ULTIMATE BENDING STRENGTH OF TIMBER BEAMS

by

IBRAHIM M. MAHDY BAZAN

A Thesis Submitted to the

Faculty of Graduate Studies

in Partial Fulfillment of the Requirement

for the Degree of

DOCTOR OF PHILOSOPHY

Major Subject: Civil Engineering

Approved

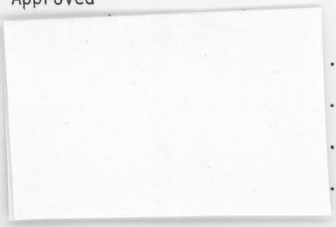

...

...

...

...

NOVA SCOTIA TECHNIICAL COLLEGE

Halifax, Nova Scotia

1980

NOVA SCOTIA TECHNICAL COLLEGE LIBRARY

"AUTHORITY TO DISTRIBUTE MANUSCRIPT THESIS"

TITLE: "Ultimate Bending Strength of Timber Beams"

The above Library may make available or authorize another library to make available individual photo/microfilm copies of this thesis without restrictions.

Full Name of Author IBRAHIM M. MAHDY BAZAN

Signature of Author 

Date 25 April 1980

TABLE OF CONTENTS

LIST OF TABLES

LIST OF FIGURES

NOTATION

a = Distance between two loads placed a/2 each side of midspan of beam.

b = Width of beam.

c = Coefficient to account for the reduced stress at extreme compression fiber of beam.

d = Depth of beam.

E_c = Compressive modulus of elasticity.

E_t = Tensile modulus of elasticity.

f = Stress at extreme fiber of beam.

f_o = Nominal stress at fracture of a structure of a specified shape and loading condition.

f_t = Tensile stress at extreme fiber of beam in inelastic range.

F_c = Maximum compressive stress in beam.

F_{cu} = Ultimate compressive strength as obtained from direct tests.

F_{pl} = Proportional limit stress in bending.

F_t = Maximum tensile stress developed at extreme fiber in beam at failure.

F_{tu} = Ultimate tensile strength as obtained from direct test.

I = Moment of inertia of beam section about the neutral axis.

k_e = Maximum knot size at edge of wide face of beam.

k_n = Maximum knot size on narrow face of beam.

k_w = Maximum centerline knot size on wide face of beam.

ℓ = Characteristic length that defines the size of a structure.

L = Span of beam.

m = Moisture content in percent.

M = Bending moment in beam section in inelastic range.

M_u = Ultimate bending moment capacity of beam.

n = f_t/F_{cu}

N = F_{tu}/F_{cu}

N' = F_t/F_{cu}

r_c = Reduction factor to account for the reduced maximum compressive stress in beam due to knots.

r_t = Reduction factor to account for the reduced maximum tensile stress in beam due to knots.

R = Modulus of rupture.

R_d = Modulus of rupture of beam having depth "d".

R_2 = Modulus of rupture of beam having 2 inches depth.

s = Size coefficient ≥ 0.

S = Size factor ≤ 1.

Y = Distance from the neutral axis to a given fiber of beam.

α = Maximum compressive stress position factor measured from top of beam.

β = Maximum compressive stress position factor measured from neutral axis.

γ = Neutral axis position factor measured from bottom of beam.

ε_c = Maximum compressive strain at extreme fiber of beam.

ε_o = Compressive strain at proportional limit stress in bending.

ε_t = Maximum tensile strain developed in extreme fiber of beam at failure.

σ = Standard deviation.

$\phi = [1 - \frac{kn}{b}][1 - \frac{kw}{d}][1 - \frac{ke}{d}]^2$

ϕ_c = Parameter ϕ for knots appeared in compression zone of beam.

ϕ_t = Parameter ϕ for knots appeared in tension zone of beam.

ACKNOWLEDGEMENTS

This research project was carried out under the supervision of Dr. S.K. Malhotra, to whom I wish to express my appreciation and sincere gratitude for his guidance, interest and helpful advice during all phases of the project.

I wish to extend my sincere appreciation to Dr. G.G. Meyerhof, Dr. D.S. Chehil and Mr. A.R. Ritchie for their continued interest and valuable assistance during my studies. Many thanks are extended to Dr. J.R. Goodman of Colorado State University for his comments and assistance in this research.

I am grateful to Mr. D. Yeadon for his assistance and help in the experimental phase of the research. Thanks are also due to Mr. A. Regala and Mrs. L. Schimp for typing the manuscript.

I gratefully acknowledge the financial assistance provided for this research by the Natural Science and Engineering Research Council of Canada.

Finally, I am deeply grateful to my wife, Nagwa, for her patience, understanding and encouragement which helped me immensely.

ABSTRACT

The current design method of calculating bending strength of timber beams is based on elastic theory, that is, on working stress approach. The elastic theory does not hold true beyond the proportional limit of stress and thus does not describe the actual behavior of timber beams in the inelastic range up to failure.

The broad objective of this study is to develop a rational approach of evaluating the ultimate bending strength of timber beams. The scope of the research is to cover various sizes of clear beams and of beams with strength reducing characteristics such as knots.

An ultimate bending strength theory for timber beams is developed. The theory predicts the ultimate moment capacity of the beam using compressive and tensile strength values of the beam material obtained from direct tests on small clear specimens.

A comprehensive experimental program is carried out to verify the theory. Tests were conducted on some two hundred and fifty-five (255) eastern spruce and Douglas-fir beams. Beams of five different sizes were subjected to central and third-point loading. Good agreement is observed between the theory and experimental results. Tests were also performed on some one thousand and nine hundred (1900) small specimens matched with the beams to determine direct compressive and tensile strengths of the test material. The ultimate tensile strength of the test material is observed to be two to three times the ultimate compressive strength.

The actual behavior of the test beams is investigated by measuring strain at various levels along the beam depth. A linear variation of the strain distribution is observed along the depth for all stages of loading

up to failure. It is observed that, at the proportional limit in bending as obtained from the load-deflection curve, the neutral axis is approximately at the center of beam depth. Beyond the proportional limit, the neutral axis shifted gradually towards the tension side, and at ultimate load, the movement of the neutral axis ranged between five to fifteen percent of the beam depth.

The proportional limit stress in bending is not significantly affected by the depth of the beam. For beams subjected to third-point loading, this stress is equal to the ultimate compressive strength of the beam material obtained from direct tests. But for centrally loaded beams, the proportional limit stress in bending is about eleven percent greater than the corresponding value for similar beams loaded at third-span points.

The maximum tensile stress developed at the extreme fiber of a beam at failure is statistically less than the ultimate strength in direct tension obtained from tests on small size standard specimens. The actual value is dependent on the depth of the beam and is smaller as the depth is increased. The effect of method of loading of the beam on maximum tensile stress at failure is found to be the same as the effect on the proportional limit-stress. The difference between both methods of loading is about eleven percent. An empirical formula relating the maximum tensile stress at failure in a beam to its size is derived.

It is observed that the presence of knots influenced the type of failure of the beam. Beams containing small knots failed in a compression-tension sequence, while beams with relatively large knots near the edge of the tension zone failed in tension without any compression failure. The load-deflection and load strain curves of the beams with large knots

indicated that the flexural behavior of these beams is elastic up to failure. To account for the weakening effect of knots on compressive and tensile strengths in a beam, correlation equations between the strength and size and location of knots, are obtained.

The concept presented in this thesis has the advantage that the ultimate moment capacity of a given timber beam for both elastic and inelastic behaviors, could be predicted from two known mechanical properties of the beam material, and it is simple to apply.

CHAPTER 1

INTRODUCTION

Timber is considered one of the most common and useful of materials for building construction. Some of the advantages of timber are its availability, economy and ease of fabrication. Today, wood structural members of almost any size and shape can be fabricated. However, owing to the fact that timber, unlike other engineering material, is of organic origin and anisotropic, its strength and mechanical properties are subject to considerable variation. Thus, more extensive testing research is needed to meet the demand and the development of timber construction.

The determination of strength characteristics of timber beams is one of the major problems in the field of timber engineering. The current design method of calculating bending strength of timber beams is based on elastic theory. Experimental investigations on timber beams have shown that elastic design with the application of high factor of safety is not adequate in many respects. As the cost of building materials is increasing, there is a need for a better and more fundamental understanding of the behavior of timber beams which leads to a more economical use of timber.

1.1 Present Design Method

The present design method of calculating bending strength of timber beams is based on elastic theory. The following assumptions are made to study the elastic behavior of a beam subjected to bending loads:

1. Plane section normal to the centriodal axis of the beam remains plane after bending. In other words, strains are linearly distributed in a section as a result of bending.
2. Stresses and strains in a section are linearly related by the modulus of elasticity of the material.

The preceding assumptions lead to the classical elastic beam formula (10):

$$f = \frac{MY}{I} \qquad [1.1]$$

where:

f = Stress at a given fiber;

M = Bending moment in the section;

Y = Distance from the neutral axis to the given fiber;

and I = Moment of inertia of the section about the neutral axis.

It can be shown that for a linearly elastic material the neutral axis contains the geometric centriod of the section, and the relation between bending moments and curvatures (or loads and deflections) is linear.

The present design practice for wood beams (8,24) is based on Eq.[1.1]. The extreme fiber stress of a given section subjected to a bending moment is equal to, or less than, the allowable unit stress in bending. Wilson (41) has discussed the overall procedure of determination of allowable unit stress in bending for Canadian lumber. His commentary provides a background to the requirements used to assign allowable unit stress in bending according to the CSA Standard 086-1976: code for engineering design of wood (8). The requirements follow the general principles of ASTM Standard D245 (3) and have been modified to reflect Canadian data and philosophy.

1.2 Inconsistencies between Elastic and Actual Behavior

Experimental research on clear timber beams has shown the following departures from simple elastic behavior:

1. The relation between bending moments and curvatures (or loads and deflections) is approximately linear in the initial stage of loading up to a point known as the proportional limit. Beyond this point, the relation is no longer linear.
2. The neutral axis remains approximately at the geometric centroid of the section up to the proportional limit point. Further loading of the beam beyond this point causes the neutral axis to move downwards rapidly.
3. The modulus of rupture defined as the maximum bending stress given by Eq.[1.1] is larger than the strength of wood under direct compression but it is smaller than the strength of wood under direct tension.
4. The modulus of rupture depends on the depth and shape of the section.

It can be seen from these results that the elastic theory does not hold true beyond the proportional limit of stress and thus does not describe the actual behavior of timber beams in the inelastic range up to failure. The inelastic concept can be used to explain some of these inconsistencies for timber beams. In the recent past, there have been some studies conducted on the inelastic behavior of timber beams. Though these studies have made a very valuable contribution to the knowledge on the subject, they were exploratory in nature and rather limited in scope.

1.3 Objectives and Scope of the Study

A timber beam can fail in any of the following modes of failure:

1. Flexural failure in compression or in tension.
2. Shear failure by maximum horizontal shear .
3. Combination of flexural and shear failure.

Only flexural behavior of timber beams is considered in this investigation.

The broad objective of this study is to develop a rational approach of evaluating the ultimate bending strength of timber beams. The theory should predict the failing load using basic strength values which could be obtained by mechanical tests on small representative samples. The scope of the research is to cover various sizes of clear beams and of beams with strength-reducing characteristics such as knots.

In order to achieve the above objective, the following program of study is adopted:

1. Review of literature on inelastic behavior of timber beams.
2. Review of the available theories and studies that dealt with and attempted to explain the size effect phenomenon on bending strength of timber beams.
3. Development of an ultimate bending strength theory for timber beams.
4. To verify the theory, a comprehensive experimental program is conducted on some two hundred and fifty-five (255) beams of various sizes. The actual behavior of the beams is investigated through strain measurements. Also, some one thousand and nine hundred (1900) compression and tension tests are conducted to obtain strength properties for test beams.

5. Test results are analysed statistically in order to determine the reliability of the proposed theory to predict the ultimate bending strength of timber beams.
6. The effect of beam size on bending strength is investigated and a relationship between the maximum tensile stress at failure in a beam to its size is derived.
7. The weakening effect of knots on bending strength is considered and correlation equations relating the compressive and tensile strengths in a beam to the size and location of knots are obtained.
8. Conclusions are drawn and recommendations are made on further research on the subject.

CHAPTER 2

REVIEW OF THE LITERATURE

The literature review is divided into two sections. The first section presents the studies that dealt with inelastic bending of timber beams. The second section deals with the size effect phenomenon on the bending strength of timber beams.

2.1 Inelastic Bending of Timber Beams

The development of an ultimate bending strength theory for timber beams depends to a large extent on the accuracy of determination of the longitudinal stress distribution in beams. Bach and Baumann (4), according to Dietz (11), proposed the first approximation of this distribution by superimposing the stress-strain curves obtained from tests on compression and tension specimens. A mathematical approach for determination of an ultimate bending strength of timber beams, which takes into account the actual stress distribution, is too complicated for practical application in design. For this reason it is not surprising that a simplified stress distribution was assumed in the development of an ultimate bending strength theory for timber beams. Several investigators have used various forms of simplified stress distributions in their research. In the following sections these studies are reviewed and discussed according to the assumed stress distributions and presented in chronological order.

2.1.1 Trapezoidal-Like Stress Distribution -- After Prager (31)

Several researchers (5,16,22,27,31,35,38,39) proposed a simplified stress distribution as shown in Fig. 2.1. This distribution is based on the following assumptions.

1) Plane section remains plane during bending up to failure.
2) The modulus of elasticity in tension is the same as in compression.
3) In tension the wood behaves as a linearly elastic material up to failure.
4) In compression the wood behaves as an ideally elastic-plastic material.
5) The maximum compressive and tensile stresses in beams are the same as the direct compressive and tensile strengths of the material.

The stress distribution in the cross-section of a beam must be such that the conditions of equilibrium are satisfied:

(i) Internal compressive force = Internal tensile force.

(ii) Internal bending moment = External bending moment.

Under these conditions of equilibrium, a relationship between ultimate bending moment, M_u, of a beam having a rectangular cross-section and the ultimate compressive and tensile strengths of the material, F_{cu} and F_{tu}, are derived as follows:

Considering the stress distribution shown in Fig. 2.1, equilibrium condition (i) yields

$$\frac{1}{2} F_{cu} \, bd \, (\beta + 2\alpha) = \frac{1}{2} F_{tu} \, bd \, \gamma \qquad [2.1]$$

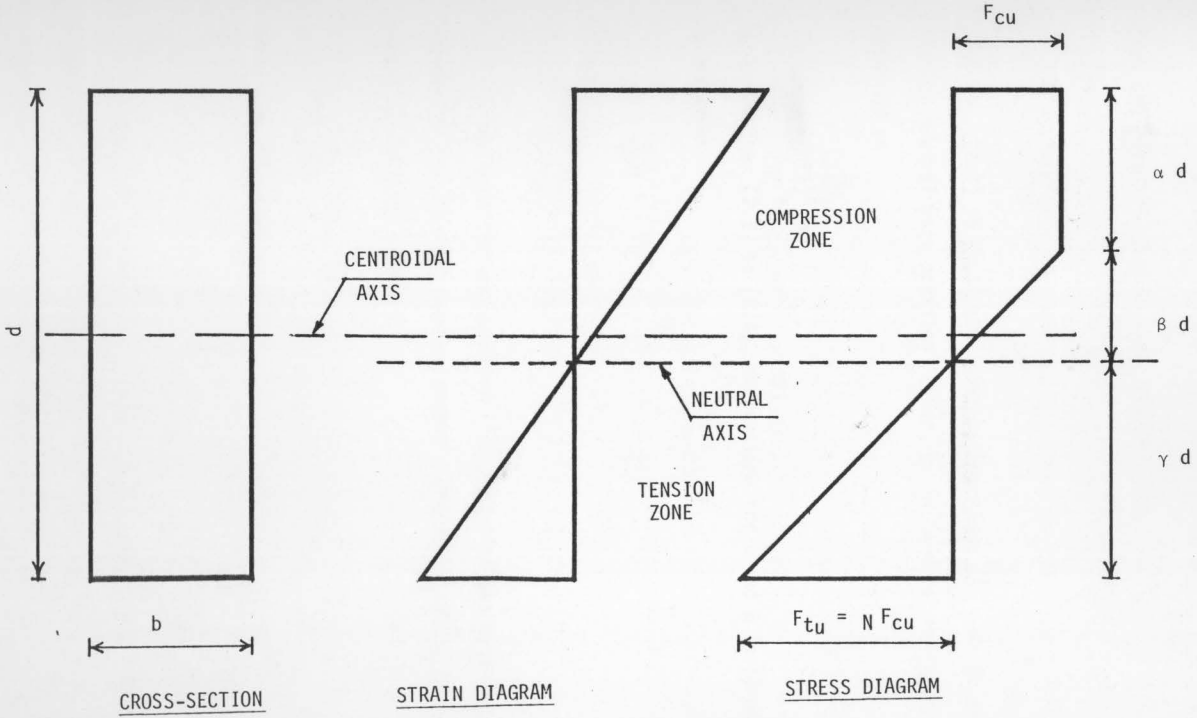

FIG. 2.1 THEORETICAL STRAIN AND STRESS DISTRIBUTIONS ACROSS DEPTH OF BEAM AT FAILURE -- AFTER PRAGER (31)

From the geometry of the stress diagram, Fig. 2.1

$$\alpha = 1 - \beta - \gamma \qquad [2.2]$$

$$\beta = \gamma\left(\frac{F_{cu}}{F_{tu}}\right) \qquad [2.3]$$

From Eqs. [2.1] to [2.3] and substituting ratio $\frac{F_{tu}}{F_{cu}} = N$, an expression for the neutral axis postiion factor, γ, in terms of ratio N can be obtained as

$$\gamma = \frac{2N}{(N+1)^2} \qquad [2.4]$$

By using Eqs. [2.2] to [2.4], expressions for α and β in terms of N can be written

$$\alpha = \frac{N-1}{N+1} \qquad [2.5]$$

$$\beta = \frac{2}{(N+1)^2} \qquad [2.6]$$

As per equilibrium condition (ii), equating the external bending moment to the internal bending moment computed by taking moments of forces about the neutral axis:

$$M_u = F_{cu}\left(\frac{bd^2}{6}\right)\left[2N\gamma^2 + 2\beta^2 + 3\alpha^2 + 6\alpha\beta\right] \qquad [2.7]$$

From Eqs. [2.4] to [2.7]

$$M_u = F_{cu}\left(\frac{bd^2}{6}\right)\left[\frac{3N-1}{N+1}\right] \qquad [2.8]$$

Equation [2.8] is derived to predict the ultimate bending moment of clear wood beams. The ultimate behavior of beams made of low grade materials, in which there are strength reducing effects due to knots

and other defects, may not be predicted exactly by Eq. [2.8].

Bechtel and Norris (5) have used the simplified stress distribution shown in Fig. 2.1 and an assumed circular function to derive a combined stress equation for all three modes of failure (flexural, shear and combined flexural and shear). They conducted tests on fourteen small clear beams, and observed that the theoretical value of bending strength is always higher than the measured value. They stated that this discrepancy is due to the fact that the compression area under the simplified stress curve, Fig. 2.1, is larger than the corresponding area under the actual curve.

Mazur (22) has used the same simplified stress distribution of Fig. 2.1 and followed similar theoretical development, but his final equation appeared more complex than Eq. [2.8]. He conducted tests on eighteen small clear beams to check the validity of the theory. He concluded that his study was too small to be considered as conclusive, but it was intended to be a pilot study for a more extensive investigation.

Ramos (33) developed a method to determine the longitudinal stress distribution in a timber beam loaded beyond its proportional limit. His test results and other experimental investigations (9,11,42) showed a satisfactory validity of the three initial assumptions of the preceding theory. The assumption that the plane section of a beam remains plane during bending was proven by the fact that the strain distribution in the cross-section of the beam was approximately limear. The modulus of elasticity in both tension and compression was not always the same but the difference between the two values was small. [Dietz (11) found the tensile modulus of elasticity was only five to six percent greater than the corresponding value in compression.

According to an experimental study by Comben (9), the bending proportional limit, as obtained from the load-deflection curve, was approximately equal to the ultimate direct compressive strength. Ramos (33) measured the maximum compressive stress in the beams and found it approximately equal to the maximum crushing strength of matched specimens. Nwokoye (27) gave the following regression equations of the relationship between the bending proportional limit stress, F_{pl}, and the ultimate compressive strength, F_{cu}:

$$F_{pl} = 1.095\ F_{cu} + 189 \text{ psi, for dry condition} \qquad [2.9]$$

$$F_{pl} = 1.28\ F_{cu} - 98 \text{ psi, for green condition} \qquad [2.10]$$

Equations [2.9] and [2.10] were based on regression analysis of the data given in (9,21,37) of more than 290 species. Nwokoye (27) concluded that the maximum compressive stress occurred at the extreme fibers in a beam just before the proportional limit stress in bending is reached and for practical purposes the bending proportional limit stress is to be taken equal to the compressive strength.

Gurfinkel (14) has used the actual stress-strain diagrams of compression and tension tests to construct a simplified stress distribution qualitatively similar to the stress distribution of Fig. 2.1. It was assumed that the maximum capacity of the beam is achieved when ultimate compressive strain is attained in the extreme fiber of the section. The maximum tensile stress in the bottom fiber was assumed to be smaller than the ultimate tensile strength in direct tension. Accordingly, the maximum tensile stress in beams depends on the actual stress-strain diagrams of the compression and tension tests. Comben (9), according to his test

results, noted that the maximum tensile stress in beams was smaller than the ultimate tensile strength, but the value was dependent on the depth of the beam. To predict the ultimate bending moment of a beam, according to Gurfinkel (14), the actual stress-strain diagrams of compression and tension tests must be available.

Several experimental investigations (17,23,32,34) showed that the stress in the compression failing zone was not constant. It was recognized that, close to the extreme compression fibers, the stress becomes smaller. This conclusion leads to some studies based on other various stress distributions which will be discussed in a later part of this chapter.

2.1.2 Parabolic-Linear Stress Distribution -- After Suenson (36)

Some investigators (7,36,42) assumed that the compressive stresses be represented by a parabolic distribution and the tensile stresses by a linear relationship, as illustrated in Fig. 2.2.

To compute the ultimate bending moment, M_u, in terms of the ultimate compressive and tensile strengths of the material, F_{cu} and F_{tu}, the conditions of equilibrium (see section 2.1.1) must be satisfied.

Referring to the stress diagram of Fig. 2.2, and using the condition of equilibrium for horizontal forces in beam section,

$$\frac{2}{3} F_{cu}\, bd\, (1-\gamma) = \frac{1}{2} F_{tu}\, bd\, \gamma \qquad [2.11]$$

Substituting $\frac{F_{tu}}{F_{cu}} = N$ in Eq. [2.11], the neutral axis position factor, γ, can be obtained as

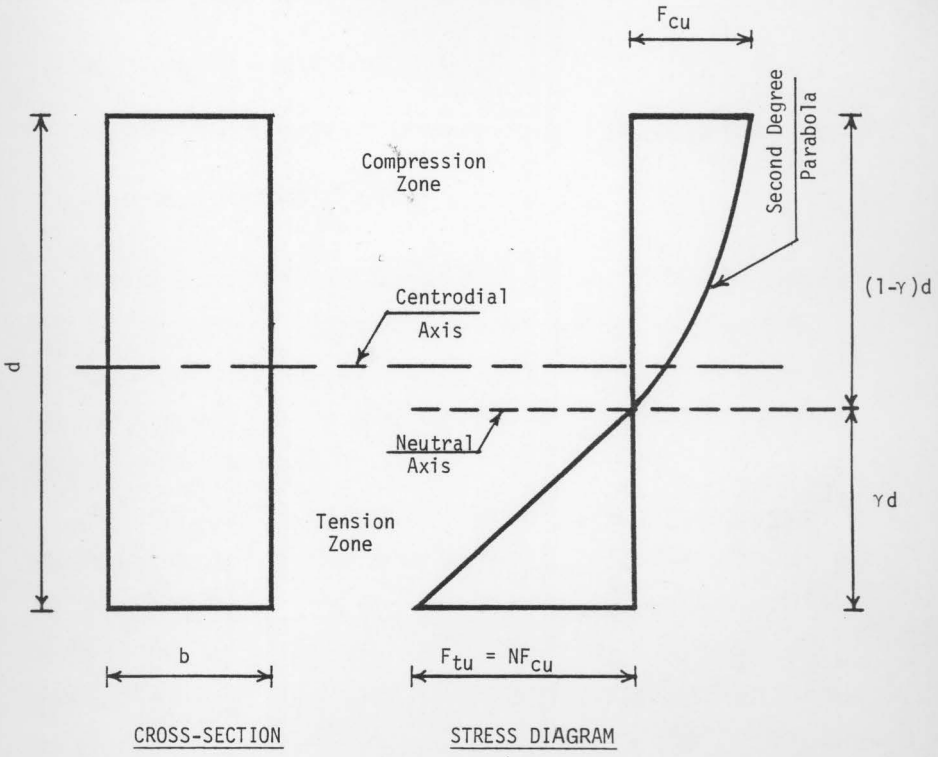

FIG. 2.2 THEORETICAL STRESS DISTRIBUTION ACROSS DEPTH OF BEAM AT FAILURE--AFTER SUENSON (36)

$$\gamma = \frac{4}{3N+4} \qquad [2.12]$$

From the moment condition of equilibrium

$$M_u = F_{cu} \left(\frac{bd^2}{6}\right) [2.5(1-\gamma)^2 + 2N\gamma^2] \qquad [2.13]$$

Substituting the value of γ from Eq. [2.12] into Eq. [2.13], yields

$$M_u = F_{cu} \left(\frac{bd^2}{6}\right) \left[\frac{22.5N^2+32N}{(3N+4)^2}\right] \qquad [2.14]$$

Recently, Zakic (42) has expressed the stress distribution curves of Fig. 2.2 by mathematical expressions and has developed equations for position of the neutral axis and the ultimate bending moment similar to Eqs. [2.12] and [2.13]. He conducted tests on only three glue-laminated beams to verify the theory.

The assumed stress distribution, Fig. 2.2, does not seem to describe the actual behavior of timber beams at failure. According to the form of the stress distribution, the maximum compressive stress occurs at the extreme fiber, and fibers close to it are subjected to smaller values. However, test results by several investigators (9,11,23) indicated that the compression failure was initiated at the extreme fiber, and then the further loading of the beam caused failure of fibers in the compression zone up to one-third of beam depth and greater in some cases. Also, Eqs. [2.12] and [2.14] do not seem to satisfy the elastic limit boundary conditions. At and below the bending proportional limit stress, the extreme fiber stresses should be equal (N=1) and the neutral axis should be at the center of depth (γ = 0.5), whereas Eq. [2.12] gives γ = 0.571, for N = 1, which mean that the neutral axis is well above the center of

depth. Nwokoye (28) has pointed out some other anomalies in the treatment by Zakic.

2.1.3 Idealized Stress Distribution -- After Radok et al (32)

Radok, Silberstein and Wills (32) proposed an idealized stress distribution of the type shown in Fig. 2.3. Their study dealt with Wooden box beams. The hypothesis of this stress distribution is that, at failure, the maximum compressive stress in a failing timber beam occurs somewhere between the extreme fiber and the neutral axis, and the stress decreases from this maximum value linearly towards the extreme compression fiber. The analysis was based on a large number of tests of box beams. The authors (32) have also considered other stress distribution which is qualitatively similar to the form of the stress distribution of Fig. 2.1. They found that the stress distribution of Fig. 2.3 provided the best explanation of the behavior of the beams tested, and that the analysis based on this stress distribution reduced the random scatter of the test results to a minimum.

The results of the study (32) were given in the form of semi-empirical curves. These curves are applicable only to beams with a solidity ratio less than 0.8. The solidity ratio was defined as the ratio of timber in the cross-section of any rectangular beam to that in a solid beam with the same overall dimensions. However, the authors (32) conducted tests on some eighteen small solid beams and they concluded that the idealised stress distribution of Fig. 2.3 could be expected to approximate the actual stress distribution of solid beams with sufficient accuracy.

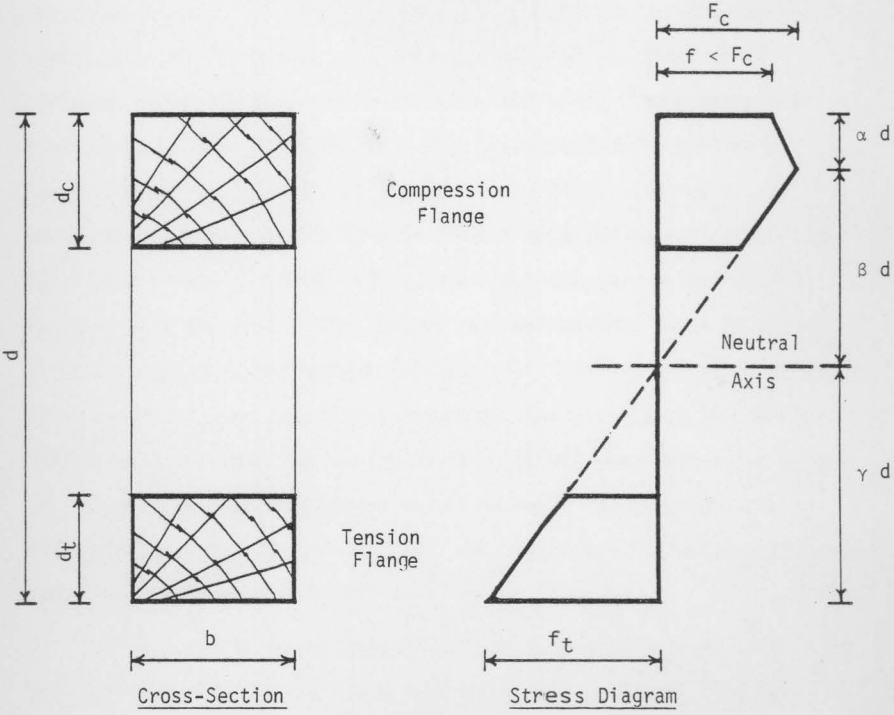

FIG. 2.3 IDEALIZED STRESS DISTRIBUTION IN BOX BEAM AFTER COMPRESSION FAILURE-- AFTER RADOK et al (32)

2.1.4 Assumed Stress Distribution -- After RRobinson and Cooper (34)

Robinson and Cooper (34) suggested a strress distribution of the form presented in Fig. 2.4. The distribution was obtained by assuming that a combination of compression, tension and shear failure occurred at collapse. They conducted tests on fifty-four solid timber beams with strength-reducing characteristics. The cross-sectional dimensions of the beams ranged from 1 x 2 to 3 x 8 inches. The stress diagram of Fig. 2.4 was a representation of the type of failure observed on forty-four beams out of the fifty-four beams tested, the remainder gave rather erratic failure. The position of the neutral axis was assumed to be at the horizontal splitting of the tension failure. The limit of the visible compression wrinkle was observed to extend to roughly halfway to the horizontal splitting and it was taken as the position of maximum compressive stress. The value of maximum compressive stress in beams was assumed to be the direct compressive strength of small clear specimens, although the beams contained strength-reducing characteristics.

Considering the stress diagram of Fig. 2.4, and from the moment condition of equilibrium, the ultimate bending moment, M_u, is given by

$$M_u = F_{cu} \left(\frac{bd^2}{6}\right) \left[\frac{1}{2} (1-\gamma) (3-\gamma)\right] \qquad [2.15]$$

From the force condition of equilibrium, the maximum tensile stress in the beam at failure, F_t, can be obtained as

$$F_t = \frac{(1-\gamma)}{\gamma} F_{cu} \qquad [2.16]$$

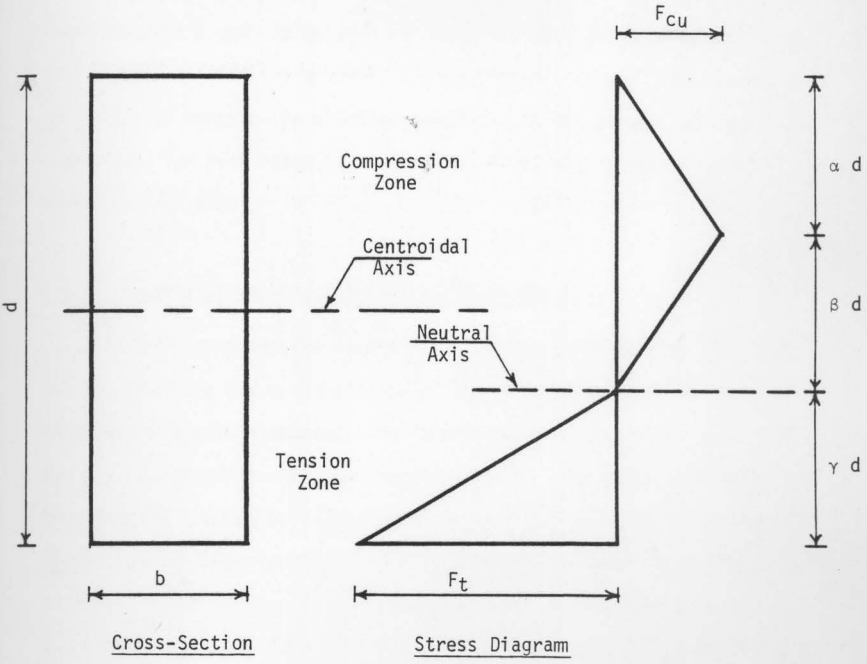

FIG. 2.4 ASSUMED STRESS DISTRIBUTION ACROSS DEPTH OF BEAM AT COLLAPSE--AFTER ROBINSON AND COOPER (34)

Equation [2.15] was used to calculate the theoretical ultimate bending moment of the test beams. The authors noted that the extremely low position of the neutral axis, according to the stress diagram, Fig. 2.4, would require a very large rate of change of tension stress down from the neutral axis to the extreme tension fibers. It was also observed that smaller compression wrinkles developed in the deeper beams and was suggested, for such beams, the use of a stress distribution such as that given in Fig. 2.3.

2.1.5 Assumed Stress Distribution -- After Moe (23)

Moe (23) proposed the stress distribution given in Fig. 2.5. He assumed that the reduction of stress in the compression zone, due to wrinkles, occurred suddenly. The experimental investigation was carried out on a large number of glue-laminated beams. The beams were produced from materials which contained strength-reducing characteristics such as knots. It was observed that, at a load ranging between 70 to 100 percent of the ultimate value, there appeared a number of wrinkles in the compression zone of the beam. These wrinkles often started out from knots and developed gradually further deeper into the compression zone. The maximum compressive stress in the cross-section of the beam was found to be, on the average, slightly smaller than the direct compressive strength of clear specimens, which is to be expected on account of the knots in the beams.

Referring to Fig. 2.5, and applying the conditions of equilibrium, the following expressions for the ultimate bending moment, M_u, and maximum tensile stress in the beam, F_t, can be obtained as

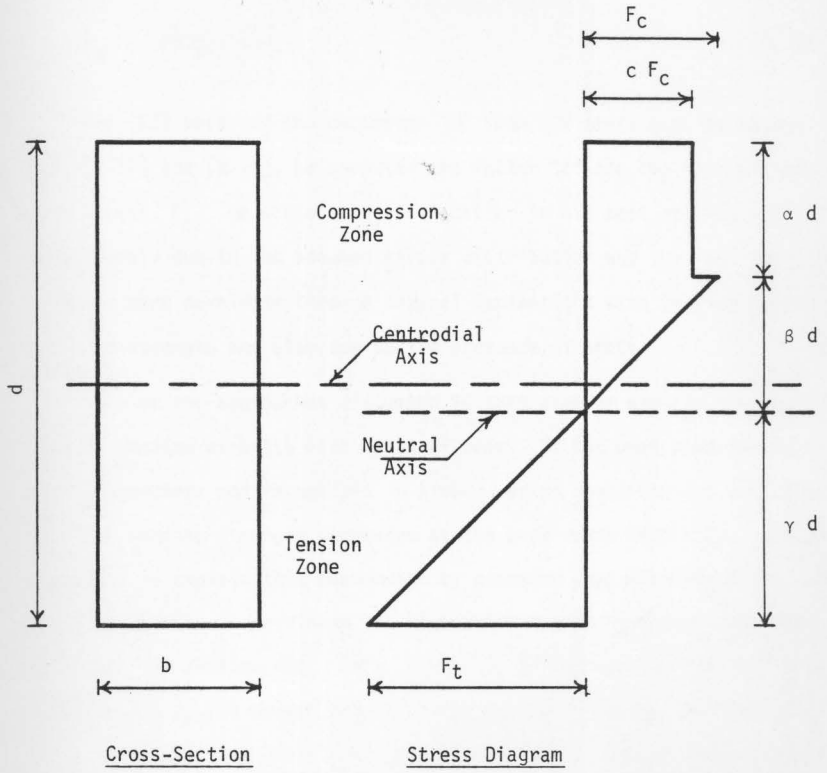

FIG. 2.5 ASSUMED STRESS DISTRIBUTION ACROSS DEPTH OF BEAM AT FAILURE--AFTER MOE (23)

$$M_u = F_c \left(\frac{bd^2}{6}\right) [(1-\alpha)^2 + c\alpha(4-\alpha)] \quad [2.17]$$

$$F_t = \left[\frac{1-\alpha(1+2c)}{(1-\alpha)}\right] F_c \quad [2.18]$$

Moe (23) measured the parameter "α" ffrom his tests and, by using Eqs. [2.17] and [2.18], he computed the factor "c" and the maximum tensile stress, F_t. He stated that the scatter in his test results was large partly due to the assumed stress distribution and the fact that the wrinkles were developed through several laminations with varying compressive strength and also due to the presence of knots.

None of the approaches discussed in this chapter explain the variation of bending strength with depth of beam. It has been observed by many researchers and recognized in timber design specification and codes that the bending strength decreases as the beam depth increases. Moe (23) attempted to explain this phenomenon by assuming that when the first compression wrinkle is developed, it penetrates deeper into the deep beam than into the shallow one. Thus, the value of compression stress in the failing zone of the deeper beam would be smaller than the corresponding value in the shallow beam on account of the larger deformations in the wrinkles. However, this assumption was not confirmed by his test results since all the tests were conducted on beams having the same depth. In addition, this assumption is in a marked contrast with the test results by Robinson and Cooper (34) where they observed smaller compression wrinkles in the deeper beams.

In recent years, two theories, namely, theory of fiber support and statistical strength theory, have been put forward to explain the variation

of bending strength with depth of beam. These theories are discussed in the following section.

2.2 Effect of Beam Size on Bending Strength of Timber Beams

2.2.1 Theory of Fiber Support

Newlin and Trayer (26) proposed the fiber support theory to explain the variation of modulus of rupture with depth of timber beams. It is assumed that wood fibers under compression act as minute column restrained against buckling as whole and against individual buckling of their cell walls by the lignin. In a block subjected to axial load, all fibers are equally strained and tend to buckle simultaneously, offering one another little support. In a beam subjected to bending, the compressive strain decreases from a maximum value of the extreme fiber to zero at the neutral axis. Hence, support of the extreme fibers by the other less-restrained fibers is possible.

The variation of modulus of rupture with depth was explained, according to this theory, by assuming that the same strain is developed at the extreme fiber of shallow and deep beams. The fibers under small strain in deep beams, being distant from the extreme fibers, may not offer much support. In shallow beams, however, the fibers under small strains are quite close to the extreme fibers and offer more support.

Newlin and Trayer (26) proposed the following equation for the ratio of modulus of rupture, R_d, of beam of depth, d, (in inches) to modulus of rupture, R_2, of two-inch deep beam.

$$\frac{R_d}{R_2} = 1.07 - 0.07\sqrt{d/2} \qquad [2.19]$$

Equation [2.19] was derived from test data obtained from beams having depths up to twelve inches.

Freas and Selbo (13) published the following equation relating R_d, R_2 and d

$$\frac{R_d}{R_2} = \left(\frac{5}{8}\right)\left(\frac{d^2+143}{d^2+88}\right) \qquad [2.20]$$

Equation [2.20] was developed on the basis of data obtained from beams having maximum depth of sixteen inches.

The validity of the fiber support theory depends on the assumption that additional support is received by the extreme compression fibers from those which are less strained. Comben (9) pointed out that, according to his experimental results, the basic philosophy of this theory was not confirmed. He observed that the proportional limit stress in bending was very slightly affected by the depth of beam and the value was in agreement with the compressive strength of the beam material as obtained from direct tests. On the other hand, the results (9) showed a marked decrease of maximum stress developed in the extreme tension fibers as the depth increased. Comben suggested that the reduced modulus of rupture with increasing depth is due to the decreased tensile stress at the extreme tension fiber.

2.2.2 Statistical Strength Theory

A study by Bohannan (6) explained the variation of modulus of rupture of timber beams with depth from a statistical point of view. The general statistical strength theory given by Weibull (40) was used. This theory

assumes that the failure of a specimen will occur when the stress in the specimen is the same as the stress that would cause failure of the weakest element of volume if tested independently. Thus, the theory assumes the existence of a weakest link where failure, once initiated, propagates without additional loads. Since final failure in bending of a timber beam is a tension failure of brittle nature, the theory assumes a cascade-type tension failure occurring when any element of volume fails in the tension zone of the beam. The application of this theory leads to the conclusion that the modulus of rupture of timber beams is dependent on the product depth times length and on the method of loading, but it is independent of the beam width.

The mathematical relationship connecting modulus of rupture with beam size and method of loading of the beam can be summarized as follows: For two beams under two equal concentrated loads applied symmetrically to the mid span points, the ratio of modulus of rupture of beam-1 to modulus of rupture of beam-2 is given by the formula

$$\frac{R_1}{R_2} = \left[\frac{d_2 b_2 \left(1 + s \frac{a_2}{L_2}\right)}{d_1 L_1 \left(1 + s \frac{a_1}{L_1}\right)} \right]^{\frac{1}{s}} \qquad [2.21]$$

where: Subscripts 1 and 2 refer to beam-1 and beam-2;

R = Modulus of rupture;

d = Depth of the beam;

L = Span of the beam;

a = Distance between loads placed $\frac{a}{2}$ each side of mid-span;

and s = Constant.

According to Eq. [2.21], the difference between modulus of rupture of a centrally loaded beam and modulus of rupture of a similar beam subjected to two-points load is given by the expression $[1 + s\frac{a}{L}]\frac{1}{s}$. For Douglas-fir beams, Bohannan (6) found the value of constant "s" equal to 18 and, accordingly, the modulus of rupture of a beam subjected to central load was 11.4 percent greater than the modulus of rupture of a similar beam loaded at third-span points.

The variation of the strength ratio $\frac{R_d}{R_2}$ with the depth of the beam for the same span-depth ratio and same method of loading, as per Eq. [2.21], is given by the following expression:

$$\frac{R_d}{R_2} = (\frac{2}{d})^{\frac{1}{9}} \qquad [2.22]$$

The CSA Standards 086-1976 (8) have adopted Eq. [2.22] for the determination of the variation of the strength ratio with depth of beams.

More recently, Leicester (18) defined the magnitude of size effect, in general, by the equation:

$$f_o = \frac{A_o}{\ell^s} \qquad [2.23]$$

where:

f_o = Nominal stress at fracture of a structure of a specified shape and loading condition;

ℓ = Characteristic length that defines the size of the structure;

s = Size coefficient ($s \geq 0$);

and A_o = Constant.

It can be seen that Eq. [2.23] is the general form of Eq. [2.22].

2.3 Conclusions

The literature review of the studies on inelastic bending of timber beams reveals that the scope of these studies was rather limited. The size of the beams or the number of tests were too small. The investigations on beams with knots were not very well suited for such a study since the size and locations of knots were not taken into account.

The statistical strength theory provides an acceptable explanation for the decreasing of bending strength with increase in beam depth. The linear stress distribution in the beam section at failure was used because of its simplicity in the mathematical computations.

CHAPTER 3

ULTIMATE BENDING STRENGTH THEORY FOR TIMBER BEAMS

3.1 General Considerations and Assumptions

The occurrence of compression failure, before tension failure, in timber beams subjected to bending loads has been recognized by many researchers (4,5,9,11,23,30,33). The reason for this behavior is that wood is, in general, much stronger in tension than in compression, parallel to the grain. Figure 3.1 shows a typical overall stress-strain relationships for tension and compression specimens under direct axial load. In tension, the curve is almost linear up to failure. In compression, the curve is essentially linear up to about 80 percent of the maximum load. Thereafter, the load or stress, reduces rapidly with increasing strain and then attains a fairly constant reduced value until the specimen split or fail in shear.

If each of the fibers of a bent timber beam are considered to behave as infinitesimally small axially loaded rods stressed to levels that depend on the corresponding strain, the characteristics of the stress-strain diagram shown in Fig. 3.1 can be used to prescribe the stress patterns in these fibers.

When a timber beam is subjected to bending, compression failure occurs initially at the extreme fibers. Further loading of the beam causes these fibers to lose some of their capacity to sustain stress and there is a redistribution of stresses along the beam depth. The adjacent fibers, at

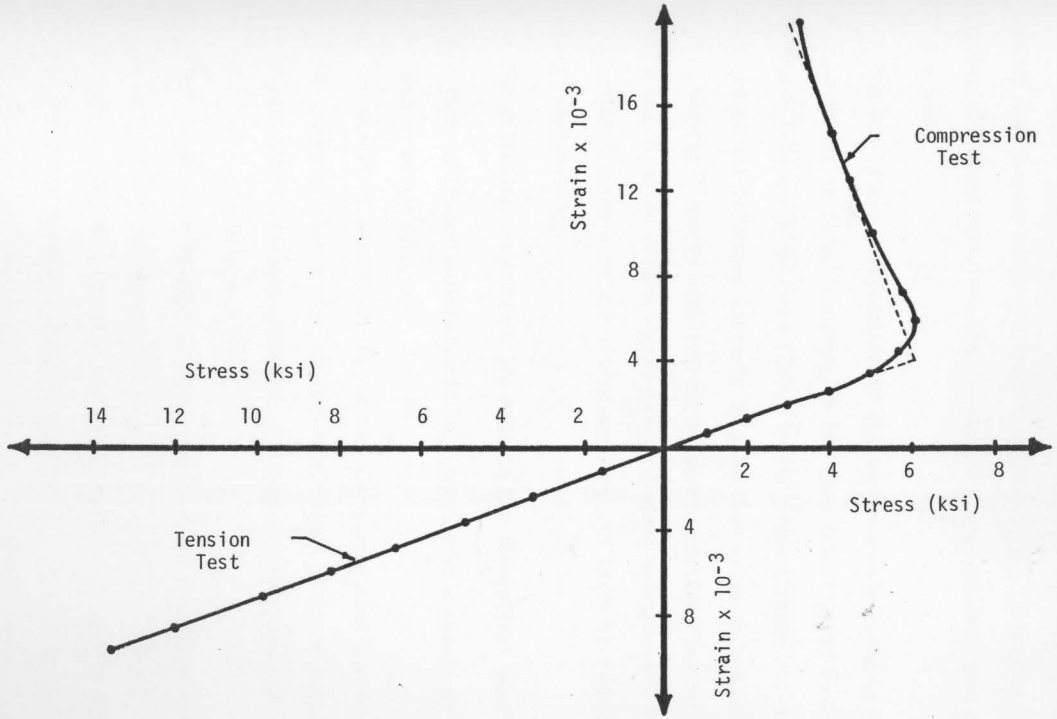

FIG. 3.1 STRESS-STRAIN RELATIONSHIPS IN DIRECT COMPRESSION AND TENSION TESTS

this stage, are subjected to a greater stress, and the neutral axis shifts towards the tension side resulting in higher stress in tension. This process continues until tension failure occurs at maximum load capacity of the beam.

The non-linear relationship of the stress-strain curve up to the maximum stress in direct compression has been investigated by Malhotra and Mazur (20) and O'Halloran (29). In the present study, it is assumed that the stress increases linearly to a maximum value beyond which the stress reduces linearly with increasing strain (dotted line in Fig. 3.1). This simplification of the stress-strain diagram approximates the actual stress distribution with sufficient accuracy and leads to simple mathematical computations.

The following assumptions are made in the theoretical development:

1) Strain is linearly distributed in a section as a result of bending up to failure.
2) The moduli of elasticity in tension and compression are equal.
3) The extreme fiber stress at the proportional limit in bending equals the ultimate compressive strength of the beam material as obtained from direct tests.
4) The stress distribution is linear up to the proportional limit stress in bending beyond which the distribution is of the form shown in Fig. 3.2. This figure illustrates the theoretical strain distributions and the corresponding stress distributions at the critical section of the beam, in relation to a progressive bending.

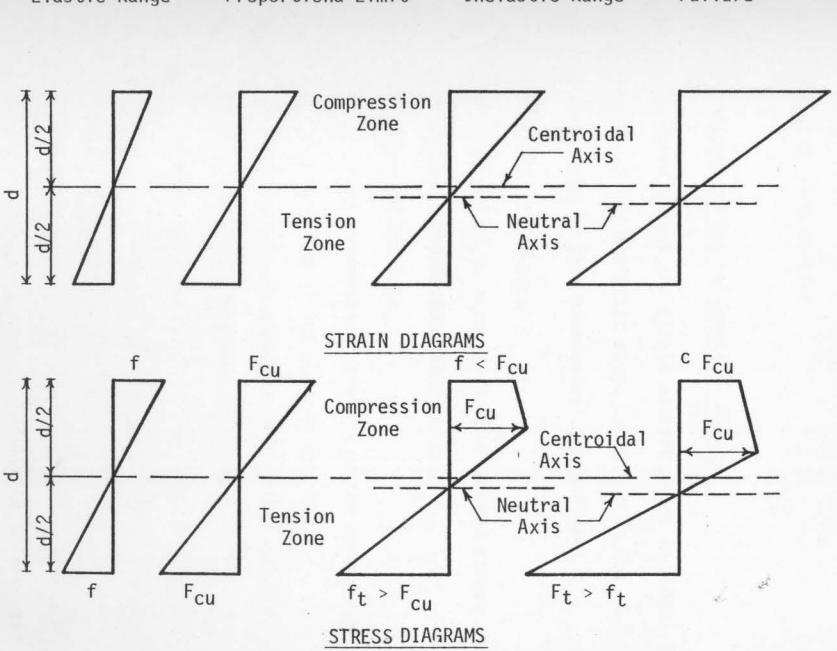

FIG. 3.2 THEORETICAL STRAIN AND STRESS DISTRIBUTIONS AT CRITICAL SECTION OF TIMBER BEAM IN RELATION TO PROGRESSIVE BENDING

The validity of assumptions 1, 2 and 3 has been proved by previous experimental investigations (9,11,33), as discussed in Chapter 2. The reason and considerations related to assumption 4 were outlined in an earlier part of this chapter.

3.2 Development of the Mathematical Models

The assumed stress and strain distributions in a beam of rectangular cross-section in the inelastic range are shown in Fig. 3.3. The following notations are used in the mathematical computations.

b = Width of the beam

c = Coefficient to account for the reduced stress at the extreme compression fiber ($c<1$)

d = Depth of the beam

F_{cu} = Ultimate compressive strength of the beam material as obtained from direct compression tests

F_{tu} = Ultimate tensile strength of the beam material as obtained from direct tension tests

F_t = Maximum tensile stress in the beam at failure ($F_t \leq F_{tu}$)

f_t = Tensile stress at the extreme fiber in inelastic range ($f_t < F_t$)

M = Bending moment in the beam section in inelastic range

M_u = Ultimate bending moment capacity of the beam

$$N = \frac{F_{tu}}{F_{cu}} > 1$$

$$N' = \frac{F_t}{F_{cu}} > 1, \quad (N' \leq N)$$

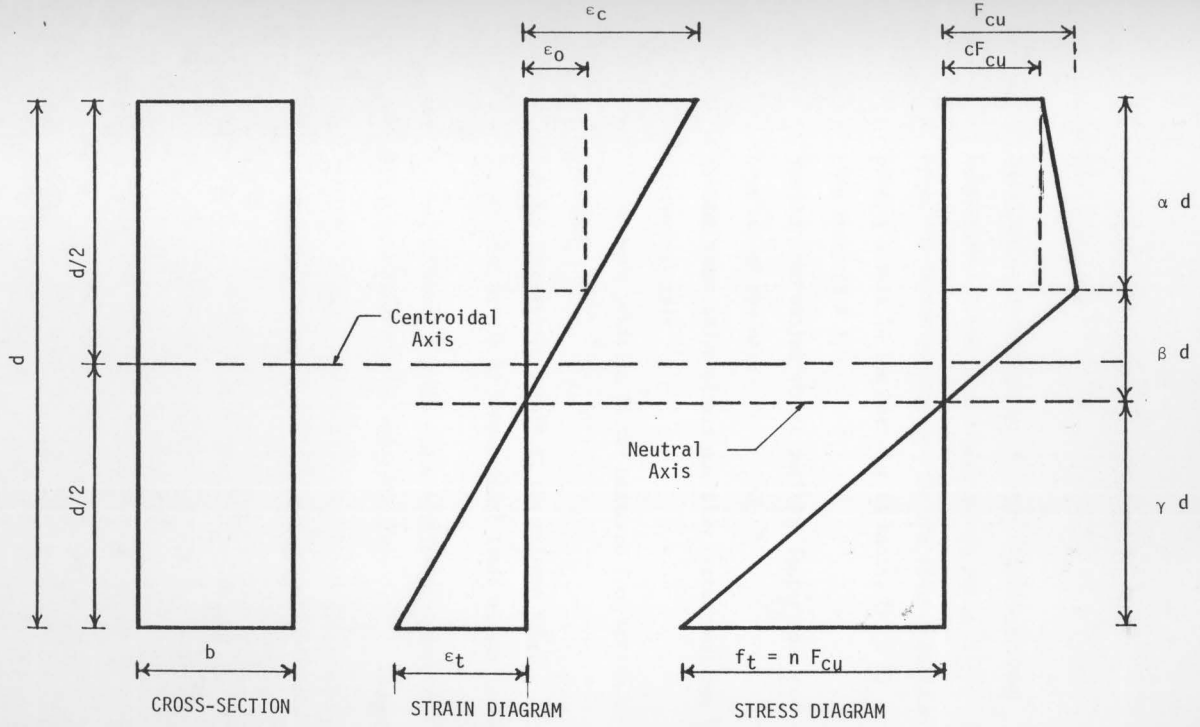

FIG. 3.3 THEORETICAL STRAIN AND STRESS DISTRIBUTIONS ACROSS DEPTH OF BEAM IN INELASTIC RANGE

$n = \frac{f_t}{F_{cu}} > 1$

r_c = Reduction factor to account for the reduced maximum compressive stress in the beam due to knots. ($r_c \leq 1$)

r_t = Reduction factor to account for the reduced maximum tensile stress in the beam due to knots. ($r_t \leq 1$)

S = Size factor($S \leq 1$)

α = Maximum Compressive stress position factor measured from top of the beam

β = Maximum compressive stress position factor measured from the neutral axis

γ = Neutral axis position factor measured from bottom of the beam

ε_c = Maximum compressive strain at the extreme fiber

ε_o = Compressive strain at proportional limit stress in bendin.

The stress distribution in the cross-section of a beam must be uch that the conditions of equilibrium are satisfied.

(i) Internal compressive force = Internal tensile force

(ii) Internal bending moment = External bending moment

Considering the stress distribution shown in Fig. 3.3, the resu tant compressive and tensile forces, respectively are:

$$\frac{1}{2} F_{cu}\, bd\, [\beta + (1+c)\, \alpha] \qquad [3.1]$$

$$\frac{1}{2} F_{cu}\, bd\, n\, \gamma \qquad [3.2]$$

Substituting Eqs. [3.1] and [3.2] into equilibrium condition (i) yields

$$\beta + (1+c)\,\alpha = n\,\gamma \qquad [3.3]$$

From the geometry of stress diagram in Fig. 3.3,

$$\alpha = 1 - \beta - \gamma \qquad [3.4]$$

$$\beta = \frac{\gamma}{n} \qquad [3.5]$$

From Eqs. [3.3] to [3.5], an expression for γ in terms of c and n can be obtained as

$$\gamma = \frac{n(1+c)}{(n+1)(n+c)} \qquad [3.6]$$

By using Eqs. [3.4] to [3.6], expressions for α and β in terms of c and n can be written:

$$\alpha = \frac{(n-1)}{(n+c)} \qquad [3.7]$$

$$\beta = \frac{(1+c)}{(n+1)(n+c)} \qquad [3.8]$$

As per equilibrium condition (ii), equating the external bending moment to the internal bending moment computed by taking moments of forces about the neutral axis:

$$M = F_{cu}\,\frac{bd^2}{6}\,[2n\,\gamma^2 + 2\beta^2 + (1+2c)\,\alpha^2 + 3(1+c)\,\alpha\beta] \qquad [3.9]$$

From Eqs. [3.6] to [3.9],

$$M = F_{cu}\,\frac{bd^2}{6}\left[\frac{n + (2n-1)c}{(n+c)}\right] \qquad [3.10]$$

Now, the reducing stress after the initial occurrence of compression failure is proportional to the increasing strain in the compression zone. Thus,

$$1 - c = \text{constant} \times (\varepsilon_c - \varepsilon_o) \qquad [3.11]$$

From the strain distribution of Fig. 3.3,

$$\varepsilon_c - \varepsilon_o = \frac{\alpha}{\beta}\,\varepsilon_o \qquad [3.12]$$

From Eqs. [3.11] and [3.12],

$$1 - c = \text{constant} \times \frac{\alpha}{\beta}\,\varepsilon_o \qquad [3.13]$$

Since the compressive strain, ε_o, at the proportional limit is constant and dependent only on the beam material, thus

$$1 - c = A\left(\frac{\alpha}{\beta}\right) \qquad [3.14]$$

where A is a constant to be determined.

Substituting the value of α and β from Eqs. [3.7] and [3.8] into Eq. [3.14] and rearranging the results,

$$c = \sqrt{1-A(n^2-1)} \qquad [3.15]$$

From Eqs. [3.10] and [3.15], an expression for the bending moment, M, can be obtained as

$$M = F_{cu}\,\frac{bd^2}{6}\left[\frac{n + (2n-1)\sqrt{1-A(n^2-1)}}{n + \sqrt{1-A(n^2-1)}}\right] \qquad [3.16]$$

The bending moment capacity of the beam will be maximum when

$$\left(\frac{dM}{dn}\right)_{n=N'} = 0$$

Differentiating Eq. [3.16] with respect to n and substituting N' for n and then equating the result to zero, an expression for constant A can be obtained as:

$$A = \frac{2N' + 1}{(N' + 1)^3(N'-1)} \qquad [3.17]$$

Substituting the value of A from Eq. [3.17] into Eq. [3.16] and replacing N' for n, the following expression for the ultimate bending moment capacity of the beam, M_u, is obtained

$$M_u = F_{cu} \frac{bd^2}{6} \left[\frac{3N'}{N' + 2} \right] \qquad [3.18]$$

From Eqs. [3.15] and [3.17], and replacing N' for n, an expression for c at ultimate bending moment is obtained,

$$c = \frac{N'}{N' + 1} \qquad [3.19]$$

Substituting the value of c from Eq. [3.19] into Eq. [3.6], and replacing N' for n, an expression for the neutral axis position factor, γ, at ultimate bending moment can be obtained as

$$\gamma = \frac{2N' + 1}{(N' + 2)(N' + 1)} \qquad [3.20]$$

The ultimate bending moment, M_u, can be obtained by using Eq. [3.18]. To predict the ultimate bending moment capacity of a beam, one requires the values of cross-sectional dimensions, b and d, and the maximum tensile and compressive stress values of the beam material, F_t and F_{cu}. However, due to the size effect, the maximum tensile stress in the beam at failure, F_t, may be smaller than the ultimate tensile strength of beam material, F_{tu}, as obtained from direct tests (9). Thus,

$$F_{t/F_{tu}} = S, \text{ where } S \leq 1 \qquad [3.21]$$

$$N' = S \cdot N \qquad [3.22]$$

Substituting the value of N' from Eq. [3.22] into Eqs. [3.18] and [3.20],

$$M_u = F_{cu} \frac{bd^2}{6} \left[\frac{3\ S \cdot N}{S \cdot N + 2}\right] \qquad [3.23]$$

$$\gamma = \frac{2\ S \cdot N + 1}{(S \cdot N + 2)(S \cdot N + 1)} \qquad [3.24]$$

In the case of beams with knots, the values of tensile and compressive strength of the beam will be smaller than the corresponding values for clear beam of the same size, due to the presence of knots. To account for the weakening effect of knots on strength, Eqs. [3.23] and [3.24] can be modified as

$$M_u = F_{cu} \frac{bd^2}{6} \left[\frac{3 r_c \cdot r_t \cdot S \cdot N}{r_t \cdot S \cdot N + 2\ r_c}\right] \qquad [3.25]$$

$$\gamma = \frac{r_c(2 r_t \cdot S \cdot N + r_c)}{(r_t \cdot S \cdot N + 2\ r_c)(r_t \cdot S \cdot N + r_c)} \qquad [3.26]$$

It should be noted that, if the value of the expression between parentheses in Eq. [3.25] is smaller than r_c, the behavior of the beam is elastic to failure and the ultimate bending moment, in this case, is given by

$$M_u = F_{cu} \frac{bd^2}{6} [r_t \cdot S \cdot N]; \qquad [3..27]$$

and the corresponding value of γ is 0.5.

In this investigation, the theory is verified by experimental tests on different sizes of clear beams and beams with knots. The values of maximum tensile stress at failure are obtained by means of strain measurement in beam specimens and they are compared with the ultimate tensile strength of the beam material in direct tension.

CHAPTER 4

EXPERIMENTAL PROGRAM

4.1 Test Material

Test material was selected from two species of lumber. The first was eastern spruce available in the Maritime Provinces of Canada, and the second was Douglas-fir. The lumber used can be divided into three groups depending on its grade. The first group was select structural grade eastern spruce of 2 x 4, 2 x 6, 2 x 8, and 4 x 12 nominal sizes. The corresponding actual cross-sectional dimensions were approximately 1.5 x 3.5, 1.5 x 5.5, 1.5 x 7.3, and 3.5 x 11.3 inches, respectively. The second group was structural grade No. 1 Douglas-fir of 2 x 6 nominal size, and the third group was construction grade No. 1 eastern spruce of 2 x 4 and 2 x 6 nominal dimensions.

Lumber of the first and second groups was visually inspected and only straight-grained clear pieces free of knots were selected for fabrication of clear beam test specimens. Beam specimens fabricated from the third group contained knots.

Each piece of lumber used was of sufficient length to provide enough material for the required length of the beam specimen, at least three compression test specimens, and three or more tension test specimens. A cutting diagram for obtaining beam and matched compression and tension specimens is given in Fig. 4.1. The length of 4 x 12 lumber was not enough to accommodate compression and tension specimens. As a result,

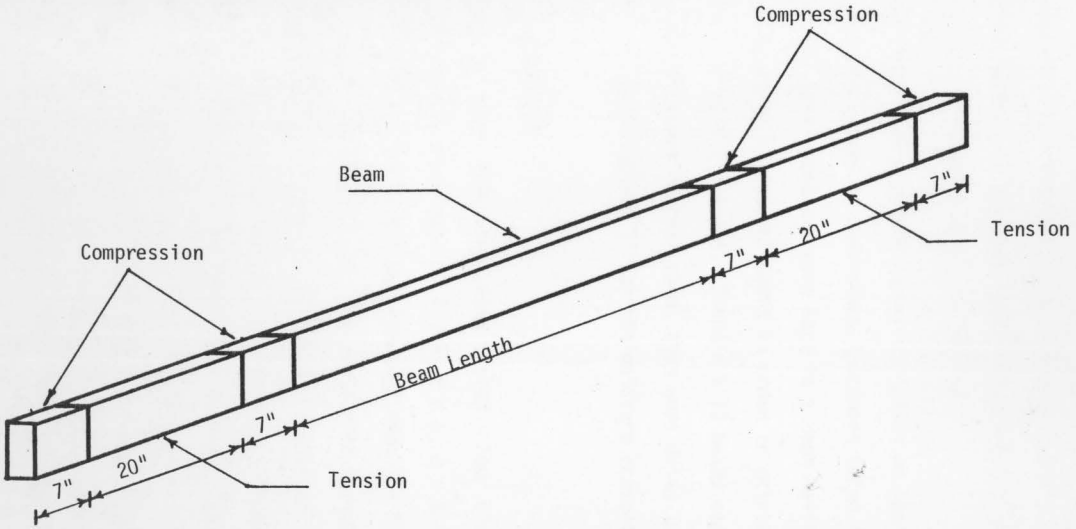

FIG. 4.1 LOCATIONS OF BEAM SPECIMEN AND MATCHED COMPRESSION AND TENSION SPECIMENS IN A LUMBER PIECE

the matched specimens for compression and tension tests were obtained from the unstressed ends of the beam specimens after testing. A summary of the experimental program is given in Table 4.1.

Before cutting, each piece of lumber was given an identification number which was then given to subsequent specimens taken from this piece. After cutting, all test specimens were kept in a room having a controlled atmosphere for a period of several weeks in order to maintain a steady moisture content of 12 ± 1 percent. Since 4 x 12 beams could not be accommodated in the moisture control room, they were dried in the open air for a few days to approximately 17 percent moisture content.

4.2 Beam Test Specimens

Five groups of clear beam sizes were tested. Four sizes were actual lumber sizes of nominal dimensions of 2 x 4, 2 x 6, 2 x 8 and 4 x 12. The fifth size, 1.50 x 1.65 inches was obtained from 2 x 6 lumber. In addition, two groups of knotted beam sizes were also tested. They were actual lumber sizes of 2 x 4 and 2 x 6 nominal dimensions. The beams were tested as simply supported beams and under two methods of loading, namely, central and third-point loading. The selected length of each beam was such to provide a span-depth ratio of about 16. This span-depth ratio was selected to ensure that the effect of shear would be relatively insignificant on the failure mode and that the type of failure would be predominantly flexural in character. A special group of 2 x 6 nominal size clear beams were stiffened at the ends and tested under third-point loading. The purpose of the stiffeners was to decrease the probability of shear effect and to observe if any differences occurred in the type of

TABLE 4.1: Experimental Program

Actual Size of Beam (in.)			No. of Beam Test Specimens		No. of Matched Compression Specimens	No. of Matched Tension Specimens
Width (b)	Depth (d)	Span (L)	Central Loading	Third-point Loading		
			Clear Beams			
1.50	1.65	27	13(S)[a],9(D)	14(S),9(D)	184	176
1.50	3.50	57	20(S)	20(S)	120	120
1.50	5.50	90	21(S),8(D)	17(S),8(D)	226	206
1.50	5.50	90[b]	-	24(S),8(D)	132	132
1.50	7.30	123	10(S)	10(S)	60	60
3.50	11.30	180	5(S)	2(S)	28	28
3.50	11.30	162	-	3(S)	12	12
			Knotted Beams			
1.50	3.50	57	15(S)	15(S)	120	120
1.50	5.50	90	6(S)	12(S)	72	72
1.50	5.50	80	6(S)	-	24	24
TOTAL			113	142	978	950

a: (S) and (D) refer to spruce and Douglas-fir Lumber, respectively.

b: Stiffened beams.

failure between stiffened and unstiffened beams. The stiffeners were glued to the outer ends of each beam as shown in Fig. 4.2.

After the beam specimens were machined to their final lengths, the positions of supports, applied loads and the center line of span were marked. The size and location of knots in the knotted beams were measured according to the ASTM Standard D245 (3) and recorded. An illustration of record of knots is given in Fig. 4.3.

A group of 6.3 mm diameter stainless steel discs (Demec points) for a mechanical gage were glued at intervals across the two faces of each beam at midspan to allow strain measurement. The number and the longitudinal distance between these gage points were varied depending on the beam size. The number was chosen such that a representative strain distribution could be obtained, and the time taken to read the gages would not be excessive. The arrangement of the gage points is shown in Fig. 4.4.

4.3 Compression and Tension Test Specimens

The dimensions of test specimen for compression parallel to grain as per ASTM Standard D143(1) are 2 x 2 x 8 inches. Since most of the lumber used in testing was 1.5-inch thick (actual size), compression specimens were 1.5 x 1.5 x 6 inches. All specimens were free from knots and each one was surfaced on all four faces. The ends of each specimen were plane and normal to its longitudinal axis.

The tension test specimens were made in accordance with the ASTM Standard D143 (1). The minimum cross-section of the specimen was 3/8 by 3/16 inch over a $2\frac{1}{2}$ inches central length and the curved portion had a

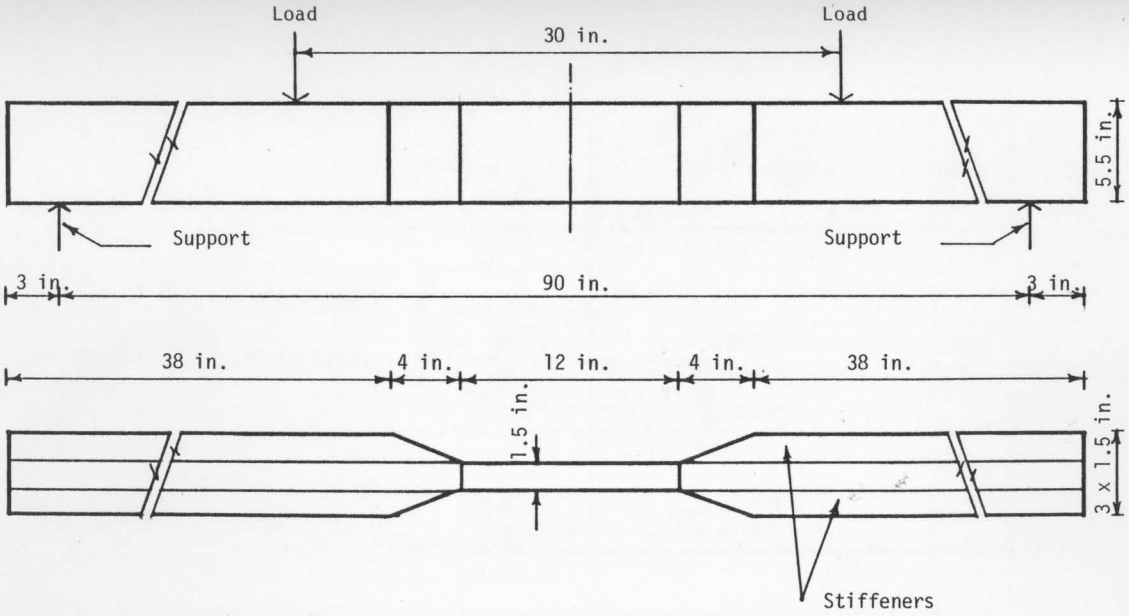

FIG. 4.2 DETAIL OF A 2 x 6 STIFFENED BEAM SPECIMEN

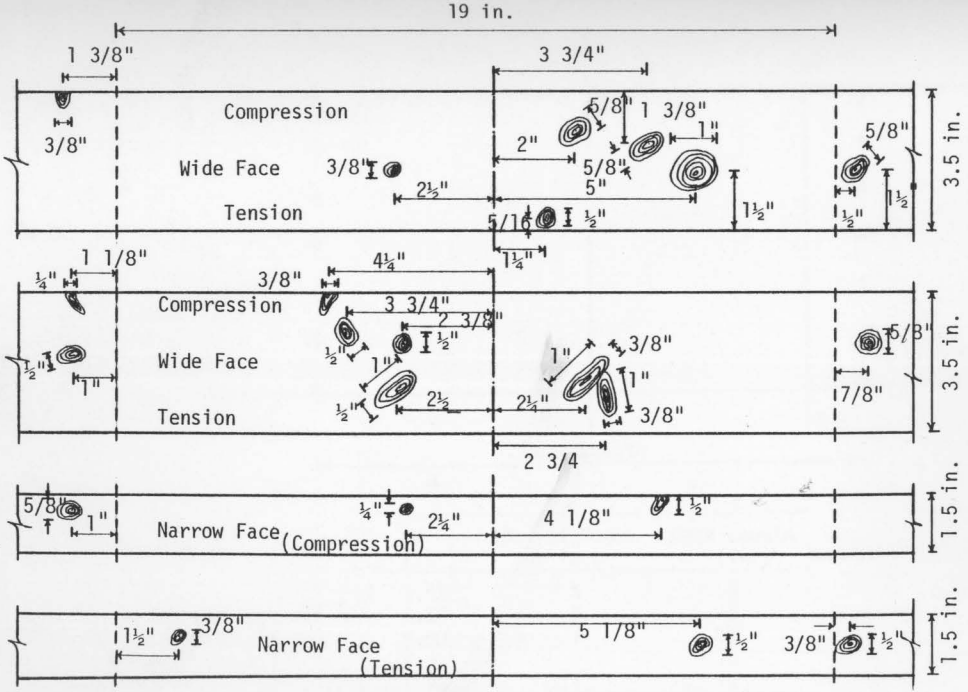

FIG. 4.3 MEASUREMENTS OF KNOTS IN A 2 x 4 BEAM SPECIMEN

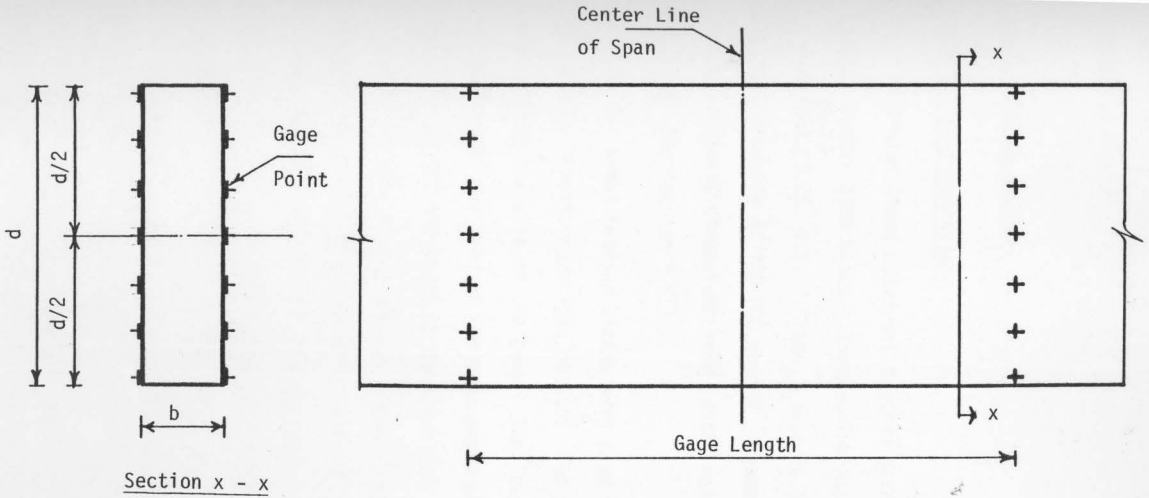

d (in.)	No. of Gages per face	Gage Length (in.)
1.65	5	4
3.50	5	6
5.50	7	10
7.30	7	10
11.30	11	10

FIG. 4.4 ARRANGEMENT OF GAGE-POINTS FOR MEASURING STRAINS IN BEAMS

radius of $17\frac{1}{2}$ inches. The detailed dimensions of a tension specimen are given in Fig. 4.5.

4.4 Bending Tests

4.4.1 Instrumentation

A Tinius Olsen universal testing machine was used for testing the actual lumber size beams. The machine has four speeds of movement of the cross-head (0.05, 0.3, 1.0 and 7 in./min.), and three load ranges with maximum capacity of 100,000 pounds. Beams having 1.50 X 1.65 inches cross-sectional dimensions were tested using an Instron universal testing machine (see section 4.5.1).

Steel metal bearing plates were used to prevent damage to the beams at support reactions and load points. The size of the bearing plate was varied with the size of the beam. The length of the bearing plate was approximately one half of the beam depth and its width was extended entirely across the width of the beam (2). Each beam was supported by fixed knife edge at one end and roller support at the other end. The load was applied perpendicular to the longitudinal axis of the beam using a cross-head of knife edge. In the case of third-point loading, the load was transferred to the beam through a steel I-beam which was supported on the beam by two rollers.

Deflections were measured at midspan and at load points, using dial gages indicated to the nearest 0.001 inch. The fiber strains were measured at the installed gage points by a mechanical gage with an adjustable gage length and read to the nearest 0.0001 inch.

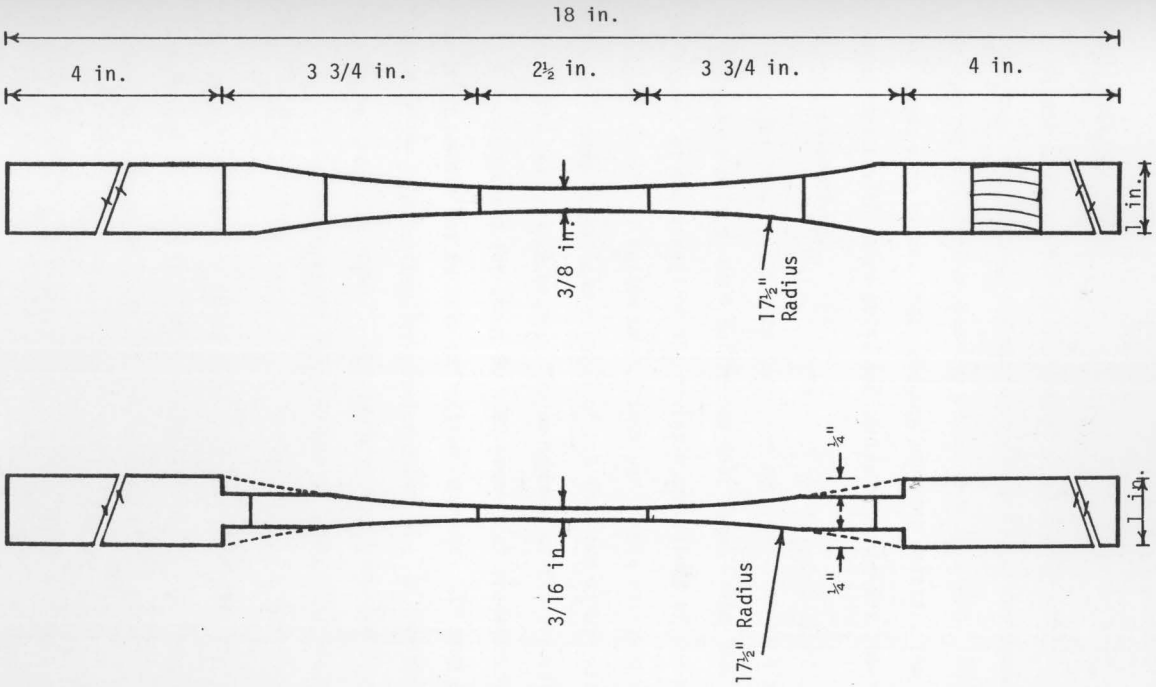

FIG. 4.5 DIMENSIONS OF TENSION PARALLEL TO GRAIN TEST SPECIMEN

4.4.2 Test Procedure

Actual cross-sectional dimensions of each beam were measured prior to testing. The beam was located symmetrically on the supports where load bearing and reaction bearing plates were in place. The deflection dial gages were placed under midspan and load points. The set-up for bending tests with third-point and central loading are shown in Figs. 4.6 and 4.7, respectively.

Initial reading, at zero load, was recorded from each strain gage on the beam and from each deflection dial gage. The load was applied vertically at two speeds of the moveable cross-head of the testing machine. A rate of motion of 0.1 inch per minute was used in testing the 1.65-inch deep beams, and a speed of 0.3 inch per minute was applied to the actual lumber size beams. The continuity of the gradual application of load was stopped for about 30 - 60 seconds at predetermined load levels to record strain and to take deflection readings. In some cases, it was necessary to stop loading for about another 30 - 60 seconds to readjust the deflection dial gages. The tests were carried until ultimate failure occurred. The maximum load was achieved in about 20 - 45 minutes for a beam test.

Immediately after the bending test was completed, at least three pieces were cut from the beam for determining the moisture content in the test specimen. Moisture content at test was obtained as:

$$\text{Moisture content (percent)} = \frac{\text{weight at test - oven-dried weight}}{\text{oven-dried weight}} \times 100$$

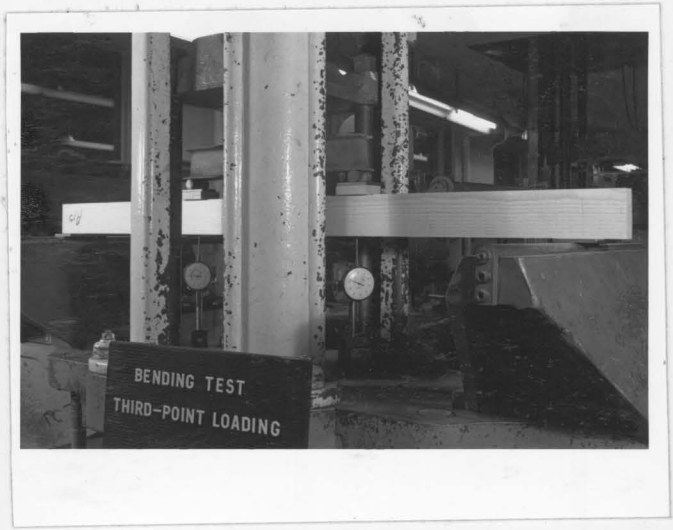

FIG. 4.6 SET-UP FOR BENDING TEST WITH THIRD-POINT LOADING

FIG. 4.7 SET-UP FOR BENDING TEST WITH CENTRAL LOADING

4.4.3 Type of Failure

It was observed that once the load had reached a value corresponding to the proportional limit as indicated by the load-deflection curve, there appeared a number of wrinkles in the extreme compression fibers. In the case of central loading, these wrinkles appeared near the point of application of load. For the third-point loading case, the wrinkles appeared first near the load points followed by other wrinkles throughout the central part of the beam. In the special group of stiffened beam, there was no sign of compression failure near the load points since the width of the beam at these points was three times the width of the critical section (see Fig. 4.2). The compression wrinkles appeared only throughout the length of the critical section (the minimum cross-section).

When the load exceeded the proportional limit, the wrinkles developed gradually further down into the compression zone. This process continued with increasing load until the final tension failure occurred. At this stage, the compression wrinkles developed up to 0.2 to 0.5 of the beam depth. In some cases, the tension failure was a splintering on the bottom of the beam. In other cases, the failure was a combination of a vertical crack (fracture across the bottom) and a horizontal crack running from the top of the vertical crack.

In the case of knotted beams, 47 beams (87% of the total number) failed similar to the clear beams. The failure followed a compression-tension sequence. The remainder, 7 beams, failed in tension without any compression failure. The knots and the associated cross-grain influenced the failure of the beams. Compression wrinkles formed through knots near

the compression edge, or detoured around the knots along the distorted grain. Tension failure was also started from a knot near the tension edge and, in most cases, the failure was associated with cross-grain tension. Typical failures in clear beams of 2 x 6 and knotted beams of 2 x 4 are shown in Figs. 4.8 to 4.11. Typical failure in beams of other sizes are shown in Figs. B.49 to B.58 (Appendix B).

4.5 Compression and Tension Tests

4.5.1 Instrumentation

Compression and tension tests were conducted on an Instron universal testing machine having a maximum load capacity of 10,000 kg. The X-Y plotter of the machine automatically recorded the load-deformation curve for each test specimen. Special gages were used in combination with an X-Y chart drive amplifier to measure deformations in the specimens. The gages were specially designed using metal foil electrical resistance strain gages bonded to beryllium cooper metal. The gage length was two inches and the deformations were measured on two faces of each specimen. The gage was calibrated using a Huggenberger portable calibrator having a least count of $\pm$ 0.01 mm. The relationship between the chart movement and the deformation was found to be linear and resulted in a strain of 0.00055 inch per inch for one centimeter of chart movement.

4.5.2 Compression Test Procedure

Dimensions of the compression specimens were measured to the nearest 0.001 inch. Before testing, each specimen was weighed and this weight

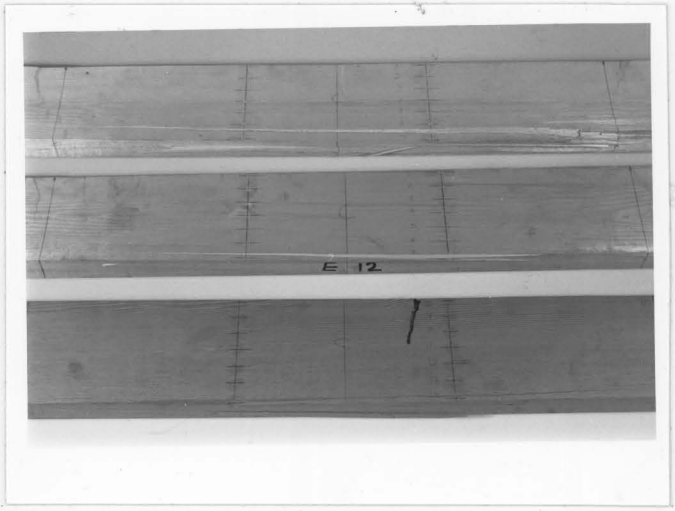

FIG. 4.8 TYPICAL FAILURE IN 2 x 6 CLEAR BEAMS SUBJECTED TO THIRD-POINT LOADING

FIG. 4.9 TYPICAL FAILURE IN 2 x 6 CLEAR BEAMS SUBJECTED TO CENTRAL LOADING

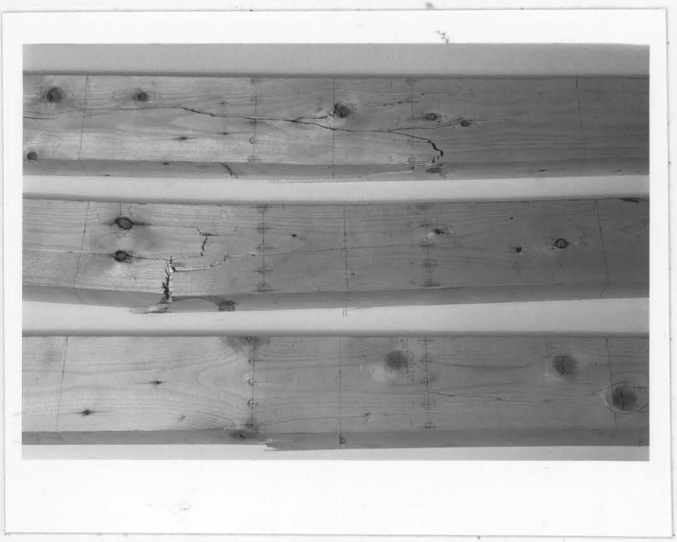

FIG. 4.10 TYPICAL FAILURE IN 2 x 4 KNOTTED BEAMS SUBJECTED TO THIRD-POINT LOADING

FIG. 4.11 TYPICAL FAILURE IN 2 x 4 KNOTTED BEAMS SUBJECTED TO CENTRAL LOADING

was recorded as initial weight which was used for determination of moisture content. The gages, for measuring deformations, were placed on two faces of the specimen as indicated in Fig. 4.12. A vertical load was applied through the geomteric centre of each specimen and parallel to its grain. Vertical load was obtained using loading plates at each end of the specimen as shown in Fig. 4.12. The load was applied gradually at a rate of motion of the moveable cross-head of 0.5 mm/min. The Compression test set-up is shown in Fig. 4.13.

The compression tests were carried well beyond the maximum load in order to get a complete history of the load-deformation curve. In most of the compression test specimens, crushing, shearing or wedge split failures were obtained. Figure 4.14 shows the types of failures obtained in compression specimens. After testing, the compression specimens were oven-dried at about 105^{o}C, and the final weights recorded. Moisture content at test for each specimen was obtained, and specific gravity was determined using the oven-dried weight and the volume at test.

4.5.3 Tension Test Procedure

Actual cross-sectional dimensions, at minimum section, of the tension specimens were measured to the nearest 0.001 inch. The gages, for measuring deformations, were placed on two faces of the central length of the specimen as shown in Fig. 4.15, and the specimen was fastened in special grips (Fig. 4.15). The parallel to grain load was applied continuously throughout the test at a rate of motion of the moveable cross-head of 1 mm/min. until failure occurred. Figure 4.16 shows a set-up for tension test, and typical failures in tension specimens are shown in Fig. 4.17.

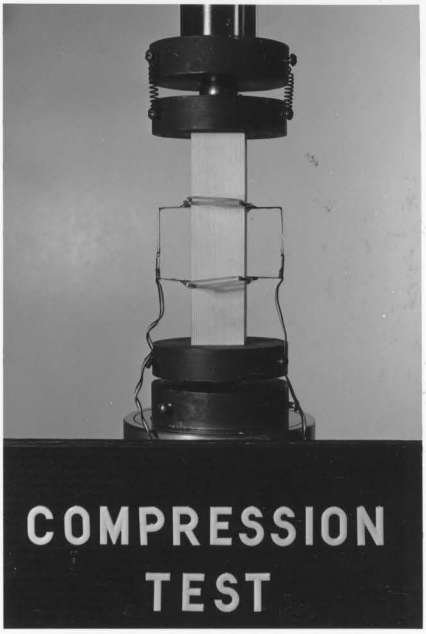

FIG. 4.12 LOCATION OF STRAIN GAGE IN COMPRESSION TEST

FIG. 4.13 COMPRESSION TEST SET-UP

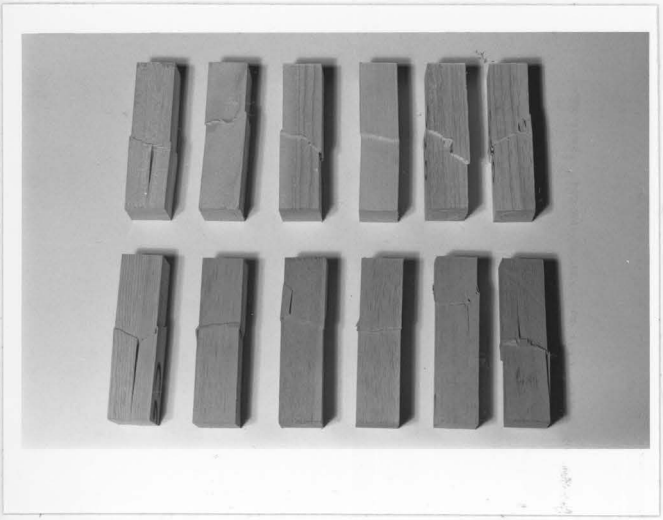

FIG. 4.14 TYPICAL FAILURE IN COMPRESSION SPECIMENS

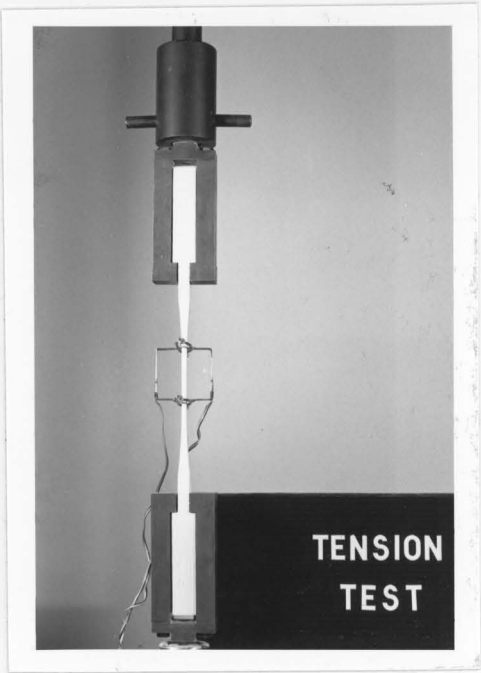

FIG. 4.15 LOCATION OF STRAIN GAGE IN TENSION TEST

FIG. 4.16 TENSION TEST SET-UP

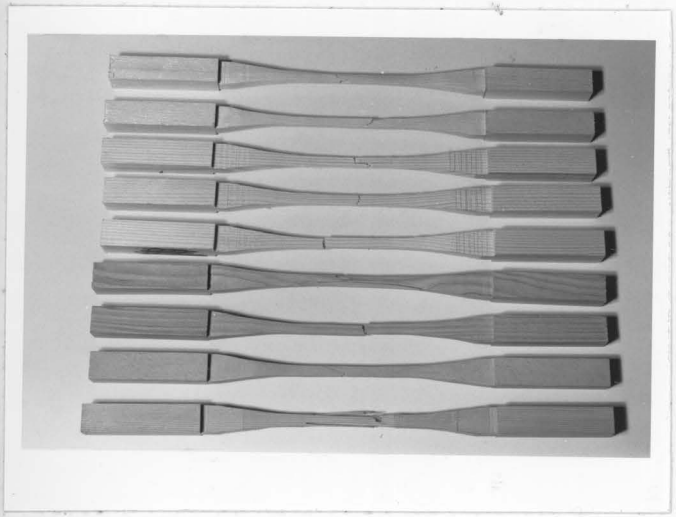

FIG. 4.17 TYPICAL FAILURE IN TENSION SPECIMENS

Moisture content of each tension specimen was determined by oven-dried method using a small piece which was obtained from the tension specimen immediately after testing.

CHAPTER 5

PRESENTATION OF MATERIAL PROPERTY TEST RESULTS

5.1 General

Ultimate compressive and tensile strengths of the beam material are obtained by conducting direct compression and tension tests on specimens matched with the beams as described in Chapter 4. Specific gravity of each beam is determined using oven-dried weight and volume at test of the matched compression specimens. To minimize any difference in moisture content between the beam test specimens and the matched compression and tension specimens, prior to test, all specimens of one group of beams and the corresponding compression and tension specimens were maintained together at the same moisture conditions (approximately 12 ± 1 %) for several weeks in a moisture control room. By adopting this procedure the strength properties obtained from direct compression and tension tests would represent directly the direct compressive and tensile strength of the corresponding beam specimens. Moisture contents at time of testing for each beam specimen and the matched compression and tension specimens were measured by oven-dried method (Chapter 4) and were found to be approximately the same. Since 4 x 12 beams could not be accommodated in the moisture control room, the moisture content values of the matched compression and tension specimens were about 4 to 5 percent smaller than the corresponding values for the beams. It was then necessary to adjust the compressive strength values of these specimens to values at the moisture content of the corresponding beams. But no adjustment was applied to the tensile

strength values as this property is not significantly affected by the moisture content variation encountered in this case (9,11,12).

Since the compression tests of this study were not suited for obtaining such relationship between the compressive strength and moisture content, a relationship between the two properties which was obtained by Malhotra (19) from test program on eastern spruce, was used to adjust the ultimate compressive strength values of compression specimens to values at the moisture content of the corresponding 4 x 12 beams. The relationship can be written in the form:

$$(F_{cu})_1 = (F_{cu})_2 \, e^{0.058\,(m_2 - m_1)} \qquad [5.1]$$

where

F_{cu} = Ultimate compressive strength;

and m = Moisture content in percent.

5.2 Test Results and Discussion

Load-deformation curve for each test specimen in compression or tension was automatically recorded on the X-Y plotter of the testing machine (Chapter 4). A typical stress-strain curve of compression test is shown in the top portion of Fig. 3.1 and a typical curve for tension test can be seen in the bottom portion of Fig. 3.1.

The values of specific gravity, mositure content, ultimate compressive strength and ultimate tensile strength of the material for each test beam are tabulated in Tables A.1.1 to A.1.20 (Appendix A). Each value listed in these tables is the average value of three or more test results.

The average values and the coefficients of variation of these properties for each group of beams are summarized in Tables 5.1 and 5.2.

To study the variation in the properties of the material used in the tests, the average values and the corresponding coefficients of variation of specific gravity, moisture content and compressive and tensile strengths for eastern spruce and Douglas-fir, are computed (Table 5.3). The ratios between the average values of tensile and compressive strengths of eastern spruce and Douglas-fir, respectively, are 2.43 and 2.14. The coefficient of variation of the tensile strength is greater than the corresponding value of compressive strength. The larger variability of tensile strength compared to compressive strength is probably due to that the tensile strength is quite sensitive to small deviation in the slope of grain in test specimens. Table 5.3 indicates that the variation in strength properties is greater in Douglas-fir than in eastern spruce. This more variability in strength properties of Douglas-fir is clearly due to the larger variation in specific gravity of the test specimens.

A statistical approach, as outlined in the following paragraph, is adopted to study the variation in strength properties of eastern spruce since the largest number of test specimens were obtained from this species. The average value of a group is a single value that typifies the whole group but does not generally give adequate information about the variability of observations within the group. This variability is a factor of significant importance to the code writers and designers and it is essential that they should have some means of taking it into account if they are to make a judicious and effective use of the material. Standard deviation, or coefficient of variation, and histogram are the most useful measures of variability. The histograms for compressive and tensile

TABLE 5.1: Summary of Material Property Test Results for Beams Subjected to Third-Point Loading

Beam Depth (in.)	Specific Gravity	Moisture Content (%)	Ultimate Compressive Strength of Matched Specimens (ksi)	Ultimate Tensile Strength of Matched Specimens (ksi)
		Clear Beams		
1.65(S)[a]	0.407[b] (6.5)	11.6 (1.2)	7.7 (12.2)	14.47 (13.3)
1.65(D)	0.482 (12.8)	11.8 (4.8)	8.64 (10.9)	15.41 (24.7)
3.50(S)	0.399 (6.2)	12.0 (1.5)	6.80 (7.5)	18.17 (16.2)
5.50(S)	0.404 (4.9)	12.4 (2.5)	6.29 (11.0)	15.65 (7.43)
5.50(D)	0.465 (13.5)	12.8 (4.3)	7.26 (18.0)	16.76 (28.2)
5.50(S) (Stiffened beams)	0.409 (8.3)	11.9 (4.7)	5.54 (14.7)	13.13 (19.7)
5.50(D) (Stiffened beams)	0.457 (2.7)	11.9 (3.1)	6.63 (9.0)	14.27 (10.0)
7.30(S)	0.399 (7.7)	12.5 (0.9)	6.04 (9.7)	15.02 (19.7)
11.30(S)	0.395 (3.8)	16.6 (7.4)	4.62 (8.8)	12.17 (16.0)
		Knotted Beams		
3.50(S)	0.415 (9.0)	11.9 (2.1)	6.19 (15.0)	15.89 (19.4)
5.50(S)	0.399 (11.7)	11.0 (4.0)	6.83 (10.5)	15.25 (16.6)

a: (S) and (D) refer to spruce and Douglas-fir lumber, respectively.

b: Values in first lines are averages and those in parentheses are coefficients of variation in percent.

TABLE 5.2: Summary of Material Property Test Results for Beams Subjected to Central Loading

Beam Depth (in.)	Specific Gravity	Moisture Content (%)	Ultimate Compressive Strength of Matched Specimens (ksi)	Ultimate Tensile Strength of Matched Specimens (ksi)
		Clear Beams		
1.65(S)[a]	0.407[b] (6.7)	11.6 (1.3)	7.28 (10.2)	15.64 (14.5)
1.65(D)	0.481 (12.8)	11.6 (3.0)	8.25 (15.6)	19.61 (28.7)
3.50(S)	0.399 (6.2)	13.0 (1.4)	6.40 (8.9)	16.93 (16.9)
5.50(S)	0.390 (6.0)	13.1 (1.0)	6.11 (12.0)	15.70 (13.8)
5.50(D)	0.490 (19.5)	12.3 (4.0)	8.17 (20.2)	17.31 (28.3)
7.30(S)	0.379 (7.3)	13.5 (1.1)	5.27 (9.4)	15.92 (15.2)
11.3(S)	0.377 (5.3)	18.4 (6.3)	3.87 (11.6)	10.97 (13.7)
		Knotted Beams		
3.50(S)	0.415 (9.0)	11.9 (2.1)	6.18 (13.3)	15.61 (19.2)
5.50(S)	0.422 (9.0)	10.7 (6.9)	7.18 (11.3)	16.24 (11.4)

a: (S) and (D) refer to spruce and Douglas-fir lumber, respectively.

b: Values in first lines are averages and those in parentheses are coefficients of variation in percent.

TABLE 5.3: Properties of Test Materials

Property	Eastern Spruce			Douglas-Fir		
	Average	Standard Deviation	Coefficient of Variation (%)	Average	Standard Deviation	Coefficient of Variation (%)
Specific gravity	0.402	0.031	7.8	0.475	0.061	12.8
Moisture content (%)	12.1	0.790	6.5	12.1	0.62	5.1
Ultimate compressive strength (ksi)	6.35	0.900	14.1	7.82	1.36	17.4
Ultimate tensile strength (ksi)	15.46	2.850	18.5	16.71	4.55	27.2

strengths of eastern spruce are shown in Figs. 5.1 and 5.2. The statistical normal distribution curves are also plotted onto these histograms. The general mathematical equation of the normal distribution curve is

$$y = \frac{1}{\sigma\sqrt{2\pi}} e^{-(\frac{1}{2\sigma^2})(x - \text{Mean})^2} \qquad [5.2]$$

where

y = Vertical ordinate of the curve at point x on the x - axis;

σ = Standard deviation;

and Mean = Arithmetic mean of observations

By using the normal distribution, it is possible to predict the percentage probability occurrence of observations falling within any range. Based on normal distribution, the predicted percentages of observations lying within ranges (Mean $\pm$ σ), (Mean $\pm$ 1.645 σ) and (Mean $\pm$ 2.33 σ), are given in Table 5.4. The percentages of the actual test results in these ranges are also given in Table 5.4. It can be seen that the theoretical predictions are in fairly close agreement with the experimental data. From Figs. 5.1 and 5.2 and Table 5.4, it can be concluded that, for the test results under consideration, the actual distributions are approximately normal.

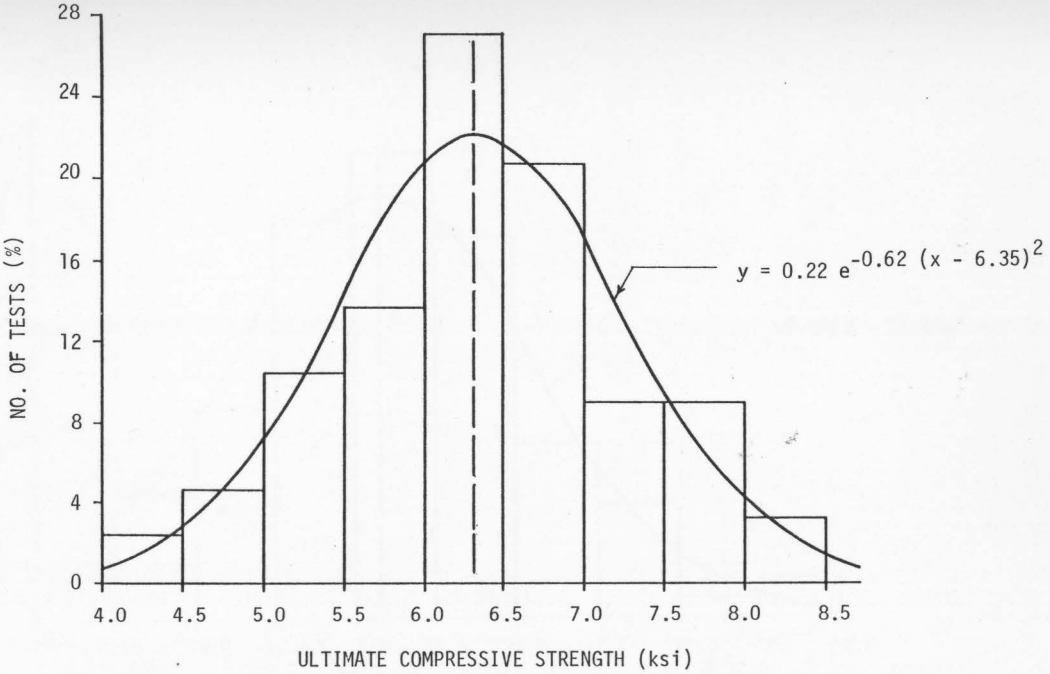

FIG. 5.1 HISTOGRAM AND NORMAL DISTRIBUTION CURVE OF ULTIMATE COMPRESSIVE STRENGTH OF EASTERN SPRUCE

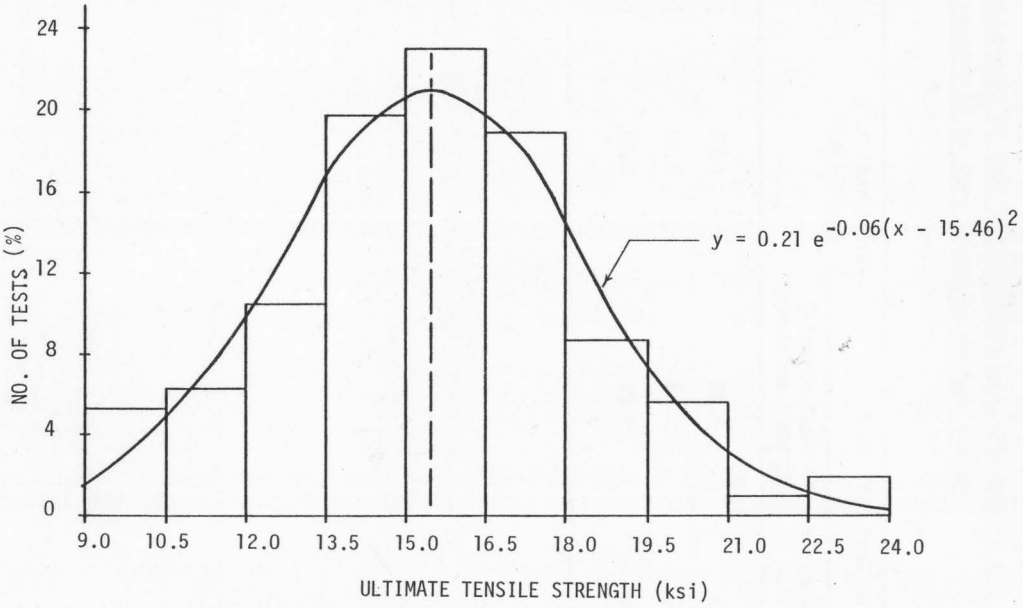

FIG. 5.2 HISTOGRAM AND NORMAL DISTRIBUTION CURVE OF ULTIMATE TENSILE STRENGTH OF EASTERN SPRUCE

TABLE 5.4: Percentages of Test Values of Ultimate Compressive and Tensile Strengths of Eastern Spruce in Various Ranges

Range	% of Theoretical Predictions	% of Test Results	
		Ultimate compressive Strength	Ultimate Tensile Strength
(Mean ± 1.000 σ)	68.2	68.1	71.1
(Mean ± 1.645 σ)	90.0	89.7	88.7
(Mean ± 2.330 σ)	98.0	99.5	98.1

CHAPTER 6

ANALYSIS OF CLEAR BEAM TEST RESULTS

6.1 Test Results and Discussion

Load-deflection curves, load-strain curves and diagrams representing strain distribution across beam depth are produced for each beam test. As an illustration, these diagrams for a 2 x 6 beam specimen subjected to both third-point and central loading are given in Figs. 6.1 to 6.6. Similar diagrams for each group of beams are presented in Figs. B.1 to B.42 (Appendix B). By using these diagrams, the following results are computed for each beam:

1. Moduli of elasticity in tension and compression, E_t and E_c. These values are computed from the load-strain curves of the extreme tension and compression fibers.
2. Extreme fiber stress at the proportional limit, F_{pl}, as indicated by the load-deflection curve

$$\left(F_{pl} = \frac{\text{Bending moment at proportional limit}}{\text{Section modulus}}\right)$$

3. Maximum tensile and compressive strains at the proportional limit.
4. Position of the neutral axis at the proportional limit and at the ultimate load.
5. Ultimate bending moment, M_u.
6. Maximum tensile strain at ultimate load, ε_t.
7. Maximum tensile stress at ultimate load, $F_t = E_t \times \varepsilon_t$.

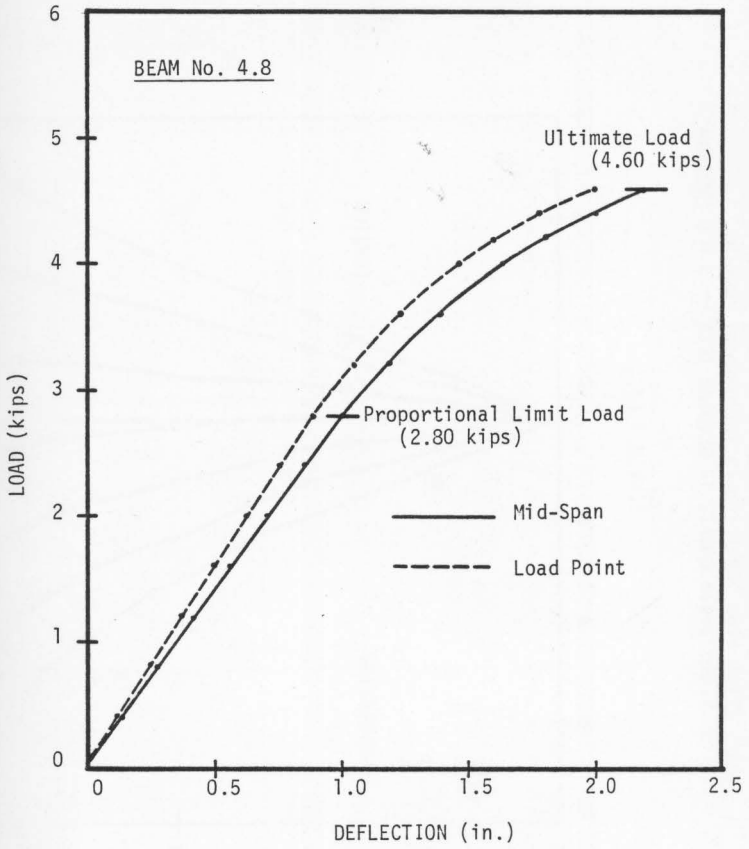

FIG. 6.1 TYPICAL LOAD-DEFLECTION CURVES IN BENDING TEST -- 2 x 6 EASTERN SPRUCE CLEAR BEAM SUBJECTED TO THIRD-POINT LOADING

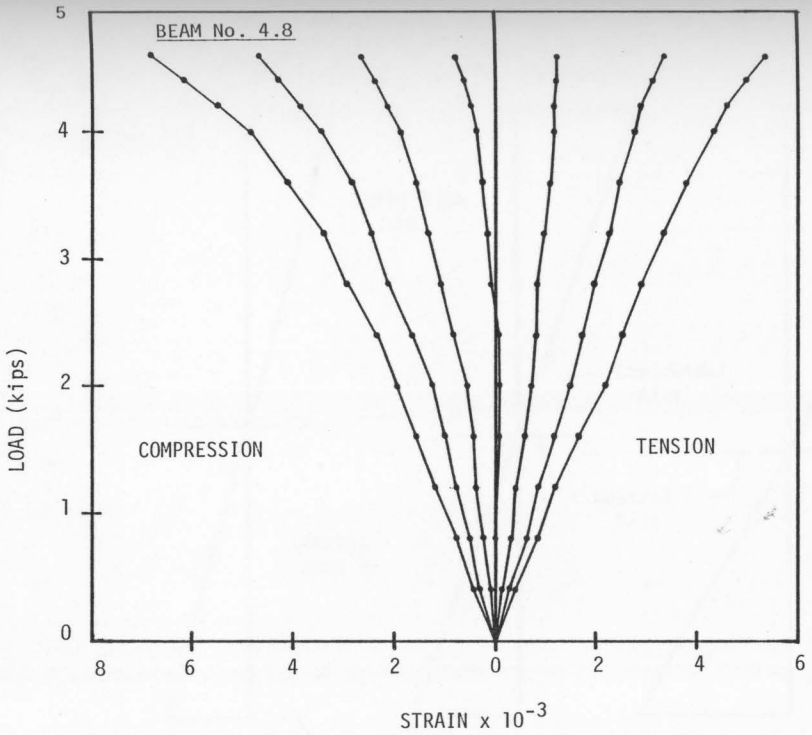

FIG. 6.2 TYPICAL LOAD-STRAIN CURVES IN BENDING TEST -- 2 x 6 EASTERN SPRUCE CLEAR BEAM SUBJECTED TO THIRD-POINT LOADING

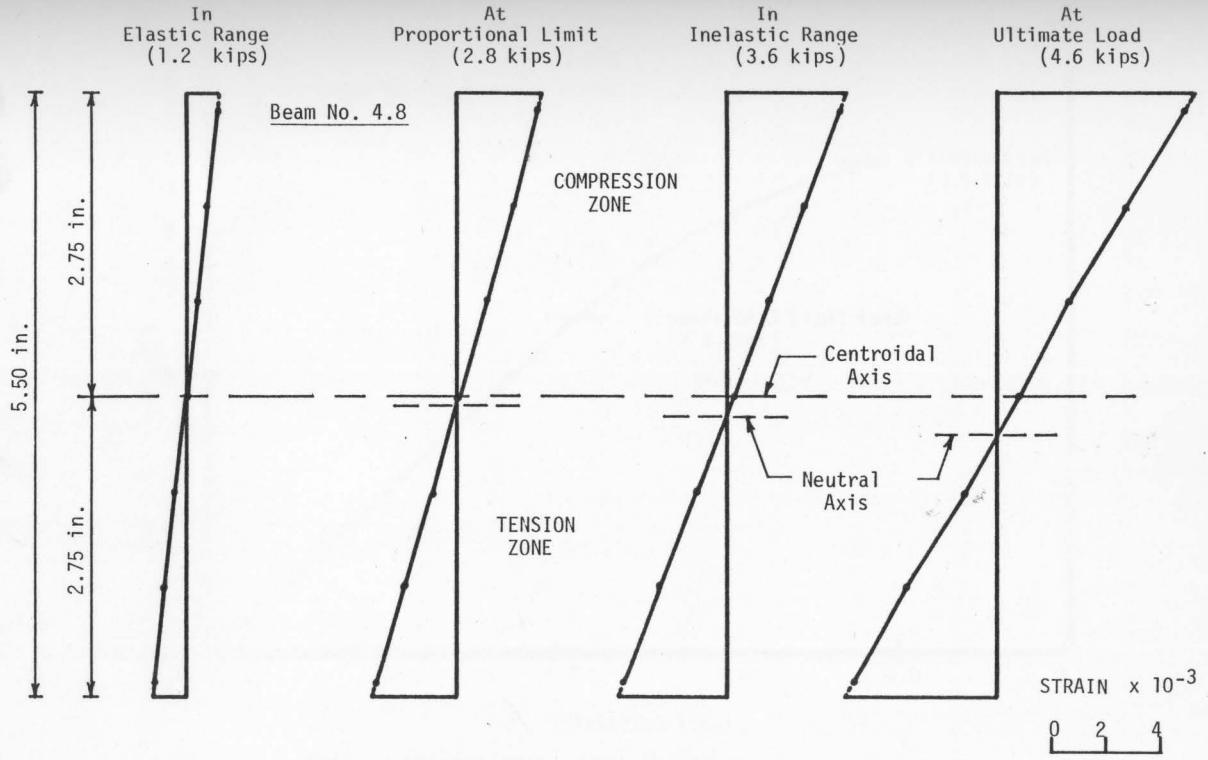

FIG. 6.3 TYPICAL STRAIN DISTRIBUTIONS IN BENDING TEST--2 x 6 EASTERN SPRUCE CLEAR BEAM SUBJECTED TO THIRD-POINT LOADING

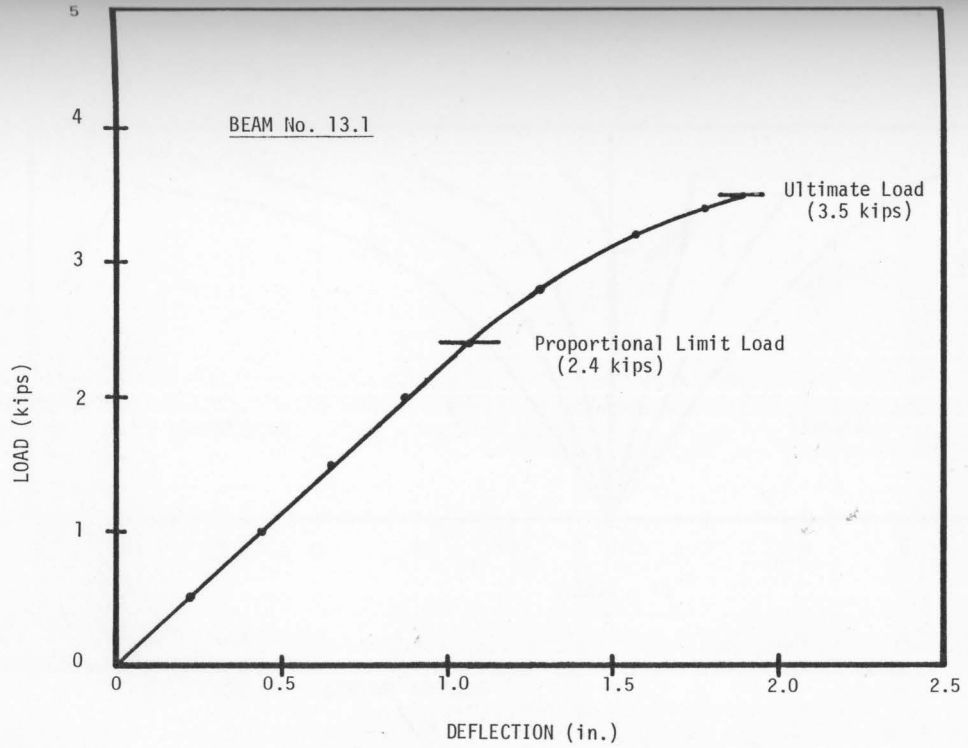

FIG. 6.4 TYPICAL LOAD-DEFLECTION CURVE IN BENDING TEST -- 2 x 6 EASTERN SPRUCE CLEAR BEAM SUBJECTED TO CENTRAL LOADING

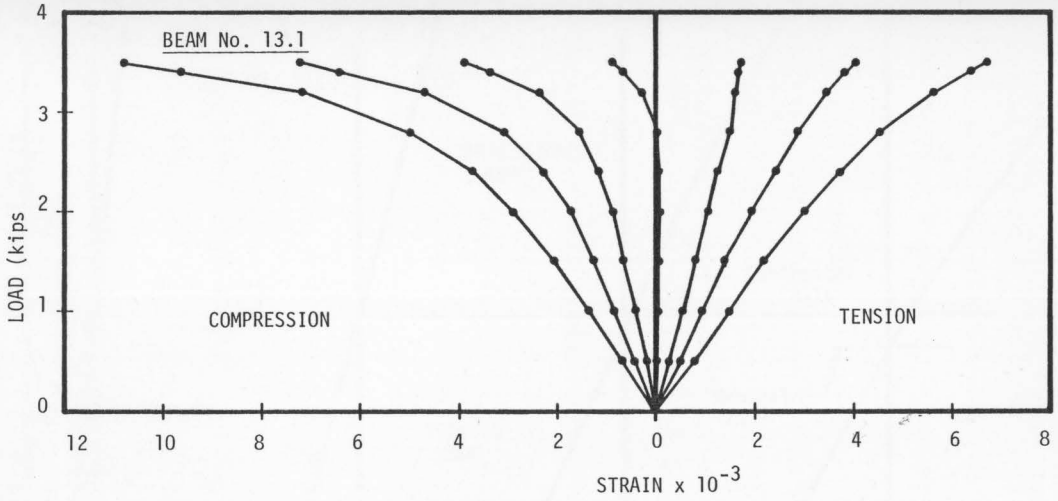

FIG. 6.5 TYPICAL LOAD-STRAIN CURVES IN BENDING TEST -- 2 x 6 EASTERN SPRUCE CLEAR BEAM SUBJECTED TO CENTRAL LOADING

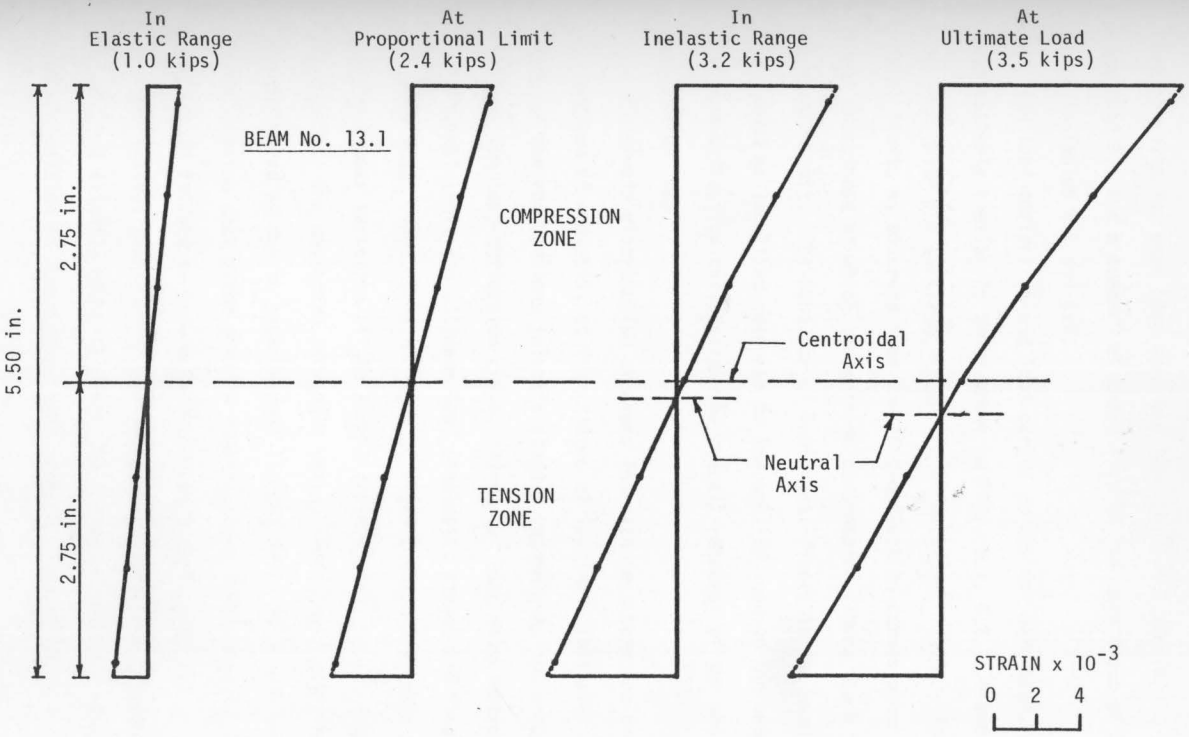

FIG. 6.6 TYPICAL STRAIN DISTRIBUTIONS ACROSS BEAM DEPTH IN BENDING TEST -- 2 x 6 EASTERN SPRUCE CLEAR BEAM SUBJECTED TO CENTRAL LOADING

These results for each test beam are tabulated in Tables A.2.1 to A.2.16 (Appendix A), and a summary of these results for each group of beams is given in Tables 6.1 and 6.2.

The load-deflection and load-strain curves for each beam, which are qualitatively similar to those shown in Figs. 6.1, 6.2, 6.4 and 6.5, show that the beams are stressed beyond the proportional limits. The proportional limits as observed from the load-deflection curves occur, at higher loads than those at which the extreme compression fibers reach their proportional limit. The behavior of individual fibers in the beam could be considered as localized response to the applied load on the beam while the load-deflection curve gives the overall response of the whole beam to the applied load.

The strain distribution diagrams for each test beam are drawn, for the purpose of analysis, at four stages of loading. Initially at a small value of the applied load (elastic stage), secondly at the proportional limit of the load-deflection curve, thirdly at load value between the proportional limit and ultimate load (inelastic stage) and finally at the ultimate load. These strain diagrams, Figs. 6.3 and 6.6, show a satisfactory linear variation of the strain distributions in all four stages of loading. The deviation of strain values from linear distribution may be considered as due to experimental limitations. Thus, the validity of the assumption that plane section remains plane during bending of timber beams up to failure is proven by the present test results.

The initial position of the neutral axis (when small load is applied) is slightly above or below the center of the beam depth. The initial position of the neutral axis probably depends on the relative

TABLE 6.1: Summary of Clear Beam Test Results -- Third-point Loading

Beam Depth (in.)	Compressive Modulus of Elasticity E_c ($X10^3$ksi)	Tensile Modulus of Elasticity E_t ($X10^3$ksi)	At Proportional Limit Load: Stress F_{pl} (ksi)	Maximum Compressive Strain ($X10^{-3}$)	Maximum Tensile Strain ($X10^{-3}$)	N.A. Position Factor from Bottom of Beam	At Ultimate Load: Ultimate Bending Moment M_u (in-k)	Maximum Tensile Strain ε_t ($X10^{-3}$)	Maximum Tensile Stress F_t (ksi)	N.A. Position Factor from Bottom of Beam γ
1.65(S)[a]	1.77[b] (13.0)	1.84 (12.7)	7.20 (12.1)	4.10 (9.8)	3.94 (14.2)	0.490 (3.2)	7.30 (12.1)	6.98 (19.3)	12.65 (14.8)	0.437 (5.5)
1.65(D)	2.04 (21.0)	2.08 (19.7)	8.94 (18.8)	4.60 (10.5)	4.28 (8.1)	0.480 (3.8)	8.51 (22.4)	6.90 (14.1)	14.46 (29.0)	0.445 (5.2)
3.50(S)	2.00 (11.0)	2.00 (11.5)	7.23 (10.6)	3.67 (8.5)	3.64 (10.6)	0.492 (3.0)	33.42 (8.1)	7.38 (16.0)	14.57 (14.2)	0.411 (2.4)
5.50(S)	1.88 (12.3)	1.92 (15.0)	6.29 (9.9)	3.40 (8.4)	3.29 (10.9)	0.489 (2.9)	70.80 (7.5)	5.98 (16.8)	11.31 (13.6)	0.437 (6.1)
5.50(D)	1.93 (20.6)	2.04 (19.9)	7.24 (21.6)	3.82 (12.6)	3.55 (11.3)	0.480 (4.7)	77.25 (21.3)	5.98 (23.0)	12.18 (31.9)	0.437 (7.2)
5.50(S) (Stiffened Beams)	1.62 (16.9)	1.65 (16.1)	5.74 (16.7)	3.71 (13.8)	3.49 (12.9)	0.498 (1.1)	61.48 (16.7)	6.06 (15.7)	9.97 (19.5)	0.438 (6.3)

TABLE 6.1 (Cont'd.)

Beam Depth (in.)	Compressive Modulus of Elasticity E_c ($X10^3$ksi)	Tensile Modulus of Elasticity E_t ($X10^3$ksi)	At Proportional Limit Load: Stress F_{pl} (ksi)	At Proportional Limit Load: Maximum Compressive Strain ($X10^{-3}$)	At Proportional Limit Load: Maximum Tensile Strain ($X10^{-3}$)	At Proportional Limit Load: N.A. Position Factor from Bottom of Beam	At Ultimate Load: Ultimate Bending Moment M_u (in-k)	At Ultimate Load: Maximum Tensile Strain ε_t ($X10^{-3}$)	At Ultimate Load: Maximum Tensile Stress F_t (ksi)	At Ultimate Load: N.A. Position Factor from Bottom of Beam γ
5.50(D) (Stiffened Beams)	1.97 (11.7)	1.99 (14.7)	6.87 (10.7)	3.61 (4.5)	3.48 (9.1)	0.495 (1.2)	72.00 (9.9)	5.60 (13.1)	11.06 14.5)	0.454 (4.0)
7.30(S)	1.96 (17.3)	2.04 (13.9)	6.13 (11.4)	3.25 (14.8)	3.05 (10.3)	0.489 (3.7)	113.67 (12.8)	4.90 (21.4)	9.96 (24.4)	0.443 (5.3)
11.30(S)	1.51 (11.7)	1.90 (11.5)	4.63 (11.5)	2.89 (16.7)	2.44 (9.4)	0.463 (3.6)	471.30 (12.9)	3.78 (17.6)	7.14 (17.6)	0.425 (8.3)

a: (S) and (D) refer to spruce and Douglas-fir lumber, respectively.

b: Value in first lines are averages and those in parentheses are coefficients of variation in percent.

TABLE 6.2: Summary of Clear Beam Test Results -- Central Loading

Beam Depth (in.)	Compressive Modulus of Elasticity E_c ($X10^3$ksi)	Tensile Modulus of Elasticity E_t ($X10^3$ksi)	At Proportional Limit Load: Stress F_{pl} (ksi)	At Proportional Limit Load: Maximum Compressive Strain ($X10^{-3}$)	At Proportional Limit Load: Maximum Tensile Strain ($X10^{-3}$)	At Proportional Limit Load: N.A. Position Factor from Bottom of Beam	At Ultimate Load: Ultimate Bending Moment M_u (in-k)	At Ultimate Load: Maximum Tensile Strain ε_t ($X10^{-3}$)	At Ultimate Load: Maximum Tensile Stress F_t (ksi)	At Ultimate Load: N.A. Position Factor from Bottom of Beam γ
1.65(S)[a]	1.87[b] (15.0)	1.87 (15.9)	7.94 (13.9)	4.52 (9.8)	4.32 (10.1)	0.506 (2.1)	7.66 (13.5)	7.74 (16.1)	14.44 (20.0)	0.441 (6.5)
1.65(D)	2.07 (20.0)	2.13 (21.8)	9.40 (19.9)	5.06 (13.7)	4.48 (11.5)	0.496 (2.6)	9.43 (21.1)	9.02 (14.4)	19.33 (30.0)	0.411 (10.1)
3.50(S)	1.81 (12.2)	1.95 (14.8)	7.33 (8.6)	4.86 (11.6)	3.82 (13.0)	0.502 (2.5)	31.96 (9.5)	7.81 (18.3)	15.15 (19.7)	0.397 (9.7)
5.50(S)	1.69 (15.3)	1.83 (15.9)	6.50 (11.1)	4.23 (11.1)	3.64 (13.1)	0.492 (4.5)	70.82 (12.1)	7.06 (13.8)	12.66 (18.9)	0.415 (8.3)
5.50(D)	2.20 (31.6)	2.23 (29.0)	9.19 (25.6)	4.53 (18.4)	4.21 (13.0)	0.502 (5.5)	91.13 (24.8)	6.66 (21.2)	14.71 (33.0)	0.440 (9.7)
7.30(S)	1.80 (12.4)	2.03 (14.5)	5.79 (8.0)	3.94 (13.5)	2.87 (13.2)	0.490 (2.4)	115.0 (11.9)	5.80 (17.2)	11.74 (21.6)	0.409 (9.0)
11.30(S)	1.20 (22.7)	1.44 (22.5)	4.24 (14.9)	4.02 (19.5)	3.00 (17.4)	0.500 (0.0)	434.25 (13.8)	5.22 (27.8)	7.22 (18.6)	0.413 (11.6)

a: (S) and (D) refer to spruce and Douglas-fir lumber, respectively.

b: Value in first lines are averages and those in parentheses are coefficients of variation in percent.

strength of the tension and compression fibers in the beam. At the proportional limit, the position of the neutral axis, in some cases, is the same as the initial position. But in other cases, the neutral axis shifts slightly towards the tension side of the beam by amount varying up to two percent of the depth. It can be concluded that, up to the proportional limit, the neutral axis is approximately at the center of depth. Beyond the proportional limit, the neutral axis gradually moves downwards rapidly and at ultimate load the movement of the neutral axis varies from about five to fifteen percent of the beam depth.

Tables 6.1 and 6.2 indicate that at the proportional limit, the maximum compressive strain is slightly greater than the maximum tensile strain. The average value of maximum compressive strain is about fifteen percent greater than the average value of maximum tensile strain. The larger difference between the two values is for the cases where the moisture content of the beams is relatively high. Tables 6.1 and 6.2 also show that the moduli of elasticity in tension and compression are not significantly different. The modulus of elasticity in tension is about six percent higher than the value in compression. The larger difference between the two values is observed in beams with higher moisture content.

The test results show that, up to the proportional limit as indicated by the load-deflection curve, the strain distribution is approximately a straight line passing close to the center of depth. Thus, the stress distribution up to this stage of loading (proportional limit) is very nearly a straight line passing through the center of depth, that is, the stresses in the fibers are proportional to their distance from the neutral axis and to the load on the beam. Further increase in load on

the beam is accompanied by a redistribution of stresses as a result of the development of compression wrinkles and consequently the downward movement of the neutral axis.

The behavior of the wood fibers at different points across the depth of beam in the inelastic stage of loading can be analyzed by dividing the fibers into three groups. The first is the fibers near the compression edge of the beam. The second is the fibers near the tension edge of the beam and the third is the fibers close to the center of depth.

It is observed that, at a load corresponding to the proportional limit, compression failure occurs initially at the extreme fibers. Further loading of the beam beyond this point causes these fibers to lose some of their capacity to sustain stress. This is revealed by the stress-strain curve of axial compression test (Fig. 3.1). As a result, there is a redistribution of stresses along the beam depth and the adjacent fibers, at this stage, are subjected to greater stresses. This may not be revealed by the load-strain curve of these fibers (Figs. 6.2 and 6.3), since the actual stress is not now proportional to the load on the beam as a result of the redistribution of stresses.

The load-strain curves of the fibers near the tension edge of the beam, Figs. 6.2 and 6.5, indicate a non-linear relationship between the load and strain in the inelastic stage of loading; whereas, when wood is stressed in direct tension, the relationship between load and strain is almost linear up to failure (Fig. 3.1). An explanation for this behavior is that, as a result of the downward movement of the neutral axis and the redistribution of compressive stresses, the tension fibers are subjected

to relatively increased stresses in order to maintain equilibrium of the beam. These relatively increased tension stresses are no longer proportional to the load on the beam. Although, the load-strain curve for tension fibers is not linear in the inelastic stage, the relationship between actual tensile stresses and strains of these fibers may still be a straight line up to the ultimate load on the beam. As the neutral axis moves progressively towards the tension side, fibers just above the center of depth are subjected to increasing strains while those just below the center of depth are subjected to somewhat reducing values. The fibers close to the center of depth originally strained in tension are later strained in compression. This can be seen from the load-strain curves of these fibers, Figs. 6.2 and 6.5, where the curve turned "backwards".

The results (see Table 7.1 of Chapter 7) show that the proportional limit stress in bending is not significantly affected by the depth of beam. For beams subjected to third-point loading, the proportional limit stress is equal to the ultimate compressive strength of the beam material as obtained from direct tests. But for beams subjected to central loading, the proportional limit stress in bending is about eleven percent greater than the ultimate strength in direct compression tests. For practical purposes, it can be assumed that the proportional limit stress in bending is equal to the ultimate compressive strength of the beam material as obtained from direct tests.

The test results (Table 7.1) also show that the maximum tensile stress in the beam at failure is statistically smaller than the ultimate strength in direct tension tests. The actual value is dependent on the

beam depth and is proportionally smaller as the depth of beam is increased.

Based on the test results of this study, it can be concluded that the assumptions made in the proposed theory (Chapter 3) for bending behavior of timber beams are quite valid.

6.2 Comparison Between Theory and Test Results

In order to compare the proposed theory with the experimental results, Figs. 6.7 and 6.8 are presented. In Fig. 6.7, a theoretical curve, based on Eq. [3.18], of the relationship between ratio $\frac{M_u}{F_{cu}\frac{bd^2}{6}}$ and ratio $\frac{F_t}{F_{cu}}$, is shown. Experimental results for individual beam tests are also plotted on this graph. A theoretical curve, based on Eq. [3.20], of the relationship between the neutral axis position factor, γ, and ratio $\frac{F_t}{F_{cu}}$, together with the results of beam tests are given in Fig. 6.8. For comparison purposes, theoretical curves (curve 1) based on Eqs. [2.4] and [2.8] and test data by Comben (9) and Ramos (33) are also plotted on the graphs.

Figures 6.9 and 6.10 show the frequency distributions of the percentage difference between the theoretical predictions of M_u and γ, and the experimental values. The first distribution, Fig. 6.9, is for the percentage difference between the theoretical and experimental values of the ultimate bending moment, M_u. Figure 6.9 shows the following:

a) 35.0 percent of all test results are within ± 3 percent of theoretical predictions.

b) 67.0 percent of all test results are within ± 6 percent of theoretical predictions.

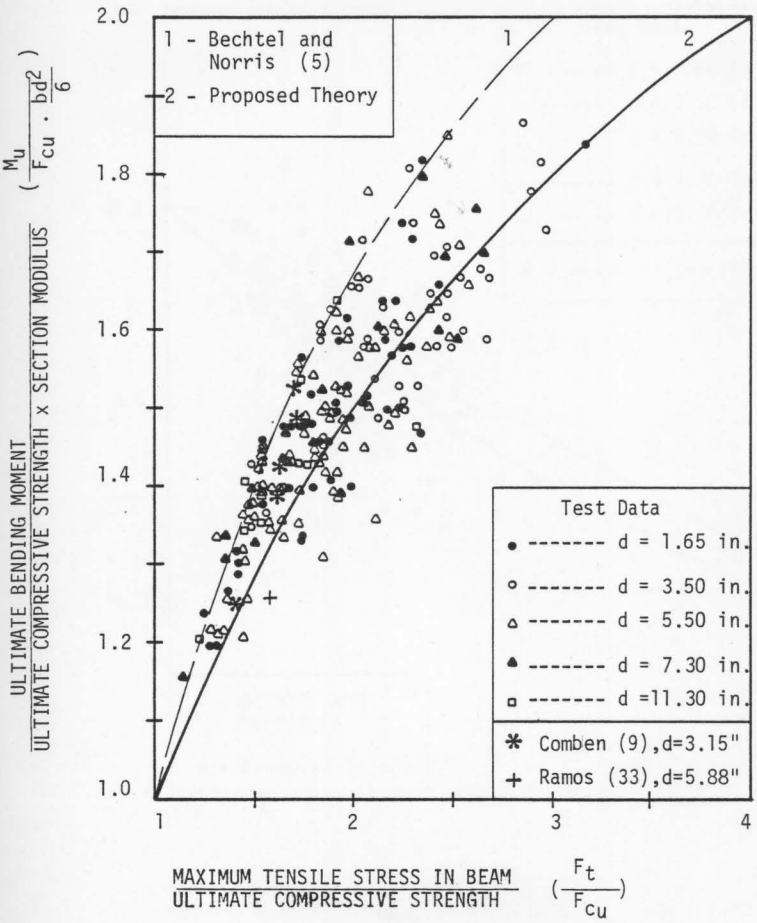

FIG. 6.7 COMPARISON BETWEEN THEORETICAL PREDICTIONS OF ULTIMATE BENDING MOMENT AND TEST RESULTS OF CLEAR BEAMS

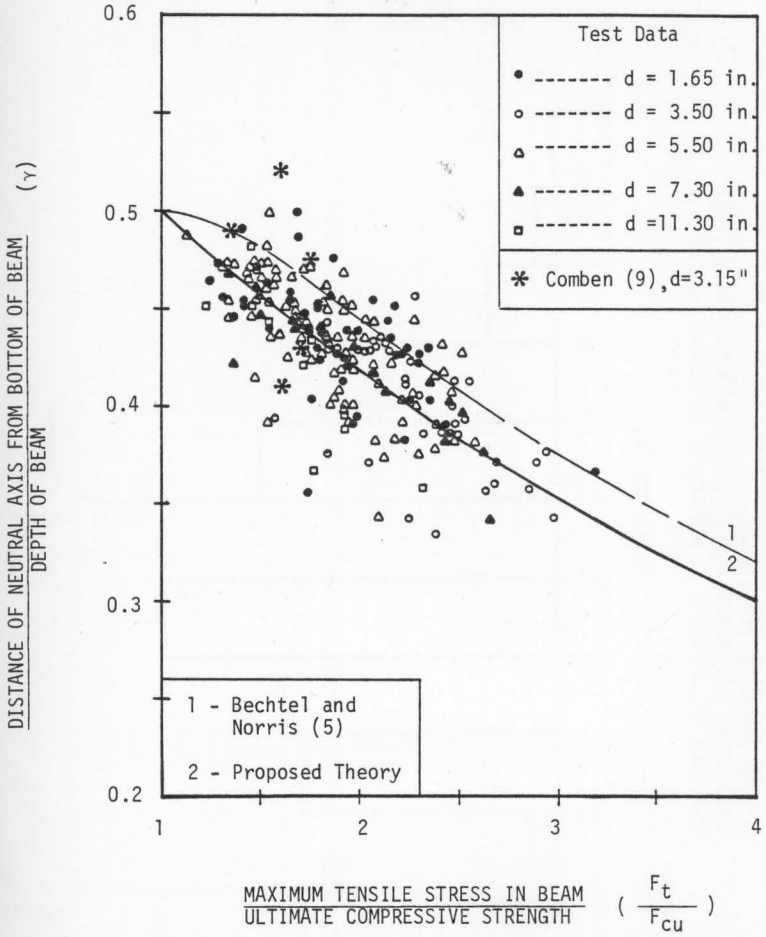

FIG. 6.8 LOCATION OF NEUTRAL AXIS - COMPARISON BETWEEN THEORY AND TEST RESULTS OF CLEAR BEAMS

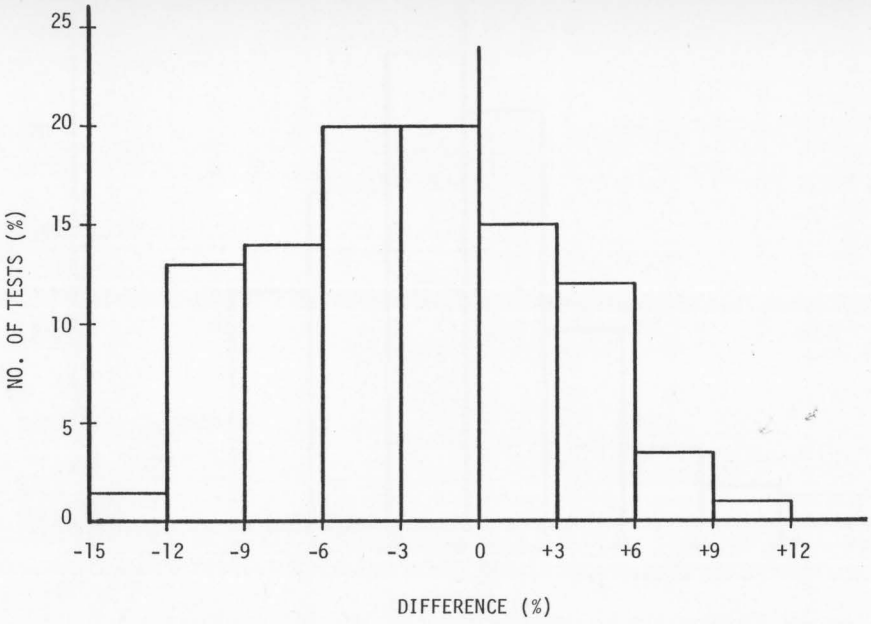

FIG. 6.9 FREQUENCY DISTRIBUTION OF PERCENTAGE DIFFERENCE BETWEEN THEORETICAL PREDICTIONS AND EXPERIMENTAL VALUES OF ULTIMATE BENDING MOMENT OF CLEAR BEAMS

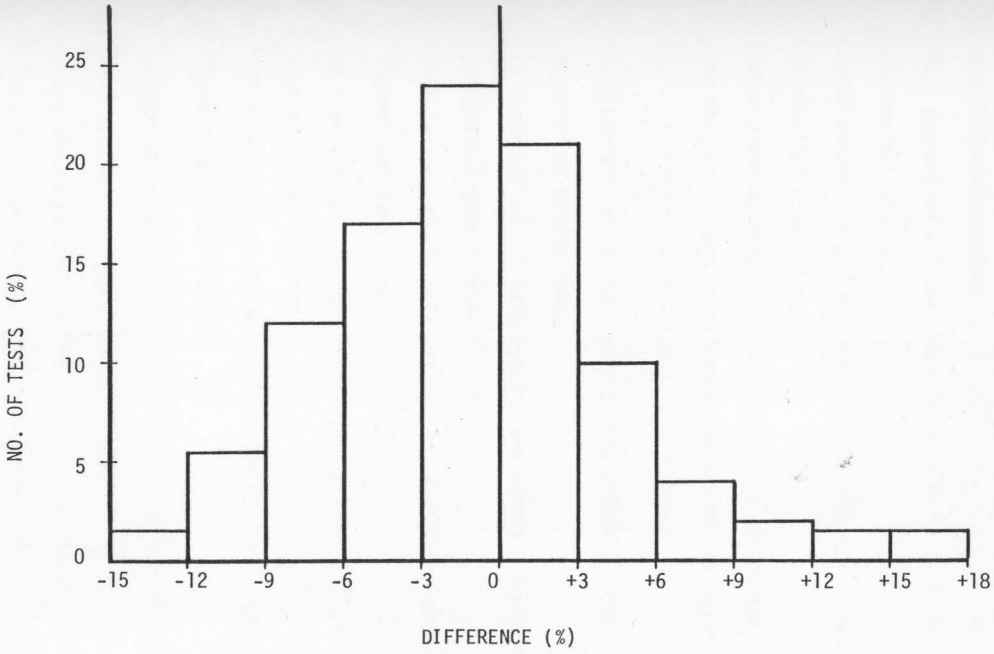

FIG. 6.10 FREQUENCY DISTRIBUTION OF PERCENTAGE DIFFERENCE BETWEEN THEORETICAL PREDICITONS AND EXPERIMENTAL VALUES OF NEUTRAL AXIS POSITION FACTOR OF CLEAR BEAMS

c) 84.5 percent of all test results are within ± 9 percent of theoretical predictions.

d) 98.5 percent of all test results are within ± 12 percent of theoretical predictions.

e) 100.0 percent of all test results are within ± 15 percent of theoretical predictions.

The second distribution, Fig.6.10, is for the percentage difference between the theoretical and experimental values of the neutral axis position factor, γ. In this case, the trend is as follows:

a) 45.0 percent of all test results are within ± 3 percent of theoretical predictions.

b) 72.0 percent of all test results are within ± 6 percent of theoretical predictions.

c) 88.0 percent of all test results are within ± 9 percent of theoretical predictions.

d) 98.5 percent of all test results are within ± 15 percent of theoretical predictions.

e) 100.0 percent of all test results are within ± 18 percent of theoretical predictions.

Comparison of the results shown in Figs. 6.6 to 6.10 indicates good agreement between the theory and test data. In practical application, the thoery should predict the ultimate bending moment of a beam using the ultimate tensile strength of the beam material as obtained from direct tension tests on small representative specimens. This necessitates that the effect of beam size on maximum tensile stress in the beam at

failure, in relation to the ultimate tensile strength in direct tests, must be determined. This issue of the size effect is investigated in the following chapter.

CHAPTER 7

EFFECTS OF BEAM SIZE AND METHOD OF LOADING ON STRESSES IN BEAMS

The proportional limit stress in bending and maximum tensile stress at failure in individual beams are compared with the ultimate compressive and tensile strengths of the beam material as obtained from direct tests on small specimens. Table 7.1 and Figs. 7.1 to 7.4 present a summary of the proportional limit stress and maximum tensile stress at failure in beams, expressed as ratios of the ultimate compressive and tensile strengths of the beam material, F_{pl}/F_{cu} and F_t/F_{tu}.

7.1 Effects of Beam Size and Method of Loading on Proportional Limit Stress in Bending

The results in Table 7.1 and Figs. 7.1 and 7.2 show that the average values of F_{pl}/F_{cu}, for the same method of loading, are virtually the same for beams of all depths. Thus, the proportional limit stress in bending is not significantly affected by depth of beams. However, for centrally loaded beams, the average value of F_{pl}/F_{cu} for all depths, is about eleven percent greater than the corresponding value for similar beams with third-point loading. An explanation of this difference due to method of loading can be offered by applying the statistical strength theory (6). For the beam with third-point loading, the maximum moment occurs a third of the span. In the case of centrally loaded beam, the maximum moment occurs theoretically at midspan; or in practice it may be assumed to

TABLE 7.1: Proportional Limit Stress in Bending and Maximum Tensile Stress in Clear Beams Expressed as Ratios of Ultimate Compressive and Tensile Strengths of Beam Material

Beam Depth (in.)	Proportional limit stress in Bending / Ultimate Compressive Strength ($\frac{F_{pl}}{F_{cu}}$)					Maximum Tensile Stress in Beams / Ultimate Tensile Strength ($\frac{F_t}{F_{tu}}$)				
	Central Loading		Third-point Loading		Ratio Between Central & Third-point Loading	Central Loading		Third-point Loading		Ratio Between Central & Third-point Loading
	Average	Coefficient of Variation (%)	Average	Coefficient of Variation (%)	(6) = (2)/(4)	Average	Coefficient of Variation (%)	Average	Coefficient of Variation (%)	(11) = (7)/(9)
(1)	(2)	(3)	(4)	(5)		(7)	(8)	(9)	(10)	
1.65	1.10	7.5	1.01	8.8	1.09	0.95	12.8	0.90	8.0	1.06
3.50	1.16	9.3	1.00	10.7	1.16	0.90	14.4	0.81	16.8	1.10
5.50	1.08	9.6	1.00	10.7	1.08	0.82	12.1	0.73	13.2	1.13
5.50[a]	-	-	1.04	4.2	-	-	-	0.77	11.3	-
7.30	1.11	11.1	1.01	6.8	1.10	0.74	15.2	0.66	13.3	1.12
11.30	1.09	5.09	0.98	2.6	1.11	0.66	10.8	0.59	13.9	1.12

a: Stiffened Beams.

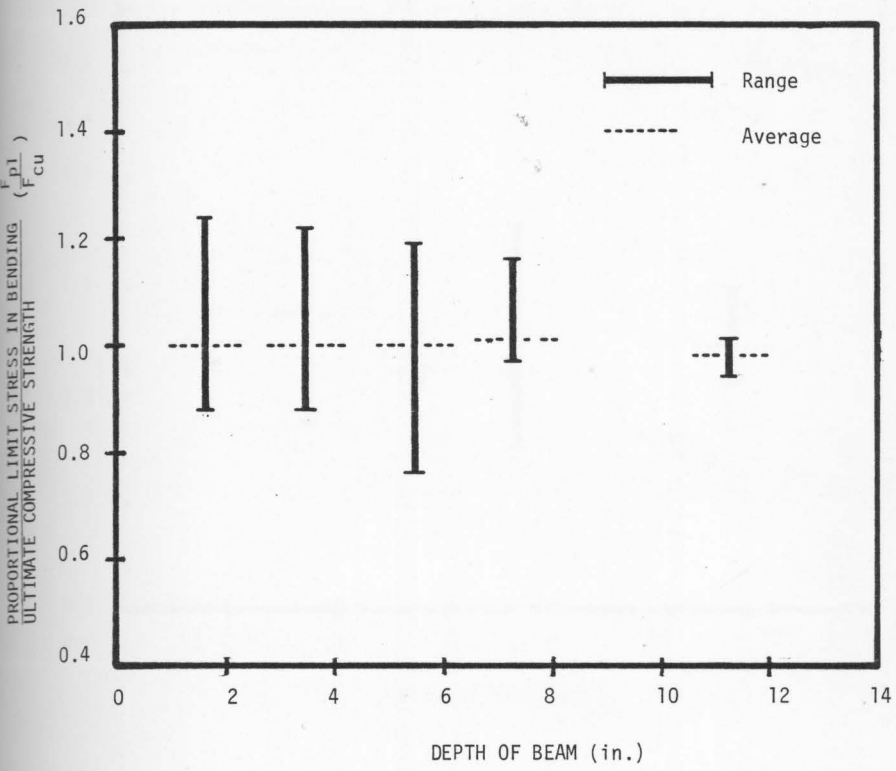

FIG. 7.1 RELATIONSHIP BETWEEN THE RATIO OF PROPORTIONAL LIMIT STRESS IN BENDING TO ULTIMATE COMPRESSIVE STRENGTH AND DEPTH OF BEAM--THIRD-POINT LOADING

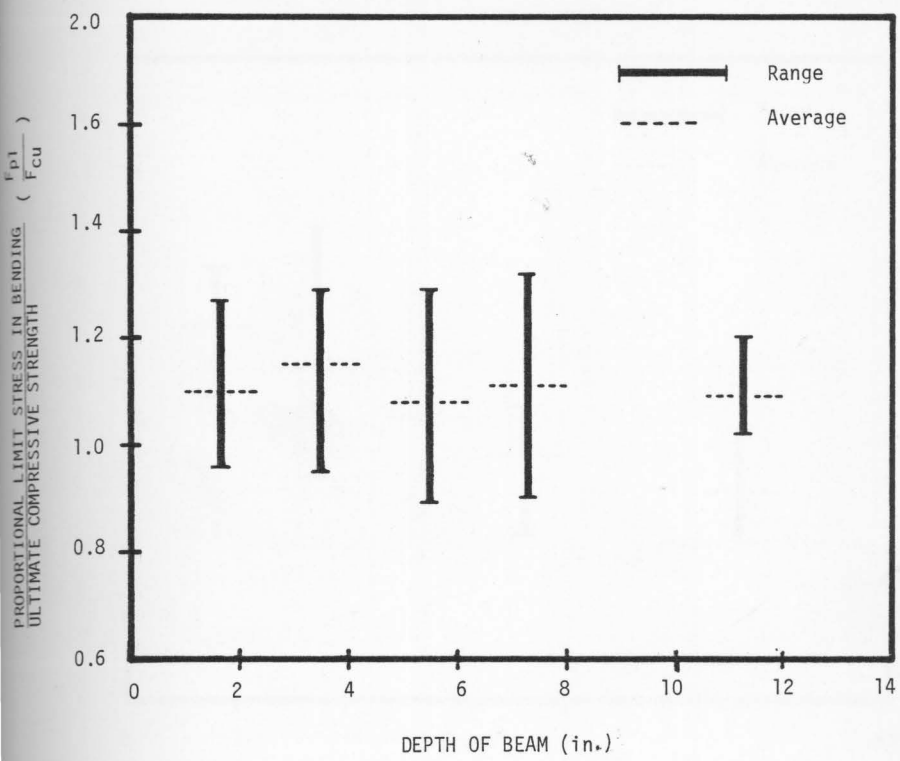

FIG. 7.2 RELATIONSHIP BETWEEN THE RATIO OF PROPORTIONAL LIMIT STRESS IN BENDING TO ULTIMATE COMPRESSIVE STRENGTH AND DEPTH OF BEAM -- CENTRAL LOADING

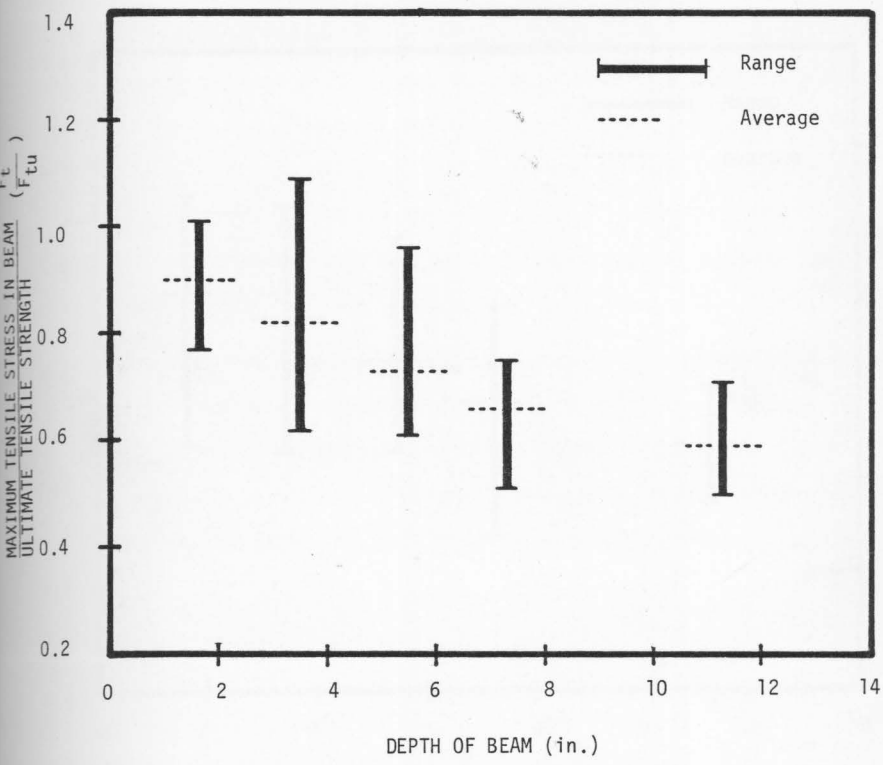

FIG. 7.3 RELATIONSHIP BETWEEN THE RATIO OF MAXIMUM TENSILE STRESS IN BEAM TO ULTIMATE TENSILE STRENGTH AND DEPTH OF BEAM -- THIRD-POINT LOADING

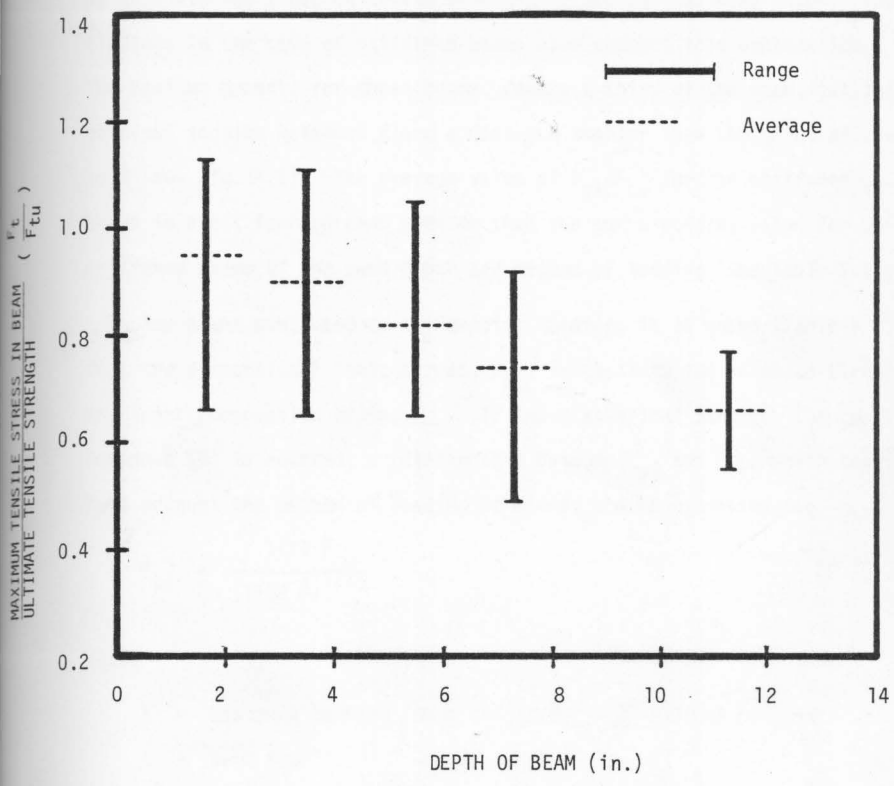

FIG. 7.4 RELATIONSHIP BETWEEN THE RATIO OF MAXIMUM TENSILE STRESS IN BEAM TO ULTIMATE TENSILE STRENGTH AND DEPTH OF BEAM -- CENTRAL LOADING

extend a small distance on either side of midspan. As the region of maximum moment is larger in beams with third-point loading, the probability of encountering a region of low strength is greater in these beams. The findings in the case of stiffened beams also support this explanation. The maximum moment, for these beams, covers a third of the span, but the critical section extended along a distance smaller than the third of the span (see Fig. 4.2). The average value of F_{pl}/F_{cu} for the stiffened beams is about four percent greater than the corresponding value for unstiffened beams of the same depth and method of loading (see Table 7.1).

For beams subjected to third-point loading, it is noted (Table 7.1) that the proportional limit stress, F_{pl}, is equal to the ultimate strength in direct compression tests, F_{cu}. If the statistical strength theory by Bohannan (6) is adopted, a relationship between F_{pl} and F_{cu}, which takes into account the method of loading of beams, can be expressed as:

$$F_{pl} = \frac{1.11\ F_{cu}}{(1+18\ \frac{a}{L})^{1/18}} \qquad [7.1]$$

where

a = Distance between loads placed a/2 each side of midspan

L = Beam span

Equation [7.1] gives a difference of eleven percent between a beam loaded at the center and a similar beam loaded at third-span points. This agrees very well with the test results, Table 7.1. It should be noted that, for practical purposes, it is assumed that the proportional limit stress in bending is equal to the ultimate compressive strength of the beam material.

7.2 Effects of Beam Size and Method of Loading on Maximum Tensile Stress in Beams

The results in Table 7.1 and Figs. 7.3 and 7.4 indicate that, for the same method of loading, there is an appreciable decrease in the average values of F_t/F_{tu} with increase in beam depth. This behavior suggests that the maximum tensile stress at failure, in bending of timber beams, is statistically less than the tensile strength of the beam material as obtained from direct tests, and the average value is proportionally smaller as the depth of the beam is increased. The effect of method of loading on maximum tensile stress at failure is found to be similar to the effect on proportional limit stress. The difference between the two methods of loading is about eleven percent (see Table 7.1).

The statistical strength theory provides an acceptable explanation for the decrease of maximum tensile stress at failure with the increase in beam depth. The probability of encountering regions of low strength that would reduce the maximum tensile stress at failure is greater in the deeper beams. Tension failure of a timber beam is brittle, and once initiated, it propagates without the application of additional loads.

An attempt is made to apply the statistical strength theory to the proposed stress distribution (Fig. 3.3). However, the evaluation of an expression that accounts for the size effect on maximum tensile stress in beams is mathematically intractable. A possible alternative is to derive an empirical formula which is a best fit to the available test data. The results from beams loaded at third-points are adjusted to the case of central loading and the combined average values for each depth are used

in the statistical curve fitting. Several forms of equations are considered in the statistical curve fitting between ratio F_t/F_{tu}, or size factor, S, and the depth of beam, d, in inches. Three best fit equations of the various forms considered are presented here:

$$S = 1.12 \left(\frac{1}{d}\right)^{0.21} \qquad [7.2]$$

with a correlation coefficient of 0.96;

$$S = 1.18 - 0.16\sqrt{d} \qquad [7.3]$$

with a correlation coefficient of 0.97,

$$S = 0.60 \left(\frac{57 + d^2}{34 + d^2}\right) \qquad [7.4]$$

with a correlation coefficient of 0.99. The three curves corresponding to Eqs. [7.2] to [7.4] and the combined average values are shown in Fig. 7.5.

It can be seen that Eq. [7.4] is the best fit to the test data. As Eq. [7.4] is derived for beams loaded at center, for beams loaded at third-points the values of the size factor, S, obtained from this equation should be reduced by eleven percent. Thus Eq. [7.4], for third-point loading, becomes:

$$S = 0.54 \left(\frac{57 + d^2}{34 + d^2}\right) \qquad [7.5]$$

the two curves corresponding to Eqs. [7.4] and [7.5] together with the average test results for both methods of loading are shown in Fig. 7.6. For purpose of comparison, test data by Comben (9) is also plotted on this graph.

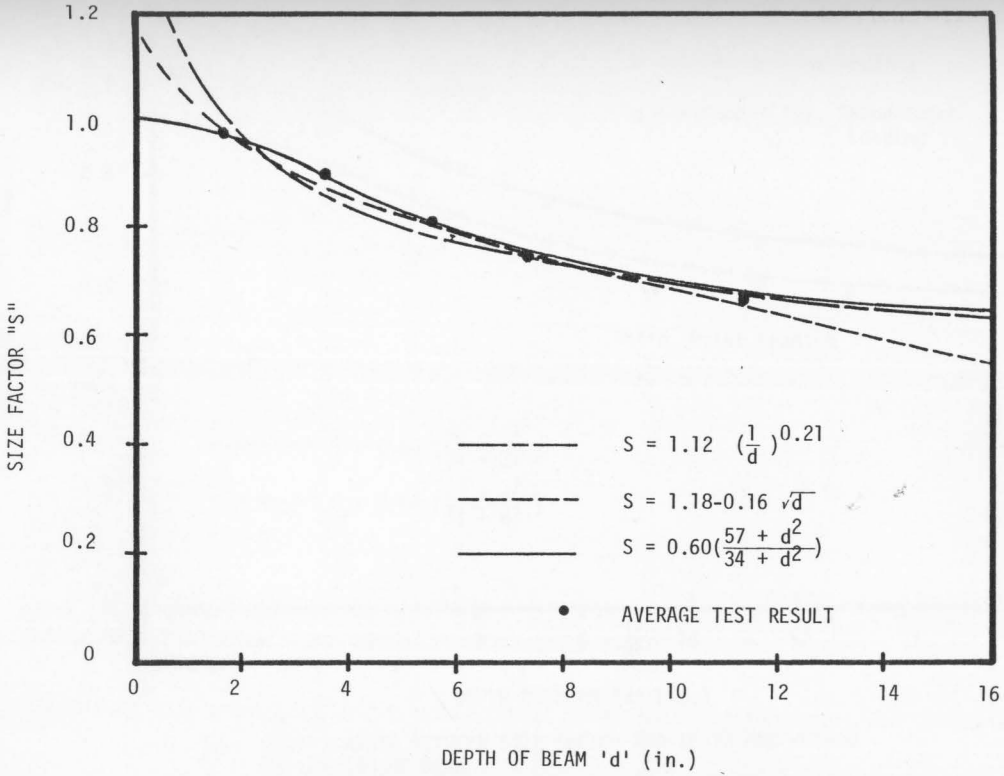

FIG. 7.5 RELATIONSHIP BETWEEN SIZE FACTOR AND DEPTH OF BEAM

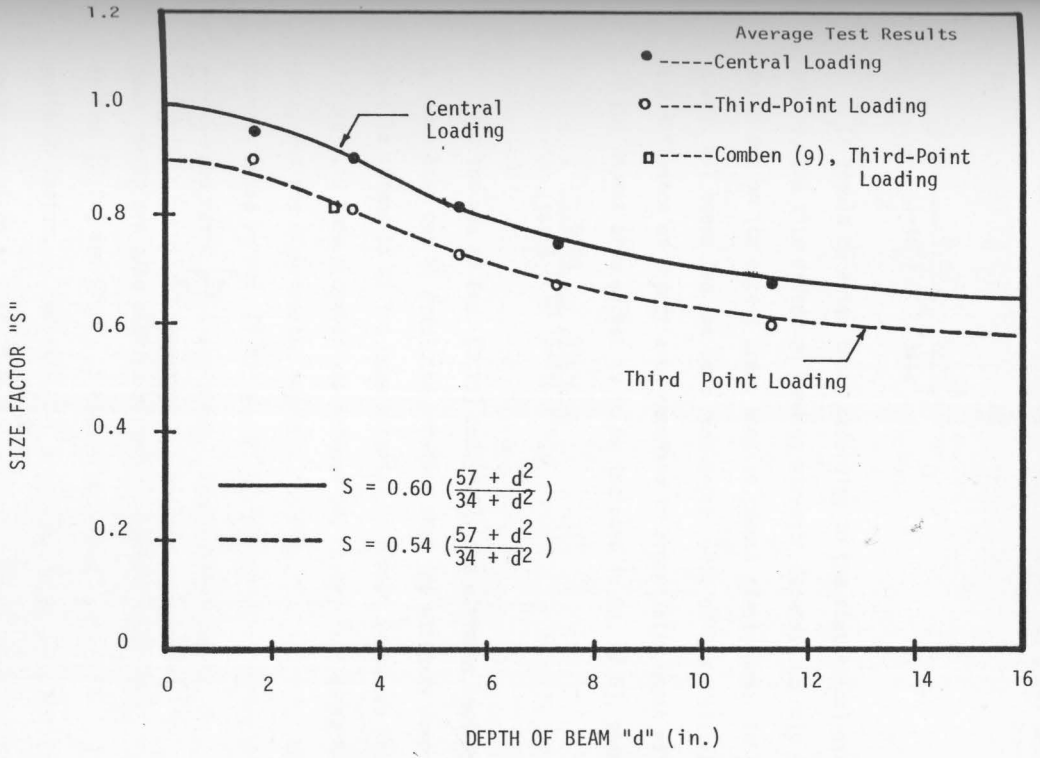

FIG. 7.6 RELATIONSHIP BETWEEN SIZE FACTOR AND DEPTH AND METHOD OF LOADING OF BEAM

If the effects of both beam depth and method of loading are to be incorporated into one single empirical formula, Eq. [7.4] can be expressed as:

$$S = \frac{0.60}{(1+18\frac{a}{L})^{1/18}} \left(\frac{57+d^2}{34+d^2}\right) \qquad [7.6]$$

It should be noted that, according to the statistical strength theory, the size effect on bending strength depends not only on the beam depth but on its aspect area, that is, depth times span. In the present study, all beams had the same span-depth ratio of about sixteen and thus the influence of aspect area amounted to essentially depth effect only. If the aspect area effect is to be included in Eq. [7.6], then

$$S = \frac{0.60}{(1+18\frac{a}{L})^{1/18}} \left(\frac{912+L\cdot d}{544+L\cdot d}\right) \qquad [7.7]$$

By the use of Eqs. [3.23] and [7.7], the ultimate bending moment for a given beam can be predicted provided that the ultimate compressive and tensile strengths of the beam material in direct tests are known. Figures 7.7 to 7.10 show a comparison between the theory (including the size effect) and the experimental results. In Figs. 7.7 and 7.8, theoretical curves, based on Eqs. [3.23] and [7.6], of the relationship between ratio $\frac{M_u}{F_{cu}\frac{bd^2}{6}}$ and ratio $\frac{F_{tu}}{F_{cu}}$, are shown. Experimental results for individual beam tests are also plotted on these graphs. Theoretical curves, based on Eqs. [3.24] and [7.6], of the relationship between the neutral axis position factor, γ, and ratio $\frac{F_{tu}}{F_{cu}}$, together with the results of beam tests are given in Figs. 7.9 and 7.10. For comparison purposes, a theoretical curve (curve 1) based on Eq. [2.4] is plotted in Figs. 7.7 and 7.8,

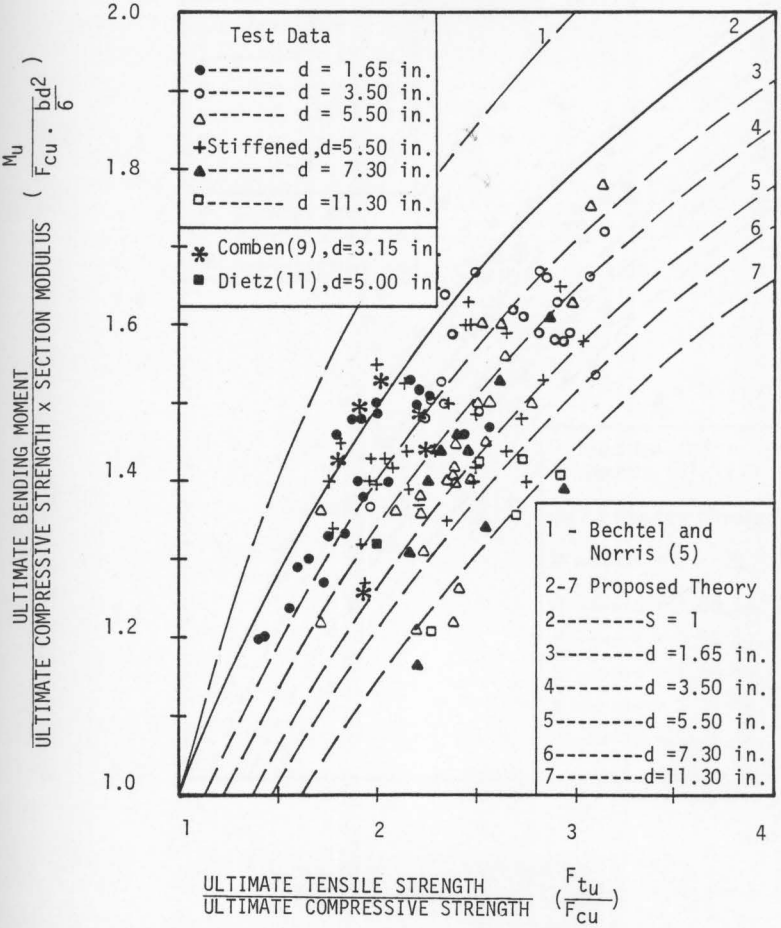

FIG. 7.7 COMPARISON BETWEEN THEORETICAL AND EXPERIMENTAL VALUES OF ULTIMATE BENDING MOMENT OF CLEAR BEAMS SUBJECTED TO THIRD-POINT LOADING

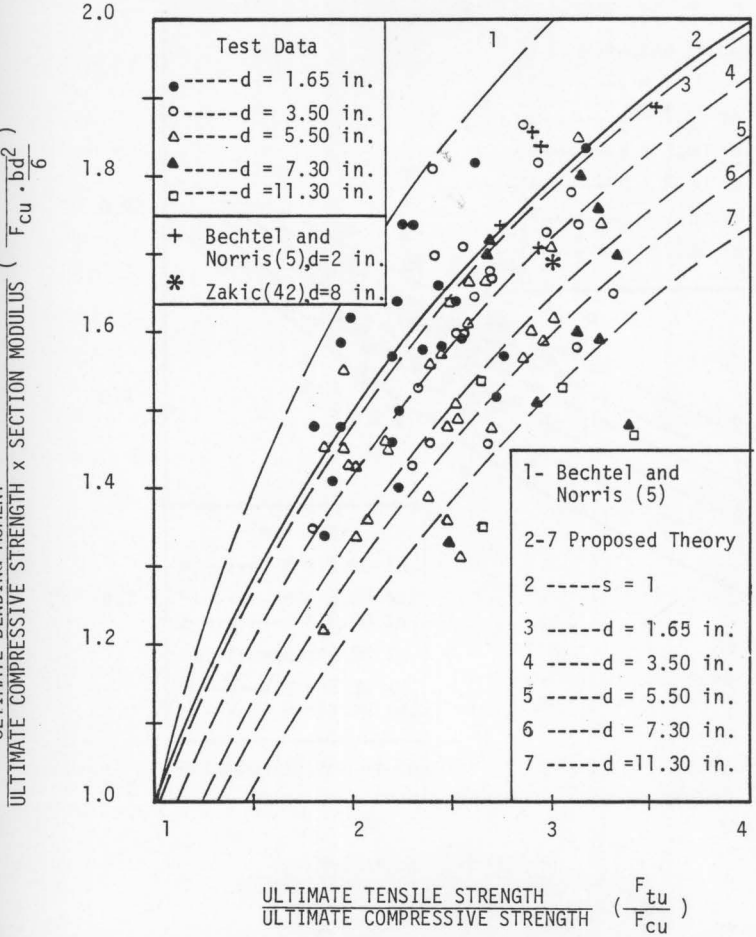

FIG. 7.8 COMPARISON BETWEEN THEORETICAL AND EXPERIMENTAL VALUES OF ULTIMATE BENDING MOMENT OF CLEAR BEAMS SUBJECTED TO CENTRAL LOADING

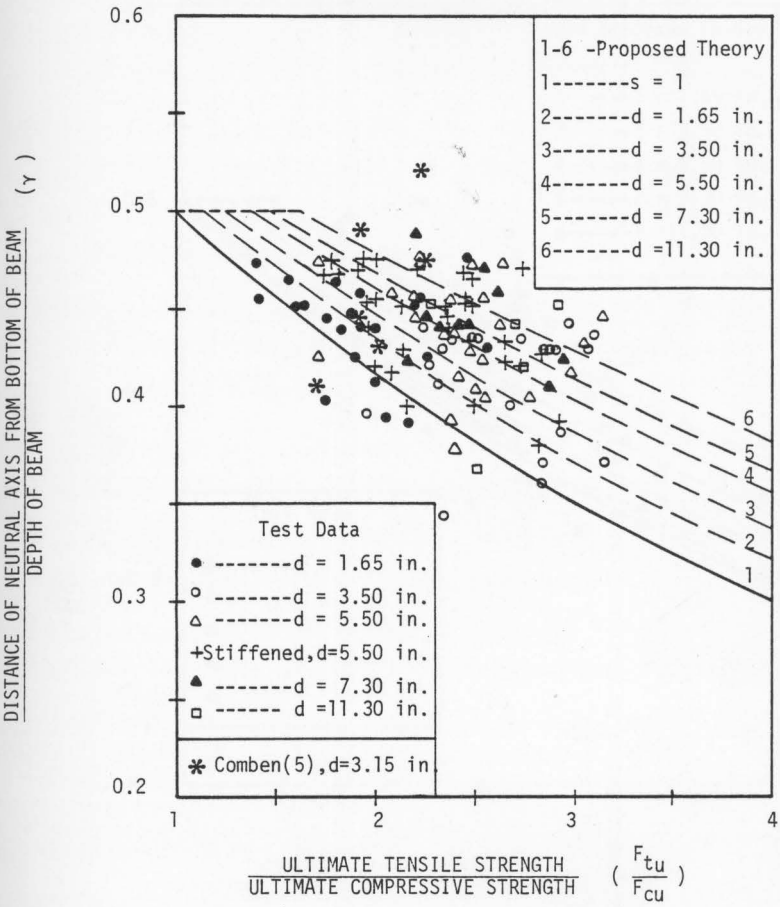

FIG. 7.9 LOCATION OF NEUTRAL AXIS -- COMPARISON BETWEEN THEORY AND TEST DATA OF CLEAR BEAM SUBJECTED TO THIRD-POINT LOADING

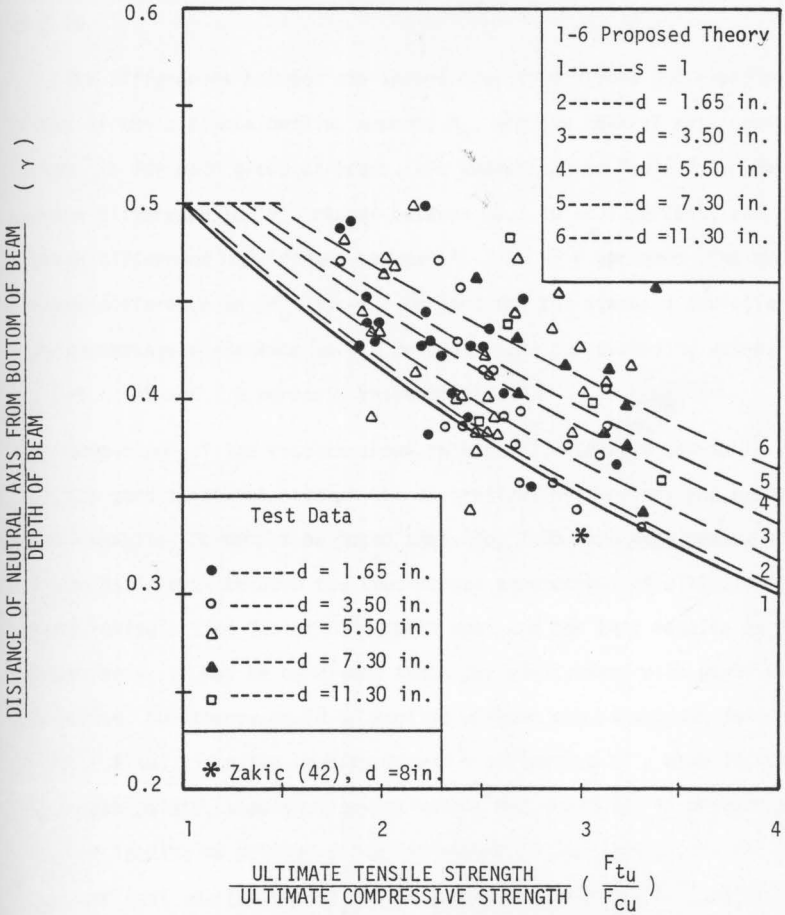

FIG. 7.10 LOCATION OF NEUTRAL AXIS--COMPARISON BETWEEN THEORY AND TEST DATA OF CLEAR BEAMS SUBJECTED TO CENTRAL LOADING

and test data by several investigators (5,9,11,42) are shown in Figs. 7.7 to 7.10.

The differences between the theoretical predictions and experimental values of the ultimate bending moment, M_u, and the neutral axis position factor, γ, for each group of beams, are summarized in Table 7.2. The average difference in "M_u" ranges between -0.3 to -2.9 percent, and the average difference in "γ" ranges between +1.7 to -5.6 percent. The overall average difference in "M_u" is -1.7 percent and the standard deviation of this percentage difference is 6.4 percent. The corresponding values for "γ" are -1.8 and 7.8 percent, respectively.

Comparison of the results shown in Figs. 7.7 to 7.10 and Table 7.2 indicate good agreement between the theoretical predictions and experimental results. It should be noted that, for 1.65-inch deep beams, the average difference between the theoretical predictions of ultimate bending moment, using a size factor "S" equals one, and the test results is less than two percent. It may be concluded that, for small beams with depth up to two inches, the theory could be applied without any adjustment for size effect. Also, since the bending moment distribution of a beam loaded at third-span points, simulates approximately the condition of uniformly distributed loading to develop a bending moment of the same magnitude, it is suggested that Eq. [7.5] of the size factor for third-point loading case, can be used for beams subjected to uniformly distributed loading.

TABLE 7.2: Comparison Between Theory and Experimental Results

Depth OF Beam (in.)	Percentage Difference in M_u				Percentage Difference in γ			
	Third-point Loading		Central Loading		Third-point Loading		Central Loading	
	Average	Standard Deviation	Average	Standard Deviation	Average	Standard Deviation	Average	Standard Deviation
1.65	-2.2	4.3	-0.3	6.7	-0.1	6.4	-5.6	6.2
3.50	-2.3	4.8	-0.8	6.8	-1.7	9.1	-2.0	6.7
5.50	-2.3	6.9	-2.1	6.7	-1.5	6.7	-1.1	6.7
7.30	-2.9	7.3	-1.5	9.0	-0.4	4.9	-3.4	8.5
11.30	-1.7	4.8	-2.0	11.0	-4.4	8.7	+1.7	9.0

CHAPTER 8

ANALYSIS OF KNOTTED BEAM TEST RESULTS

8.1 Test Results and Discussion

Load-deflection curves, load-strain curves and diagrams representing strain distribution across beam depth are produced for each beam test. Samples of these diagrams can be seen in Figs. 8.1 to 8.9 and Figs. B.43 to B.48 (Appendix B). The results obtained, using these diagrams, are tabulated in Table A.2.17 to A.2.20 (Appendix A), and summarized in Table 8.1.

The behavior of knotted beams can be divided into two marked groups, depending on the type of failure. In the first group (47 beams, or 87% of the total number of test beams), the failure followed a compression-tension sequence. In the second group (7 beams), the tension failure occurred before any compression failure. The load-deflection and load-strain curves of the first group (Figs. 8.1, 8.2, 8.4 and 8.5) are qualitatively similar to those obtained for clear beams. These curves have very well defined proportional limits which indicate that the plastification in the beams took place. The load-deflection and load-strain curves of the second group (Figs. 8.7 and 8.8) show that the proportional limit load values virtually coincide with the ultimate loads, indicating that the flexural behavior of these beams is elastic up to failure.

The strain distribution diagrams of both groups (Figs. 8.3, 8.6 and 8.9) show a satisfactory linear variation of the strain distribution at

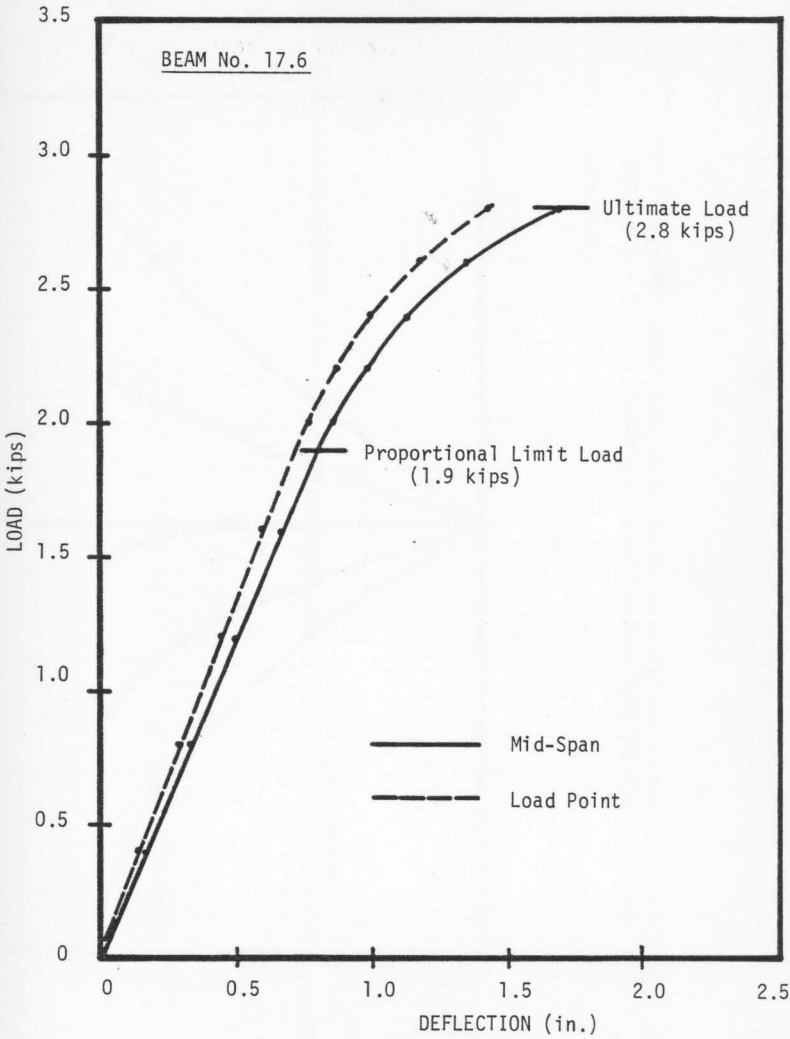

FIG. 8.1 TYPICAL LOAD-DEFLECTION CURVES IN BENDING TEST -- 2 x 4 - EASTERN SPRUCE KNOTTED BEAM SUBJECTED TO THIRD-POINT LOADING

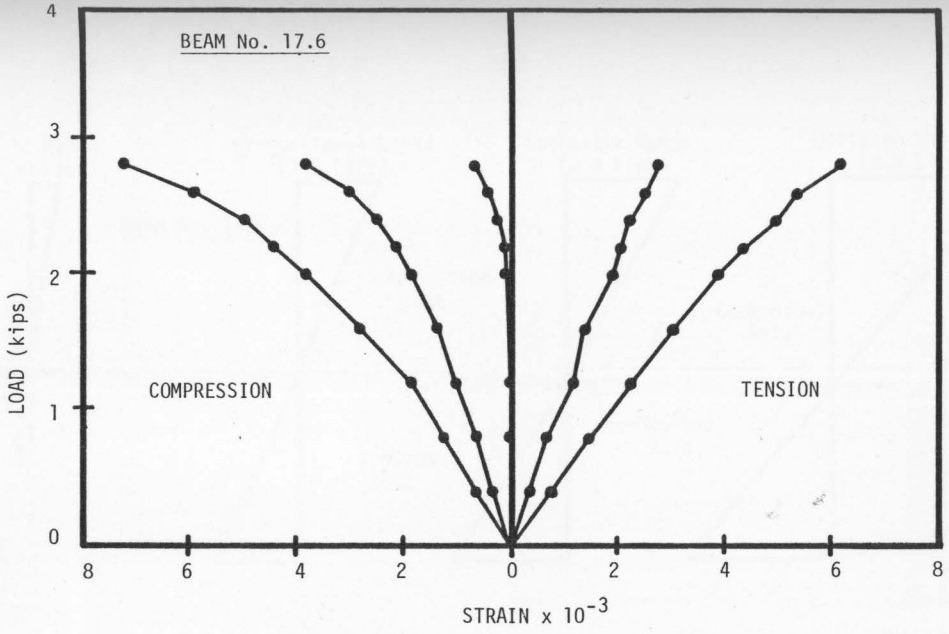

FIG. 8.2 TYPICAL LOAD-STRAIN CURVES IN BENDING TEST-- 2 x 4 EASTERN SPRUCE KNOTTED BEAM SUBJECTED TO THIRD-POINT LOADING

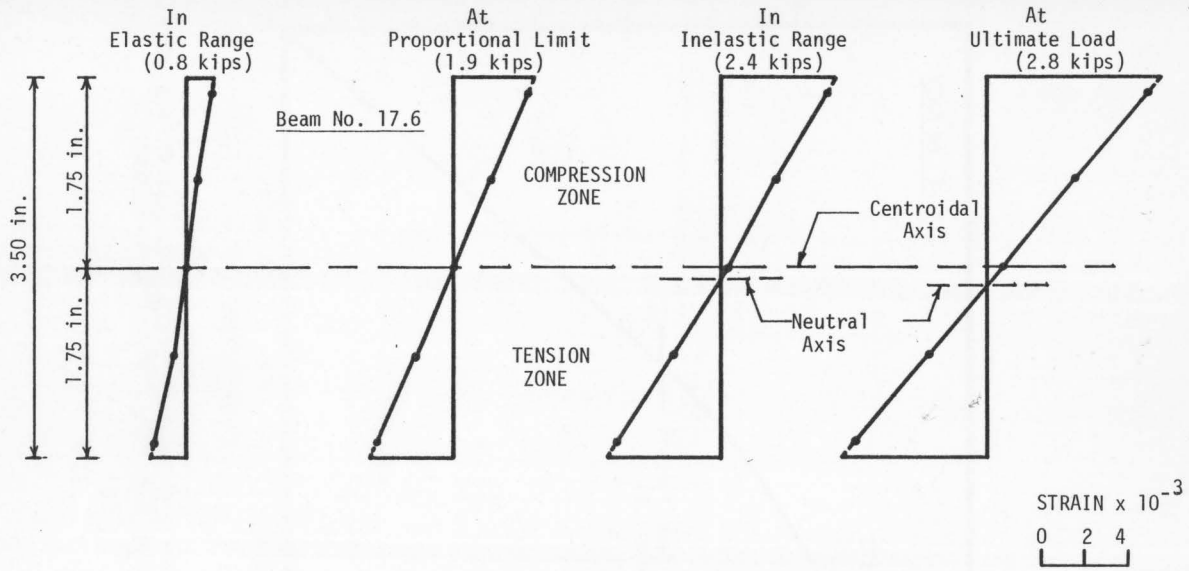

FIG. 8.3 TYPICAL STRAIN DISTRIBUTIONS ACROSS BEAM DEPTH IN BENDING TEST -- 2 x 4 EASTERN SPRUCE KNOTTED BEAM SUBJECTED TO THIRD-POINT LOADING

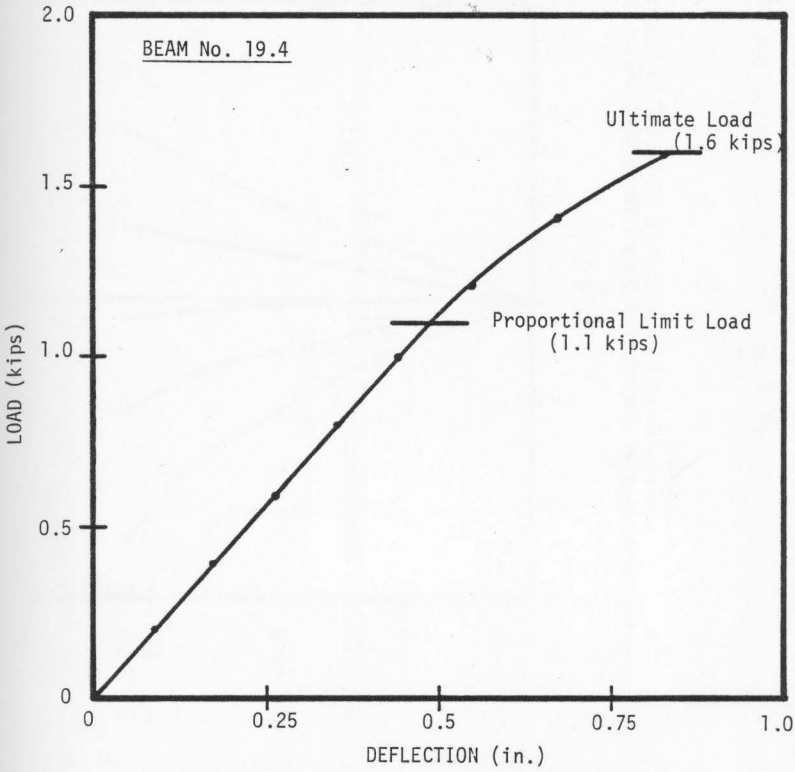

FIG. 8.4 TYPICAL LOAD-DEFLECTION CURVE IN BENDING TEST -- 2 x 4 EASTERN SPRUCE KNOTTED BEAM SUBJECTED TO CENTRAL LOADING

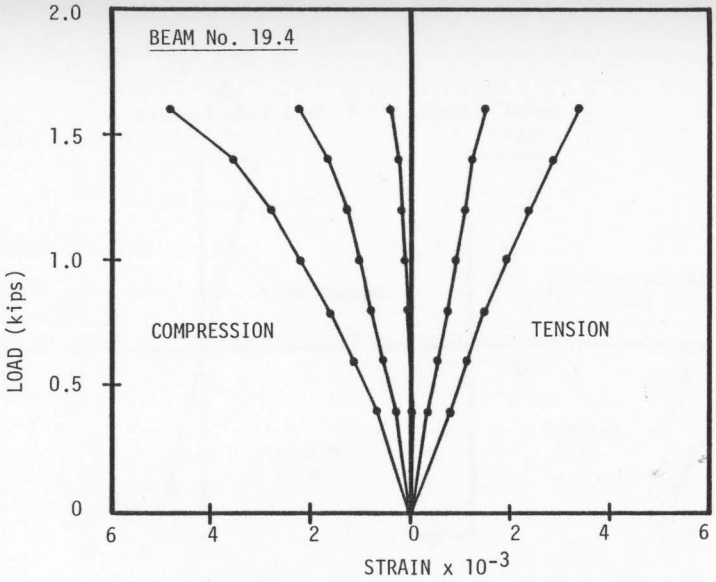

FIG. 8.5 TYPICAL LOAD-STRAIN CURVES IN BENDING TEST -- 2 x 4 EASTERN SPRUCE KNOTTED BEAM SUBJECTED TO CENTRAL LOADING

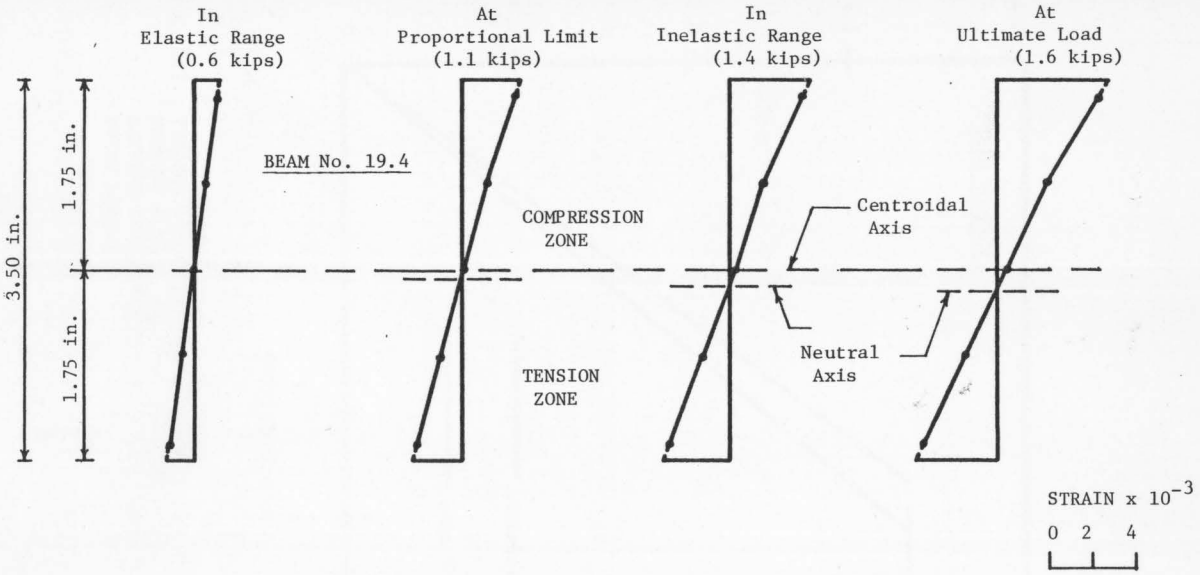

FIG. 8.6 TYPICAL STRAIN DISTRIBUTIONS ACROSS BEAM DEPTH IN BENDING TEST -- 2 x 4 EASTERN SPRUCE KNOTTED BEAM SUBJECTED TO CENTRAL LOADING

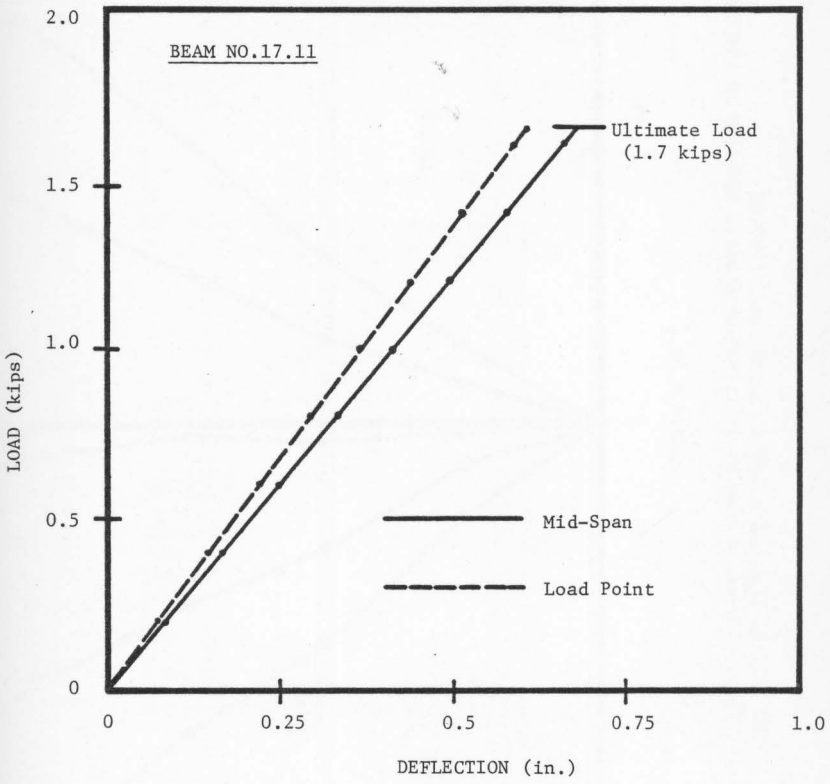

FIG. 8.7 TYPICAL LOAD-DEFLECTION CURVES IN BENDING TEST SHOWING ELASTIC BEHAVIOR TO FAILURE -- 2 x 4 EASTERN SPRUCE KNOTTED BEAM SUBJECTED TO THIRD-POINT LOADING

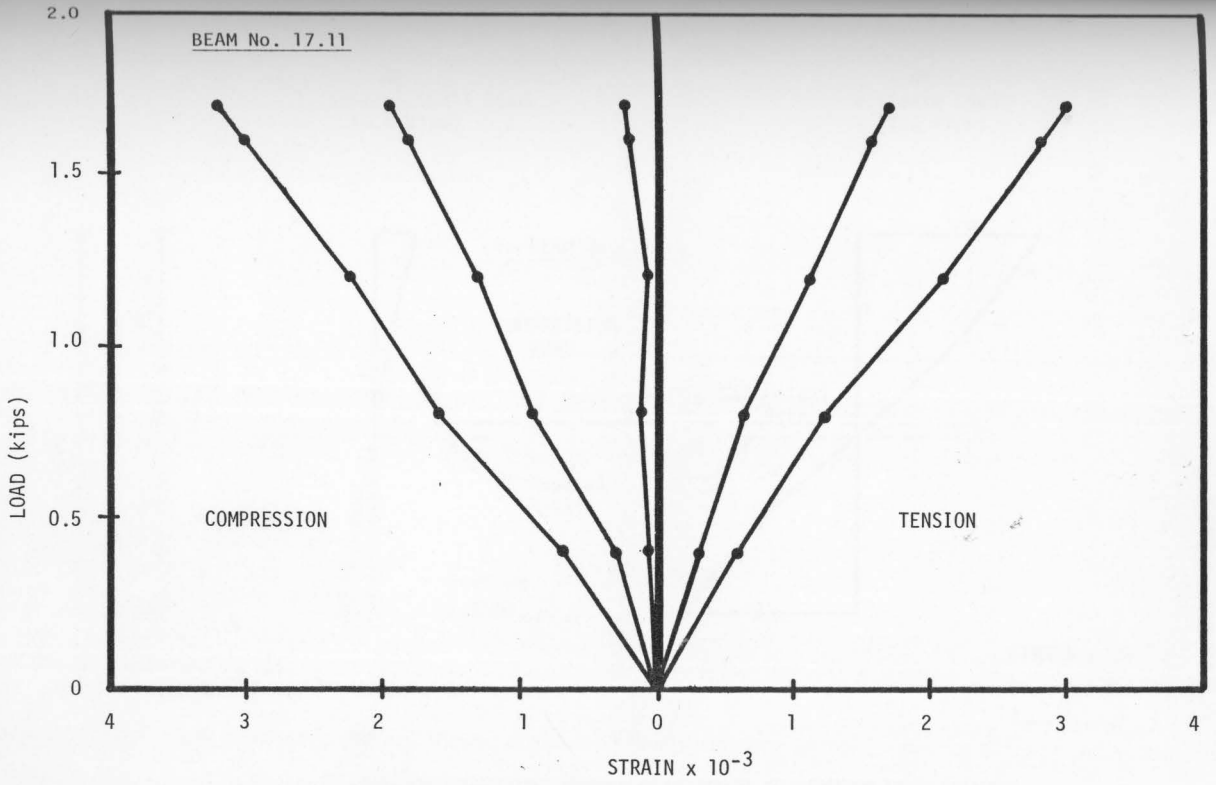

FIG. 8.8 TYPICAL LOAD-STRAIN CURVES IN BENDING TEST SHOWING ELASTIC BEHAVIOR TO FAILURE -- 2 x 4 EASTERN SPRUCE KNOTTED BEAM SUBJECTED TO THIRD-POINT LOADING

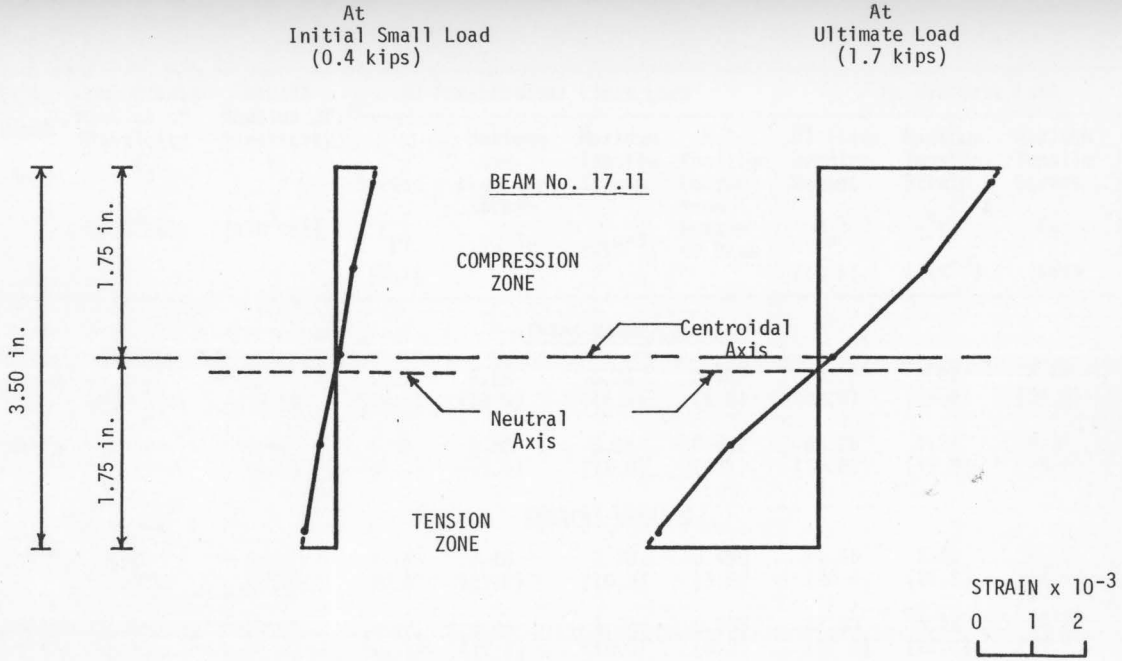

FIG. 8.9 TYPICAL STRAIN DISTRIBUTIONS ACROSS BEAM DEPTH IN BENDING TEST SHOWING ELASTIC BEHAVIOR TO FIALURE -- 2 x 4 EASTERN SPRUCE KNOTTED BEAM SUBJECTED TO THIRD-POINT LOADING

TABLE 8.1: Summary of Knotted Beam Test Results

Beam Depth (in.)	Compressive Modulus of Elasticity E_c ($X10^3$ksi)	Tensile Modulus of Elasticity E_t ($X10^3$ksi)	At Proportional Limit Load: Stress F_{pl} (ksi)	At Proportional Limit Load: Maximum Compressive Strain ($x10^{-3}$)	At Proportional Limit Load: Maximum Tensile Strain ($X10^{-3}$)	At Proportional Limit Load: N.A. Position Factor from Bottom of Beam	At Ultimate Load: Ultimate Bending Moment M_u (in-k)	At Ultimate Load: Maximum Tensile Strain ε_t ($X10^{-3}$)	At Ultimate Load: Maximum Tensile Stress F_t (ksi)	At Ultimate Load: N.A. Position Factor from Bottom of Beam γ
				Third-point Loading						
3.50(S)[a]	1.70[b] (20.3)	1.77 (19.7)	5.80 (16.2)	3.58 (18.8)	3.36 (16.5)	0.487 (4.5)	23.72 (22.6)	5.01 (28.4)	8.69 (29.8)	0.451 (8.6)
5.50(S)	1.93 (10.0)	1.96 (12.7)	6.35 (16.0)	3.38 (11.6)	3.24 (13.0)	0.497 (3.1)	63.75 (18.62)	4.74 (19.4)	9.31 (19.4)	0.458 (7.8)
				Central Loading						
3.50(S)	1.58 (22.0)	1.66 (21.8)	6.12 (16.8)	4.18 (21.2)	3.78 (19.3)	0.494 (3.9)	24.65 (20.4)	5.65 (25.9)	9.16 (24.5)	0.455 (8.8)
5.50(S)	1.73 (16.0)	1.87 (17.2)	6.17 (15.1)	3.83 (17.2)	3.36 (15.0)	0.503 (5.2)	61.33 (17.9)	5.56 (27.5)	10.25 (28.5)	0.433 (13.5)

a: (S) refers to spruce lumber.

b: Values in first lines are averages and those in parentheses are coefficients of variation in percent.

different stages of loading, up to failure. But the deviation of the strain values from linear distribution, in some knotted beams, is more pronounced than for the case of clear beams which is to be expected due to knots.

The test results (Table 8.1) indicate that, at the proportional limit, the average value of maximum compressive strain is about nine percent greater than the average value of maximum tensile strain, while the modulus of elasticity in tension is only about five percent larger than the value in compression. Table 8.1 also indicates that, at the proportional limit, the neutral axis is approximately at the center of depth. But, at ultimate load of the beams in the first group (inelastic behavior), the neutral axis shifts towards the tension side of the beam by varying amounts up to about ten percent of the beam depth.

The results show that the presence of knots influences the behavior of the beams. In the second group where the behavior of the beams is elastic to failure, it is observed that these beams have relatively larger knots near the tension edge of the beams. It is observed that the knots reduce the compressive and tensile strengths of the beams. This issue is further investigated in a later part of this chapter. It should be noted here that the proportional limit stress in bending, F_{pl}, is, on the average, about seven percent smaller than the compressive strength of the beam material, F_{cu}, as obtained from direct tests on small clear specimens. In other words, the average value of the ratio F_{pl}/F_{cu} is 0.93. The smallest value of this ratio (F_{pl}/F_{cu}) is observed to be 0.70. The average value of ratio between the maximum tensile stress in the beam at failure

and the ultimate tensile strength of the beam material as obtained from direct tests on small clear specimens, F_t/F_{tu}, is 0.63 with a minimum value of 0.35.

8.2 Comparison Between Theory and Test Results

To check the validity of the proposed theory (Chapter 3) to knotted beams failing in the inelastic range, a comparison between the theoretical predictions and test results of the first group of beams (47 beams) is made, Figs. 8.10 and 8.11. In Fig. 8.10, a theoretical curve (curve 2) based on Eq. [3.18], of the relationship between ratio $\frac{M_u}{F_{cu} \cdot \frac{bd^2}{6}}$ and ratio $\frac{F_t}{F_{cu}}$, is shown. Experimental results for individual beam tests are also plotted on this graph. A theoretical curve (curve 2) based on Eq. [3.20], of the relationship between the neutral axis position factor, γ, and ratio $\frac{F_t}{F_{cu}}$, together with the results of beam tests are shown in Fig. 8.11. Theoretical curves (curves 3 and 4) based on Eqs. [3.18] and [3.20] with modified compressive strength values by the average and minimum reduction factors of 0.93 and 0.70, respectively, are also plotted on the graphs. For comparison purposes, theoretical curves (curve 1) based on Eqs. [2.8] and [2.4] are shown in Figs. 8.10 and 8.11.

The frequency distributions of the percentage difference between the theoretical predictions of M_u and γ (curve 2) and the experimental values, are given in Figs. 8.12 and 8.13. For the ultimate bending moment, M_u, Fig. 8.12 shows the following:

a) 31.8 percent of the test results are within $\pm$ 3 percent of theoretical predictions

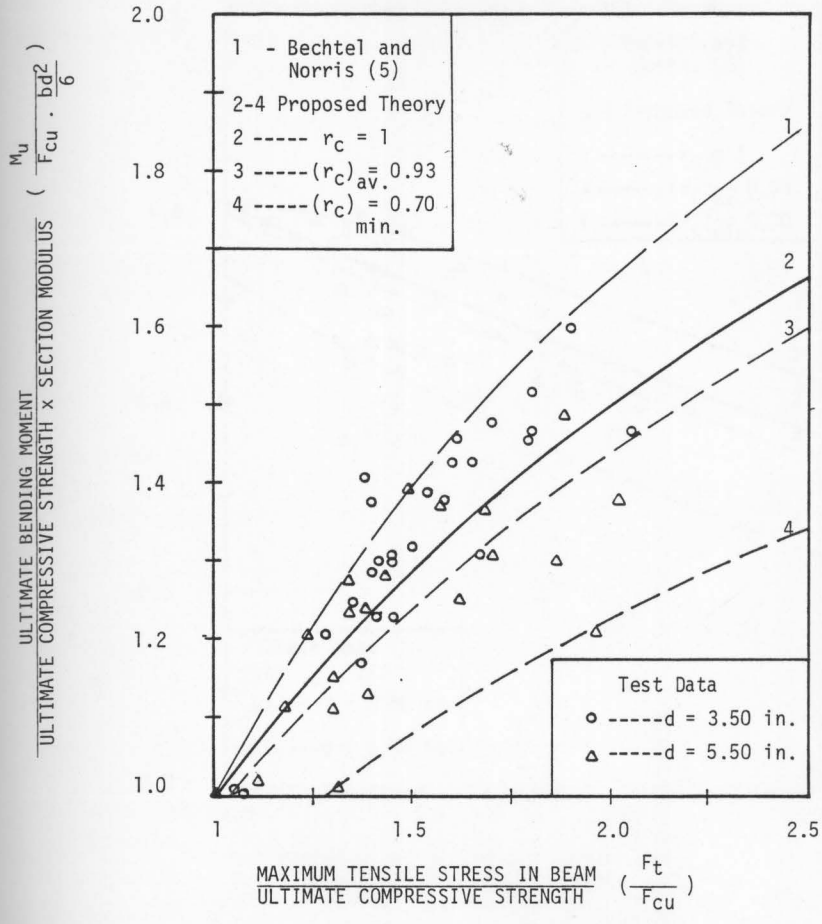

FIG. 8.10 COMPARISON BETWEEN THEORETICAL PREDICTIONS OF ULTIMATE BENDING MOMENT AND TEST RESULTS OF KNOTTED BEAMS

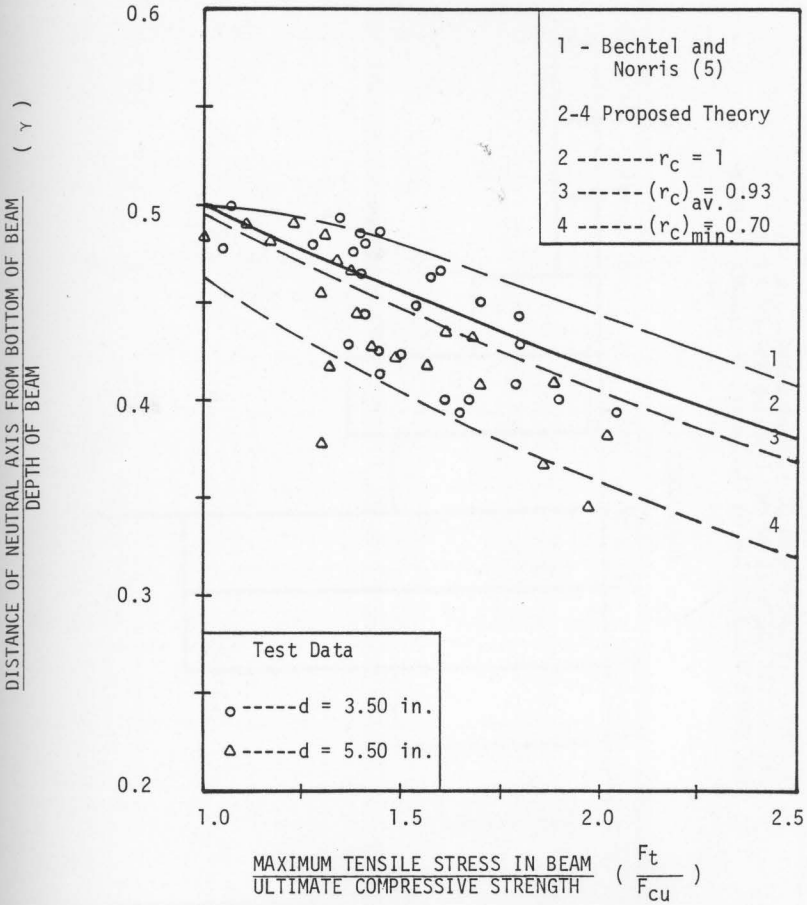

FIG. 8.11 LOCATION OF NEUTRAL AXIS -- COMPARISON BETWEEN THEORY AND TEST RESULTS OF KNOTTED BEAMS

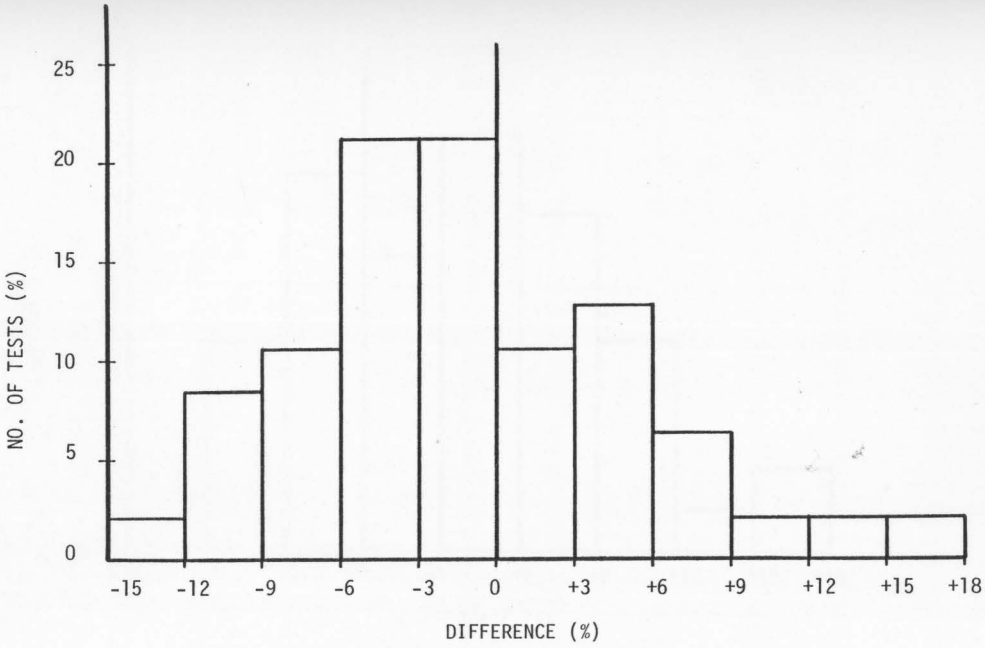

FIG. 8.12 FREQUENCY DISTRIBUTION OF PERCENTAGE DIFFERENCE BETWEEN THEORETICAL PREDICTIONS AND EXPERIMENTAL VALUES OF ULTIMATE BENDING MOMENT OF KNOTTED BEAMS

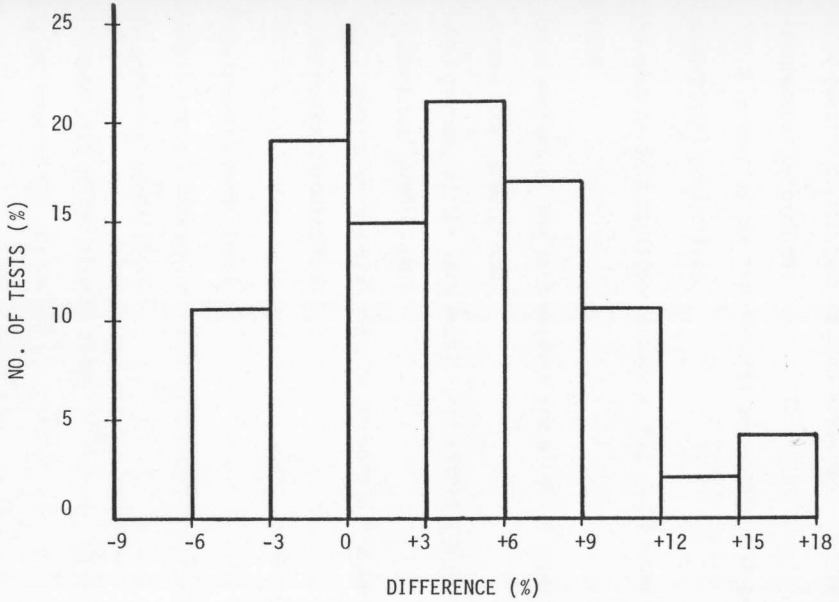

FIG. 8.13 FREQUENCY DISTRIBUTION OF PERCENTAGE DIFFERENCE BETWEEN THEORETICAL PREDICTIONS AND EXPERIMENTAL VALUES OF NEUTRAL AXIS POSITION FACTOR OF KNOTTED BEAMS

b) 65.8 percent of the test results are within ± 6 percent of theoretical predictions

c) 82.8 percent of the test results are within ± 9 percent of theoretical predictions

d) 97.9 percent of the test results are within ± 15 percent of theoretical predictions

e) 100.0 percent of the test results are within ± 18 percent of theoretical predictions

For the neutral axis position factor, γ, Fig. 8.13 shows the following:

a) 34.0 percent of the test results are within ± 3 percent of theoretical predictions.

b) 65.7 percent of the test results are within ± 6 percent of theoretical predictions.

c) 82.7 percent of the test results are within ± 9 percent of theoretical predictions.

d) 95.4 percent of the test results are within ± 15 percent of theoretical predictions.

e) 100.0 percent of the test results are within ± 18 percent of theoretical predictions.

Comparisons of the results shown in Figs. 8.10 to 8.13 indicate good agreement between the theory and experimental results. In practice, one should be able to predict the ultimate bending load using the ultimate compressive and tensile strengths of the beam material as obtained from direct tests on small clear specimen. This requires that the effect of knots on the stresses in beams must be determined.

8.3 Effects of Knots on Stresses in Beams

Knots reduce the stresses in beams principally because knots interrupt the direction of grain and cause localized cross-grain with steep slopes. Intergrown or live knots resist some stresses but encased knots or knotholes transmit little or no stresses. On the other hand, distortion of grain is greater around an intergrown or live knot than around an encased or dead knot. As a result, overall effects are roughly equalized (12).

The effect of a knot on bending strength depends approximately on the proportion of the cross-section of the piece of lumber occupied by the knot, upon knot location and upon the distribution of stress across the depth of the beam. A knot located close to the neutral axis will have less effect on bending strength than a knot located close to the edge. Also, the effect of knots on strength is greater in tension than in compression (14,15).

The true effects of knots on bending strength are not completely known. The present design practice of timber beams (8,24) uses a hypothetical strength ratio to account for the weakening effect of knots. The ASTM Standard D245 (3) provides formulas for this strength ratio. These formulas are based on the assumption that the knot is effectively a hole through the piece reducing the cross-section of the beam. Hence, for a bending member, the strength ratio is the ratio of the bending moment capacity of a beam with the reduced cross-section will carry to the bending moment of the beam without knot. According to the ASTM Standard, three knot ratios should be considered. The first is the maximum knot ratio on the narrow face of the beam, $\frac{K_n}{b}$. The second is the maximum

centerline knot ratio on the wide face of the beam, $\frac{K_w}{d}$, and the third is the maximum knot ratio at the edge of wide face of the beam, $\frac{K_e}{d}$. The hypothetical strength ratios corresponding to these knot ratios are, respectively, $[1 - \frac{K_n}{b}]$, $[1 - \frac{K_w}{d}]$ and $[1 - \frac{K_e}{d}]^2$. The smallest of the three strength ratios is the controlling value used to determine the strength property.

In the present study, a combined effect of all three knot ratios is considered. It is assumed that the effect of knots is dependent on a parameter ϕ, where ϕ is defined as:

$$\phi = [1 - \frac{K_n}{b}][1 - \frac{K_w}{d}][1 - \frac{K_e}{d}]^2 \qquad [8.1]$$

The size of the knots in each test beam is measured according to the ASTM Standard D245 (3). For the purpose of the analysis, knots located in the top half of the beam (compression zone) are considered to affect the compressive strength while knots appearing in the bottom half of the beam are considered to influence the tensile strength. The maximum knot ratios and the corresponding values of the parameter ϕ_c^* and ϕ_t, as computed from Eq. [8.1], are given in Tables A.3.1 to A.3.8 (Appendix A).

The proportional limit stress in bending and the maximum tensile stress at failure in individual knotted beams are expressed as ratios of the ultimate compressive and tensile strength of the beam material as obtained from direct tests on small clear specimens, F_{pl}/F_{cu} and f_t/F_{tu}. The ratio F_{pl}/F_{cu} for clear beams is observed to be unaffected by the depth of the beam and practically equals one (see Chapter 7). Thus, this ratio (F_{pl}/F_{cu}) for knotted beams only is affected by the knots. But the

---

* Parameters ϕ_c and ϕ_t refer to knots in compression and tension zones, respectively.

ratio F_t/F_{tu} for clear beams is dependent on the beam depth, and it is reducing as the depth of the beam is increased, although there are no visible knots. In order to obtain the effect of visible knots on the maximum tensile stress in the beam, the values of ratio F_t/F_{tu} for knotted beams are adjusted to the size of the beam using Eq. [7.6], that is, the values of F_t/F_{tu} are divided by the appropriate size factor "S". The ratios F_{pl}/F_{cu} and $F_t/S \cdot F_{tu}$ for knotted beams are referred to it as reduction factors r_c and r_t, respectively. These reduction factors are usually smaller than one and they account for the weakening effects of the knots. The reduction factors r_c and r_t for the test beams are given in Tables A.3.1 to A.3.8 (Appendix A).

Correlations between the reduction factor r_c and the parameter ϕ_c, and between the reduction factor r_t and the parameter ϕ_t, are obtained. They are derived with first order regression equation fitting one independent variable and one response variable. The parameter ϕ is taken as the independent variable and the reduction factor r is taken as the response variable. The following results are obtained:

$$r_c = 0.71 + 0.35\ \phi_c, \qquad [8.2]$$

with a correlation coefficient of 0.80 and a standard error of estimate of 0.05 for r_c;

$$r_t = 0.31 + 0.79\ \phi_t, \qquad [8.3]$$

with a correlation coefficient of 0.82 and a standard error of estimate of 0.07 for r_t. The two curves representing Eqs. [8.2] and [8.3] and the corresponding test data are shown in Figs. 8.14 and 8.15.

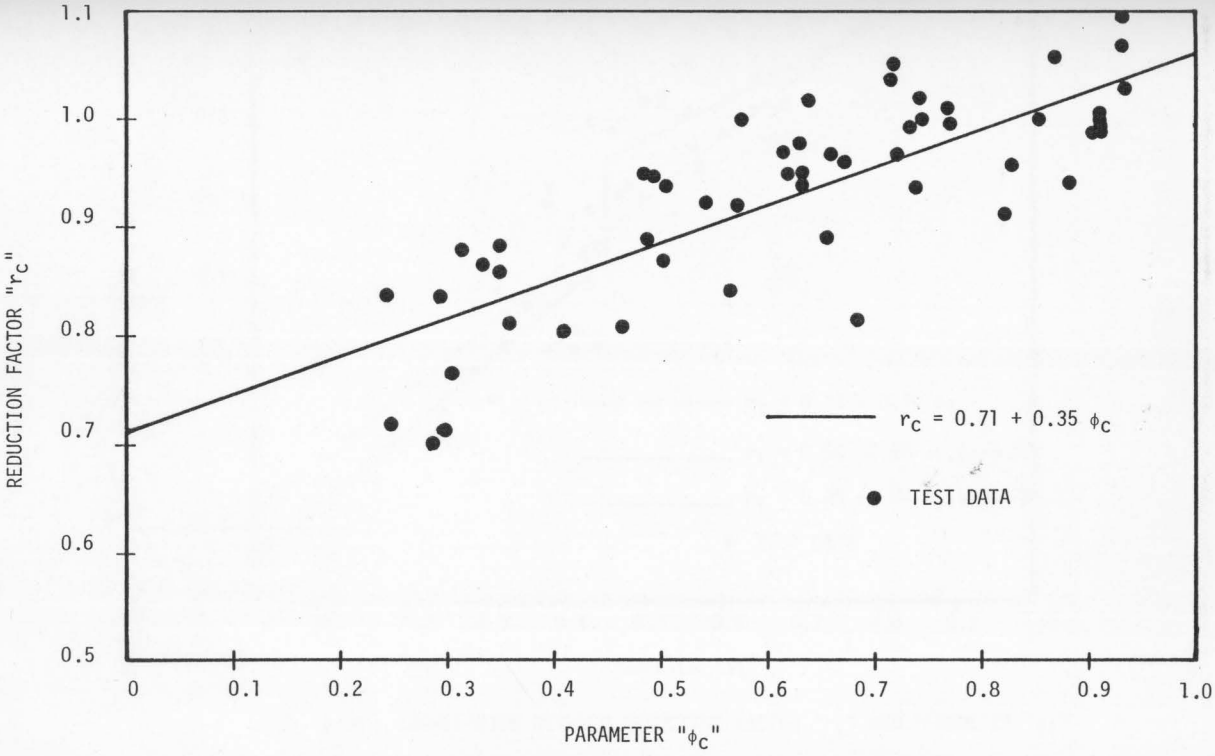

FIG. 8.14 CORRELATION BETWEEN REDUCTION FACTOR "r_c" AND PARAMETER "ϕ_c"

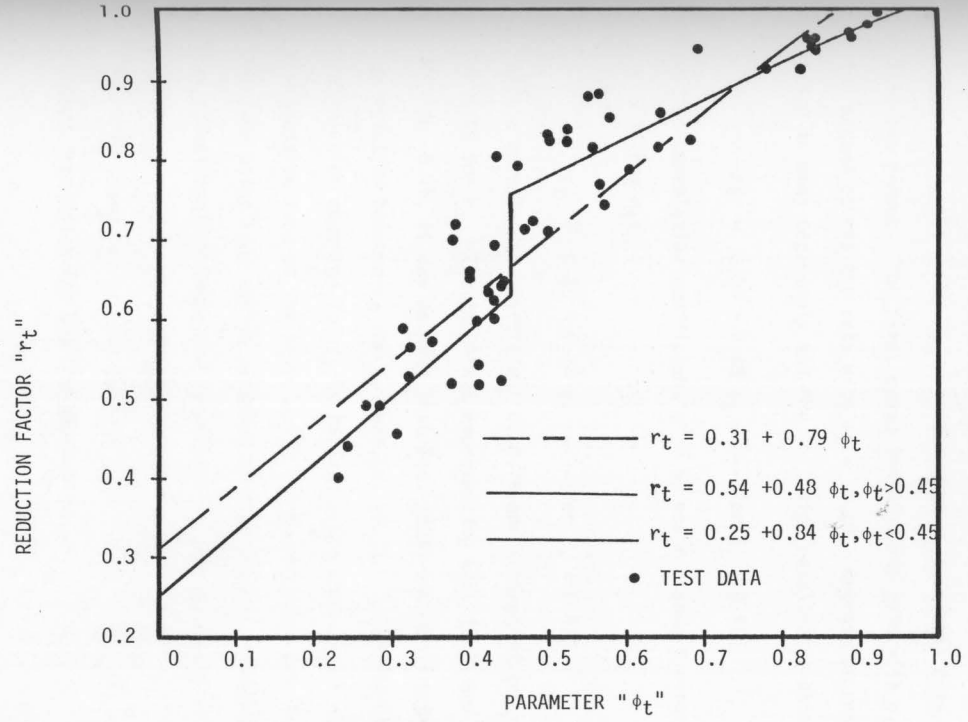

FIG. 8.15 CORRELATION BETWEEN REDUCTION FACTOR "r_t" AND PARAMETER "ϕ_t"

Equation [8.2] and Fig. 8.14 indicate a good correlation between r_c and ϕ_c. But Fig. 8.15 indicates that Eq. [8.3] predicts values of r_t larger than the test data for beams with large knots ($\phi_t < 0.45$) and that the equation giv es values of r_t smaller than the experimental results for beams with small knots ($\phi_t > 0.45$). The experimental data is divided into two groups. The first group includes the data with $\phi_t \geq 0.45$, and the second covers the data with $\phi_t < 0.45$. Regression analysis on each group is made separately and the following results are obtained:

$$r_t = 0.54 + 0.48\ \phi_t \text{ -----(for } \phi_t \geq 0.45), \qquad [8.4]$$

with a correlation coefficient of 0.89 and a standard error of estimate of 0.04 for r_t;

$$r_t = 0.25 + 0.84\ \phi_t \text{ -----(for } \phi_t < 0.45), \qquad [8.5]$$

with a correlation coefficient of 0.78 and a standard error of estimate of 0.05 for r_t. The two lines representing Eqs. [8.4] and [8.5] are shown in Fig. 8.15. It can be seen that Eqs. [8.4] and [8.5] provide a better correlation between r_t and ϕ_t than Eq. [8.3]. It should be noted that the correlation equation for r_c is derived using knot ratios measured on the compressive zone of the beam, while the correlation equations for r_t are derived using knot ratios measured on the tension zone of the beam. For practical applications, the parameters ϕ_c and ϕ_t should be replaced by one parameter ϕ which could be obtained using Eq. [8.1]. The three knot ratios, $\frac{K_n}{b}$, $\frac{K_w}{d}$ and $\frac{K_e}{d}$ are the maximum knot ratios measured on a piece of lumber from which the beam is fabricated.

By the use of Eqs. [3.25], [3.27] and [7.7] together with Eqs. [8.2], [8.4] and [8.5], the ultimate bending moment for a given beam with knots, can be predicted provided that the ultimate compressive and tensile strengths of the beam material in direct test on small clear specimens are known. Figures 8.16 and 8.17 show a comparison between the theory (including the effects of beam depth and knots) and the experimental results. In these figures, theoretical curves based on Eqs. [3.25], [3.27], [7.7], [8.2], [8.4] and [8.5], of the relationship between ratio $\frac{M_u}{F_{cu}\frac{bd^2}{6}}$ and ratio $\frac{F_{tu}}{F_{cu}}$, are shown. Experimental results for individual beam tests including those where the behavior is elastic to failure, as well as the average test results for each beam depth, are also plotted on these graphs. Curve 1 represents the theory with no adjustment for depth or knot effects. Curves 2 and 3 represent the theory with size factor and reduction factors corresponding to the average knot ratios for each depth. Curves 4 and 5 represent the theory with size factor and reduction factors corresponding to the largest knot ratios for each depth. For comparison purposes, test data by Mazur (22) is shown in Fig. 8.16. It should be noted that, if the theoretical value of $\frac{M_u}{F_{cu}\frac{bd^2}{6}}$ is equal to, or less than r_c, the behavior of the beam is elastic to failure. The point below which the behavior of the beam is elastic to failure is marked in the graphs.

Comparison of the results shown in Figs. 8.15 and 8.16 indicates good agreement between the theoretical predictions and experimental results. The following example illustrates the prediction of bending strength for a 2 x 4 beam of eastern spruce:

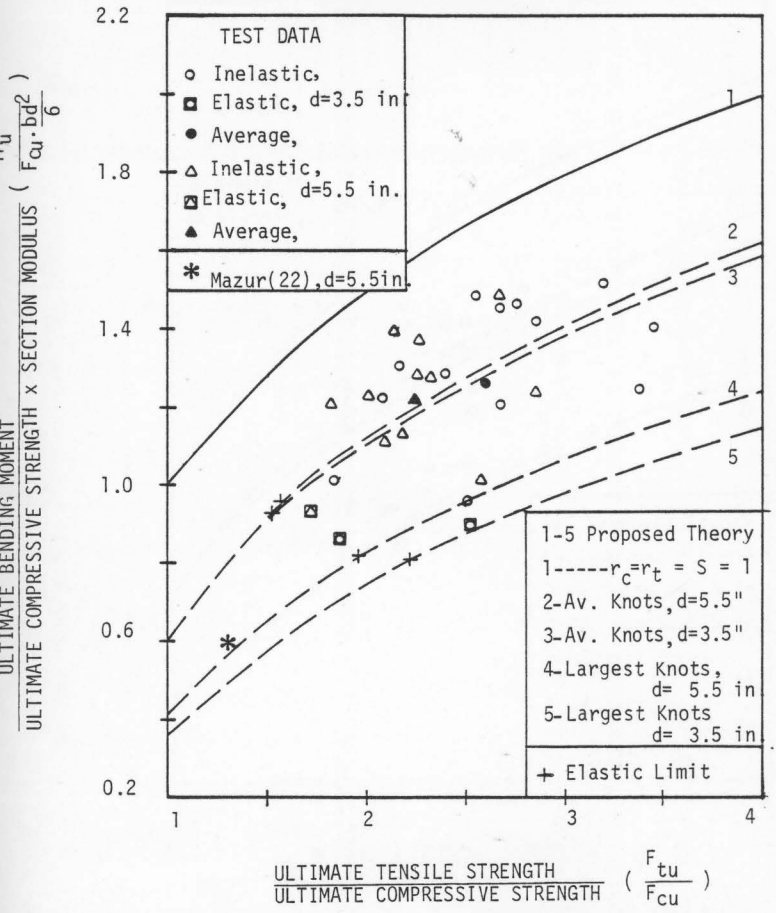

FIG. 8.16 COMPARISON BETWEEN THEORETICAL AND EXPERIMENTAL VALUES OF ULTIMATE BENDING MOMENT OF KNOTTED BEAMS SUBJECTED TO THIRD-POINT LOADING

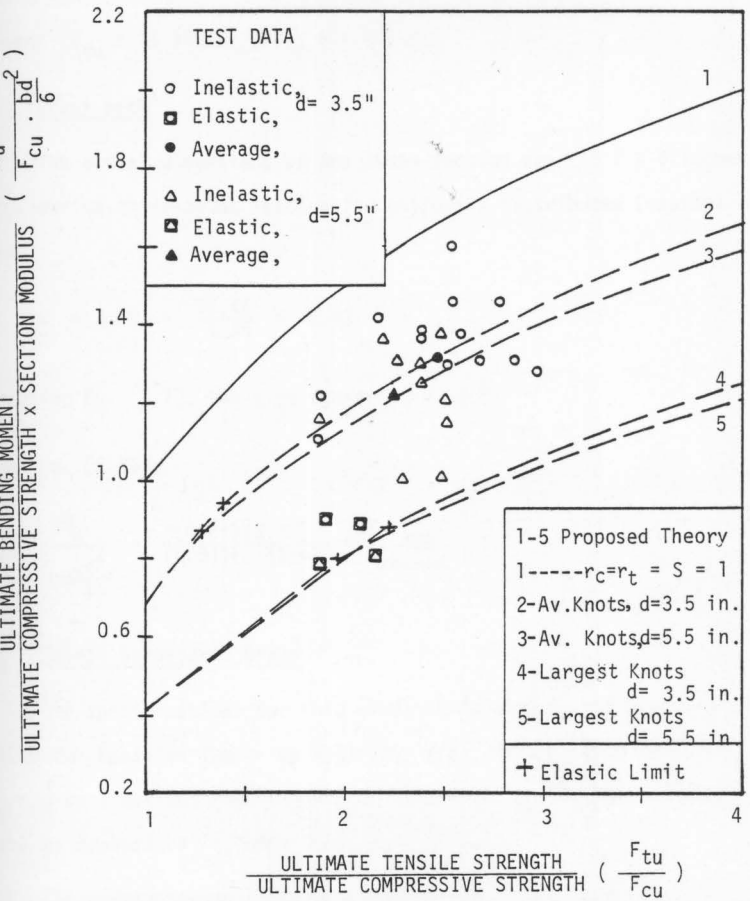

FIG. 8.17 COMPARISON BETWEEN THEORETICAL AND EXPERIMENTAL VALUES OF ULTIMATE BENDING MOMENT OF KNOTTED BEAMS SUBJECTED TO CENTRAL LOADING

Example

Given: F_{tu} = 15.46 ksi , F_{cu} = 6.35 ksi

a) Clear Beam

The actual dimensions of the cross-section are 1.5 x 3.5 inches. Considering third-point loading (or uniformly distributed loading) on the beam,

$$N = \frac{F_{tu}}{F_{cu}} = \frac{15.46}{6.35} = 2.43$$

By using Eq. [7.7], the size factor S = 0.81

From Eq. [3.23],

$$\frac{M_u}{F_{cu}\frac{bd^2}{6}} = \frac{3(0.81)(2.43)}{(0.81)(2.43)+2} = 1.488$$

b) Select Structural Grade

The specifications for this grade as defined by the standard grading rules for Canadian lumber by NLGA (25) are: maximum knot on narrow face, $k_n = \frac{3}{8}$ in.; maximum knot at edge of wide face, $k_e = \frac{3}{4}$ in.; and maximum knot at centerline of wide face, $k_w = \frac{7}{8}$ in.

The corresponding three knot ratios are: $\frac{K_n}{b}$ = 0.25; $\frac{k_w}{d}$ = 0.25; and $\frac{k_e}{d}$ = 0.21.

From Eq. [8.1], $\phi = [1 - 0.25]\,[1 - 0.25]\,[1 - 0.21]^2 = 0.35$

By using Eq. [8.2], $r_c = 0.71 + 0.35\,(0.35) = 0.83$

From Eq. [8.5], $r_t = 0.25 + 0.84\,(0.35) = 0.54$

By using Eq. [3.25],

$$\frac{M_u}{F_{cu}\frac{bd^2}{6}} = \frac{3(0.83)(0.54)(0.81)(2.43)}{(0.54)(0.81)(2.43)+2(0.83)} = 0.97 > r_c \text{ (inelastic behavior)}$$

Strentth Ratio = $\frac{0.97}{1.488} = \underline{\underline{0.65}}$

According to the ASTM Standard D245 (3), the strength ratio = $\underline{\underline{0.67}}$

c) No. 1 Grade

The specifications for this grade according to NLGA (25) are: $k_n = \frac{1}{2}$ in.; $k_w = 1\frac{1}{2}$ in. and $k_e = 1$ in.

The corresponding three knot ratios are: $\frac{k_n}{b} = 0.33$, $\frac{k_w}{d} = 0.43$ and $\frac{k_e}{d} = 0.29$.

From Eq. [8.1], $\phi = [1 - 0.33]\,[1 - 0.32]\,[1 - 0.29]^2 = 0.19$

By using Eq. [8.2], $r_c = 0.71 + 0.35\,(0.19) = 0.78$

From Eq. [8.5], $r_t = 0.25 + 0.84\,(0.19) = 0.41$

By using Eq. [3.25],

$$\frac{M_u}{F_{cu}\frac{bd^2}{6}} = \frac{3(0.78)(0.41)(0.81)(2.43)}{(0.41)(0.81)(2.43)+2(0.78)} = \underline{\underline{0.80}} > r_c \text{ (inelastic behavior)}$$

Strength ratio = $\frac{0.80}{1.488} = \underline{\underline{0.54}}$

According to the ASTM Standard, the strength ratio = $\underline{\underline{0.57}}$

It can be seen that the strength ratios calculated by using the proposed theory and the correlations accounting for the weakening effect

due to knots are in good agreement with the strength ratios given by the ASTM standard.

CHAPTER 9

CONCLUSIONS AND RECOMMENDATIONS

9.1 Conclusions

The following conclusions are drawn from the present investigation with a comprehensive appraisal of the study:

1. An ultimate bending strength theory for timber beams is developed. The theory predicts the ultimate bending moment capacity of the beam, using compressive and tensile strength values of the beam material obtained from direct tests on small clear specimens.
2. By conducting tests on different sizes of clear beams and beams with strength-reducing characteristics such as knots, and subjected to central and third-point loading, good agreement is observed between the theory and the experimental results.
3. By measuring strain at various levels along the depth of the beam, a linear variation of strain distribution is observed along the depth for all stages of loading up to failure.
4. The modulus of elasticity in tension is only about six percent greater than the corresponding value in compression.
5. At the proportional limit, as indicated by the load deflection curve, the neutral axis is approximately at the center of the beam depth. But at ultimate load, the neutral axis shifts towards the tension side of the beam by an amount varying between five to fifteen percent of the beam depth.

6. Based on direct tension and compression tests on small clear specimens matched with the beams, the ultimate tensile strength is found to be two to three times the ultimate compressive strength.
7. The proportional limit stress in bending is not significantly affected by the beam depth. For beams subjected to third-point loading, this stress is equal to the ultimate compressive strength of the beam material as obtained from direct tests. But for centrally loaded beams, the proportional limit stress in bending is about eleven percent greater than the value for similar beams loaded at third-span points.
8. The maximum tensile stress developed in the extreme fiber of a beam at failure is statistically less than the ultimate strength in direct tension obtained from tests on small size standard specimens. The actual value is dependent on the beam depth and is smaller as the depth of the beam is increased.
9. The maximum tensile stress at failure for a centrally loaded beam is about eleven percent greater than the corresponding value for a similar beam loaded at third-span points.
10. An empirical formula relating the maximum tensile stress at failure in a beam to its size, is derived.
11. The presence of knots influences the behavior of beams. For beams with small knots, the failure is of a compression-tension sequence; whereas beams with relatively large knots near the edge in the tension zone behave elastically up to the ultimate load and fail in tension only.
12. Correlation equations accounting for the weakening effect of knots on compressive and tensile strengths in beams, are obtained.

9.2 Recommendations

The following recommendations are made to further research on the behavior of timber beams:

1. Further experimental investigations should be carried out on bending of timber beams with high moisture content (green condition).
2. The effect of shear on the mode of failure should be investigated. The influence of shear might reduce the ultimate flexural moment capacity of the beam and failure could occur at a lower flexural moment corresponding to a combined flexural and shear mode of failure.
3. The study should be extended to cover other shapes of cross-sections such as box beams and I-beams.
4. The effect of end forces (compressive and tensile forces) on a beam under bending loads should also be investigated.

CHAPTER 10

REFERENCES

1. AMERICAN SOCIETY FOR TESTING AND MATERIALS. 1978. "Standard methods of testing small clear specimens of timber". ASTM D143-72. Philadelphia, Pennsylvania.
2. AMERICAN SOCIETY FOR TESTING AND MATERIALS. 1978. "Standard methods of static tests of timbers in structural sizes". ASTM D198-76. Philadelphia, Pennsylvania.
3. AMERICAN SOCIETY FOR TESTING AND MATERIALS. 1978. "Standard methods of establishing structural grades and related allowable properties for visually graded lumber". ASTM D245-74. Philadelphia, Pennsylvania.
4. BACH, C., and R. BAUMANN. 1924. "Elastizität und Festigkeit (Elasticity and Strength of Materials)". 9th edition, Berlin, Germany, pp. 300-308.
5. BECHTEL, S.C., and C.B. NORRIS. 1952. "Strength of wood beams of rectangular cross-section as affected by span-depth ratio". USDA Forest Service, Forest Products Laboratory Report No. 1910, Madison, Wisconsin.
6. BOHANNA, B. 1966. "Effect of size on bending strength of wood members". USDA Forest Service, Forest Products Laboratory Research paper FPL 56, Madison, Wisconsin.
7. BROCHARD, F.X. 1960. "Boiset charpente en Bois (Wood and Wood Structures)". Eyrolles, Paris, France, pp. 114-119.

8. CANADIAN STANDARDS ASSOCIATION. 1976. "Code for the engineering design of wood". CSA Standard 086-1976, Canadian Standards Assoc., Rexdale, Ontario, Canada.

9. COMBEN, A.J. 1957. "The effect of depth on the strength properties of timber beams with an analysis of the stresses and strains developed". Department of Scientific and Industrial Research, Forest Products Research, Special Report No. 12, London, England.

10. DEN HARTOG, J.P. "Strength of Materials". Dover Publications, Inc., New York.

11. DIETZ, A.G.H. 1941. "Stress-strain relationship in wooden beams subjected to pure bending". D.SC. dissertation, Massachusetts Institute of Technology, Cambridge, Massachusetts.

12. FOREST PRODUCTS LABORATORY. 1974. "Wood Handbook -- Wood as an engineering material". USDA Agricultural Handbook No. 72, Washington, D.C.

13. FREAS, A.D., and M.L. SELBO. 1954. "Fabrication and design of glue-laminated wood structural members". U.S. Forest Products Laboratory Technical Bulletin No. 1069, Madison, Wisconsin.

14. GURFINKEL, G. 1973. "Wood Engineering". Southern Forest Products Association. New Orleans, Louisiana.

15. KOLLMANN, F.F.P., and W.A. COTE, JR. 1968. "Principles of Wood Science and Technology -- Solid Wood" Springer-Verlag, New York, Inc.

16. KON, T. 1949. "On the laws of flexural rupture of wood". Hokkaido University Report, Sapporo, Japan.

17. KRUEGER, G.P. 1964. "Ultimate strength design of reinforced timber rigid frames with semi-rigid joints". Ph.D. dissertation, University of Wisconsin, Madison, Wisconsin.

18. LEICESTER, R.H. 1973. "Effect of size on the strength of structures". CSIRO, Australian Forest Products Laboratory, Division of Building Research Technological paper No. 71, Highett, Australia.

19. MALHOTRA, S.K. 1969. "Buckling strength of solid timber columns". Ph.D. dissertation, Nova Scotia Technical College, Halifax, Nova Scotia, Canada.

20. MALHOTRA, S.K. and S.J. MAZUR. 1970. "Buckling strength of solid timber columns". Transactions of the Engineering Institute of Canada, published in the Engineering Journal. 13(A-4): I-VII.

21. MARKWARDT, L.J., and T.R.C. WILSON. 1935. "Strength and related properties of woods grown in the United States". USDA Technical Bulletin No. 479. Madison, Wisconsin.

22. MAZUR, S.J. 1965. "Symposium on timber and timber structures -- Ultimate strength theory for rectangular wooden beams". Transactions of the Engineering Institute of Canada. 8(A-16): 7-11.

23. MOE, J. 1961. "The mechanism of failure of wood in bending". Publication International Association for Bridge and Structural Engineering. 21: 163-178.

24. NATIONAL FOREST PRODUCTS ASSOCIATION. 1977. "National design specification for wood construction". Washington, D.C.

25. NATIONAL LUMBER GRADES AUTHORITY. 1970. "Standard grading rules for Canadian lumber". Vancouver, British Columbia, Canada.

26. NEWLIN, J.A., and G.W. TRAYER. 1924. "Form factors of beams subjected to transverse loading only". NACA Report No. 1310, Washington, D.C. (Reproduced as USDA Forest Products Laboratory Report No. 1310, Madison, Wisconsin, 1941).

27. NWOKOYE, D.N. 1972. "An investigation into an ultimate beam theory for rectangular timber beams -- solid and laminated". Timber Research and Development Assocaition, Research Report E/RR/34, Buckinghamshire, England.

28. NWOKOYE, D.N. 1974. Discussion of "Inelastic bending of wood beams -- by B.D. Zakic". Journal of the Structural Division, Proceedings of the American Society of Civil Engineers. 100(ST9): 1963-1966.

29. O'HALLORAN, M.R. 1973. "Curvilinear stress-strain relationship for wood in compression". Ph.D. dissertation, Colorado State University, Fort Collins, Colorado.

30. PINCUS, G. 1967. "Nature of compression failure in wood". Journal of the Structural Division, Proceedings of the American Society of Civil Engineers. 93(ST3): 51-61.

31. PRAGER, V.W. 1933. "Über die querschnittsbemessung zweigurtiger holzholme (cross-sectional stress-distribution of double-flanged wood beams)". Zeitschrift für Flugtechnik und Motorluftschiffart, No. 19.

32. RADOK, J.R.M., J.P.O. SILBERSTEIN, and H.A. WILLS. 1948. "A new theory for the strength of wooden box beams". Australian Aeronautical Research Report ACA. 40, Melbourne, Australia.

33. RAMOS, A.N. 1961. "Stress-strain distribution in Douglas-fir beams within the plastic range". USDA Forest Service, Forest Products Laboratory Report No. 2231, Madison, Wisconsin.

34. ROBINSON, H., and D.W. COOPER. 1958. "The ultimate strength in bending of solid beams of structural grade European Redwood". Journal of the Institute of Wood Science. 1(2): 40-65.

35. ROS, M.S. 1936. "Das Holz als Bauschtoff (Wood as Structure Material)". I. Schweiz Kongr, Förderung Holzverw., Bern, Germany, p. 274.

36. SUENSON, E. 1941. "Die Lag der Nullinie in gebogenen Holzbalken". Holz als Roh - und Werkstoff. 4: 305-314.

37. SUKAPANPOTHARAM, S. 1966. "Glue-laminated timber beams of Tang, and Yang". M.Eng. dissertation, SEATO Graduate School of Engineering, Bangkok, Thailand.

38. THUNELL, B. 1939. Ing. Vet. Akad. Stockholm, H.3.

39. THUNELL, B. 1940. Ing. Vet. Akad. Stockholm, H.4.

40. WEIBULL, W. 1939. "A statistical theory of the strength of materials". Swedish Royal Institute for Engineering Research, Stockholm, Sweden.

41. WILSON, C.R. 1978. "Commentary on section 4 Sawn lumber of CSA 086-1976 Code for the engineering design of wood". Canadian Journal of Civil Engineering. 5: 11-17.

42. ZAKIC, B.D. 1973. "Inelastic bending of wood beams". Journal of the structural Division, Proceedings of the American Society of Civil Engineers. 99(ST10): 2079-2095.

APPENDIX A

TABLES

TABLE A.1.1 Material Property Test Results for 1.50 X 1.65 inches Eastern Spruce Clear Beams Subjected to Third-point Loading

Beam No.	Specific Gravity	Moisture Content (%)	Ultimate Compressive Strength of Matched Specimens (ksi)	Ultimate Tensile Strength of Matched Specimens (ksi)
1.1	0.431	11.8	7.79	17.60
1.2	0.399	11.5	7.29	13.08
1.3	0.419	11.6	7.78	15.04
1.4	0.374	11.5	6.52	12.51
1.5	0.427	11.6	7.79	15.47
1.6	0.421	11.6	7.59	14.35
1.7	0.443	11.3	8.01	14.00
1.8	0.378	11.5	5.29	13.59
1.9	0.376	11.6	6.98	14.33
1.10	0.405	11.7	7.62	16.50
1.11	0.398	11.6	7.36	13.82
1.12	0.448	11.6	8.01	17.95
1.13	0.365	11.9	5.48	13.31
1.14	0.408	11.5	6.90	11.02

TABLE A.1.2 Material Property Test Results for 1.50 X 1.65 inches Douglas-Fir Clear Beams Subjected to Third-point Loading

Beam No.	Specific Gravity	Moisture Content (%)	Ultimate Compressive Strength of Matched Specimens (ksi)	Ultimate Tensile Strength of Matched Specimens (ksi)
2.1	0.464	12.2	8.41	16.61
2.2	0.547	13.0	8.93	13.90
2.3	0.520	12.0	9.34	20.83
2.4	0.580	11.5	9.98	21.73
2.5	0.408	11.3	8.48	11.80
2.6	0.496	11.2	8.44	11.88
2.7	0.421	11.4	7.29	13.31
2.8	0.410	11.7	7.29	12.00
2.9	0.490	11.5	9.53	16.63

TABLE A.1.3 Material Property Test Results for 2 X 4 Eastern Spruce Clear Beams Subjected to Third-point Loading

Beam No.	Specific Gravity	Moisture Content (%)	Ultimate Compressive Strength of Matched Specimens (ksi)	Ultimate Tensile Strength of Matched Specimens (ksi)
3.1	0.384	12.0	6.89	15.98
3.2	0.378	12.1	6.49	18.89
3.3	0.438	12.1	7.20	22.68
3.4	0.430	11.9	7.69	22.85
3.5	0.399	12.0	6.89	19.91
3.6	0.380	12.0	6.72	20.62
3.7	0.405	12.0	7.10	17.82
3.8	0.372	11.9	7.26	17.00
3.9	0.386	12.5	6.77	16.88
3.10	0.387	11.9	6.54	17.94
3.11	0.390	11.9	6.62	15.49
3.12	0.379	11.9	6.56	17.58
3.13	0.384	11.9	6.72	19.18
3.14	0.439	12.1	7.10	14.70
3.15	0.449	11.7	8.05	23.59
3.16	0.429	12.4	6.14	14.62
3.17	0.378	12.0	5.83	16.45
3.18	0.396	12.0	6.43	18.12
3.19	0.383	11.9	6.65	20.60
3.20	0.372	11.8	6.34	12.44

TABLE A.1.4 Material Property Test Results for 2 X 6 Eastern Spruce Clear Beams Subjected to Third-point Loading

Beam No.	Specific Gravity	Moisture Content (%)	Ultimate Compressive Strength of Matched Specimens (ksi)	Ultimate Tensile Strength of Matched Specimens (ksi)
4.1	0.410	12.8	6.55	17.31
4.2	0.432	13.0	5.00	15.68
4.3	0.362	12.8	4.34	13.24
4.4	0.430	12.6	6.69	13.97
4.5	0.415	12.6	6.88	17.22
4.6	0.392	12.5	6.35	15.66
4.7	0.399	12.3	6.53	15.75
4.8	0.418	12.2	6.45	15.15
4.9	0.444	12.3	7.30	16.06
4.10	0.396	12.2	6.34	15.74
4.11	0.385	12.1	6.54	15.67
4.12	0.416	12.2	6.85	17.44
4.13	0.396	12.3	6.17	15.69
4.14	0.399	12.2	6.37	16.70
4.15	0.394	12.1	6.34	14.10
4.16	0.396	12.0	6.23	14.88
4.17	0.390	11.9	5.99	15.78

TABLE A.1.5 Material Property Test Results for 2 X 6 Douglas-Fir Clear Beams Subjected to Third-Point Loading

Beam No.	Specific Gravity	Moisture Content (%)	Ultimate Compressive Strength of Matched Specimens (ksi)	Ultimate Tensile Strength of Matched Specimens (ksi)
5.1	0.412	12.8	6.55	11.20
5.2	0.421	12.7	6.17	14.68
5.3	0.547	14.0	7.41	22.10
5.4	0.520	13.0	9.98	22.29
5.5	0.496	12.2	7.02	16.66
5.6	0.421	12.4	5.72	12.61
5.7	0.410	12.7	7.29	12.57
5.8	0.490	12.5	7.90	21.94

TABLE A.1.6 Material Property Test Results for 2 X 6 Eastern Spruce Clear Stiffened Beams Subjected to Third-point Loading

Beam No.	Specific Gravity	Moisture Content (%)	Ultimate Compressive Strength of Matched Specimens (ksi)	Ultimate Tensile Strength of Matched Specimens (ksi)
6.1	0.368	11.1	5.95	11.64
6.2	0.417	11.8	6.00	11.51
6.3	0.446	11.7	6.10	15.00
6.4	0.443	12.1	6.67	16.56
6.5	0.397	11.5	5.67	16.56
6.6	0.396	12.7	4.70	9.13
6.7	0.399	11.1	6.24	16.56
6.8	0.417	11.8	6.23	14.71
6.9	0.350	12.3	4.70	9.41
6.10	0.410	12.9	4.95	12.14
6.11	0.460	12.2	6.19	15.38
6.12	0.445	12.1	6.26	15.72
6.13	0.394	12.4	4.02	15.34
6.14	0.493	11.0	6.24	13.38
6.15	0.430	11.6	4.40	12.10
6.16	0.385	12.7	5.19	14.71
6.17	0.434	11.5	6.18	16.86
6.18	0.414	13.1	4.58	9.83

TABLE A.1.6 (Cont'd)

Beam No.	Specific Gravity	Moisture Content (%)	Ultimate Compressive Strength of Matched Specimens (ksi)	Ultimate Tensile Strength of Matched Specimens (ksi)
6.19	0.399	11.9	5.47	9.91
6.20	0.407	12.1	5.67	9.93
6.21	0.410	11.5	6.38	12.59
6.22	0.417	11.6	6.35	14.04
6.23	0.350	12.0	4.40	10.37
6.24	0.350	12.0	4.40	11.67

TABLE A.1.7 Material Property Test Results for 2 X 6 Douglas-Fir Clear Stiffened Beams Subjected to Third-point Loading

Beam No.	Specific Gravity	Moisture Content (%)	Ultimate Compressive Strength of Matched Specimens (ksi)	Ultimate Tensile Strength of Matched Specimens (ksi)
7.1	0.480	11.4	7.70	16.36
7.2	0.462	11.7	6.95	14.06
7.3	0.467	11.5	6.82	12.13
7.4	0.441	12.5	5.57	13.85
7.5	0.457	11.9	6.67	13.32
7.6	0.450	12.1	6.48	15.21
7.7	0.452	12.1	6.44	13.37
7.8	0.450	12.1	6.44	15.88

TABLE A.1.8 Material Property Test Results for 2 X 8 Eastern Spruce Clear Beams Subjected to Third-Point Loading

Beam No.	Specific Gravity	Moisture Content (%)	Ultimate Compressive Strength of Matched Specimens (ksi)	Ultimate Tensile Strength of Matched Specimens (ksi)
8.1	0.416	12.5	6.15	15.62
8.2	0.402	12.3	5.56	12.25
8.3	0.390	12.6	6.10	15.93
8.4	0.473	12.4	7.54	22.17
8.5	0.382	12.6	6.00	14.45
8.6	0.364	12.5	5.75	14.06
8.7	0.373	12.4	6.22	13.41
8.8	0.381	12.4	5.91	16.97
8.9	0.409	12.6	5.56	12.88
8.10	0.400	12.3	5.56	12.50

TABLE A.1.9 Material Property Test Results for 4 x 12 Eastern Spruce Clear Beams Subjected to Third-point Loading

Beam No.	Specific Gravity	Moisture Content (%)	Ultimate Compressive Strength of Matched Specimens (ksi)	Ultimate Tensile Strength of Matched Specimens (ksi)
9.1	0.379	18.0	4.15	11.20
9.2	0.386	17.3	4.36	10.94
9.3	0.404	17.0	4.49	10.20
9.4	0.390	15.2	5.08	13.90
9.5	0.416	15.4	5.00	14.60

Table A.1.10 Material Property Test Results for 1.50 X 1.65 inches Eastern Spruce Clear Beams Subjected to Central Loading

Beam No.	Specific Gravity	Moisture Content (%)	Ultimate Compressive Strength of Matched Specimens (ksi)	Ultimate Tensile Strength of Matched Specimens (ksi)
10.1	0.431	11.8	7.98	16.66
10.2	0.399	11.5	7.29	13.47
10.3	0.419	11.6	7.81	17.30
10.4	0.374	11.5	6.50	14.18
10.5	0.427	11.6	7.81	14.78
10.6	0.421	11.6	7.61	16.35
10.7	0.443	11.3	7.97	13.79
10.8	0.378	11.5	6.65	16.67
10.9	0.376	11.6	7.02	13.53
10.10	0.405	11.7	7.61	18.60
10.11	0.448	11.6	8.03	20.38
10.12	0.365	11.9	5.52	15.00
10.13	0.408	11.5	6.89	12.55

TABLE A.1.11 Material Property Test Results for 1.50 X 1.65 inches Douglas-Fir Clear Beams Subjected to Central Loading

Beam No.	Specific Gravity	Moisture Content (%)	Ultimate Compressive Strength of Matched Specimens (ksi)	Ultimate Tensile Strength of Matched Specimens (ksi)
11.1	0.464	12.2	7.29	15.69
11.2	0.547	12.0	8.88	19.72
11.3	0.520	12.0	9.49	24.76
11.4	0.580	11.5	9.98	29.08
11.5	0.408	11.3	6.51	13.65
11.6	0.496	11.2	8.41	15.11
11.7	0.421	11.4	6.89	16.18
11.8	0.410	11.7	7.29	16.20
11.9	0.490	11.5	9.49	26.13

TABLE A.1.12 Material Property Test Results for 2 X 4 Eastern Spruce Clear Beams Subjected to Central Loading

Beam No.	Specific Gravity	Moisture Content (%)	Ultimate Compressive Strength of Matched Specimens (ksi)	Ultimate Tensile Strength of Matched Specimens (ksi)
12.1	0.384	13.0	6.53	14.28
12.2	0.378	13.1	6.36	17.12
12.3	0.438	13.1	6.88	20.52
12.4	0.430	12.9	7.35	22.98
12.5	0.399	13.0	6.70	17.90
12.6	0.380	13.0	5.90	18.55
12.7	0.405	13.0	6.98	15.97
12.8	0.372	12.9	6.37	15.18
12.9	0.386	13.5	5.97	15.27
12.10	0.387	12.9	5.76	17.88
12.11	0.390	12.9	5.77	13.83
12.12	0.379	12.9	6.38	15.98
12.13	0.384	12.9	5.86	17.25
12.14	0.439	13.1	6.98	17.80
12.15	0.449	12.7	7.82	21.13
12.16	0.420	13.4	6.01	14.34
12.17	0.378	13.0	5.72	14.75
12.18	0.396	13.0	6.20	16.20
12.19	0.382	12.9	6.20	20.54
12.20	0.372	12.8	6.20	11.18

TABLE A.1.13 Material Property Test Results for 2 X 6 Eastern Spruce Clear Beams Subjected to Central Loading

Beam No.	Specific Gravity	Moisture Content (%)	Ultimate Compressive Strength of Matched Specimens (ksi)	Ultimate Tensile Strength of Matched Specimens (ksi)
13.1	0.420	13.1	6.61	17.66
13.2	0.410	13.3	6.77	16.60
13.3	0.379	13.0	5.70	13.88
13.4	0.408	13.1	6.43	19.32
13.5	0.388	13.3	5.31	15.15
13.6	0.398	13.1	6.81	17.26
13.7	0.364	13.2	5.22	15.13
13.8	0.355	13.0	5.22	14.05
13.9	0.406	13.1	6.77	14.70
13.10	0.400	13.1	6.62	16.36
13.11	0.420	12.8	6.91	13.86
13.12	0.359	13.0	5.30	16.58
13.13	0.357	13.1	5.30	13.41
13.14	0.385	13.2	6.62	15.69
13.15	0.378	13.1	6.35	15.67
13.16	0.425	13.1	6.91	20.42
13.17	0.347	13.4	4.63	15.05
13.18	0.387	13.0	6.01	12.46
13.19	0.411	13.1	6.93	13.50
13.20	0.396	13.0	6.43	19.31
13.21	0.402	13.0	5.38	13.54

TABLE A.1.14 Material Property Test Results for 2 X 6 Douglas-Fir Clear Beams Subjected to Central Loading

Beam No.	Specific Gravity	Moisture Content (%)	Ultimate Compressive Strength of Matched Specimens (ksi)	Ultimate Tensile Strength of Matched Specimens (ksi)
14.1	0.465	12.7	6.49	14.05
14.2	0.390	12.8	6.56	12.44
14.3	0.658	13.1	9.98	20.28
14.4	0.580	12.0	9.98	25.60
14.5	0.543	11.9	9.98	19.84
14.6	0.408	11.8	6.56	12.51
14.7	0.409	11.9	7.17	13.24
14.8	0.468	12.4	8.64	20.54

TABLE A.1.15 Material Property Test Results for 2 X 8 Eastern Spruce Clear Beams Subjected to Central Loading

Beam No.	Specific Gravity	Moisture Content (%)	Ultimate Compressive Strength of Matched Specimens (ksi)	Ultimate Tensile Strength of Matched Specimens (ksi)
15.1	0.400	13.5	5.90	14.60
15.2	0.352	13.8	4.72	14.81
15.3	0.353	13.7	5.08	16.42
15.4	0.384	13.7	5.57	17.99
15.5	0.350	13.4	4.55	12.19
15.6	0.352	13.5	5.03	14.68
15.7	0.366	13.3	5.48	17.10
15.8	0.435	13.6	6.09	20.19
15.9	0.377	13.5	5.00	13.38
15.10	0.391	13.5	5.28	17.88

TABLE A.1.16 Material Property Test Results for 4 X 12 Eastern Spruce Clear Beams Subjected to Central Loading

Beam No.	Specific Gravity	Moisture Content (%)	Ultimate Compressive Strength of Matched Specimens (ksi)	Ultimate Tensile Strength of Matched Specimens (ksi)
16.1	0.361	20.4	3.10	9.48
16.2	0.392	17.5	4.27	11.29
16.3	0.404	18.2	4.03	10.67
16.4	0.364	18.0	3.91	13.37
16.5	0.362	17.8	4.03	10.04

TABLE A.1.17 Material Property Test Results for 2 X 4 Eastern Spruce Knotted Beams Subjected to Third-point Loading

Beam No.	Specific Gravity	Moisture Content (%)	Ultimate Compressive Strength of Matched Specimens (ksi)	Ultimate Tensile Strength of Matched Specimens (ksi)
17.1	0.443	11.9	6.12	19.55
17.2	0.433	12.1	6.47	16.43
17.3	0.371	11.9	6.30	13.06
17.4	0.421	12.1	5.55	10.19
17.5	0.480	12.1	7.80	16.93
17.6	0.369	11.7	5.23	13.22
17.7	0.374	11.6	5.37	12.86
17.8	0.425	11.8	6.97	17.44
17.9	0.417	12.1	6.35	16.94
17.10	0.400	12.1	4.72	15.97
17.11	0.390	12.3	6.07	11.33
17.12	0.430	11.4	6.73	19.19
17.13	0.428	11.8	6.97	19.18
17.14	0.478	12.0	7.41	19.81
17.15	0.361	12.3	4.72	16.26

TABLE A.1.18 Material Property Test Results for 2 X 6 Eastern Spruce Knotted Beams Subjected to Third-point Loading

Beam No.	Specific Gravity	Moisture Content (%)	Ultimate Compressive Strength of Matched Specimens (ksi)	Ultimate Tensile Strength of Matched Specimens (ksi)
18.1	0.383	11.2	6.22	16.00
18.2	0.434	11.5	7.18	19.07
18.3	0.373	11.1	6.38	18.13
18.4	0.482	11.6	8.03	18.60
18.5	0.442	11.6	7.20	16.28
18.6	0.350	10.6	5.65	11.82
18.7	0.378	10.8	6.78	14.49
18.8	0.343	10.2	6.15	13.84
18.9	0.395	11.0	6.40	12.91
18.10	0.337	10.5	6.78	11.61
18.11	0.423	11.0	7.37	16.02
18.12	0.451	10.8	7.87	14.22

TABLE A.1.19 Material Property Test Results for 2 X 4 Eastern Spruce Knotted Beams Subjected to Central Loading

Beam No.	Specific Gravity	Moisture Content (%)	Ultimate Compressive Strength of Matched Specimens (ksi)	Ultimate Tensile Strength of Matched Specimens (ksi)
19.1	0.369	11.9	5.23	13.22
19.2	0.390	12.1	6.07	11.33
19.3	0.443	12.0	6.12	17.75
19.4	0.374	11.9	5.37	12.86
19.5	0.430	12.1	6.73	19.19
19.6	0.433	12.1	6.47	16.43
19.7	0.425	11.7	6.97	17.44
19.8	0.428	11.6	6.47	19.18
19.9	0.371	11.8	6.30	13.06
19.10	0.417	12.1	6.35	16.94
19.11	0.478	12.1	7.14	19.81
19.12	0.421	12.3	5.55	10.19
19.13	0.400	11.4	4.72	15.97
19.14	0.361	11.8	5.37	13.87
19.15	0.480	12.3	7.80	16.93

TABLE A.1.20 Material Property Test Results for 2 X 6 Eastern Spruce Knotted Beams Subjected to Central Loading

Beam No.	Specific Gravity	Moisture Content (%)	Ultimate Compressive Strength of Matched Specimens (ksi)	Ultimate Tensile Strength of Matched Specimens (ksi)
20.1	0.452	9.9	7.83	17.03
20.2	0.347	9.2	5.70	13.53
20.3	0.407	10.4	7.37	18.44
20.4	0.445	10.6	7.33	18.15
20.5	0.424	10.6	6.78	15.33
20.6	0.430	11.0	8.05	14.97
20.7	0.383	11.2	7.83	17.03
20.8	0.434	11.5	5.70	13.53
20.9	0.373	11.1	7.37	18.44
20.10	0.442	11.6	7.33	18.15
20.11	0.442	11.6	6.78	15.33
20.12	0.482	10.2	8.05	14.97

TABLE A.2.1: Beam Test Results of 1.50 X 1.65 inches Eastern Spruce Clear Specimens Subjected to Third-point Loading

Beam No.	Compressive Modulus of Elasticity E_c ($X10^3$ksi)	Tensile Modulus of Elasticity E_t ($X10^3$ksi)	At Proportional Limit Load				At Ultimate Load			
			Stress F_{pl} (ksi)	Maximum Compressive Strain ($X10^{-3}$)	Maximum Tensile Strain ($X10^{-3}$)	N.A. Position Factor from Bottom of Beam	Ultimate Bending Moment M_u (in-k)	Maximum Tensile Strain ε_t ($X10^{-3}$)	Maximum Tensile Stress F_t (ksi)	N.A. Position Factor from Bottom of Beam γ
1.1	1.93	1.99	8.02	4.21	4.03	0.500	8.43	7.52	14.96	0.424
1.2	1.99	1.93	8.02	3.97	4.16	0.491	7.29	5.83	11.25	0.464
1.3	1.56	1.70	6.85	4.46	4.03	0.485	7.29	7.08	12.03	0.440
1.4	1.65	1.65	6.85	4.33	4.15	0.500	6.55	6.52	10.76	0.458
1.5	1.61	1.68	8.02	4.51	4.76	0.509	8.43	9.21	15.47	0.439
1.6	1.59	1.70	7.29	4.58	4.28	0.485	7.74	8.02	13.63	0.424
1.7	1.82	2.25	7.29	4.13	3.24	0.450	6.94	4.89	11.00	0.445
1.8	1.41	1.41	6.56	4.64	4.64	0.491	7.09	8.77	12.37	0.430
1.9	1.85	1.85	6.56	3.60	3.54	0.491	7.14	7.51	13.90	0.394

TABLE A.2.1 (Cont'd)

Beam No.	Compressive Modulus of Elasticity E_c ($X10^3$ksi)	Tensile Modulus of Elasticity E_t ($X10^3$ksi)	At Proportional Limit Load				At Ultimate Load			
			Stress F_{pl} (ksi)	Maximum Compressive Strain ($X10^{-3}$)	Maximum Tensile Strain ($X10^{-3}$)	N.A. Position Factor from Bottom of Beam	Ultimate Bending Moment M_u (in-k)	Maximum Tensile Strain ε_t ($X10^{-3}$)	Maximum Tensile Stress F_t (ksi)	N.A. Position Factor from Bottom of Beam γ
1.10	2.12	2.12	8.31	3.91	3.91	0.491	8.38	7.08	15.01	0.391
1.11	1.98	2.09	7.29	3.91	3.48	0.500	7.44	6.08	12.71	0.448
1.12	1.94	1.72	8.02	4.28	4.64	0.500	8.04	8.14	14.00	0.440
1.13	1.42	1.67	5.10	3.42	3.06	0.500	5.46	6.14	10.25	0.476
1.14	1.97	2.06	6.56	3.48	3.18	0.464	6.05	4.76	9.81	0.451

TABLE A.2.2: Beam Test Results of 1.50 X 1.65 inches Douglas-Fir Clear Specimens Subjected To Third-point Loading

Beam No.	Compressive Modulus of Elasticity E_c ($X10^3$ksi)	Tensile Modulus of Elasticity E_t ($X10^3$ksi)	At Proportional Limit Load				At Ultimate Load			
			Stress F_{pl} (ksi)	Maximum Compressive Strain ($X10^{-3}$)	Maximum Tensile Strain ($X10^{-3}$)	N.A. Position Factor from Bottom of Beam	Ultimate Bending Moment M_u (in-k)	Maximum Tensile Strain ε_t ($X10^{-3}$)	Maximum Tensile Stress F_t (ksi)	N.A. Position Factor from Bottom of Beam γ
2.1	2.38	2.38	8.75	3.67	3.67	0.500	9.08	6.77	16.11	0.412
2.2	1.75	1.93	8.75	5.19	4.52	0.500	7.54	5.76	11.12	0.464
2.3	2.63	2.29	10.93	4.52	4.77	0.500	10.91	8.46	19.37	0.455
2.4	2.40	2.67	11.66	5.07	4.13	0.450	11.71	8.14	21.73	0.450
2.5	1.67	1.73	8.31	4.70	4.64	0.482	6.94	6.27	10.85	0.473
2.6	1.85	1.96	8.02	4.64	4.09	0.464	7.14	5.64	11.05	0.455
2.7	1.90	1.73	7.29	4.28	4.22	0.482	7.14	7.39	12.78	0.439
2.8	1.36	1.47	6.56	5.13	4.46	0.482	6.45	7.02	10.32	0.452
2.9	2.40	2.53	10.20	4.40	4.03	0.464	9.72	6.64	16.80	0.403

TABLE A.2.3: Beam Test Results of 2 X 4 Eastern Spruce Clear Specimens Subjected to Third-point Loading

Beam No.	Compressive Modulus of Elasticity E_c ($X10^3$ksi)	Tensile Modulus of Elasticity E_t ($X10^3$ksi)	At Proportional Limit Load				At Ultimate Load			
			Stress F_{pl} (ksi)	Maximum Compressive Strain ($X10^{-3}$)	Maximum Tensile Strain ($X10^{-3}$)	N.A. Position Factor from Bottom of Beam	Ultimate Bending Moment M_u (in-k)	Maximum Tensile Strain ε_t ($X10^{-3}$)	Maximum Tensile Stress F_t (ksi)	N.A. Position Factor from Bottom of Beam γ
3.1	1.98	2.07	6.82	3.46	3.31	0.500	32.30	7.41	15.34	0.411
3.2	1.85	1.85	7.14	3.93	3.88	0.500	32.30	6.64	12.28	0.429
3.3	1.96	1.96	8.07	3.46	3.48	0.479	38.00	7.52	14.74	0.371
3.4	2.36	2.21	8.69	3.76	3.93	0.500	37.50	6.41	14.17	0.443
3.5	2.08	2.08	6.82	3.28	3.28	0.486	33.25	7.08	14.73	0.429
3.6	2.02	2.09	8.07	4.04	3.87	0.493	34.20	6.41	13.40	0.429
3.7	1.67	1.67	6.82	4.10	4.10	0.500	32.30	9.07	15.15	0.434
3.8	1.92	1.94	6.82	3.56	3.53	0.500	33.25	8.41	16.32	0.343
3.9	2.15	2.11	7.45	3.46	3.53	0.486	34.68	6.64	14.01	0.434
3.10	2.29	1.81	7.45	3.26	4.12	0.500	32.30	6.64	12.02	0.434
3.11	2.17	2.24	8.07	3.72	3.61	0.500	35.15	6.36	14.25	0.429
3.12	1.85	1.85	6.82	3.50	3.72	0.486	34.20	8.74	16.17	0.400
3.13	2.16	1.94	7.45	3.46	3.86	0.500	34.20	7.02	13.62	0.429

TABLE A.2.3 (Cont'd)

Beam No.	Compressive Modulus of Elasticity E_c ($X10^3$ksi)	Tensile Modulus of Elasticity E_t ($X10^3$ksi)	At Proportional Limit Load: Stress F_{pl} (ksi)	At Proportional Limit Load: Maximum Compressive Strain ($X10^{-3}$)	At Proportional Limit Load: Maximum Tensile Strain ($X10^{-3}$)	At Proportional Limit Load: N.A. Position Factor from Bottom of Beam	At Ultimate Load: Ultimate Bending Moment M_u (in-k)	At Ultimate Load: Maximum Tensile Strain ε_t ($X10^{-3}$)	At Ultimate Load: Maximum Tensile Stress F_t (ksi)	At Ultimate Load: N.A. Position Factor from Bottom of Beam γ
3.14	1.76	1.61	6.82	4.04	4.26	0.500	34.20	9.95	16.02	0.423
3.15	2.49	2.58	8.69	3.48	3.37	0.500	38.95	7.59	19.58	0.386
3.16	1.62	1.62	6.82	4.22	4.23	0.500	31.35	7.85	12.72	0.434
3.17	1.95	2.02	6.82	3.72	3.39	0.500	31.35	7.74	15.63	0.360
3.18	1.77	2.02	6.82	4.15	3.39	0.457	31.35	8.52	17.21	0.371
3.19	1.96	2.01	6.58	3.60	3.28	0.500	31.35	6.97	14.01	0.436
3.20	2.03	2.15	5.58	3.22	2.73	0.450	26.60	4.63	9.95	0.393

TABLE A.2.4 Beam Test Results of 2 X 6 Eastern Spruce Clear Specimens Subjected to Third-point Loading

Beam No.	Compressive Modulus of Elasticity E_c ($X10^3$ksi)	Tensile Modulus of Elasticity E_t ($X10^3$ksi)	At Proportional Limit Load				At Ultimate Load			
			Stress F_{pl} (ksi)	Maximum Compressive Strain ($X10^{-3}$)	Maximum Tensile Strain ($X10^{-3}$)	N.A. Position Factor from Bottom of Beam	Ultimate Bending Moment M_u (in-k)	Maximum Tensile Strain ε_t ($X10^{-3}$)	Maximum Tensile Stress F_t (ksi)	N.A. Position Factor from Bottom of Beam γ
4.1	2.18	2.25	6.94	3.17	3.08	0.500	77.25	5.00	11.25	0.473
4.2	1.80	1.80	5.95	3.33	3.28	0.491	69.00	5.75	10.35	0.445
4.3	1.51	1.49	5.16	3.38	3.44	0.482	61.50	7.02	10.46	0.431
4.4	2.15	2.25	6.35	3.20	2.81	0.482	69.00	4.47	10.06	0.458
4.5	2.30	2.41	6.74	2.88	2.78	0.482	78.00	5.43	13.09	0.409
4.6	1.87	1.96	6.35	3.42	3.23	0.473	71.25	5.59	10.96	0.427
4.7	1.40	1.47	5.55	4.02	3.74	0.473	62.25	6.54	9.61	0.415
4.8	1.84	1.81	5.55	3.14	3.06	0.491	69.00	5.69	10.30	0.436
4.9	1.69	1.69	5.55	3.32	3.27	0.491	66.75	6.27	10.60	0.445
4.10	1.69	1.46	6.15	3.49	4.18	0.527	69.00	8.30	12.12	0.473

TABLE A.2.4 (Cont'd)

Beam No.	Compressive Modulus of Elasticity E_c ($X10^3$ksi)	Tensile Modulus of Elasticity E_t ($X10^3$ksi)	At Proportional Limit Load				At Ultimate Load			
			Stress F_{pl} (ksi)	Maximum Compressive Strain ($X10^{-3}$)	Maximum Tensile Strain ($X10^{-3}$)	N.A. Position Factor from Bottom of Beam	Ultimate Bending Moment M_u (in-k)	Maximum Tensile Strain ε_t ($X10^{-3}$)	Maximum Tensile Stress F_t (ksi)	N.A. Position Factor from Bottom of Beam γ
4.11	1.98	2.08	6.74	3.54	3.23	0.482	73.50	7.23	15.04	0.377
4.12	1.93	2.05	7.54	3.81	3.65	0.476	78.75	6.21	12.73	0.404
4.13	1.79	1.92	6.35	3.61	3.28	0.478	72.75	5.81	11.14	0.455
4.14	1.97	2.05	7.14	3.78	3.46	0.482	77.25	6.11	12.53	0.441
4.15	1.81	1.77	6.15	3.32	3.45	0.509	67.50	5.34	9.45	0.476
4.16	2.02	2.27	6.35	3.26	2.78	0.500	66.00	4.26	9.67	0.436
4.17	2.04	1.96	6.35	3.14	3.23	0.491	75.00	6.60	12.94	0.422

TABLE A.2.5 Beams Test Results of 2 X 6 Douglas-Fir Clear Specimen Subjected to Third-point Loading

Beam No.	Compressive Modulus of Elasticity E_c ($X10^3$ksi)	Tensile Modulus of Elasticity E_t ($X10^3$ksi)	At Proportional Limit Load				At Ultimate Load			
			Stress F_{pl} (ksi)	Maximum Compressive Strain ($x10^{-3}$)	Maximum Tensile Strain ($X10^{-3}$)	N.A. Position Factor from Bottom of Beam	Ultimate Bending Moment M_u (in-k)	Maximum Tensile Strain ε_t ($X10^{-3}$)	Maximum Tensile Stress F_t (ksi)	N.A. Position Factor from Bottom of Beam γ
5.1	1.87	1.70	6.35	3.86	3.70	0.482	71.25	6.33	10.76	0.424
5.2	1.87	2.05	5.55	2.98	2.70	0.491	57.00	4.00	8.22	0.455
5.3	1.78	2.09	7.93	4.45	3.78	0.455	96.75	8.46	17.68	0.418
5.4	2.64	2.64	10.11	3.81	3.81	0.500	99.00	5.49	14.49	0.473
5.5	1.56	1.92	6.74	4.44	3.49	0.436	75.00	5.64	10.83	0.391
5.6	1.49	1.37	5.55	3.64	4.03	0.491	60.00	6.17	8.45	0.455
5.7	1.82	2.01	7.14	3.92	3.52	0.482	67.50	4.69	9.43	0.473
5.8	2.42	2.50	8.53	3.49	3.38	0.500	91.50	7.02	17.55	0.404

TABLE A.2.6 Beam Test Results of 2 X 6 Eastern Spruce Clear Stiffened Specimens Subjected to Third-point Loading

Beam No.	Compressive Modulus of Elasticity E_c ($X10^3$ksi)	Tensile Modulus of Elasticity E_t ($X10^3$ksi)	At Proportional Limit Load				At Ultimate Load			
			Stress F_{pl} (ksi)	Maximum Compressive Strain ($x10^{-3}$)	Maximum Tensile Strain ($X10^{-3}$)	N.A. Position Factor from Bottom of Beam	Ultimate Bending Moment M_u (in-k)	Maximum Tensile Strain ε_t ($X10^{-3}$)	Maximum Tensile Stress F_t (ksi)	N.A. Position Factor from Bottom of Beam γ
6.1	1.76	1.88	6.49	3.86	3.45	0.500	63.00	4.90	9.22	0.455
6.2	1.65	1.69	6.13	3.80	3.65	0.500	60.00	5.12	8.65	0.470
6.3	1.79	1.94	6.64	3.83	3.42	0.491	75.00	6.00	11.64	0.455
6.4	1.94	1.77	6.85	3.53	3.86	0.509	70.50	6.14	10.87	0.451
6.5	1.40	1.53	6.13	4.41	4.00	0.500	70.50	8.90	13.61	0.391
6.6	1.30	1.37	4.46	3.61	3.26	0.500	45.00	4.72	6.46	0.475
6.7	2.04	1.96	6.35	3.14	3.23	0.491	75.00	6.60	12.91	0.422
6.8	1.69	1.77	6.49	4.03	3.67	0.495	70.50	6.60	11.69	0.436
6.9	1.49	1.40	4.98	3.35	3.56	0.500	55.00	6.39	8.94	0.420
6.10	1.47	1.47	5.41	3.78	3.68	0.500	60.00	6.20	9.11	0.468
6.11	1.84	1.88	6.53	3.72	3.48	0.500	70.50	6.11	11.48	0.433
6.12	1.86	1.95	6.57	3.89	3.37	0.496	70.50	6.25	12.18	0.400

TABLE A.2.6 (Cont'd)

Beam No.	Compressive Modulus of Elasticity E_c ($X10^3$ksi)	Tensile Modulus of Elasticity E_t ($X10^3$ksi)	At Proportional Limit Load				At Ultimate Load			
			Stress F_{pl} (ksi)	Maximum Compressive Strain ($x10^{-3}$)	Maximum Tensile Strain ($X10^{-3}$)	N.A. Position Factor from Bottom of Beam	Ultimate Bending Moment M_u (in-k)	Maximum Tensile Strain ε_t ($X10^{-3}$)	Maximum Tensile Stress F_t (ksi)	N.A. Position Factor from Bottom of Beam γ
6.13	1.41	1.49	4.03	3.00	2.70	0.496	48.00	6.38	9.51	0.379
6.14	1.36	1.56	6.54	5.30	4.19	0.486	72.00	7.85	12.25	0.429
6.15	1.30	1.28	4.33	3.34	3.38	0.500	45.00	5.44	6.97	0.470
6.16	1.50	1.49	5.53	3.78	3.70	0.500	60.00	6.64	9.90	0.426
6.17	2.12	2.13	6.13	3.18	2.87	0.500	69.00	5.70	12.15	0.420
6.18	1.34	1.44	4.33	3.54	3.00	0.496	48.00	6.10	8.79	0.400
6.19	1.74	1.74	5.95	3.53	3.45	0.500	60.00	4.93	8.58	0.467
6.20	1.73	1.74	5.95	3.60	3.42	0.500	60.00	5.00	8.68	0.467
6.21	2.09	2.16	6.35	3.18	2.94	0.491	69.00	5.04	10.89	0.440
6.22	1.48	1.43	6.95	4.68	4.86	0.509	66.00	6.45	9.23	0.470
6.23	1.33	1.32	4.46	3.35	3.38	0.500	45.00	5.78	7.63	0.446
6.24	1.20	1.29	4.18	3.69	3.25	0.489	48.00	6.18	7.98	0.433

TABLE A.2.7 Beam Test Results of 2 X 6 Douglas-Fir Clear Stiffened Specimens Subject to Third-point Loading

Beam No.	Compressive Modulus of Elasticity E_c ($X10^3$ksi)	Tensile Modulus of Elasticity E_t ($X10^3$ksi)	At Proportional Limit Load				At Ultimate Load			
			Stress F_{pl} (ksi)	Maximum Compressive Strain ($x10^{-3}$)	Maximum Tensile Strain ($X10^{-3}$)	N.A. Position Factor from Bottom of Beam	Ultimate Bending Moment M_u (in-k)	Maximum Tensile Strain ε_t ($X10^{-3}$)	Maximum Tensile Stress F_t (ksi)	N.A. Position Factor from Bottom of Beam γ
7.1	2.15	2.19	7.93	3.69	3.62	0.496	84.00	5.91	12.95	0.451
7.2	2.12	2.18	7.57	3.74	3.48	0.500	75.00	4.90	10.66	0.475
7.3	1.99	1.98	7.21	3.70	3.64	0.500	69.00	4.56	9.03	0.475
7.4	1.49	1.37	5.55	3.64	4.03	0.491	60.00	6.17	8.45	0.455
7.5	2.08	2.28	6.85	3 45	3.00	0.489	70.50	4.86	11.07	0.455
7.6	1.94	1.94	6.49	3.55	3.35	0.500	70.50	6.14	11.91	0.451
7.7	1.79	1.84	6.49	3.80	3.53	0.485	69.00	6.55	12.06	0.417
7.8	2.17	2.17	6.85	3.31	3.16	0.500	78.00	5.68	12.33	0.451

TABLE A.2.8 Beam Test Results of 2 X 8 Eastern Spruce Clear Specimens Subjected to Third-point Loading

Beam No.	Compressive Modulus of Elasticity E_c ($X10^3$ksi)	Tensile Modulus of Elasticity E_t ($X10^3$ksi)	At Proportional Limit Load				At Ultimate Load			
			Stress F_{pl} (ksi)	Maximum Compressive Strain ($x10^{-3}$)	Maximum Tensile Strain ($X10^{-3}$)	N.A. Position Factor from Bottom of Beam	Ultimate Bending Moment M_u (in-k)	Maximum Tensile Strain ε_t ($X10^{-3}$)	Maximum Tensile Stress F_t (ksi)	N.A. Position Factor from Bottom of Beam γ
8.1	2.40	2.25	6.16	2.28	2.72	0.500	109.68	3.68	8.28	0.470
8.2	1.88	2.05	5.39	2.89	2.62	0.500	86.10	3.05	6.25	0.488
8.3	2.10	2.11	7.08	3.53	3.34	0.500	125.05	5.36	11.31	0.458
8.4	2.65	2.73	7.39	2.90	2.68	0.500	139.40	5.36	14.63	0.422
8.5	1.80	1.81	5.69	3.21	3.13	0.500	116.85	6.00	10.84	0.440
8.6	1.65	1.81	5.69	3.39	3.13	0.500	110.70	5.36	9.70	0.440
8.7	1.78	1.87	6.16	3.45	3.28	0.476	108.65	4.62	8.45	0.422
8.8	1.79	1.95	6.62	4.10	3.60	0.452	127.10	6.44	12.56	0.410
8.9	1.57	1.80	5.39	3.39	2.98	0.464	106.60	5.15	9.27	0.440
8.10	1.98	2.02	5.69	3.39	2.98	0.500	106.60	4.12	8.32	0.445

TABLE A.2.9 Beam Test Results of 4 X 12 Eastern Spruce Clear Specimens Subjected to Third-point Loading

Beam No.	Compressive Modulus of Elasticity E_c ($X10^3$ksi)	Tensile Modulus of Elasticity E_t ($X10^3$ksi)	At Proportional Limit Load				At Ultimate Load			
			Stress F_{pl} (ksi)	Maximum Compressive Strain ($x10^{-3}$)	Maximum Tensile Strain ($X10^{-3}$)	N.A. Position Factor from Bottom of Beam	Ultimate Bending Moment M_u (in-k)	Maximum Tensile Strain ε_t ($X10^{-3}$)	Maximum Tensile Stress F_t (ksi)	N.A. Position Factor from Bottom of Beam γ
9.1	1.38	1.82	4.03	2.62	2.21	0.465	420.00	3.50	6.37	0.440
9.2	1.31	1.64	4.23	3.75	2.57	0.447	465.00	4.74	7.77	0.367
9.3	1.49	1.89	4.53	2.72	2.39	0.456	405.00	2.91	5.50	0.451
9.4	1.76	2.24	5.08	2.67	2.26	0.456	540.00	3.91	8.76	0.420
9.5	1.59	1.89	5.26	2.67	2.77	0.491	526.50	3.86	7.30	0.451

TABLE A.2.10 Beam Test Results of 1.50 X 1.65 inches Eastern Spruce Clear Specimens Subjected to Central Loading

Beam No.	Compressive Modulus of Elasticity E_c ($X10^3$ksi)	Tensile Modulus of Elasticity E_t ($X10^3$ksi)	At Proportional Limit Load				At Ultimate Load			
			Stress F_{pl} (ksi)	Maximum Compressive Strain ($x10^{-3}$)	Maximum Tensile Strain ($X10^{-3}$)	N.A. Position Factor from Bottom of Beam	Ultimate Bending Moment M_u (in-k)	Maximum Tensile Strain ε_t ($X10^{-3}$)	Maximum Tensile Stress F_t (ksi)	N.A. Position Factor from Bottom of Beam γ
10.1	2.14	2.26	10.06	5.02	4.45	0.500	9.45	8.11	18.33	0.422
10.2	2.01	2.09	7.65	3.91	3.67	0.512	6.68	4.90	10.24	0.492
10.3	2.08	1.96	7.65	4.03	3.91	0.524	7.44	6.71	13.15	0.500
10.4	1.60	1.50	6.56	4.11	4.38	0.515	6.47	7.94	11.91	0.439
10.5	1.83	1.81	8.75	4.95	4.83	0.500	8.48	8.33	15.08	0.439
10.6	1.93	1.94	8.75	4.80	4.60	0.500	8.63	9.52	18.47	0.391
10.7	1.74	1.88	7.65	4.64	4.16	0.500	7.66	7.99	15.03	0.427
10.8	1.60	1.56	7.65	5.26	5.07	0.500	7.44	9.40	14.67	0.427
10.9	1.69	1.64	7.65	4.83	4.77	0.500	7.07	7.67	12.58	0.452
10.10	2.33	2.22	7.65	4.08	3.95	0.515	8.19	7.87	17.48	0.427
10.11	2.23	2.30	8.75	4.11	3.80	0.524	8.71	7.53	17.32	0.436
10.12	1.35	1.39	8.75	4.40	4.03	0.500	5.73	7.12	9.90	0.452
10.13	1.82	1.71	5.69	4.58	4.52	0.488	7.59	7.92	13.55	0.430

TABLE A.2.11 Beam Test Results of 1.50 X 1.65 inches Douglas-Fir Clear Specimens Subjected to Central Loading

Beam No.	Compressive Modulus of Elasticity E_c ($X10^3$ksi)	Tensile Modulus of Elasticity E_t ($X10^3$ksi)	At Proportional Limit Load				At Ultimate Load			
			Stress F_{pl} (ksi)	Maximum Compressive Strain ($x10^{-3}$)	Maximum Tensile Strain ($X10^{-3}$)	N.A. Position Factor from Bottom of Beam	Ultimate Bending Moment M_u (in-k)	Maximum Tensile Strain ε_t ($X10^{-3}$)	Maximum Tensile Stress F_t (ksi)	N.A. Position Factor from Bottom of Beam γ
11.1	2.06	2.06	7.65	3.91	3.79	0.512	8.04	7.77	16.00	0.427
11.2	1.90	1.98	10.39	6.36	5.32	0.500	10.42	9.66	19.13	0.445
11.3	2.53	2.83	11.59	5.07	4.03	0.476	11.76	7.87	22.28	0.403
11.4	2.77	2.80	12.68	4.71	4.16	0.500	12.95	11.32	31.70	0.367
11.5	1.70	1.73	8.20	5.32	4.83	0.489	8.19	8.44	14.60	0.430
11.6	1.75	1.92	8.75	5.13	4.71	0.512	8.48	7.40	14.20	0.488
11.7	1.86	1.77	7.65	4.89	4.64	0.500	7.44	8.77	15.53	0.403
11.8	1.57	1.59	7.65	5.62	5.13	0.479	7.44	10.24	16.28	0.382
11.9	2.53	2.51	10.06	4.52	4.16	0.500	10.12	9.68	24.30	0.355

TABLE A.2.12 Beam Test Results of 2 X 4 Eastern Spruce Clear Specimen Subjected to Central Loading

Beam No.	Compressive Modulus of Elasticity E_c ($X10^3$ksi)	Tensile Modulus of Elasticity E_t ($X10^3$ksi)	At Proportional Limit Load				At Ultimate Load			
			Stress F_{pl} (ksi)	Maximum Compressive Strain ($x10^{-3}$)	Maximum Tensile Strain ($X10^{-3}$)	N.A. Position Factor from Bottom of Beam	Ultimate Bending Moment M_u (in-k)	Maximum Tensile Strain ϵ_t ($X10^{-3}$)	Maximum Tensile Stress F_t (ksi)	N.A. Position Factor from Bottom of Beam γ
12.1	2.03	2.07	7.44	4.75	3.59	0.536	30.64	7.31	15.14	0.386
12.2	1.96	2.05	7.44	5.00	3.63	0.500	32.78	8.19	16.78	0.357
12.3	2.07	2.41	7.91	5.03	3.28	0.514	36.34	8.68	20.93	0.343
12.4	1.90	2.25	8.38	4.87	3.73	0.500	35.63	8.17	18.38	0.386
12.5	1.65	1.79	7.44	6.08	4.17	0.500	29.93	6.90	12.35	0.377
12.6	1.67	1.92	7.44	4.77	3.87	0.500	31.35	7.05	13.54	0.406
12.7	1.47	1.47	6.98	5.63	4.76	0.500	28.50	7.06	10.38	0.471
12.8	1.59	1.63	6.05	4.70	3.72	0.500	28.50	7.17	11.69	0.429
12.9	1.84	2.09	6.98	4.48	3.34	0.500	31.35	7.09	14.81	0.414
12.10	1.74	2.21	7.26	5.03	3.28	0.500	31.35	7.52	16.63	0.371
12.11	2.14	2.14	7.44	3.80	3.48	0.521	32.06	6.14	13.14	0.457
12.12	1.57	1.65	7.21	5.03	4.38	0.479	31.35	8.62	14.22	0.414
12.13	1.67	1.73	7.44	5.28	4.30	0.500	32.78	9.97	17.24	0.377

TABLE A.2.12 (Cont'd)

Beam No.	Compressive Modulus of Elasticity E_c ($X10^3$ksi)	Tensile Modulus of Elasticity E_t ($X10^3$ksi)	At Proportional Limit Load				At Ultimate Load			
			Stress F_{pl} (ksi)	Maximum Compressive Strain ($x10^{-3}$)	Maximum Tensile Strain ($X10^{-3}$)	N.A. Position Factor from Bottom of Beam	Ultimate Bending Moment M_u (in-k)	Maximum Tensile Strain ϵ_t ($X10^{-3}$)	Maximum Tensile Stress F_t (ksi)	N.A. Position Factor from Bottom of Beam γ
12.14	1.57	1.52	6.98	5.03	4.83	0.500	34.20	11.69	17.77	0.414
12.15	2.31	2.57	8.84	4.26	3.45	0.514	39.90	7.73	19.86	0.394
12.16	1.93	1.94	7.21	4.59	3.72	0.500	31.35	7.46	14.48	0.386
12.17	1.95	2.06	7.44	4.76	3.62	0.486	32.78	7.95	16.37	0.357
12.18	1.60	1.70	7.44	5.66	4.38	0.500	31.35	9.05	15.39	0.391
12.19	1.84	1.86	7.21	4.81	3.88	0.500	31.35	7.95	14.79	0.334
12.20	1.77	1.97	6.05	3.72	3.06	0.486	25.65	4.65	9.17	0.471

TABLE A.2.13 Beam Test Results of 2 X 6 Eastern Spruce Clear Specimens Subjected to Central Loading

Beam No.	Compressive Modulus of Elasticity E_c ($X10^3$ksi)	Tensile Modulus of Elasticity E_t ($X10^3$ksi)	At Proportional Limit Load				At Ultimate Load			
			Stress F_{pl} (ksi)	Maximum Compressive Strain ($x10^{-3}$)	Maximum Tensile Strain ($X10^{-3}$)	N.A. Position Factor from Bottom of Beam	Ultimate Bending Moment M_u (in-k)	Maximum Tensile Strain ε_t ($X10^{-3}$)	Maximum Tensile Stress F_t (ksi)	N.A. Position Factor from Bottom of Beam γ
13.1	1.95	1.88	7.14	3.91	3.93	0.509	78.75	7.14	13.42	0.445
13.2	2.01	2.35	7.59	4.39	3.33	0.464	85.50	7.42	17.43	0.382
13.3	1.75	1.90	6.84	4.34	3.76	0.500	72.00	6.28	11.94	0.343
13.4	1.98	1.88	7.14	3.63	3.82	0.536	78.75	7.81	14.68	0.405
13.5	1.46	1.42	5.95	4.41	4.21	0.500	63.00	7.58	10.76	0.436
13.6	1.56	1.83	6.40	4.65	3.49	0.483	67.50	6.88	12.60	0.400
13.7	1.32	1.34	5.95	4.50	4.44	0.482	63.00	6.81	10.29	0.455
13.8	1.70	1.89	5.36	3.38	2.83	0.500	58.50	7.38	9.13	0.473
13.9	1.82	1.85	6.84	4.04	3.70	0.500	74.25	7.54	13.96	0.413
13.10	1.70	2.00	6.55	4.18	3.38	0.491	74.25	7.20	14.40	0.382
13.11	1.90	1.80	6.84	3.86	3.91	0.500	69.75	6.39	11.50	0.464
13.12	1.54	1.82	6.84	4.97	3.75	0.500	74.25	7.20	13.10	0.409
13.13	1.50	1.57	5.65	4.97	3.60	0.491	61.88	7.00	11.00	0.382

TABLE A.2.13 (Cont'd)

Beam No.	Compressive Modulus of Elasticity E_c ($X10^3$ksi)	Tensile Modulus of Elasticity E_t ($X10^3$ksi)	At Proportional Limit Load				At Ultimate Load			
			Stress F_{pl} (ksi)	Maximum Compressive Strain ($x10^{-3}$)	Maximum Tensile Strain ($X10^{-3}$)	N.A. Position Factor from Bottom of Beam	Ultimate Bending Moment M_u (in-k)	Maximum Tensile Strain ε_t ($X10^{-3}$)	Maximum Tensile Stress F_t (ksi)	N.A. Position Factor from Bottom of Beam γ
13.14	1.64	1.92	6.69	4.55	3.49	0.473	69.75	6.62	12.71	0.400
13.15	1.59	1.92	5.65	4.02	2.94	0.473	65.25	7.00	13.48	0.373
13.16	1.94	2.15	7.74	4.39	3.60	0.500	83.25	7.98	17.15	0.382
13.17	1.20	1.19	5.65	4.97	4.76	0.509	60.75	9.49	11.29	0.418
13.18	1.47	1.49	5.65	4.12	3.81	0.514	61.88	6.35	9.47	0.467
13.19	2.00	2.31	7.14	3.72	3.09	0.491	81.00	5.14	11.88	0.436
13.20	2.10	2.00	7.14	3.73	3.58	0.500	83.25	8.10	16.22	0.427
13.21	1.32	1.89	5.65	4.44	2.96	0.422	60.75	5.00	9.48	0.422

TABLE A.214 Beam Test Results of 2 X 6 Douglas-Fir Clear Specimen Subjected to Central Loading

Beam No.	Compressive Modulus of Elasticity E_c ($X10^3$ksi)	Tensile Modulus of Elasticity E_t ($X10^3$ksi)	At Proportional Limit Load				At Ultimate Load			
			Stress F_{pl} (ksi)	Maximum Compressive Strain ($x10^{-3}$)	Maximum Tensile Strain ($X10^{-3}$)	N.A. Position Factor from Bottom of Beam	Ultimate Bending Moment M_u (in-k)	Maximum Tensile Strain ε_t ($X10^{-3}$)	Maximum Tensile Stress F_t (ksi)	N.A. Position Factor from Bottom of Beam γ
14.1	2.36	2.25	7.14	3.11	3.19	0.545	72.00	4.43	9.97	0.500
14.2	1.38	1.44	6.55	4.92	4.60	0.500	72.00	8.89	12.81	0.391
14.3	2.92	2.83	11.90	4.08	4.21	0.500	108.00	5.30	15.01	0.473
14.4	2.90	3.05	11.31	4.02	3.70	0.500	121.50	7.22	22.01	0.391
14.5	2.65	2.72	11.90	4.77	4.38	0.518	108.00	6.71	18.25	0.436
14.6	1.19	1.46	6.55	5.71	4.44	0.445	60.75	6.08	8.88	0.445
14.7	1.61	1.62	8.03	5.36	4.97	0.509	78.75	6.78	10.99	0.482
14.8	2.55	2.50	10.11	4.23	4.18	0.500	108.00	7.89	19.72	0.400

TABLE A.2.15 Beam Test Results of 2 X 8 Eastern Spruce Clear Specimens Subjected to Central Loading

Beam No.	Compressive Modulus of Elasticity E_c ($X10^3$ksi)	Tensile Modulus of Elasticity E_t ($X10^3$ksi)	At Proportional Limit Load: Stress F_{pl} (ksi)	Maximum Compressive Strain ($x10^{-3}$)	Maximum Tensile Strain ($X10^{-3}$)	N.A. Position Factor from Bottom of Beam	At Ultimate Load: Ultimate Bending Moment M_u (in-k)	Maximum Tensile Strain ε_t ($X10^{-3}$)	Maximum Tensile Stress F_t (ksi)	N.A. Position Factor from Bottom of Beam γ
15.1	1.79	2.12	5.31	3.08	2.50	0.500	104.55	4.20	8.91	0.462
15.2	1.68	1.81	6.00	4.64	3.32	0.473	113.78	6.14	11.11	0.415
15.3	1.64	1.79	5.54	4.31	3.09	0.500	107.63	7.16	12.81	0.397
15.4	2.16	2.31	6.46	3.81	2.79	0.486	138.38	6.31	14.57	0.377
15.5	1.75	1.72	6.00	4.48	3.49	0.486	104.55	5.24	9.02	0.432
15.6	1.77	1.87	5.08	3.54	2.71	0.500	101.48	5.57	10.42	0.418
15.7	1.83	2.34	5.54	3.80	2.37	0.473	116.85	5.70	13.34	0.384
15.8	2.21	2.57	6.46	3.44	2.51	0.500	138.38	6.28	16.15	0.342
15.9	1.48	1.75	6.00	4.59	3.18	0.500	119.93	7.03	12.31	0.404
15.10	1.71	2.01	5.54	3.73	2.75	0.479	104.55	4.36	8.76	0.459

TABLE A.2.16 Beam Test Results of 4 X 12 Eastern Spruce Clear Specimens Subjected to Central Loading

Beam No.	Compressive Modulus of Elasticity E_c ($X10^3$ksi)	Tensile Modulus of Elasticity E_t ($X10^3$ksi)	At Proportional Limit Load				At Ultimate Load			
			Stress F_{pl} (ksi)	Maximum Compressive Strain ($x10^{-3}$)	Maximum Tensile Strain ($X10^{-3}$)	N.A. Position Factor from Bottom of Beam	Ultimate Bending Moment M_u (in-k)	Maximum Tensile Strain ε_t ($X10^{-3}$)	Maximum Tensile Stress F_t (ksi)	N.A. Position Factor from Bottom of Beam γ
16.1	0.90	1.06	3.32	4.27	3.12	0.500	353.25	5.63	5.97	0.398
16.2	1.57	1.81	4.83	3.32	2.67	0.500	490.50	4.12	7.45	0.438
16.3	1.33	1.75	4.23	3.08	2.41	0.500	405.00	3.35	5.87	0.482
16.4	1.21	1.32	3.99	4.52	3.03	0.500	414.00	6.89	9.09	0.358
16.5	0.97	1.27	4.83	4.90	3.79	0.500	495.00	6.09	7.73	0.389

TABLE A.2.17 Beam Test Results of 2 X 4 Eastern Spruce Knotted Specimens Subjected to Third-point Loading

Beam No.	Compressive Modulus of Elasticity E_c ($X10^3$ksi)	Tensile Modulus of Elasticity E_t ($X10^3$ksi)	At Proportional Limit Load				At Ultimate Load			
			Stress F_{pl} (ksi)	Maximum Compressive Strain ($x10^{-3}$)	Maximum Tensile Strain ($X10^{-3}$)	N.A. Position Factor from Bottom of Beam	Ultimate Bending Moment M_u (in-k)	Maximum Tensile Strain ε_t ($X10^{-3}$)	Maximum Tensile Stress F_t (ksi)	N.A. Position Factor from Bottom of Beam γ
17.1	1.62	1.78	6.32	4.26	3.55	0.486	28.50	6.20	11.03	0.443
17.2[a]	1.80	2.05	5.89	3.28	2.87	0.506	18.05	2.87	5.89	0.506
17.3	1.35	1.56	5.58	5.06	3.57	0.457	23.75	5.86	9.15	0.414
17.4	1.29	1.13	4.65	3.62	4.11	0.494	17.10	5.14	5.81	0.477
17.5	2.23	2.07	7.46	3.38	3.60	0.471	31.35	5.45	11.29	0.423
17.6	1.34	1.31	5.21	3.87	3.98	0.500	26.60	6.77	8.87	0.450
17.7	1.88	1.96	4.94	2.63	2.52	0.463	21.38	3.86	7.57	0.443
17.8	2.10	2.10	4.94	2.35	2.35	0.500	20.43	3.57	7.39	0.500
17.9	1.90	1.96	6.20	3.47	3.16	0.463	28.50	5.22	10.24	0.400

TABLE A.2.17 (Cont'd)

Beam No.	Compressive Modulus of Elasticity E_c ($X10^3$ksi)	Tensile Modulus of Elasticity E_t ($X10^3$ksi)	At Proportional Limit Load				At Ultimate Load			
			Stress F_{pl} (ksi)	Maximum Compressive Strain ($x10^{-3}$)	Maximum Tensile Strain ($X10^{-3}$)	N.A. Position Factor from Bottom of Beam	Ultimate Bending Moment M_u (in-k)	Maximum Tensile Strain ε_t ($X10^{-3}$)	Maximum Tensile Stress F_t (ksi)	N.A. Position Factor from Bottom of Beam γ
17.10	1.10	1.17	4.79	4.37	4.09	0.529	18.05	5.43	6.36	0.494
17.11[a]	1.51	1.60	5.27	3.50	3.29	0.471	16.15	3.29	5.27	0.471
17.12	1.92	2.13	6.77	3.54	3.18	0.457	29.45	5.22	11.11	0.394
17.13	1.76	1.76	6.93	3.94	3.94	0.500	31.35	8.13	14.31	0.394
17.14	2.21	2.17	7.13	3.23	3.29	0.509	27.55	4.38	9.50	0.480
17.15	1.56	1.74	4.95	3.17	2.84	0.500	20.43	3.73	6.49	0.477

a: Elastic behavior to failure

TABLE A.2.18 Beam Test Results of 2 X 6 Eastern Spruce Knotted Specimens Subjected to Third-point Loading

Beam No.	Compressive Modulus of Elasticity E_c ($X10^3$ksi)	Tensile Modulus of Elasticity E_t ($X10^3$ksi)	At Proportional Limit Load				At Ultimate Load			
			Stress F_{pl} (ksi)	Maximum Compressive Strain ($x10^{-3}$)	Maximum Tensile Strain ($X10^{-3}$)	N.A. Position Factor from Bottom of Beam	Ultimate Bending Moment M_u (in-k)	Maximum Tensile Strain ε_t ($X10^{-3}$)	Maximum Tensile Stress F_t (ksi)	N.A. Position Factor from Bottom of Beam γ
18.1	1.82	2.01	4.76	2.85	2.37	0.500	48.00	3.44	6.92	0.490
18.2	1.95	2.12	7.14	3.66	3.37	0.491	81.00	6.37	13.50	0.409
18.3	1.94	2.08	5.55	2.86	2.67	0.500	60.00	4.12	8.57	0.473
18.4	2.30	2.45	7.54	3.31	3.08	0.491	8.00	4.38	10.70	0.454
18.5	1.96	2.00	7.14	4.04	3.57	0.473	75.00	5.65	11.30	0.418
18.6	1.65	1.55	4.76	2.88	3.07	0.500	48.00	4.26	6.60	0.480
18.7	1.99	1.77	6.74	3.38	3.81	0.500	72.00	5.70	10.09	0.422
18.8	1.79	1.81	5.9	3.34	3.29	0.491	60.00	4.88	8.83	0.427
18.9	1.74	1.70	6.35	3.65	3.74	0.509	60.00	5.22	8.87	0.467
18.10[a]	1.90	1.88	6.35	3.30	3.38	0.527	48.00	3.38	6.35	0.527
18.11	1.85	1.93	5.95	3.26	3.08	0.473	63.00	5.30	10.23	0.445
18.12	2.27	2.27	7.93	3.49	3.49	0.513	72.00	4.28	9.72	0.491

a: Elastic behavior to failure

TABLE A.2.19 Beam Test Results of 2 X 4 Eastern Spruce Knotted Specimens Subjected to Central Loading

Beam No.	Compressive Modulus of Elasticity E_c ($X10^3$ksi)	Tensile Modulus of Elasticity E_t ($X10^3$ksi)	At Proportional Limit Load				At Ultimate Load			
			Stress F_{pl} (ksi)	Maximum Compressive Strain ($x10^{-3}$)	Maximum Tensile Strain ($X10^{-3}$)	N.A. Position Factor from Bottom of Beam	Ultimate Bending Moment M_u (in-k)	Maximum Tensile Strain ε_t ($X10^{-3}$)	Maximum Tensile Stress F_t (ksi)	N.A. Position Factor from Bottom of Beam γ
19.1	1.17	1.49	5.77	5.11	3.87	0.471	25.65	6.66	9.93	0.400
19.2	1.23	1.24	5.77	5.35	4.65	0.500	22.80	6.92	8.58	0.480
19.3[a]	1.99	1.65	5.67	2.85	3.44	0.514	17.10	3.44	5.67	0.514
19.4	1.80	2.22	5.12	2.83	2.30	0.486	22.80	3.71	8.25	0.448
19.5	1.39	1.72	6.40	5.24	3.72	0.457	27.08	6.55	11.27	0.400
19.6	1.54	1.54	6.60	4.29	4.28	0.500	29.21	7.55	11.63	0.429
19.7	2.01	2.06	7.42	3.90	3.60	0.500	27.79	4.89	10.09	0.486
19.8	1.47	1.25	6.60	5.17	5.28	0.514	25.65	7.24	9.05	0.486
19.9[a]	1.55	1.55	5.58	3.60	3.60	0.528	17.10	3.60	5.58	0.528
19.10	1.16	1.36	6.05	5.33	4.44	0.463	25.65	7.00	9.52	0.423

a: Elastic behavior to failure

TABLE A.2.19 (Cont'd)

Beam No.	Compressive Modulus of Elasticity E_c ($X10^3$ksi)	Tensile Modulus of Elasticity E_t ($X10^3$ksi)	At Proportional Limit Load				At Ultimate Load			
			Stress F_{pl} (ksi)	Maximum Compressive Strain ($x10^{-3}$)	Maximum Tensile Strain ($X10^{-3}$)	N.A. Position Factor from Bottom of Beam	Ultimate Bending Moment M_u (in-k)	Maximum Tensile Strain ε_t ($X10^{-3}$)	Maximum Tensile Stress F_t (ksi)	N.A. Position Factor from Bottom of Beam γ
19.11	1.68	1.73	7.42	4.50	4.29	0.500	32.06	7.40	12.80	0.408
19.12	1.31	1.49	4.65	3.61	3.12	0.486	19.95	5.10	7.60	0.428
19.13	1.48	1.58	4.95	3.77	3.13	0.486	19.95	4.72	7.47	0.463
19.14	1.46	1.46	5.36	3.67	3.67	0.500	22.80	5.13	7.49	0.466
19.15	2.39	2.55	8.38	3.50	3.29	0.505	34.20	4.88	12.44	0.466

a: Elastic behavior to failure

TABLE A.2.20 Beam Test Results of 2 X 6 Eastern Spruce Knotted Specimens Subjected to Central Loading

Beam No.	Compressive Modulus of Elasticity E_c ($X10^3$ksi)	Tensile Modulus of Elasticity E_t ($X10^3$ksi)	At Proportional Limit Load				At Ultimate Load			
			Stress F_{pl} (ksi)	Maximum Compressive Strain ($X10^{-3}$)	Maximum Tensile Strain ($X10^{-3}$)	N.A. Position Factor from Bottom of Beam	Ultimate Bending Moment M_u (in-k)	Maximum Tensile Strain ε_t ($X10^{-3}$)	Maximum Tensile Stress F_t (ksi)	N.A. Position Factor from Bottom of Beam γ
20.1	1.96	2.16	7.81	4.22	3.62	0.500	81.00	6.08	13.14	0.431
20.2	1.60	1.55	5.36	3.35	3.46	0.509	54.00	5.90	9.15	0.436
20.3	1.72	2.07	5.95	4.08	2.87	0.482	67.50	7.00	14.50	0.345
20.4	1.78	1.98	7.14	4.03	3.61	0.496	76.50	7.49	14.84	0.382
20.5	1.54	1.87	6.55	4.56	3.50	0.500	67.50	6.15	11.50	0.409
20.6	1.79	2.11	7.14	4.68	3.38	0.500	67.50	4.98	10.50	0.378
20.7[a]	2.04	2.01	6.35	3.11	3.16	0.509	48.00	3.16	6.35	0.509
20.8	1.07	1.30	5.02	4.83	3.86	0.436	56.00	8.18	10.63	0.367
20.9	2.16	2.39	6.35	3.24	2.66	0.545	64.00	4.00	9.56	0.455
20.10	1.80	1.82	5.29	2.96	2.91	0.515	56.00	5.29	9.63	0.485
20.11	1.63	1.69	4.76	3.19	2.82	0.518	50.00	4.03	6.81	0.482
20.12[a]	1.72	1.44	6.35	3.69	4.41	0.522	48.00	4.41	6.35	0.522

a: Elastic behavior to failure

TABLE A.3.1 Reduction Factor "r_c" and parameter "ϕ_c" corresponding to Knot Ratios Measured in Compression Zone of 2 X 4 Beams Subjected to Third-point Loading

Beam No.	$(\frac{K_n}{b})_c$	$(\frac{K_w}{d})_c$	$(\frac{K_e}{d})_c$	ϕ_c Eq.[8.1]	Reduction Factor $r_c = \frac{F_{pl}}{F_{cu}}$
17.1	-	0.071	-	0.929	1.03
17.2[a]	0.042	0.143	-	0.821	0.91
17.3	0.417	0.250	0.107	0.349	0.89
17.4	0.417	0.250	0.179	0.295	0.84
17.5	0.125	0.054	-	0.828	0.96
17.6	0.063	0.179	-	0.769	0.99
17.7	0.333	0.143	-	0.572	0.92
17.8	0.583	0.286	-	0.298	0.71
17.9	0.083	0.143	0.071	0.627	0.98
17.10	0.083	0.161	-	0.769	1.01
17.11[a]	0.417	0.286	0.107	0.332	0.87
17.12	0.083	0.071	-	0.852	1.00
17.13	0.083	0.143	0.034	0.733	0.99
17.14	0.250	0.107	-	0.670	0.96
17.15	0.250	0.214	0.143	0.541	0.92

a: Elastic behavior to failure

TABLE A.3.2 Reduction Factor "r_c" and parameter "ϕ_c", corresponding to Knot Ratios Measured in Compression zone of 2 X 6 Beams Subjected to Third-point Loading

Beam No.	$(\frac{K_n}{b})_c$	$(\frac{K_w}{d})_c$	$(\frac{K_e}{d})_c$	ϕ_c Eq.[8.1]	Reduction Factor $r_c = \frac{F_{pl}}{F_{cu}}$
18.1	0.500	0.182	0.136	0.305	0.77
18.2	-	0.091	-	0.909	0.99
18.3	0.250	0.102	0.136	0.503	0.87
18.4	0.167	0.114	-	0.738	0.94
18.5	-	0.091	-	0.909	0.99
18.6	0.167	0.136	0.114	0.565	0.84
18.7	-	0.091	-	0.909	0.99
18.8	0.167	0.136	-	0.720	0.97
18.9	-	0.091	-	0.909	0.99
18.10[a]	-	0.114	-	0.886	0.94
18.11	0.333	0.159	0.091	0.463	0.81
18.12	-	0.091	-	0.909	1.01

a: Elastic behavior to failure

TABLE A.3.3 Reduction Factor "r_c" and parameter "ϕ_c" corresponding to Knot Ratios Measured in Compression Zone of 2 X 4 Beams Subjected to Central Loading

Beam No.	$(\frac{K_n}{b})_c$	$(\frac{K_w}{d})_c$	$(\frac{K_e}{d})_c$	ϕ_c Eq.[8.1]	Reduction Factor $r_c = \frac{F_{pl}}{F_{cu}}$
19.1	-	0.071	-	0.929	1.10
19.2	0.417	0.214	-	0.485	0.95
19.3[a]	0.167	0.179	0.143	0.502	0.94
19.4	0.417	0.161	-	0.489	0.95
19.5	0.292	0.125	-	0.620	0.95
19.6	0.208	0.196	-	0.637	1.02
19.7	0.083	0.054	-	0.867	1.06
19.8	0.167	0.107	-	0.744	1.02
19.9[a]	0.167	0.214	-	0.655	0.89
19.10	0.250	0.161	-	0.629	0.95
19.11	0.167	0.143	-	0.714	1.04
19.12	0.500	0.250	0.196	0.242	0.84
19.13	0.167	0.143	-	0.714	1.05
19.14	0.167	0.107	-	0.744	1.00
19.15	-	0.071	-	0.929	1.07

a; Elastic behavior to failure

TABLE A.3.4 Reduction Factor "r_c" and parameter "ϕ_c" corresponding to Knot Ratios Measured in Compression Zone of 2 X 6 Beams Subjected to Central Loading

Beam No.	$(\frac{K_n}{b})_c$	$(\frac{K_w}{d})_c$	$(\frac{K_e}{d})_c$	ϕ_c Eq.[8.1]	Reduction Factor $r_c = \frac{F_{pl}}{F_{cu}}$
20.1	0.250	0.159	0.045	0.575	1.00
20.2	0.250	0.159	-	0.631	0.94
20.3	0.500	0.136	0.091	0.357	0.81
20.4	0.250	0.114	-	0.665	0.97
20.5	0.250	0.182	-	0.614	0.97
20.6	0.333	0.114	0.091	0.488	0.89
20.7[a]	0.167	0.182	-	0.681	0.81
20.8	0.500	0.159	0.136	0.314	0.88
20.9	0.500	0.159	0.091	0.347	0.86
20.10	0.583	0.159	0.159	0.248	0.72
20.11	0.500	0.182	0.159	0.289	0.70
20.12[a]	0.500	0.182	-	0.409	0.80

a: Elastic behavior to failure

TABLE A.3.5 Reduction Factor "r_t" and parameter "ϕ_t" Corresponding to Knot Ratios Measured in Tension Zone of 2 X 4 Beams Subjected to Third-point Loading

Beam No.	$(\frac{K_n}{b})_t$	$(\frac{K_w}{d})_t$	$(\frac{K_e}{d})_t$	ϕ_t Eq.[8.1]	Reduction Factor $r_t = \frac{F_t}{0.81F_{tu}}$
17.1	0.500	0.143	-	0.429	0.69
17.2[a]	0.500	0.214	0.214	0.243	0.44
17.3	0.250	0.143	-	0.643	0.86
17.4	0.500	0.250	-	0.375	0.70
17.5	0.250	0.143	0.071	0.555	0.82
17.6	0.333	0.214	-	0.524	0.82
17.7	0.417	0.179	-	0.479	0.72
17.8	0.333	0.289	0.179	0.320	0.53
17.9	0.333	0.143	-	0.572	0.74
17.10	0.500	0.161	0.179	0.283	0.49
17.11[a]	0.333	0.286	0.143	0.350	0.57
17.12	0.333	0.250	-	0.500	0.71
17.13	-	0.179	-	0.821	0.92
17.14	0.500	0.214	0.179	0.313	0.59
17.15	0.500	0.214	0.214	0.265	0.49

TABLE A.3.6 Reduction Factor "r_t" and Parameter "ϕ_t" Corresponding to Knot Ratios Measured in Tension Zone of 2 X 6 Beams Subjected to Third-point Loading

Beam No.	$(\frac{K_n}{b})_t$	$(\frac{K_w}{d})_t$	$(\frac{K_e}{d})_t$	ϕ_t Eq.[8.1]	Reduction Factor $r_t = \frac{F_t}{0.73F_{tu}}$
18.1	0.500	0.182	-	0.409	0.60
18.2	-	0.091	-	0.909	0.98
18.3	0.417	0.182	0.182	0.394	0.65
18.4	0.250	0.182	0.136	0.458	0.79
18.5	0.083	0.091	-	0.834	0.96
18.6	0.167	0.136	0.114	0.565	0.77
18.7	-	0.114	-	0.886	0.96
18.8	0.167	0.159	0.114	0.550	0.88
18.9	-	0.159	-	0.841	0.95
18.10[a]	0.250	0.227	0.136	0.433	0.81
18.11	0.333	0.159	-	0.561	0.88
18.12	0.167	0.091	0.045	0.691	0.94

a: Elastic behavior to failure

TABLE A.3.7 Reduction Factor "r_t" and Parameter "ϕ_t" Corresponding to Knot Ratios Measured in Tension Zone of 2 X 4 Beams Subjected to Central Loading

Beam No.	$(\frac{K_n}{b})_t$	$(\frac{K_w}{d})_t$	$(\frac{K_e}{d})_t$	ϕ_t Eq.[8.1]	Reduction Factor $r_t = \frac{F_t}{0.90F_{tu}}$
19.1	0.167	0.250	0.107	0.498	0.83
19.2	0.333	0.214	-	0.524	0.84
19.3[a]	0.500	0.250	0.214	0.231	0.40
19.4	0.417	0.196	-	0.469	0.71
19.5	0.250	0.143	0.214	0.397	0.65
19.6	0.250	0.196	-	0.603	0.79
19.7	0.333	0.107	0.143	0.437	0.64
19.8	0.417	0.250	-	0.437	0.52
19.9[a]	0.333	0.214	0.214	0.324	0.54
19.10	0.333	0.214	0.179	0.430	0.62
19.11	0.250	0.250	0.179	0.379	0.72
19.12	0.333	0.250	-	0.500	0.83
19.13	0.500	0.250	-	0.375	0.52
19.14	0.333	0.214	0.179	0.430	0.60
19.15	0.250	0.143	-	0.643	0.82

a: Elastic behavior to failure

TABLE A.3.8 Reduction Factor "r_t" and Parameter "ϕ_t" Corresponding to Knot Ratios Measured in Tension Zone of 2 X 6 Beams Subjected to Central Loading

Beam No.	$(\frac{K_n}{b})_t$	$(\frac{K_w}{d})_t$	$(\frac{K_e}{d})_t$	ϕ_t Eq.[8.1]	Reduction Factor $r_t = \frac{F_t}{0.81F_{tu}}$
20.1	-	0.159	-	0.841	0.94
20.2	0.167	0.182	-	0.681	0.83
20.3	-	0.114	-	0.886	0.96
20.4	-	0.068	-	0.923	1.00
20.5	0.167	0.091	-	0.757	0.92
20.6	0.250	0.114	0.068	0.577	0.86
20.7[a]	0.500	0.182	0.136	0.305	0.46
20.8	-	0.159	-	0.841	0.96
20.9	0.500	0.159	0.159	0.421	0.63
20.10	0.333	0.159	0.114	0.440	0.65
20.11	0.500	0.182	-	0.410	0.54
20.12[a]	0.500	0.182	-	0.410	0.52

a: Elastic behavior to failure

APPENDIX B

FIGURES

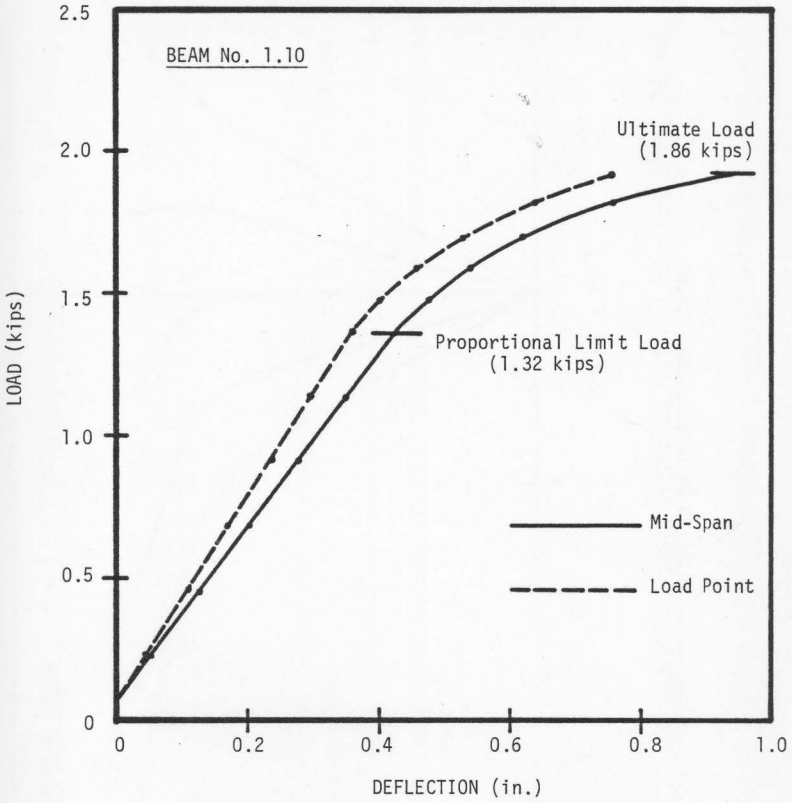

FIG. B.1 TYPICAL LOAD-DEFLECTION CURVES IN BENDING TEST --1.50 x 1.65 INCHES EASTERN SPRUCE CLEAR BEAM SUBJECTED TO THIRD-POINT LOADING

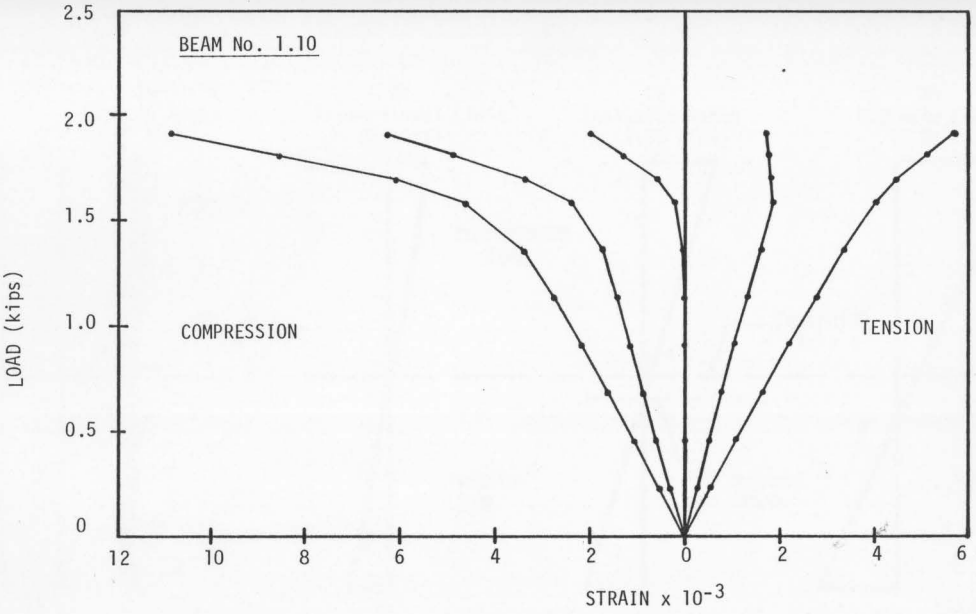

FIG. B.2 TYPICAL LOAD-STRAIN CURVES IN BENDING TEST -- 1.50 x 1.65 INCHES EASTERN SPRUCE CLEAR BEAM SUBJECTED TO THIRD-POINT LOADING

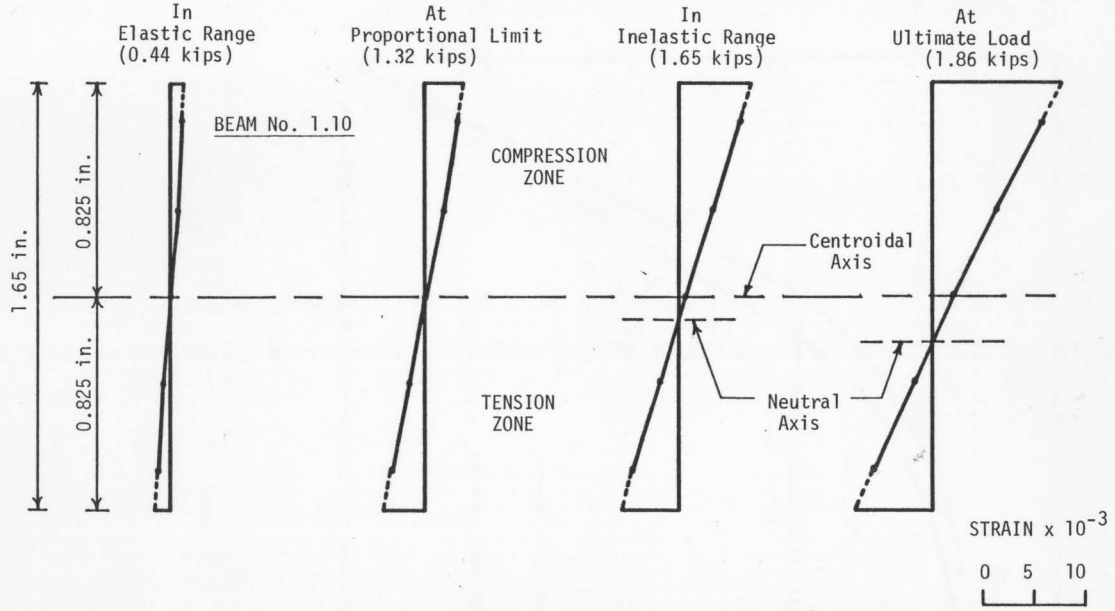

FIG. B.3 TYPICAL STRAIN DISTRIBUTIONS ACROSS BEAM DEPTH IN BENDING TEST -- 1.50 x 1.65 INCHES EASTERN SPRUCE CLEAR BEAM SUBJECTED TO THIRD-POINT LOADING

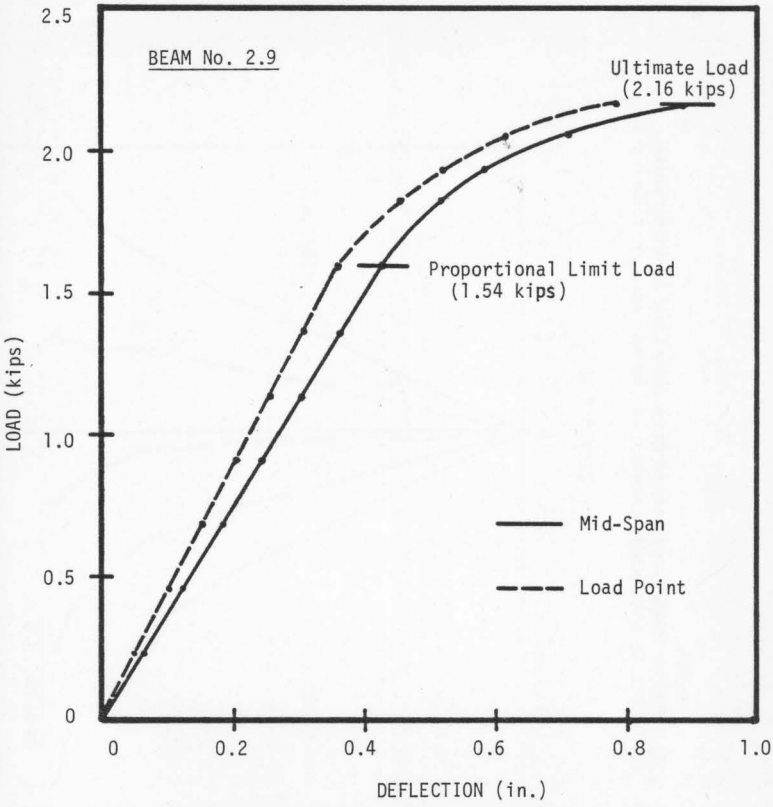

FIG. B.4 TYPICAL LOAD-DEFLECTION CURVES IN BENDING TEST --1.50 x 1.65 INCHES DOUGLAS-FIR CLEAR BEAM SUBJECTED TO THIRD-POINT LOADING

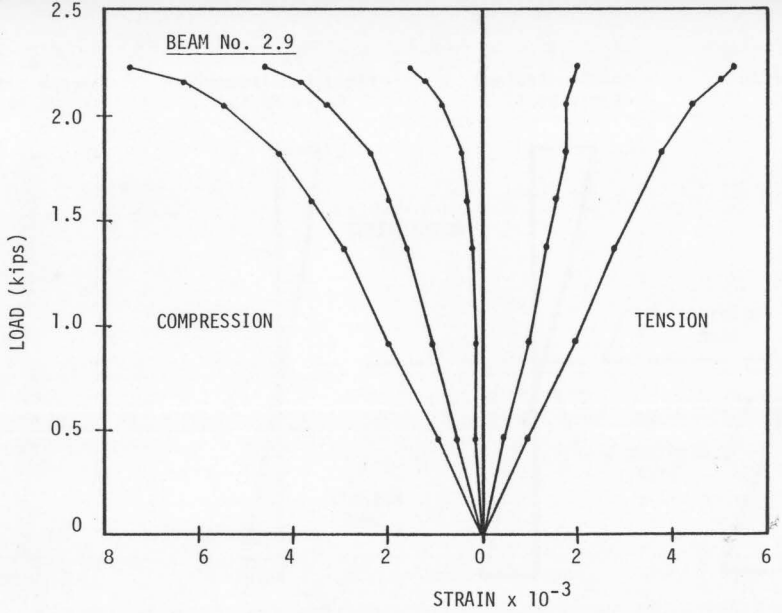

FIG. B.5 TYPICAL LOAD-STRAIN CURVES IN BENDING TEST -- 1.50 x 1.65 INCHES DOUGLAS-FIR CLEAR BEAM SUBJECTED TO THIRD-POINT LOADING

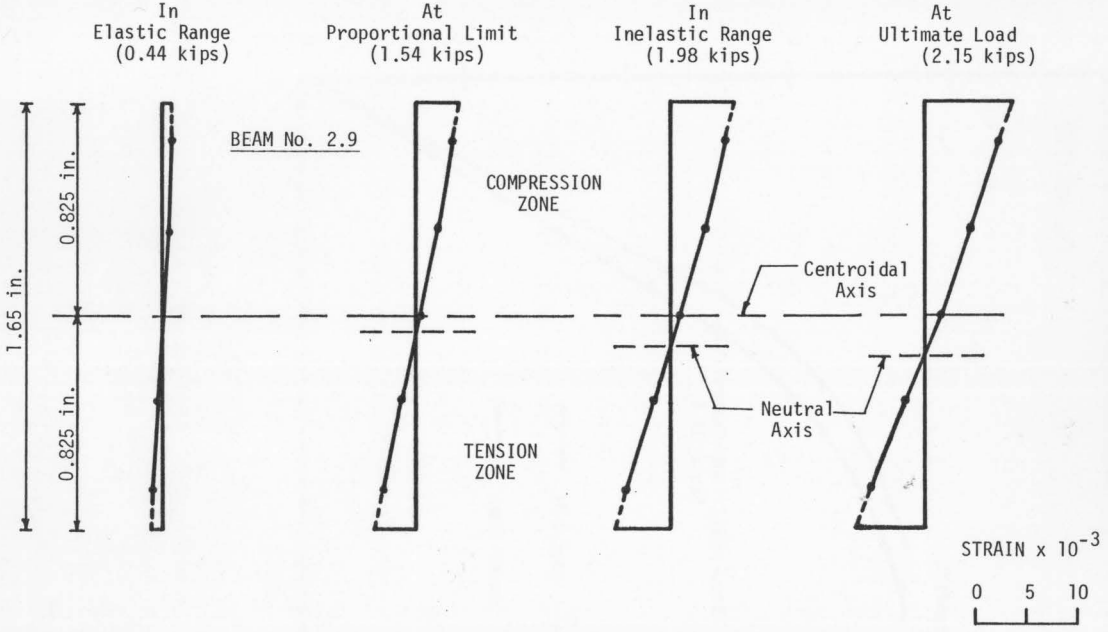

FIG. B.6 TYPICAL STRAIN DISTRIBUTIONS ACROSS BEAM DEPTH IN BENDING TEST -- 1.50 x 1.65 INCHES DOUGLAS-FIR CLEAR BEAM SUBJECTED TO THIRD-POINT LOADING

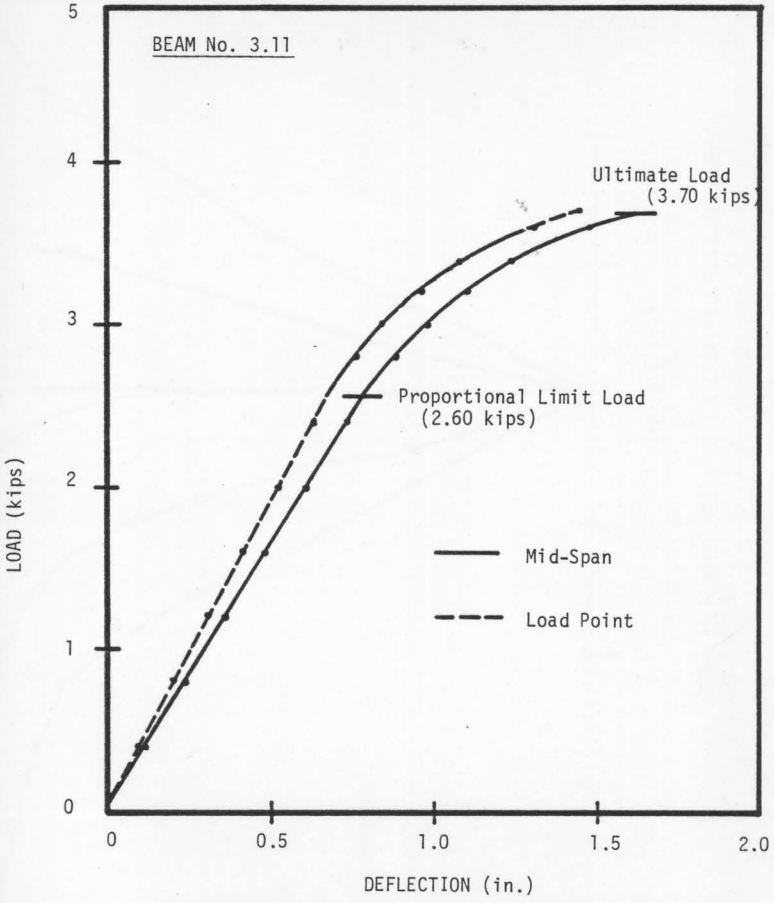

FIG. B.7 TYPICAL LOAD-DEFLECTION CURVES IN BENDING TEST -- 2 x 4 EASTERN SPRUCE CLEAR BEAM SUBJECTED TO THIRD-POINT LOADING

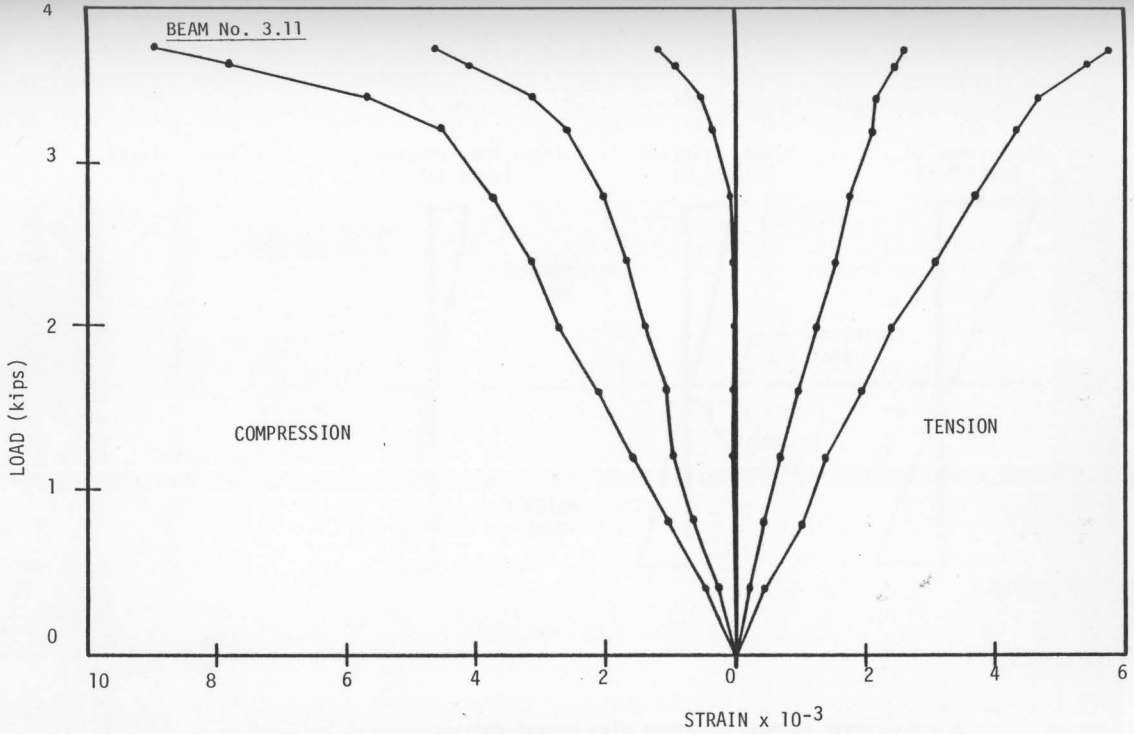

FIG. B.8 TYPICAL LOAD-STRAIN CURVES IN BENDING TEST-- 2 x 4 EASTERN SPRUCE CLEAR BEAM SUBJECTED TO THIRD-POINT LOADING

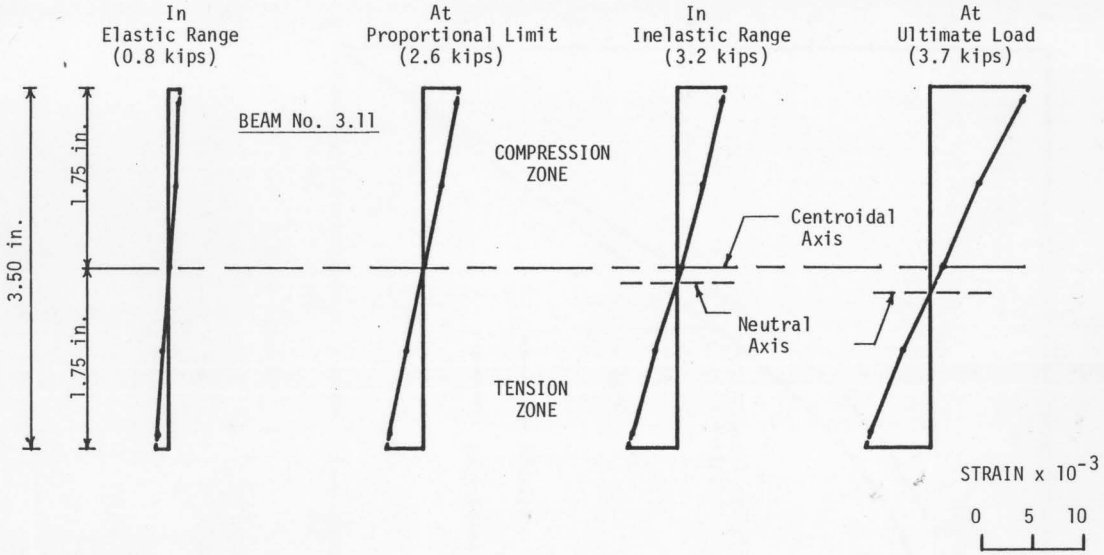

FIG. B.9 TYPICAL STRAIN DISTRIBUTIONS ACROSS BEAM DEPTH IN BENDING TEST -- 2 x 4 EASTERN SPRUCE CLEAR BEAM SUBJECTED TO THIRD-POINT LOADING

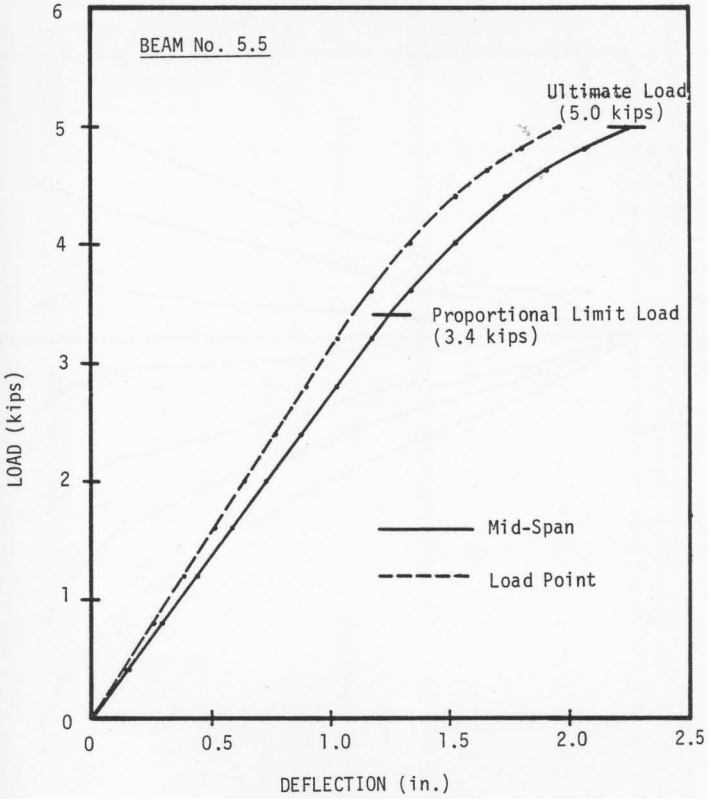

FIG. B.10 TYPICAL LOAD-DEFLECTION CURVES IN BENDING TEST -- 2 x 6 DOUGLAS-FIR CLEAR BEAM SUBJECTED TO THIRD-POINT LOADING

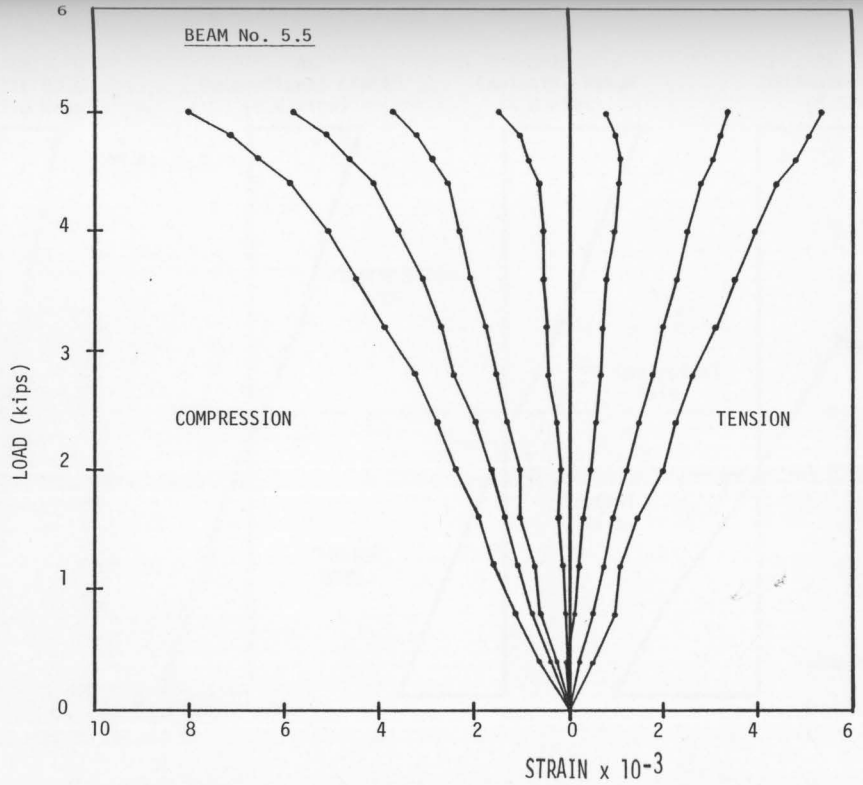

FIG. B.11 TYPICAL LOAD-STRAIN CURVES IN BENDING TEST -- 2 x 6 DOUGLAS-FIR CLEAR BEAM SUBJECTED TO THIRD-POINT LOADING

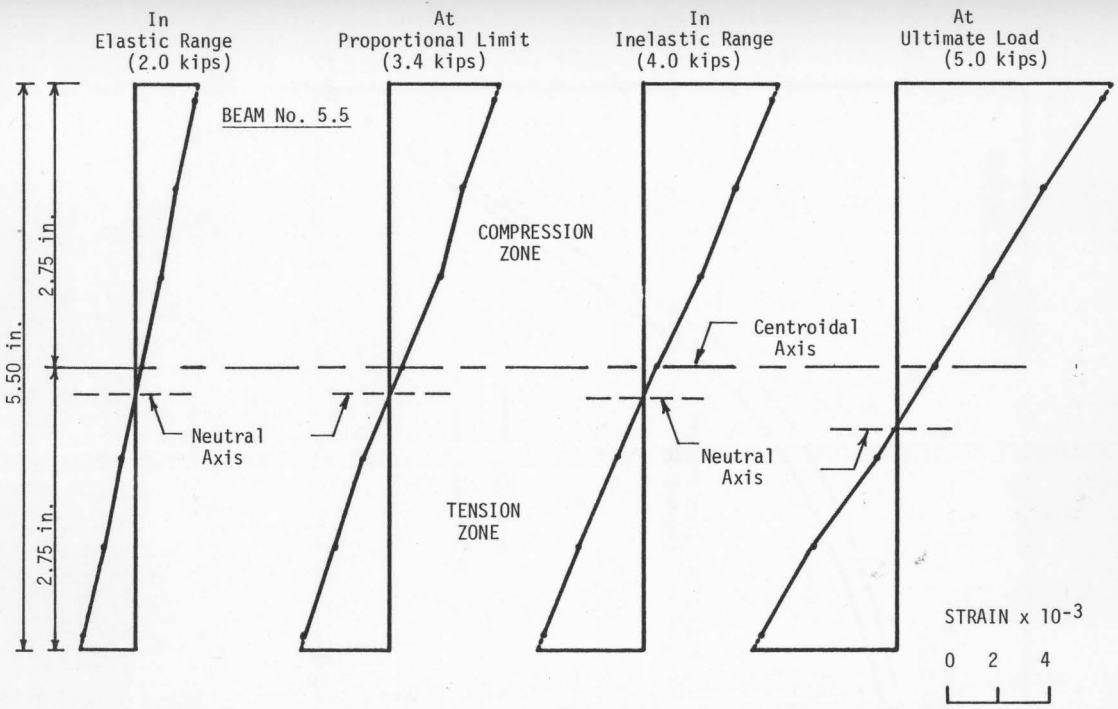

FIG. B.12 TYPICAL STRAIN DISTRIBUTIONS ACROSS BEAM DEPTH IN BENDING TEST -- 2 x 6 DOUGLAS-FIR CLEAR BEAM SUBJECTED TO THIRD-POINT LOADING

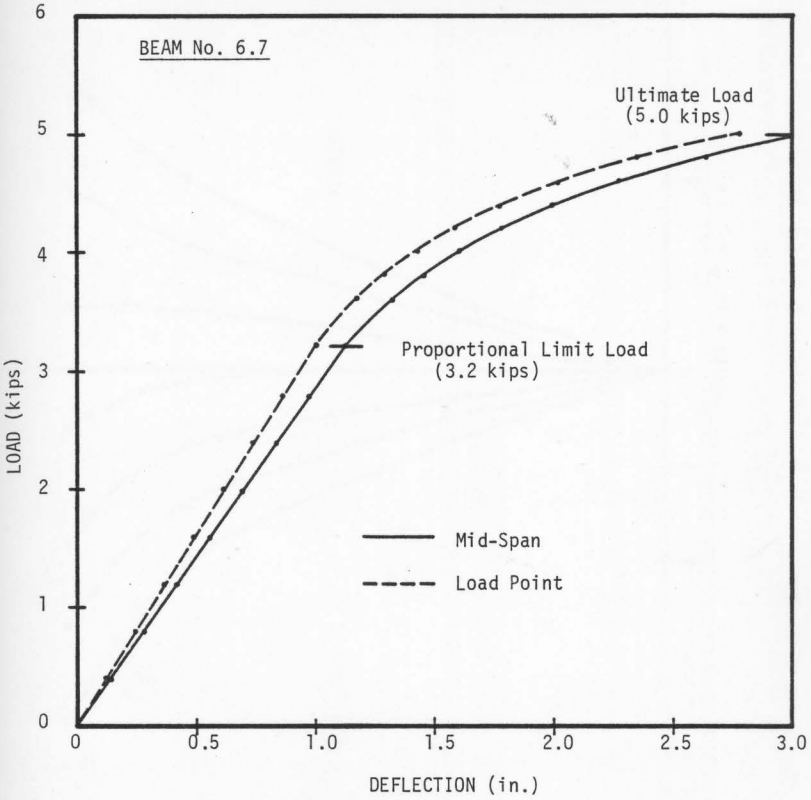

FIG. B.13 TYPICAL LOAD-DEFLECTION CURVES IN BENDING TEST -- 2 x 6 EASTERN SPRUCE STIFFENED CLEAR BEAM SUBJECTED TO THIRD-POINT LOADING

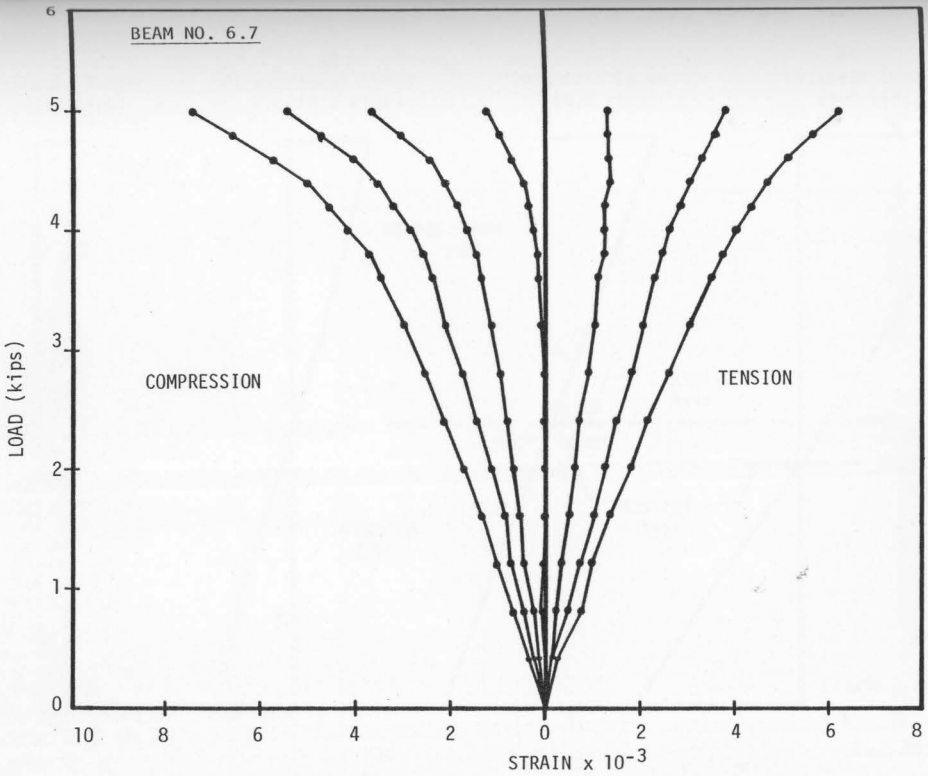

FIG. B.14 TYPICAL LOAD-STRAIN CURVES IN BENDING TEST-- 2 x 6 EASTERN SPRUCE STIFFENED CLEAR BEAM SUBJECTED TO THIRD-POINT LOADING

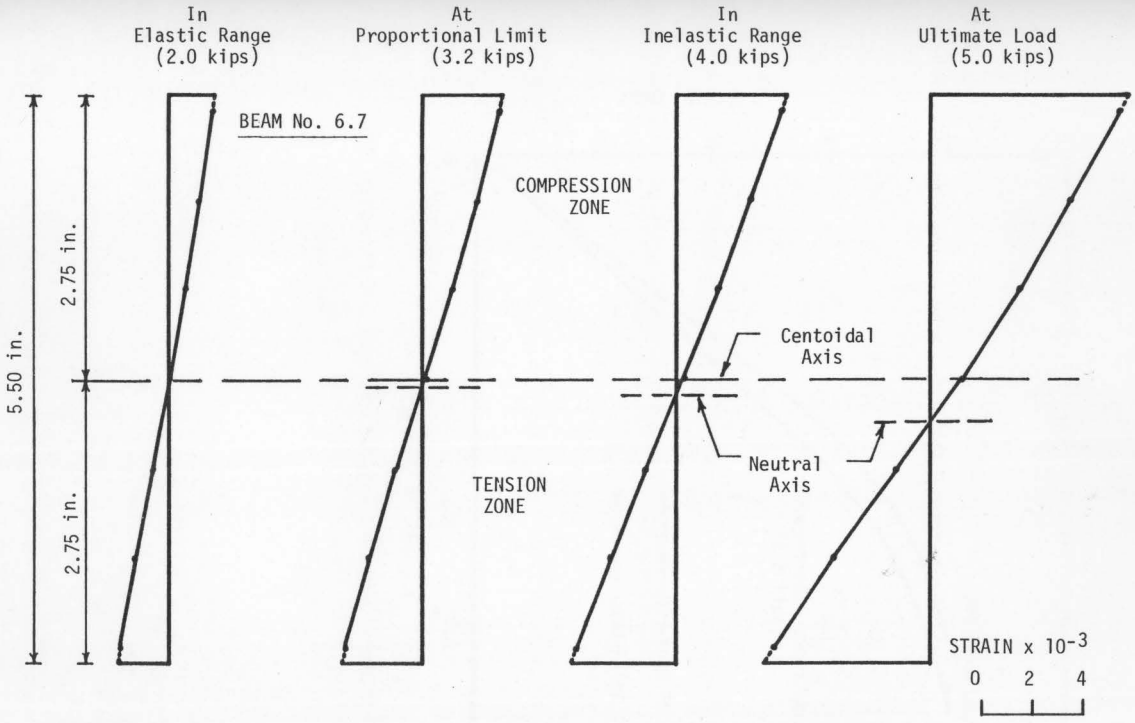

FIG. B.15 TYPICAL STRAIN DISTRIBUTIONS ACROSS BEAM DEPTH IN BENDING TEST -- 2 x 6 EASTERN SPRUCE STIFFENED CLEAR BEAM SUBJECTED TO THIRD-POINT LOADING

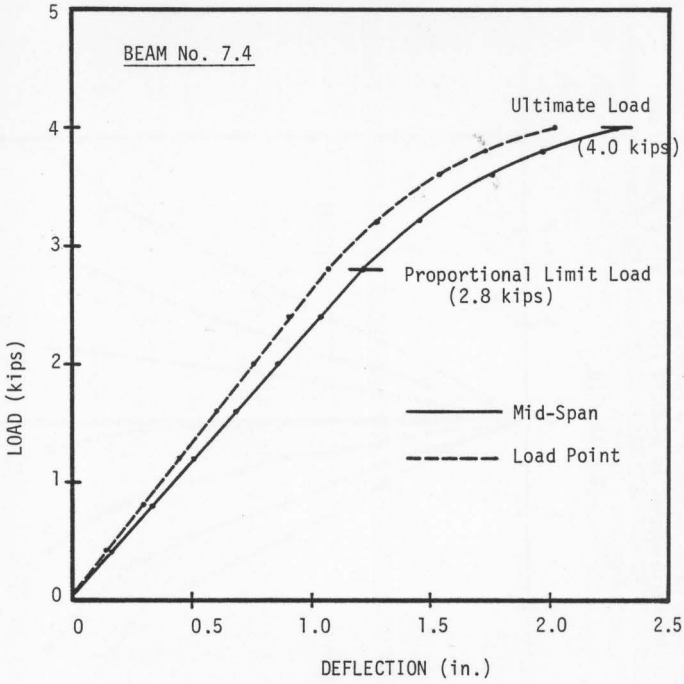

FIG. B.16 TYPICAL LOAD DEFLECTION CURVES IN BENDING TEST -- 2 x 6 DOUGLAS-FIR STIFFENED CLEAR BEAM SUBJECTED TO THIRD-POINT LOADING

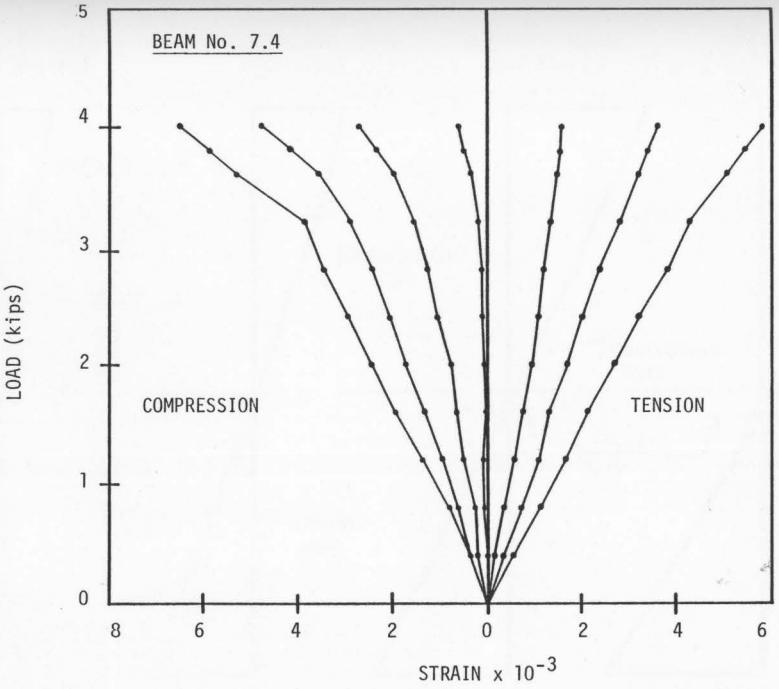

FIG. B.17 TYPICAL LOAD-STRAIN CURVES IN BENDING TEST -- 2 x 6 DOUGLAS-FIR STIFFENED CLEAR BEAM SUBJECTED TO THIRD-POINT LOADING

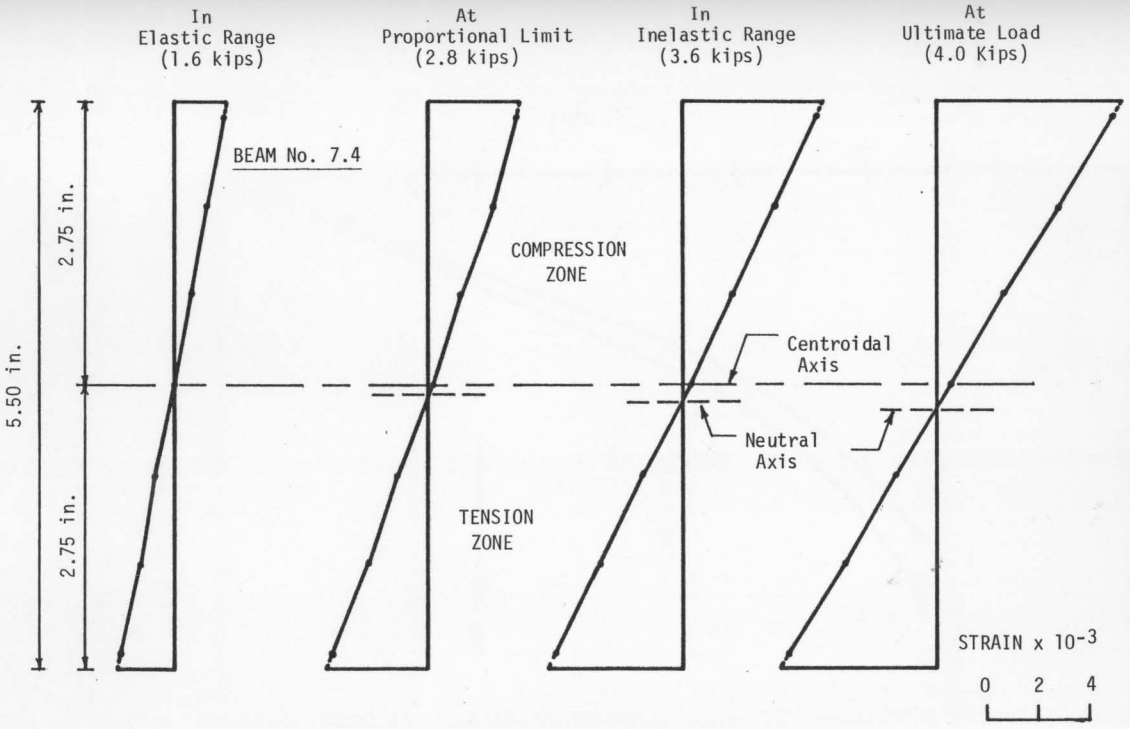

FIG. B.18 TYPICAL STRAIN DISTRIBUTIONS ACROSS BEAM DEPTH IN BENDING TEST -- 2 x 6 DOUGLAS-FIR STIFFENED CLEAR BEAM SUBJECTED TO THIRD-POINT LOADING

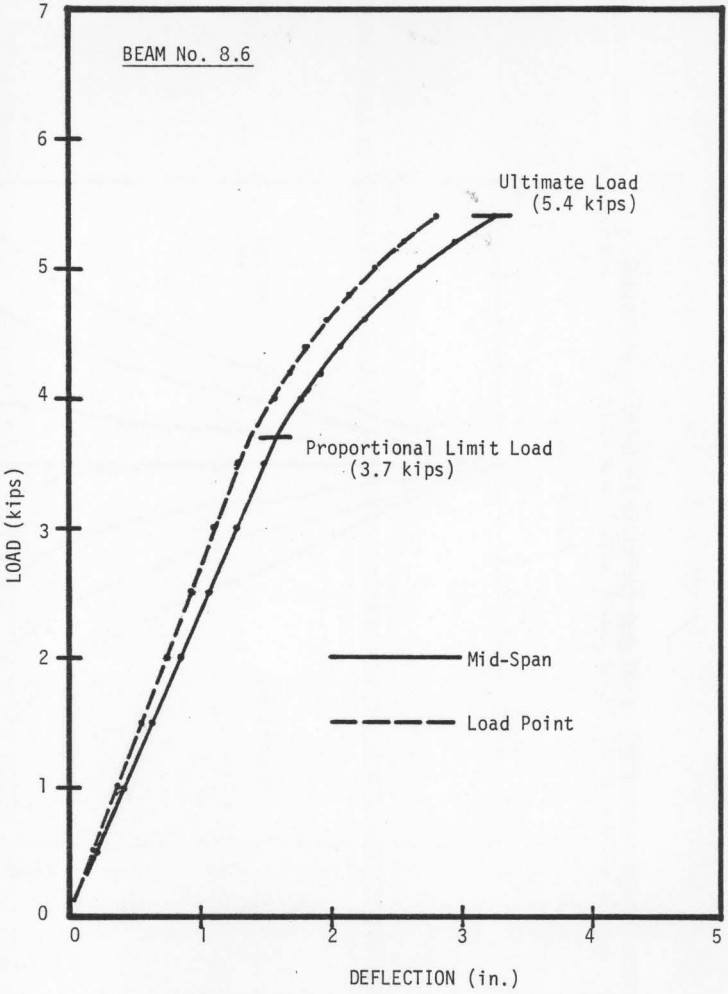

FIG. B.19 TYPICAL LOAD-DEFLECTION CURVES IN BENDING TEST -- 2 x 8 EASTERN SPRUCE CLEAR BEAM SUBJECTED TO THIRD-POINT LOADING

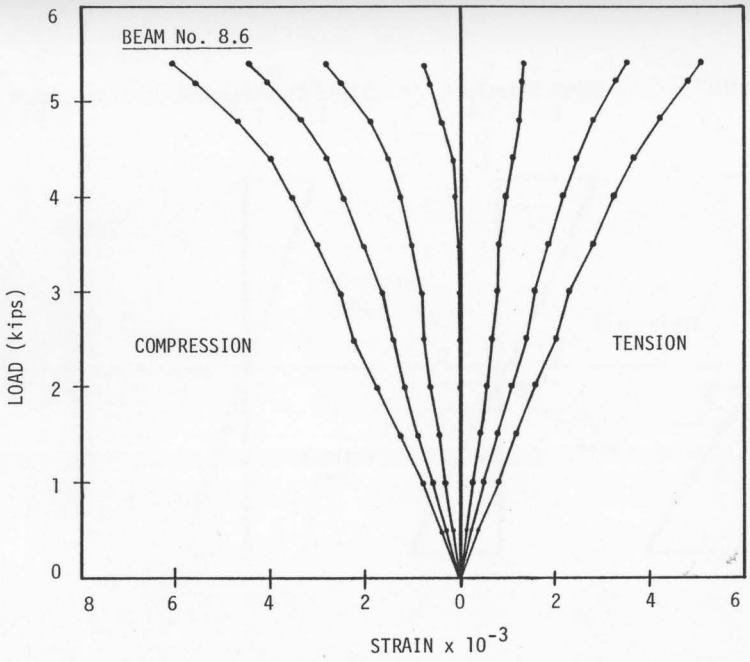

FIG. B.20 TYPICAL LOAD-STRAIN CURVES IN BENDING TEST -- 2 x 8 EASTERN SPRUCE CLEAR BEAM SUBJECTED TO THIRD-POINT LOADING

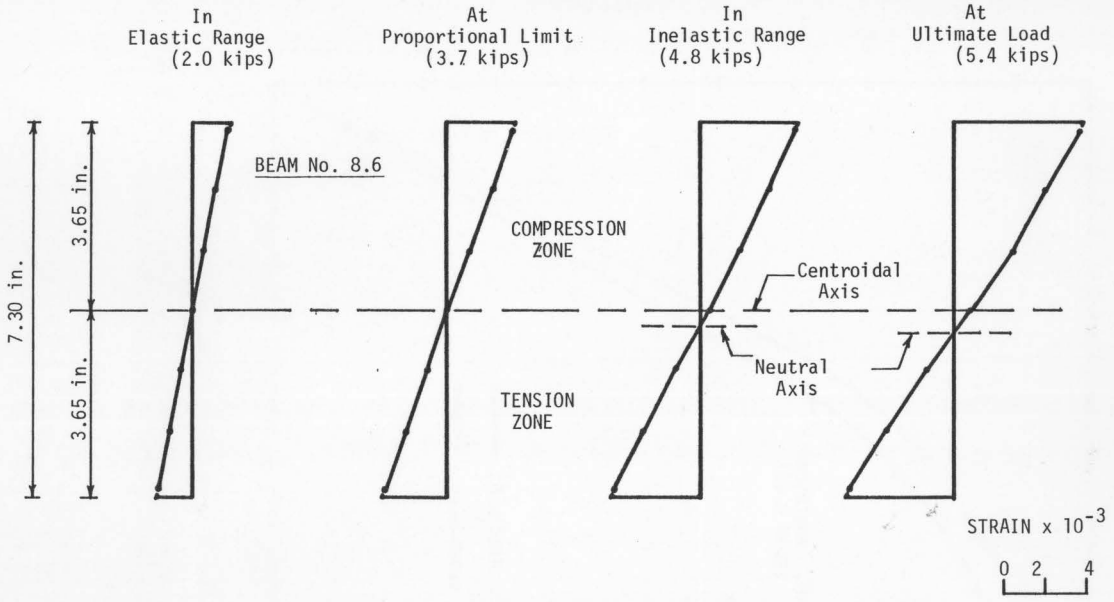

FIG. B.21 TYPICAL STRAIN DISTRIBUTIONS ACROSS BEAM DEPTH IN BENDING TEST -- 2 x 8 EASTERN SPRUCE CLEAR BEAM SUBJECTED TO THIRD-POINT LOADING

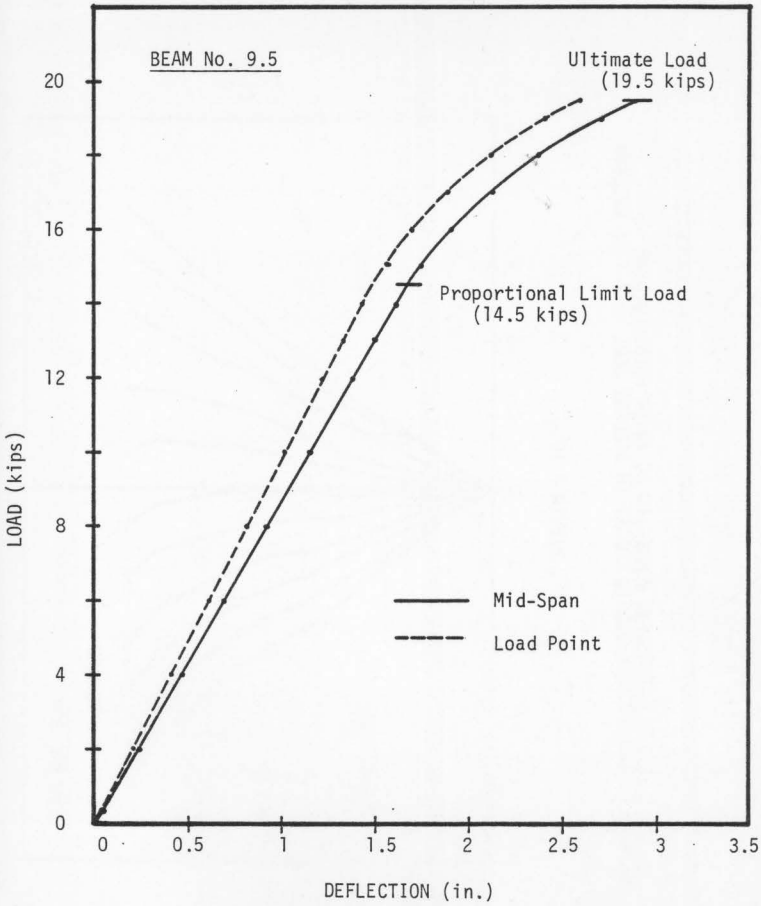

FIG. B.22 TYPICAL LOAD-DEFLECTION CURVES IN BENDING TEST -- 4 x 12 EASTERN SPRUCE CLEAR BEAM SUBJECTED TO THIRD-POINT LOADING

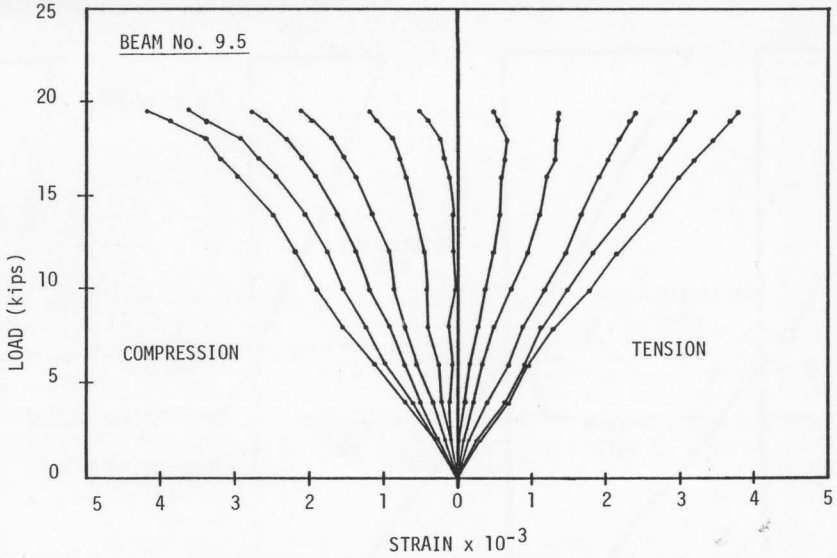

FIG. B.23 TYPICAL LOAD-STRAIN CURVES IN BENDING TEST -- 4 x 12 EASTERN SPRUCE CLEAR BEAM SUBJECTED TO THIRD-POINT LOADING

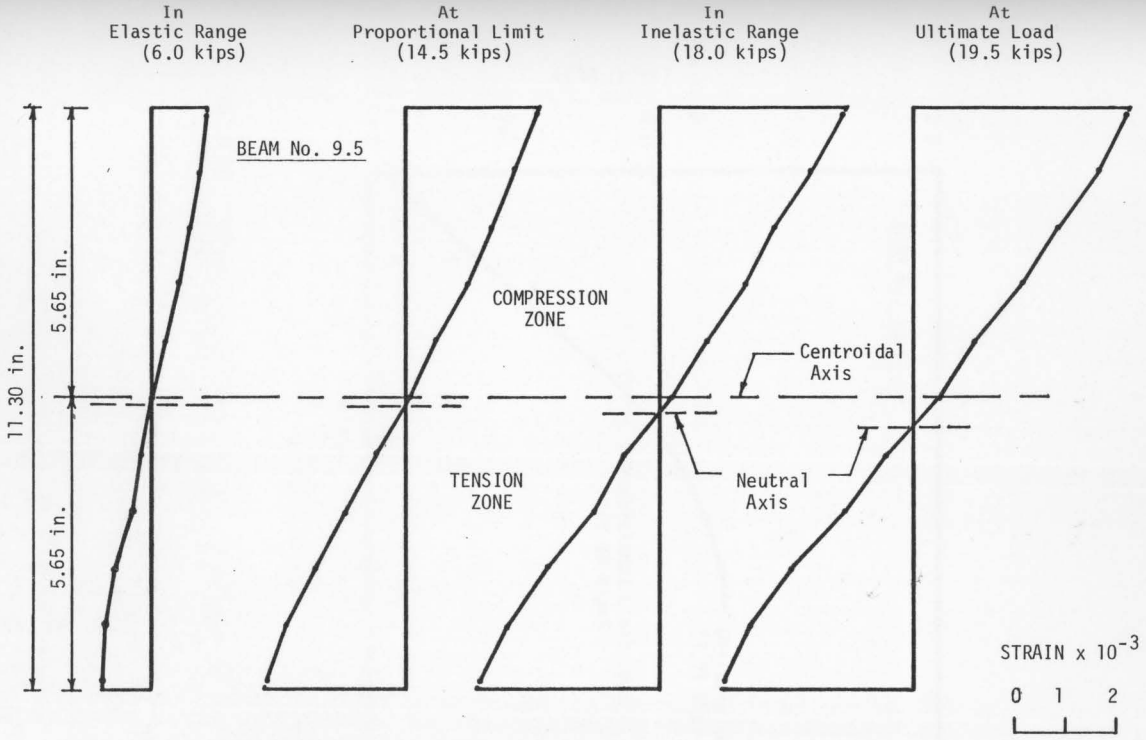

FIG. B.24 TYPICAL STRAIN DISTRIBUTIONS ACROSS BEAM DEPTH IN BENDING TEST -- 4 x 12 EASTERN SPRUCE CLEAR BEAM SUBJECTED TO THIRD-POINT LOADING

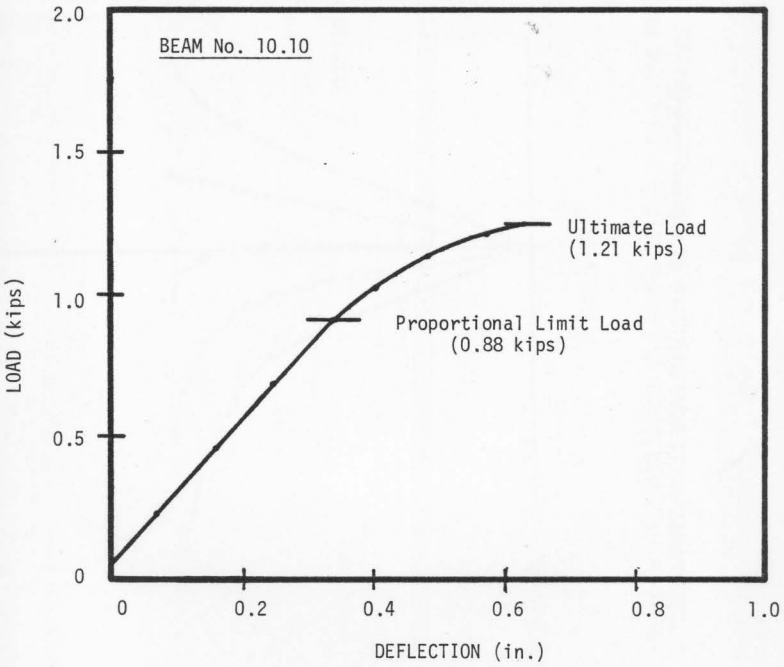

FIG. B.25 TYPICAL LOAD-DEFLECTION CURVE IN BENDING TEST -- 1.50 x 1.65 INCHES EASTERN SPRUCE CLEAR BEAM SUBJECTED TO CENTRAL LOADING

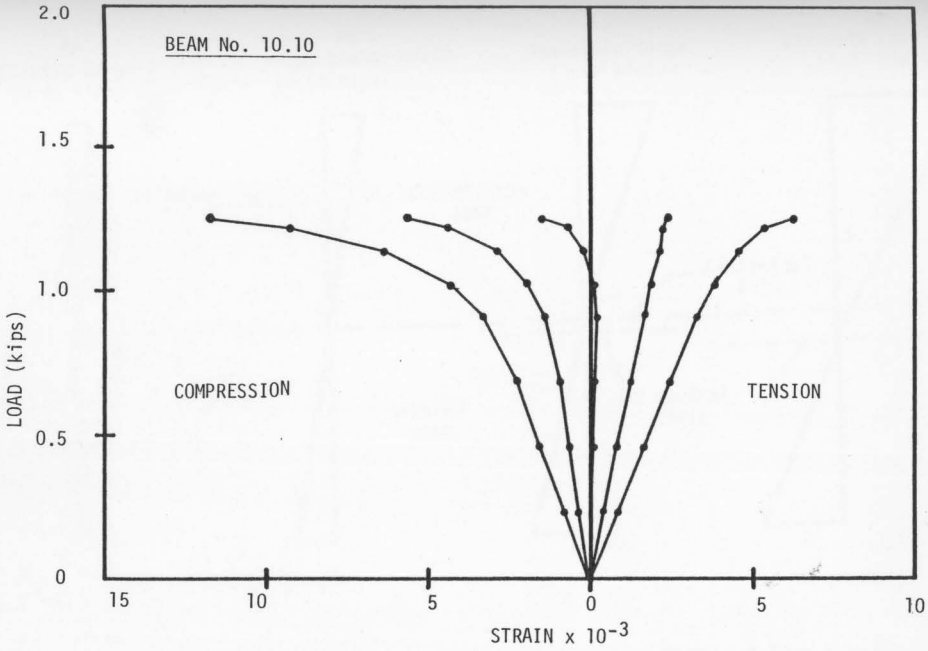

FIG. B.26 TYPICAL LOAD-STRAIN CURVES IN BENDING TEST -- 1.50 x 1.65 INCHES EASTERN SPRUCE CLEAR BEAM SUBJECTED TO CENTRAL LOADING

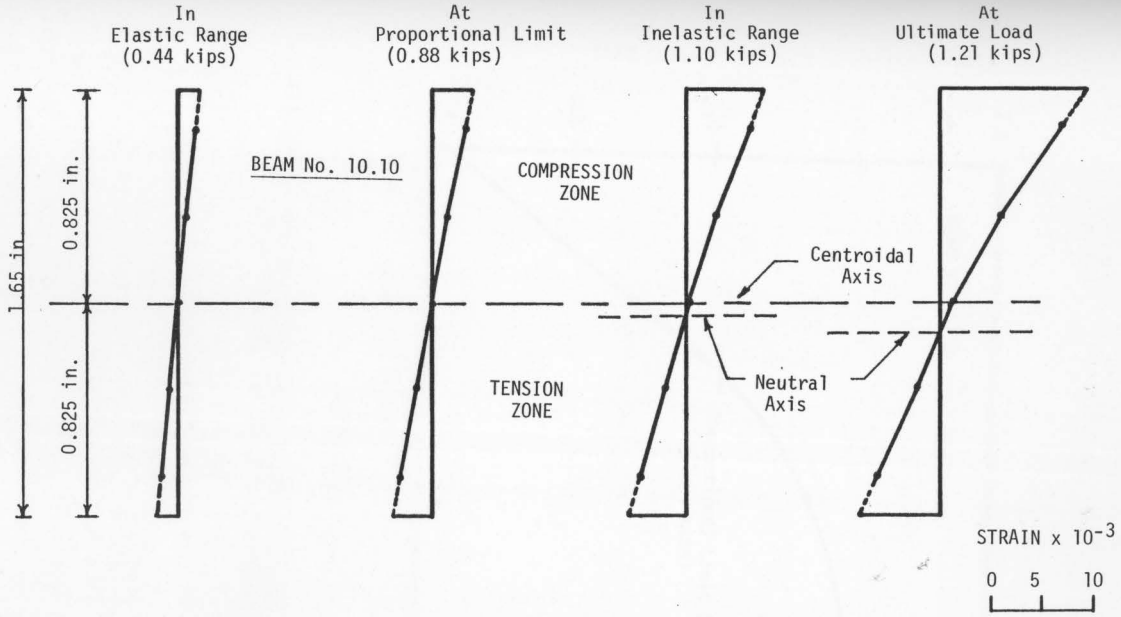

FIG. B.27 TYPICAL STRAIN DISTRIBUTIONS ACROSS BEAM DEPTH IN BENDING TEST -- 1.50 x 1.65 INCHES EASTERN SPRUCE CLEAR BEAM SUBJECTED TO CENTRAL LOADING

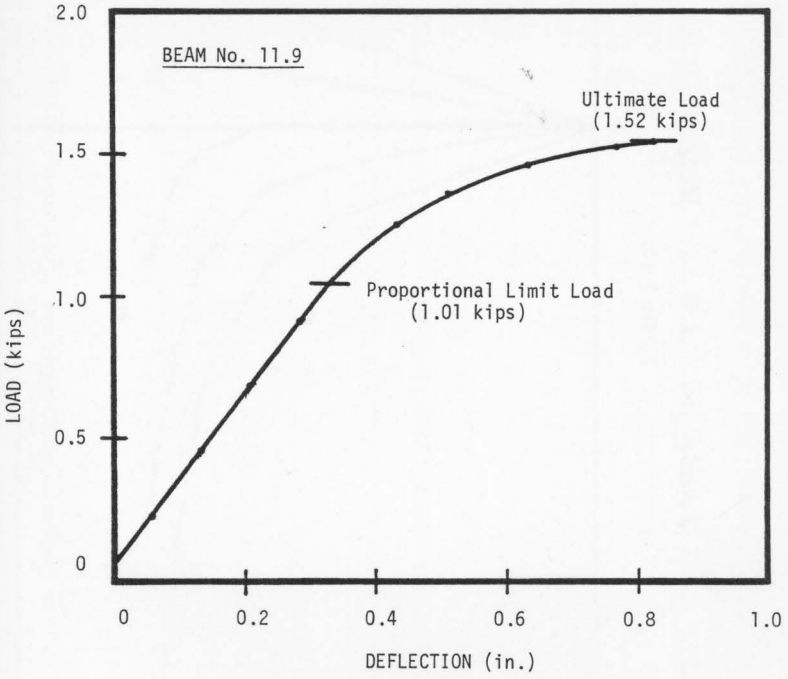

FIG. B.28 TYPICAL LOAD-DEFLECTION CURVE IN BENDING TEST -- 1.50 x 1.65 INCHES DOUGLAS-FIR CLEAR BEAM SUBJECTED TO CENTRAL LOADING

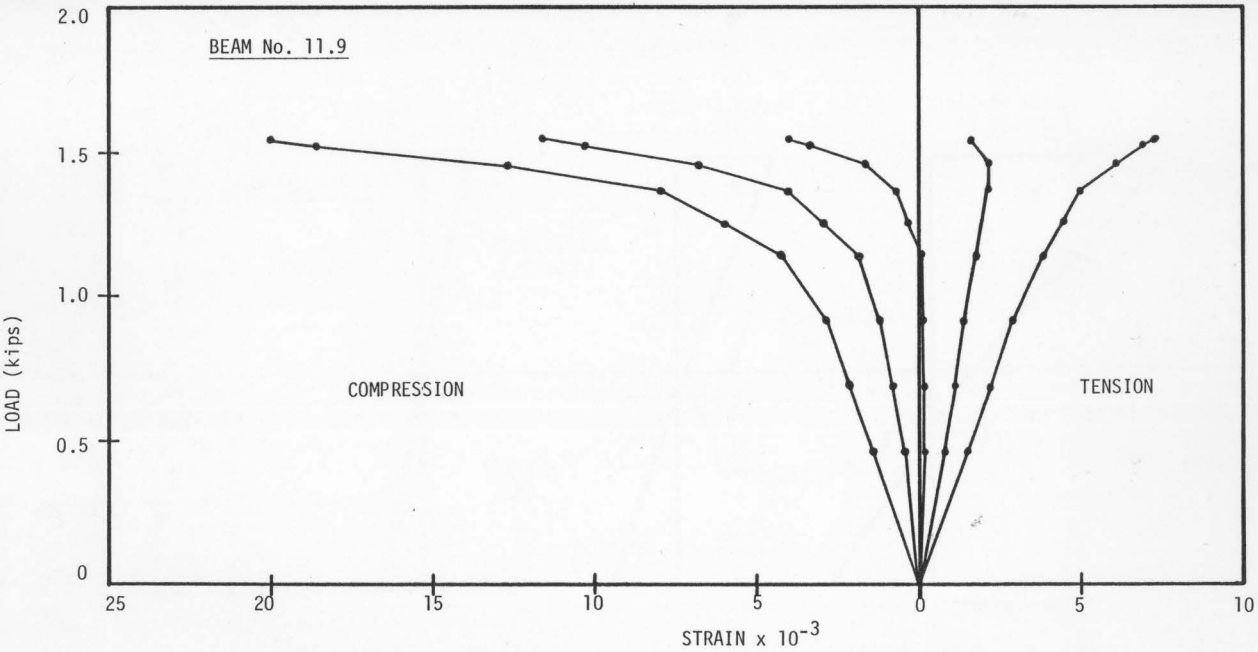

FIG. B.29 TYPICAL LOAD-STRAIN CURVES IN BENDING TEST -- 1.50 x 1.65 INCHES DOUGLAS-FIR CLEAR BEAM SUBJECTED TO CENTRAL LOADING

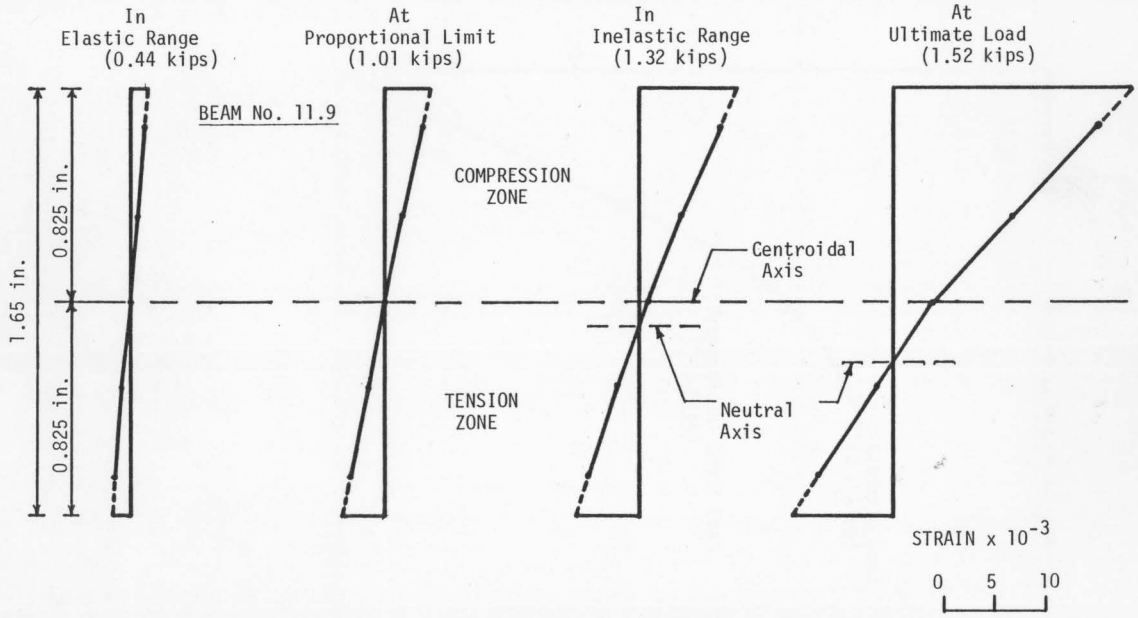

FIG. B.30 TYPICAL STRAIN DISTRIBUTIONS ACROSS BEAM DEPTH IN BENDING TEST -- 1.50 x 1.65 INCHES DOUGLAS-FIR CLEAR BEAM SUBJECTED TO CENTRAL LOADING

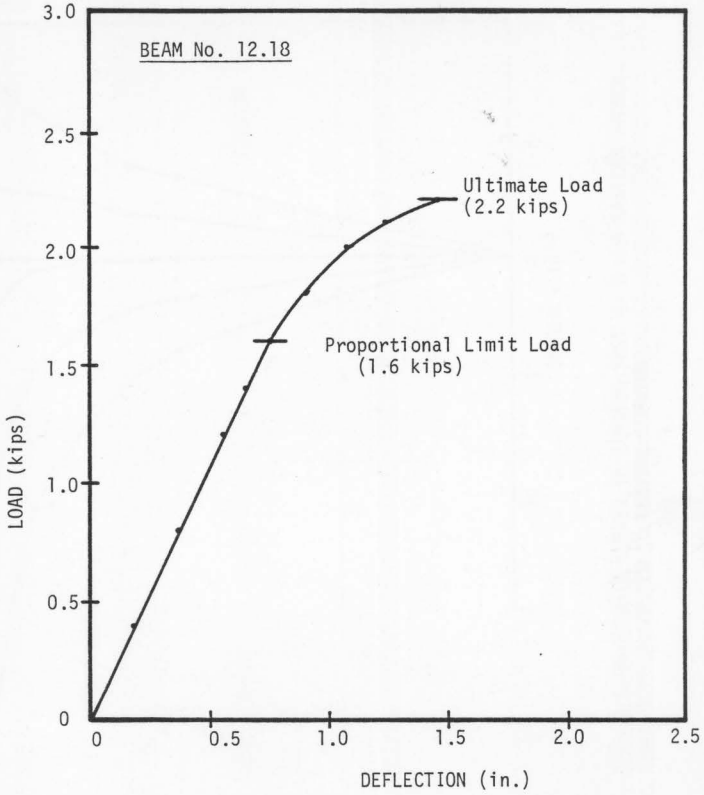

FIG. B.31 TYPICAL LOAD-DEFLECTION CURVE IN BENDING TEST -- 2 x 4 EASTERN SPRUCE CLEAR BEAM SUBJECTED TO CENTRAL LOADING

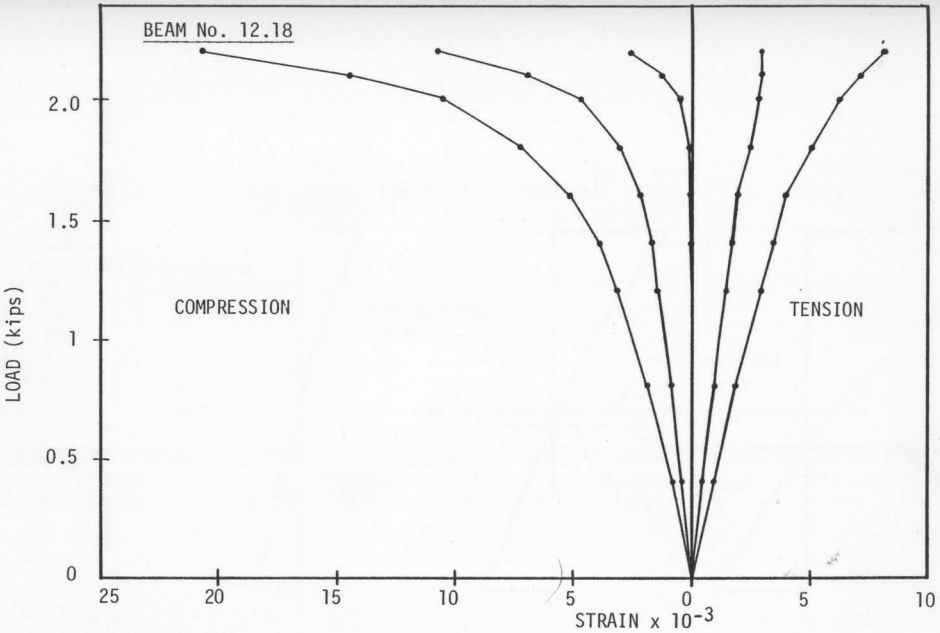

FIG. B.32 TYPICAL LOAD-STRAIN CURVES IN BENDING TEST -- 2 x 4 EASTERN SPRUCE CLEAR BEAM SUBJECTED TO CENTRAL LOADING

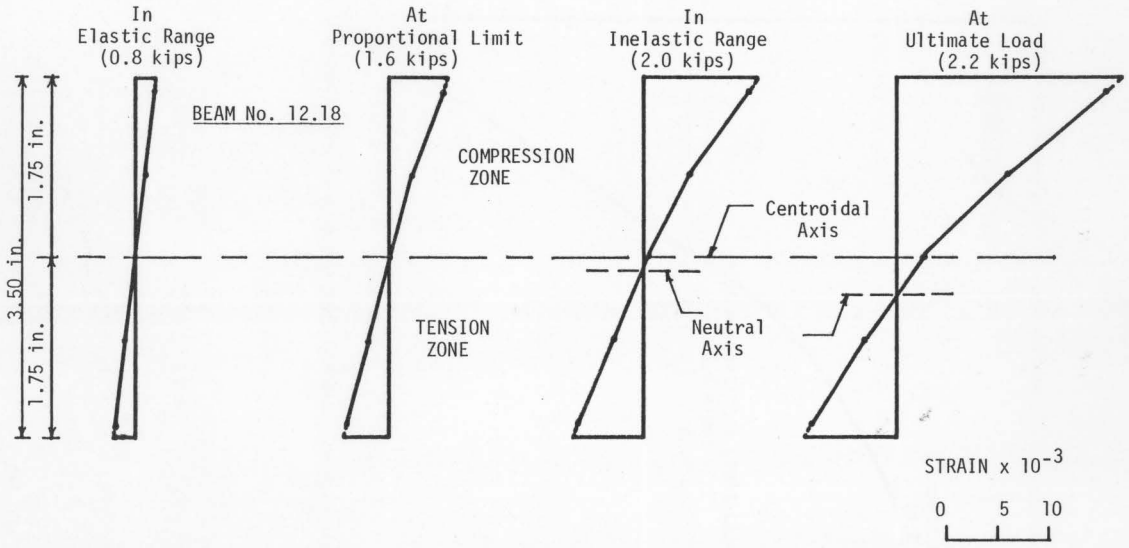

FIG. B.33 TYPICAL STRAIN DISTRIBUTIONS ACROSS BEAM DEPTH IN BENDING TEST -- 2 x 4 EASTERN SPRUCE CLEAR BEAM SUBJECTED TO CENTRAL LOADING

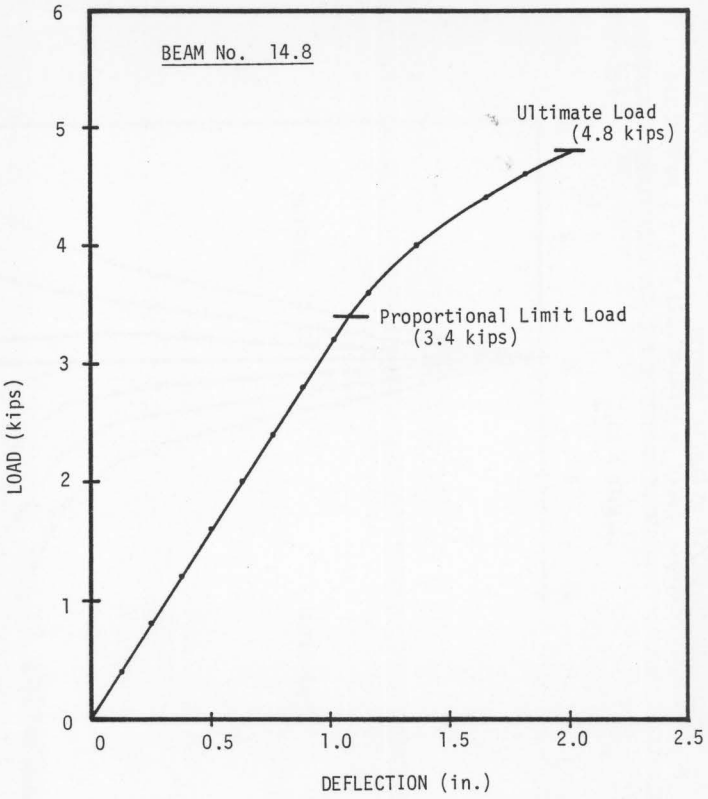

FIG. B.34 TYPICAL LOAD-DEFLECTION CURVE IN BENDING TEST -- 2 x 6 DOUGLAS-FIR CLEAR BEAM SUBJECTED TO CENTRAL LOADING

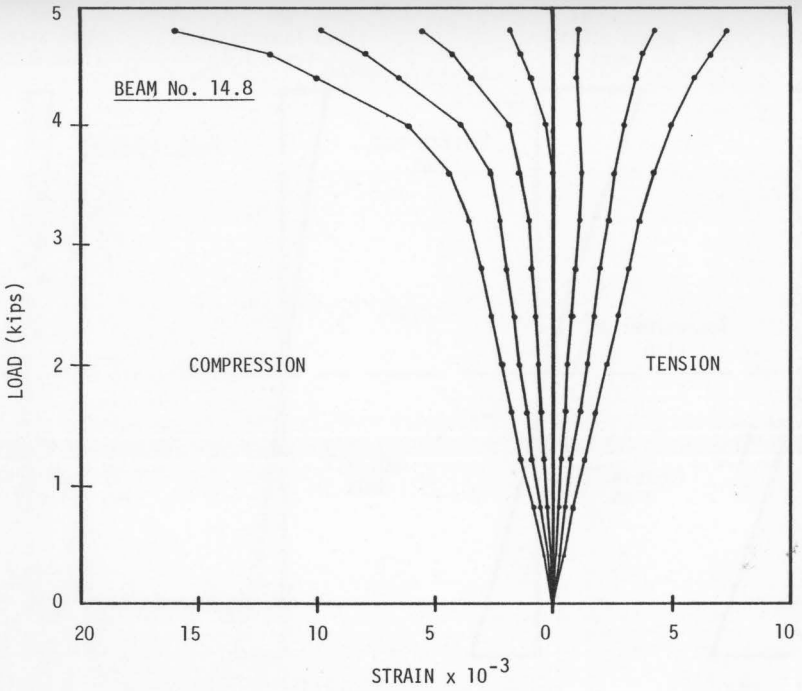

FIG. B.35 TYPICAL LOAD-STRAIN CURVES IN BENDING TEST -- 2 x 6 DOUGLAS-FIR CLEAR BEAM SUBJECTED TO CENTRAL LOADING

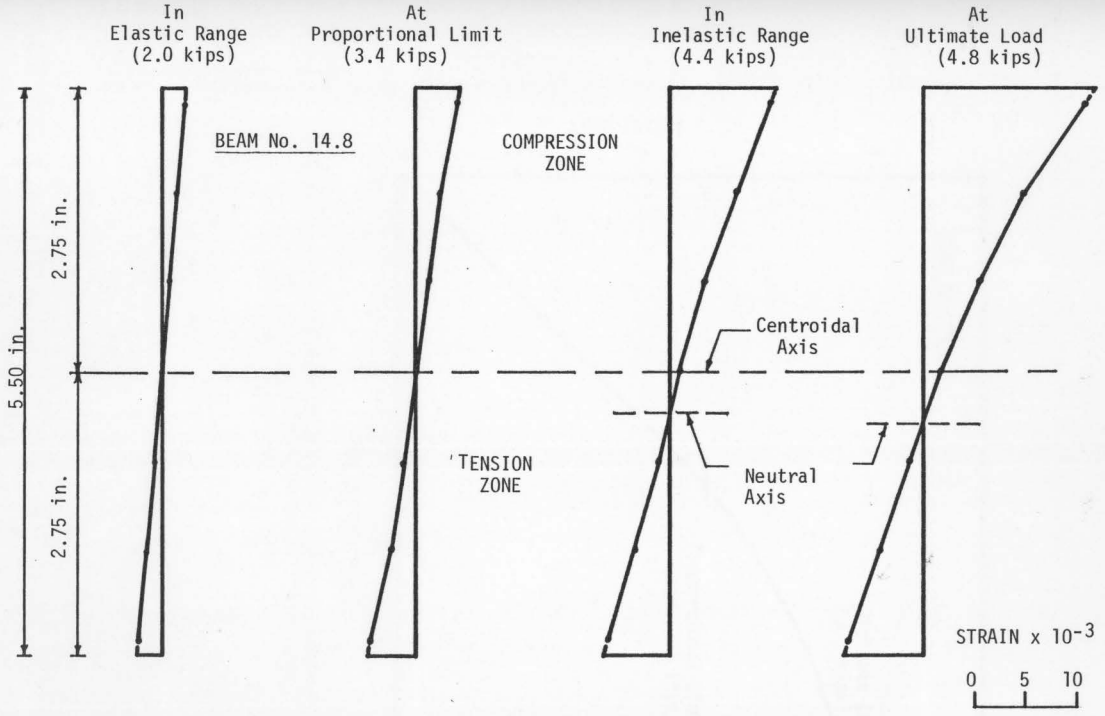

FIG. B. 36 TYPICAL STRAIN DISTRIBUTIONS ACROSS BEAM DEPTH IN BENDING TEST -- 2 x 6 DOUGLAS-FIR CLEAR BEAM SUBJECTED TO CENTRAL LOADING

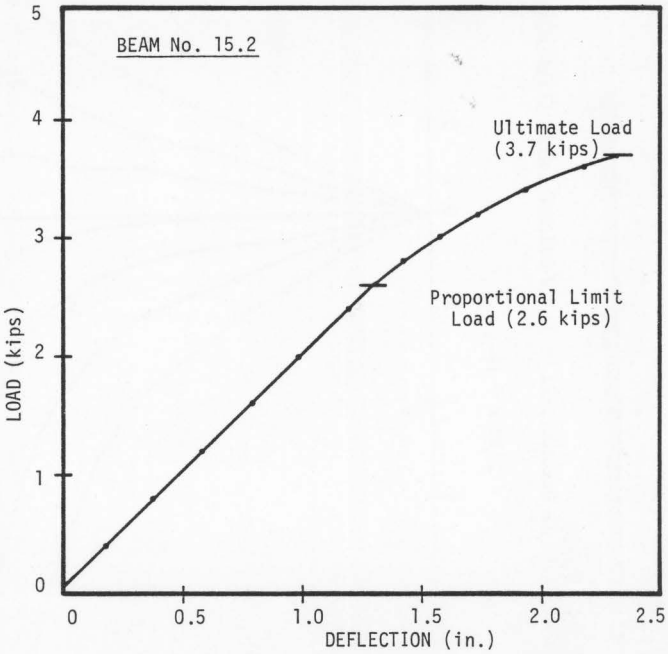

FIG. B.37 TYPICAL LOAD-DEFLECTION CURVE IN BENDING TEST -- 2 x 8 EASTERN SPRUCE CLEAR BEAM SUBJECTED TO CENTRAL LOADING

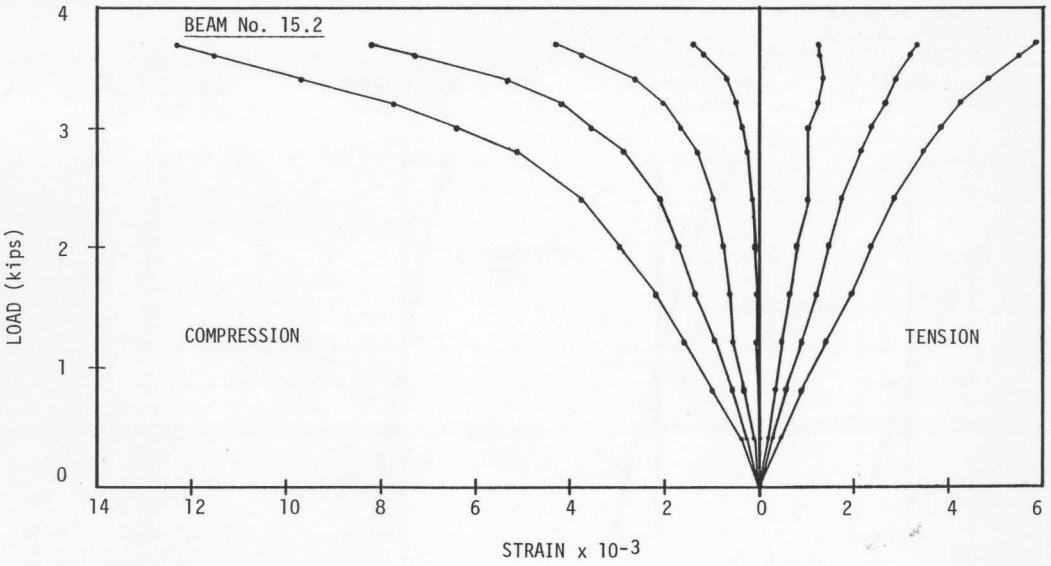

FIG. B.38 TYPICAL LOAD-STRAIN CURVES IN BENDING TEST -- 2 x 8 EASTERN SPRUCE CLEAR BEAM SUBJECTED TO CENTRAL LAODING

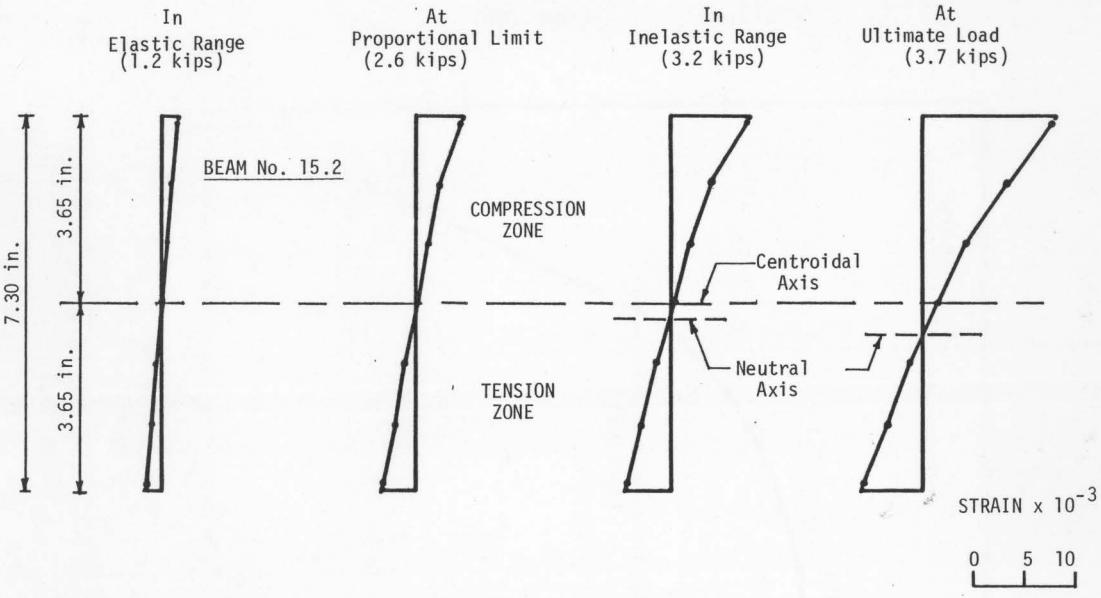

FIG. B. 39 TYPICAL STRAIN DISTRIBUTIONS ACROSS BEAM DEPTH IN BENDING TEST -- 2 x 8 EASTERN SPRUCE CLEAR BEAM SUBJECTED TO CENTRAL LOADING

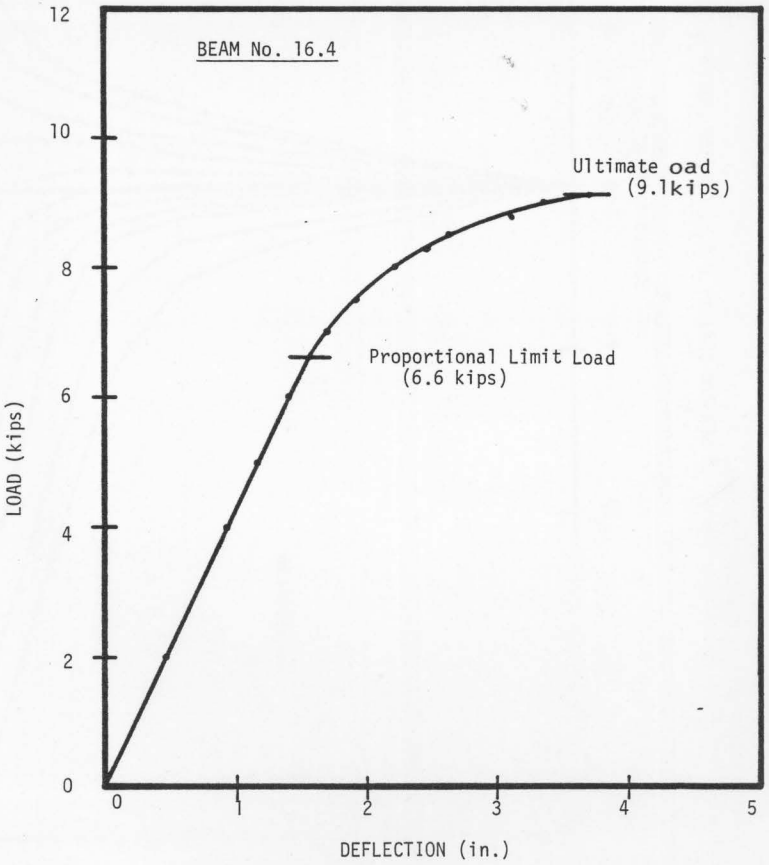

FIG. B. 40 TYPICAL LOAD-DEFLECTION CURVE IN BENDING TEST -- 4 x 12 EASTERN SPRUCE CLEAR BEAM SUBJECTED TO CENTRAL LOADING

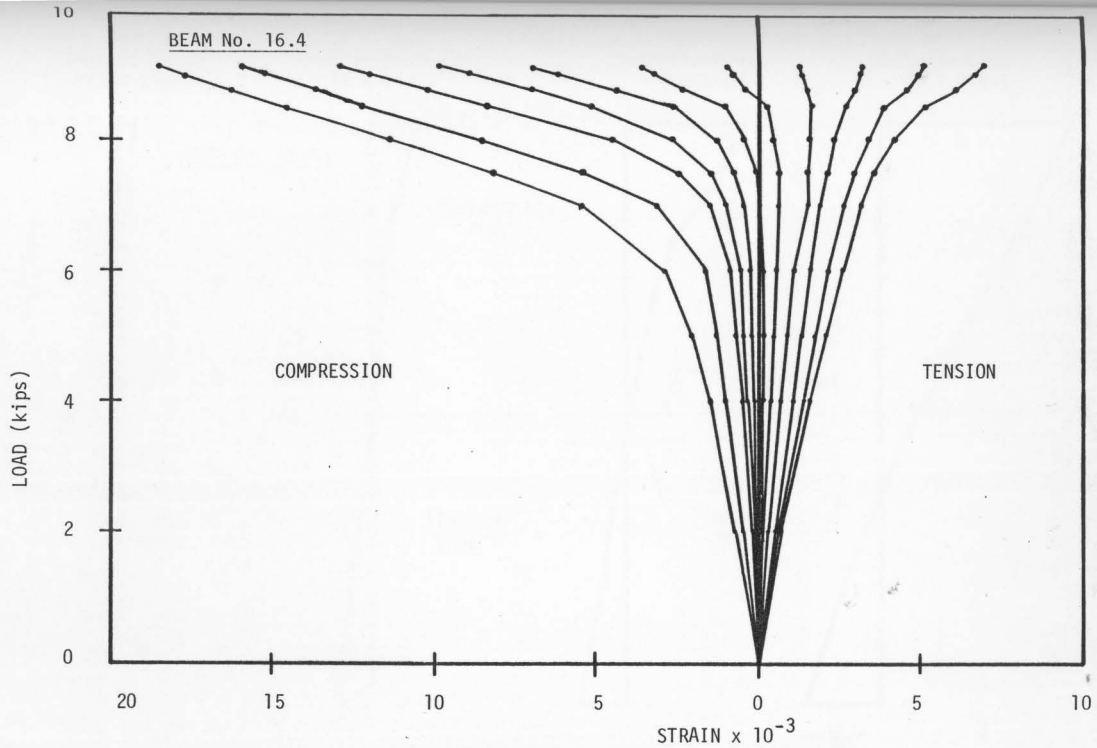

FIG. B.41 TYPICAL LOAD-STRAIN CURVES IN BENDING TEST -- 4 x 12 EASTERN SPRUCE CLEAR BEAM SUBJECTED TO CENTRAL LOADING

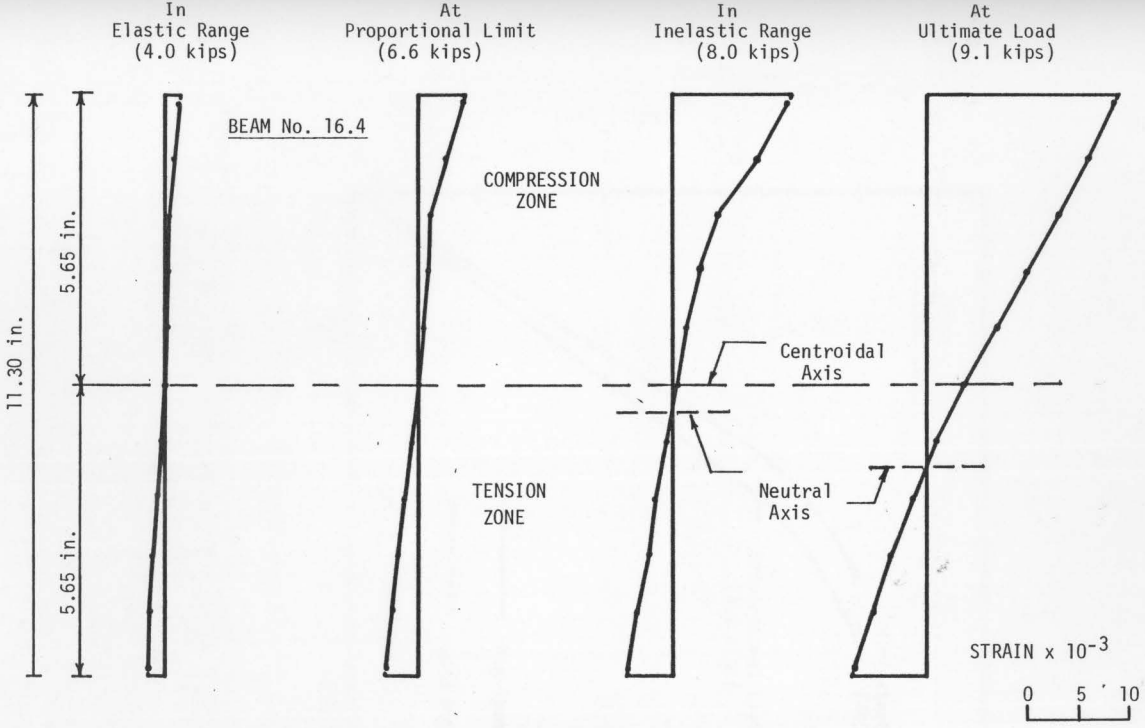

FIG. B.42 TYPICAL STRAIN DISTRIBUTIONS ACROSS BEAM DEPTH IN BENDING TEST -- 4 x 12 EASTERN SPRUCE CLEAR BEAM SUBJECTED TO CENTRAL LOADING

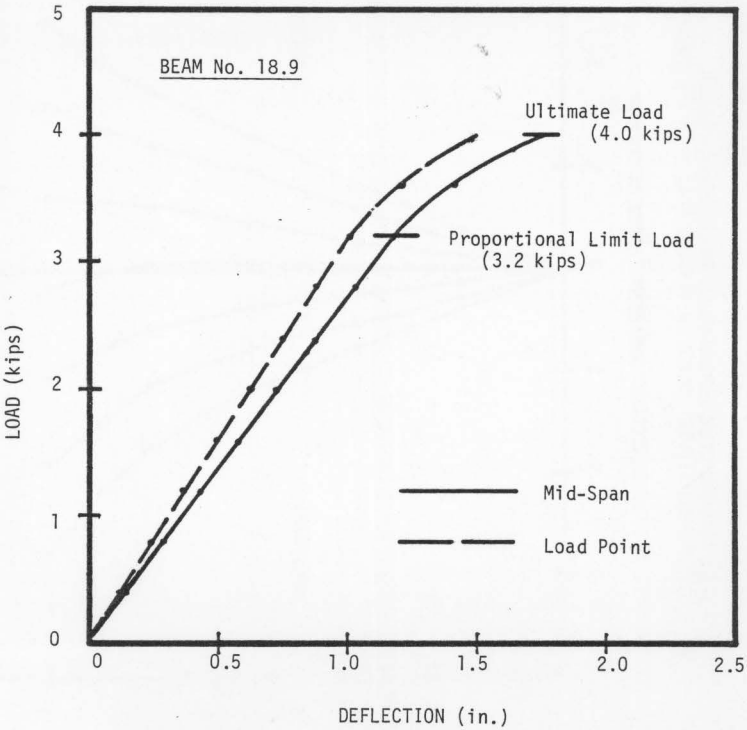

FIG. B.43 TYPICAL LOAD-DEFLECTION CURVES IN BENDING TEST -- 2 x 6 EASTERN SPRUCE KNOTTED BEAM SUBJECTED TO THIRD-POINT LOADING

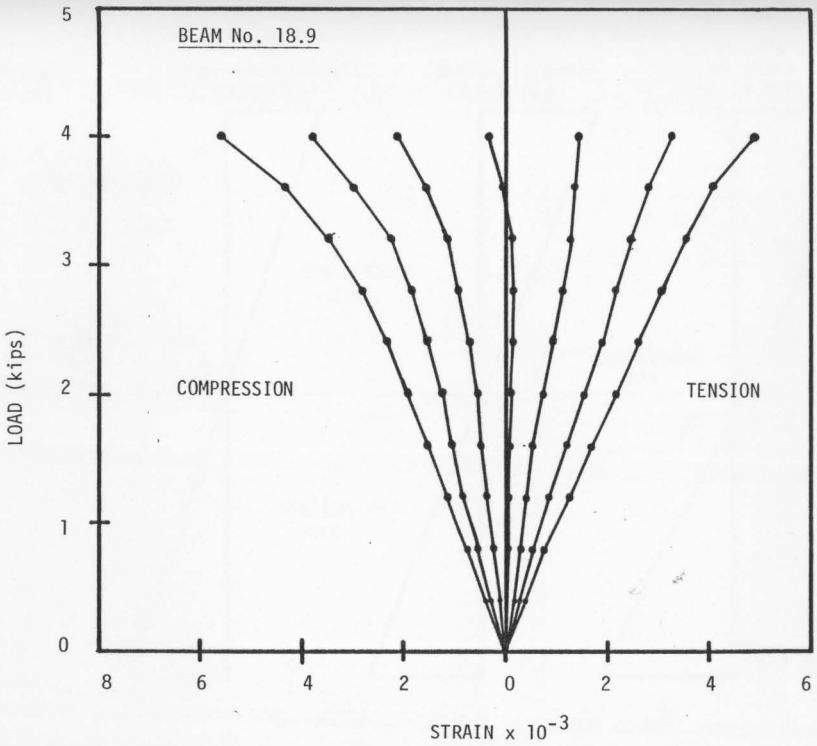

FIG. B.44 TYPICAL LOAD-STRAIN CURVES IN BENDING TEST -- 2 x 6 EASTERN SPRUCE KNOTTED BEAM SUBJECTED TO THIRD-POINT LOADING

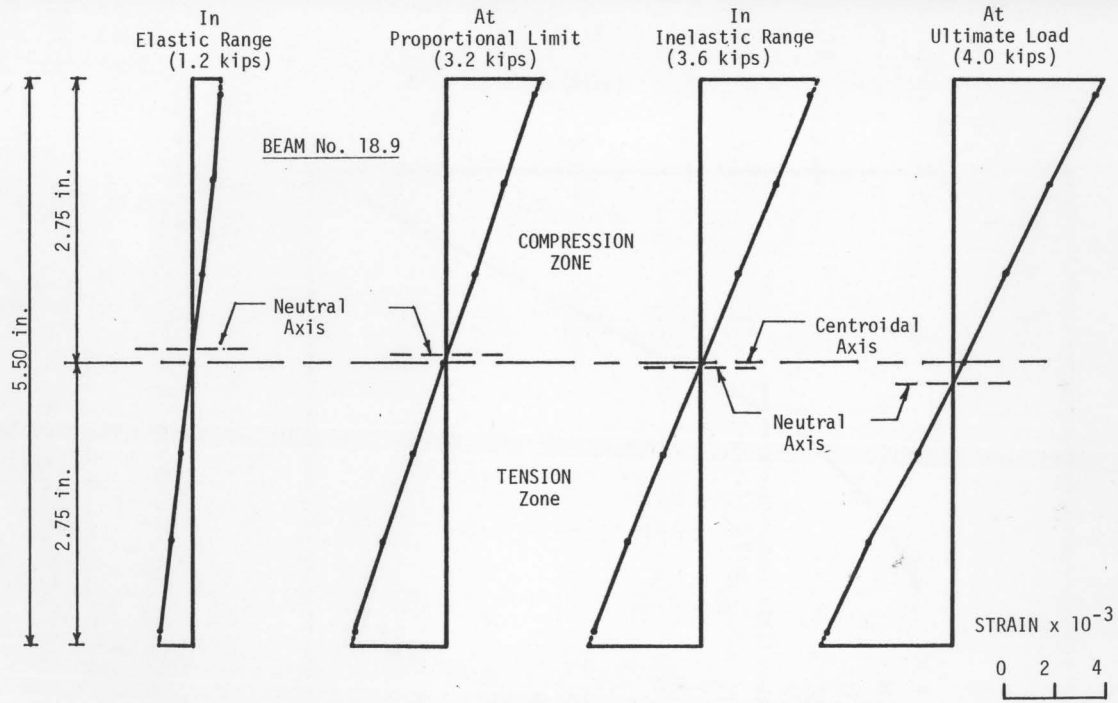

FIG. B. 45 TYPICAL STRAIN DISTRIBUTIONS ACROSS BEAM DEPTH IN BENDING TEST -- 2 x 6 EASTERN SPRUCE KNOTTED BEAM SUBJECTED TO THIRD-POINT LOADING

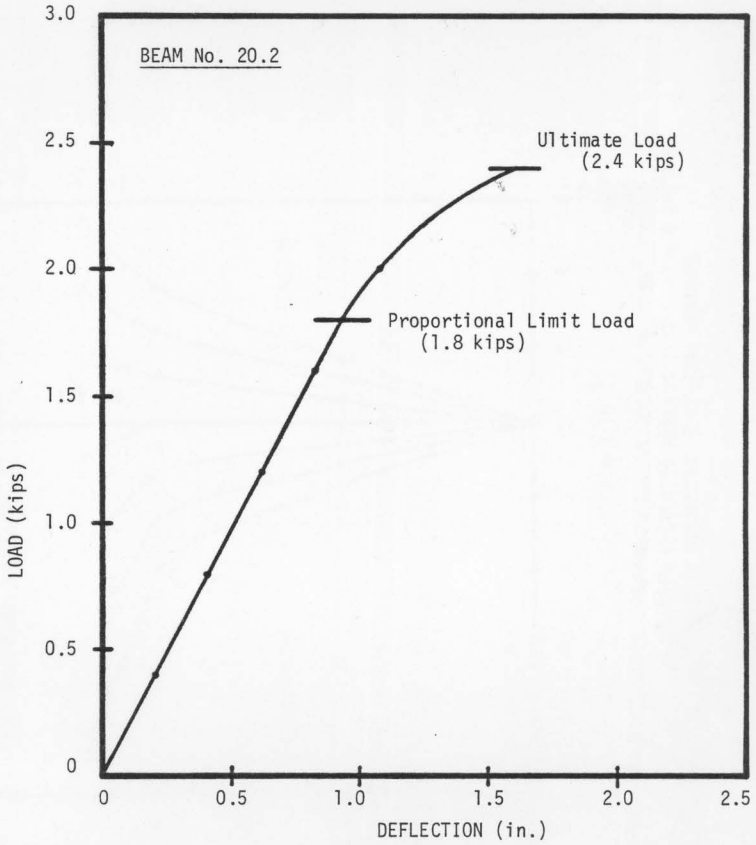

FIG. B.46 TYPICAL LOAD-DEFLECTION CURVE IN BENDING TEST -- 2 x 6 EASTERN SPRUCE KNOTTED BEAM SUBJECTED TO CENTRAL LOADING

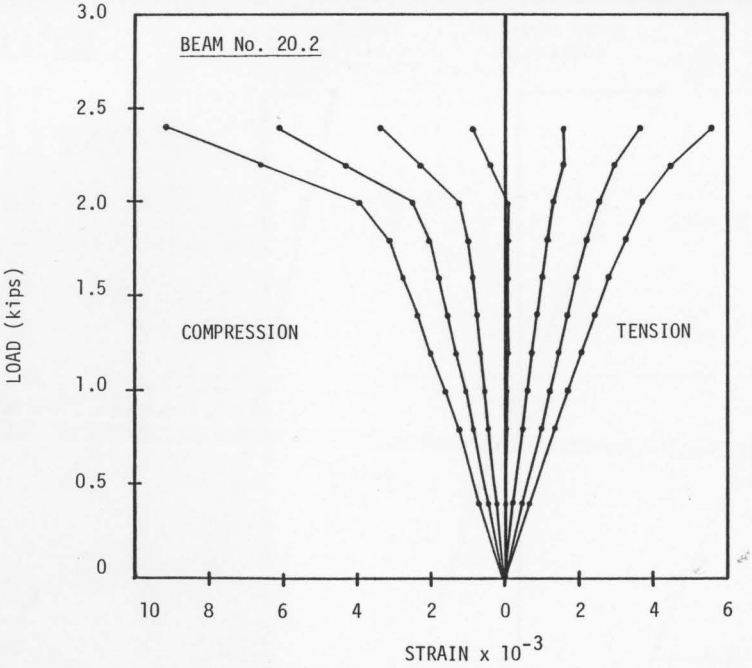

FIG. B.47 TYPICAL LOAD-STRAIN CURVES IN BENDING TEST -- 2 x 6 EASTERN SPRUCE KNOTTED BEAM SUBJECTED TO CENTRAL LOADING

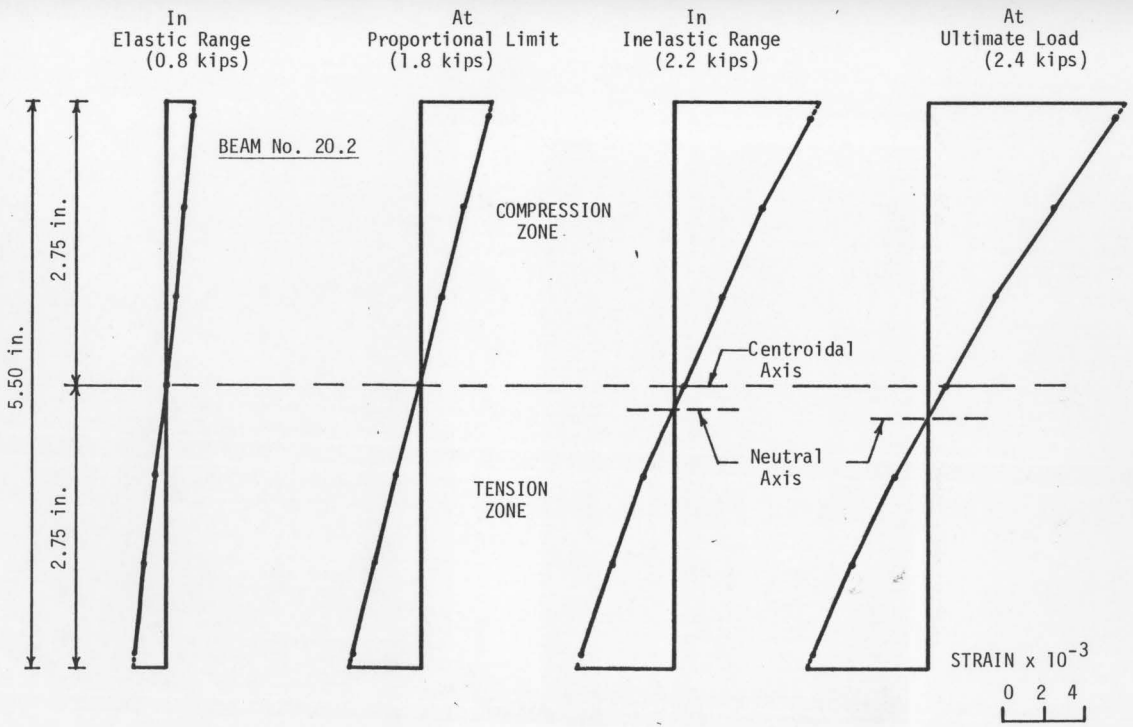

FIG. B. 48 TYPICAL STRAIN DISTRIBUTIONS ACROSS BEAM DPETH IN BENDING TEST -- 2 x 6 EASTERN SPRUCE KNOTTED BEAM SUBJECTED TO CENTRAL LOADING

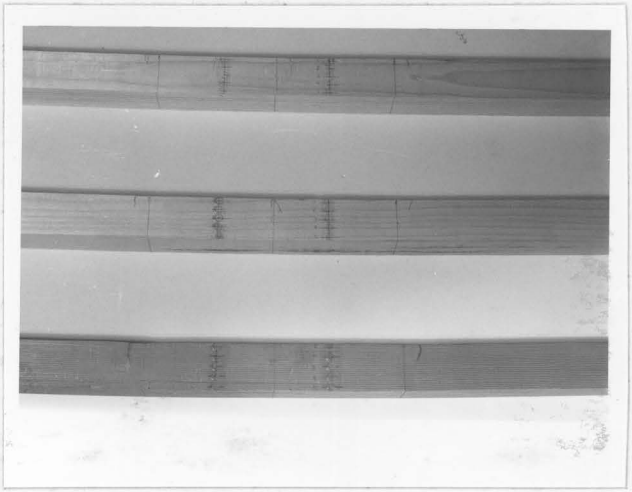

FIG. B. 49 TYPICAL FAILURE IN 1.50 x 1.65 INCHES CLEAR BEAM SUBJECTED TO THIRD-POINT LOADING

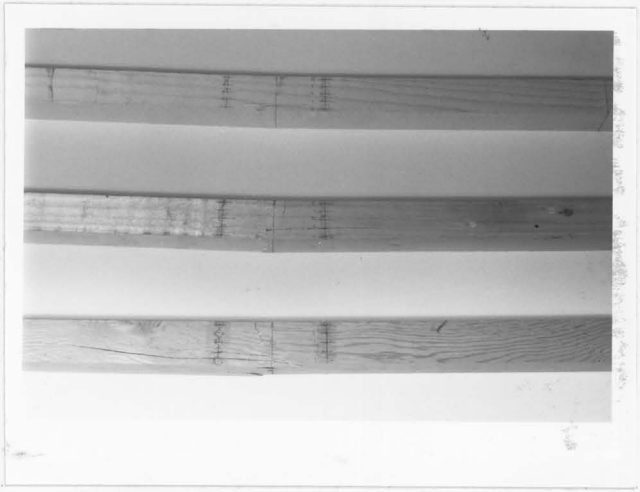

FIG. B. 50 TYPICAL FAILURE IN 1.50 x 1.65 INCHES CLEAR BEAMS SUBJECTED TO CENTRAL LOADING

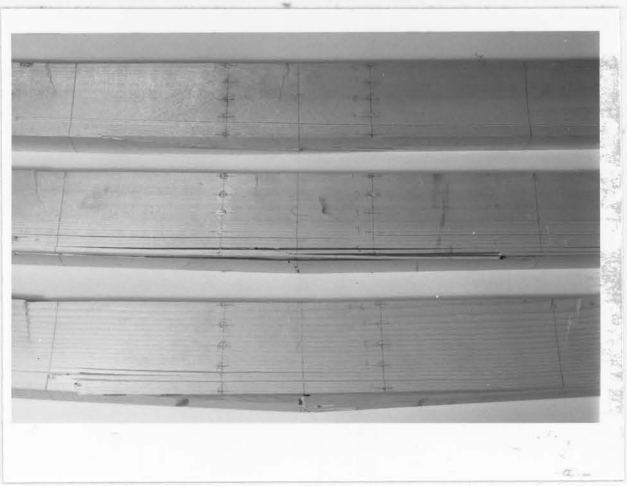

FIG. B.51 TYPICAL FAILURE IN 2 x 4 CLEAR BEAMS SUBJECTED TO THIRD-POINT LOADING

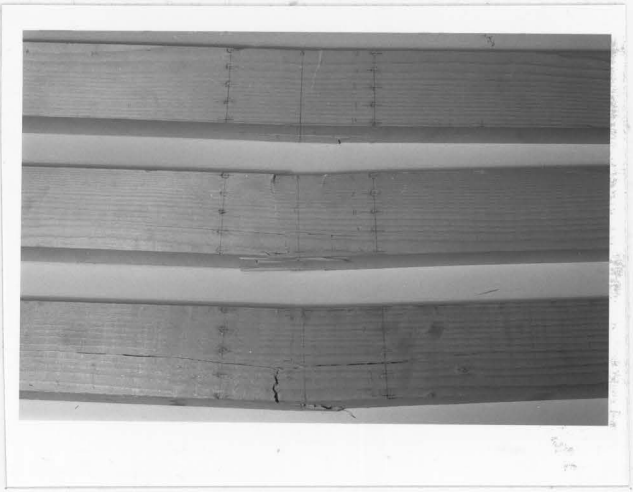

FIG. B.52 TYPICAL FAILURE IN 2 x 4 CLEAR BEAM SUBJECTED TO CENTRAL LOADING

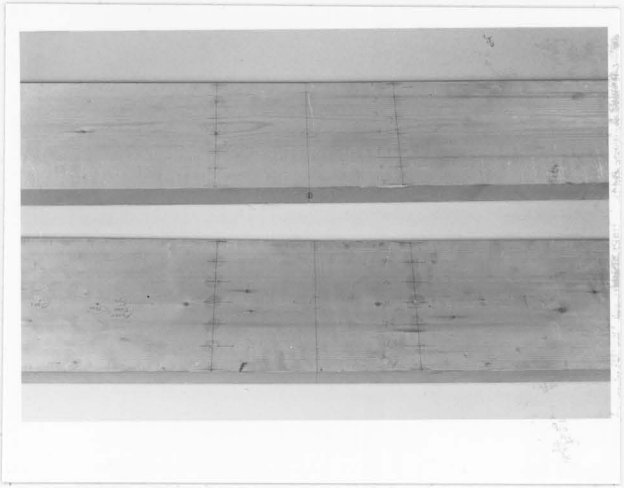

FIG. B.53 TYPICAL FAILURE IN 2 x 8 CLEAR BEAMS SUBJECTED TO THIRD-POINT LOADING

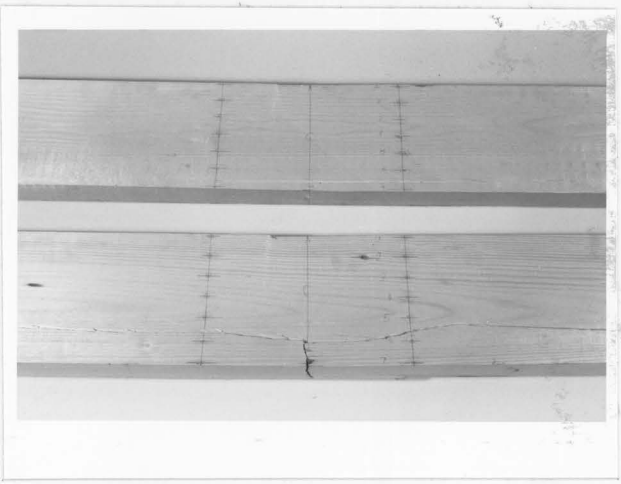

FIG. B.54 TYPICAL FAILURE IN 2 x 8 CLEAR BEAMS SUBJECTED TO CENTRAL LOADING

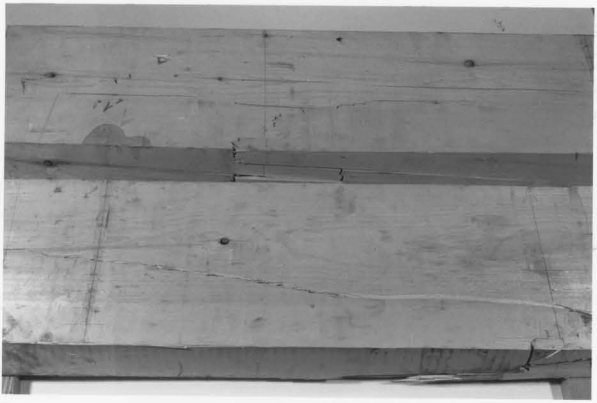

FIG. B.55 TYPICAL FAILURE IN 4 x 12 CLEAR BEAMS SUBJECTED TO THIRD-POINT LOADING

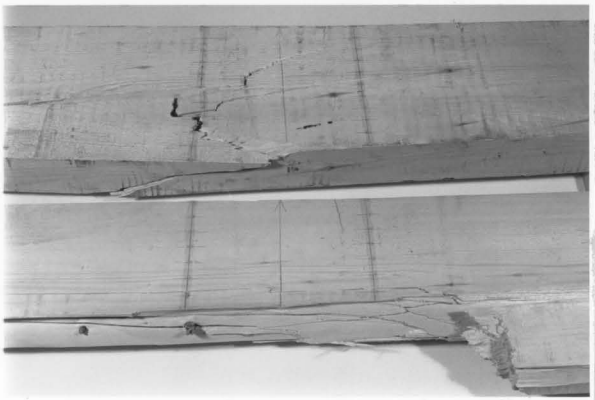

FIG. B.56 TYPICAL FAILURE IN 4 x 12 CLEAR BEAMS SUBJECTED TO CENTRAL LOADING

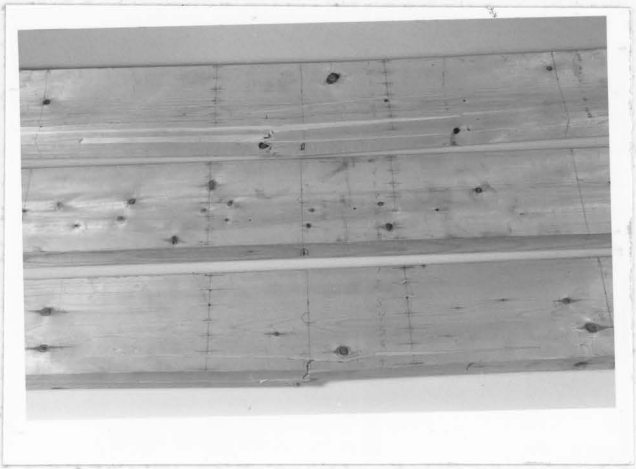

FIG. B.57 TYPICAL FAILURE IN 2 x 6 KNOTTED BEAMS SUBJECTED TO THIRD-POINT LOADING

FIG. B.58 TYPICAL FAILURE IN 2 x 6 KNOTTED BEAMS SUBJECTED TO CENTRAL LOADING